David Brandwood

Fourier Transforms
in Radar
and Signal
Processing

SECOND EDITION

DVD Included

Fourier Transforms in Radar and Signal Processing

Second Edition

DISCLAIMER OF WARRANTY

The technical descriptions, procedures, and computer programs in this book have been developed with the greatest of care and they have been useful to the author in a broad range of applications; however, they are provided as is, without warranty of any kind. Artech House, Inc. and the author and editors of the book titled *Fourier Transforms in Radar and Signal Processing, Second Edition* make no warranties, expressed or implied, that the equations, programs, and procedures in this book or its associated software are free of error, or are consistent with any particular standard of merchantability, or will meet your requirements for any particular application. They should not be relied upon for solving a problem whose incorrect solution could result in injury to a person or loss of property. Any use of the programs or procedures in such a manner is at the user's own risk. The editors, author, and publisher disclaim all liability for direct, incidental, or consequent damages resulting from use of the programs or procedures in this book or the associated software.

Fourier Transforms in Radar and Signal Processing

Second Edition

David Brandwood

Contents

Preface

The principal change, in revising this book, has been the addition of a new chapter, primarily on periodic waveforms. The subject of Fourier series has been presented using the rules-and-pairs method, in particular for the common case of real periodic functions. The topic of Fourier transforms of discrete waveforms is also included, leading to a discussion of periodic discrete waveforms in particular, with reference to the fast Fourier transform.

Errors in the original text, mainly typographical, have been corrected, and at a number of points in the text, the mathematics, and the figures have been revised for greater clarity. Some further small additions and illustrations have been included, particularly in Chapters 2 and 3.

A significant further addition is the provision of a disk containing MAT-LAB programs, including those for all the principal graphical figures. Readers can run these programs with the same parameters to reproduce the figures and vary these parameters for their particular interests or requirements.

Again grateful acknowledgment is due to the publisher's reviewer, remaining anonymous, for encouragement and for useful and perceptive comments.

DHB 2011

Preface to the First Edition

The basic material for this book has been accumulated over the author's working lifetime of about forty years. The rules-and-pairs approach to Fourier transforms has been employed with good effect in a wide variety of problems, from pulse Doppler radar spectra to delay compensation, from antenna array patterns to efficient clutter simulation. It has been found to be generally easy and effective, quickly yielding useful results and allowing the user to see clearly the relationships between functions and transforms, waveforms, and spectra, rather than losing sight of these in the complexities of integration. It seemed, however, that the benefits of this approach should be better known, and the initial intention was to produce a technical note for use by the author's colleagues and successors. However, the interest shown and encouragement given by Artech House have been gratefully received and the opportunity to publicize the technique more widely has been taken.

DHB 2002

1

Introduction

1.1   Aim of the Work

The Fourier transform is a valuable theoretical technique, used widely in fields such as applied mathematics, statistics, physics, and engineering. However, the relationship between a function and its transform is given by an integral, and a certain amount of tedious integration may be required to obtain the transform in a given application. In general, the user of this mathematical tool is interested in the functions and their transforms and not in the process of obtaining one from the other, which, even if not difficult, may be complicated and require care to avoid any small slip leading to an error in the result. If the transform function could be obtained without integration, this would be welcomed by most users. In fact, anyone performing many transforms in a particular field, such as radar, where the spectra corresponding to various, perhaps rather similar, waveforms are required, would notice that certain waveforms have certain transforms and that certain relationships between waveforms lead to corresponding relationships between spectra. By knowing a relatively small number of waveform-transform pairs and the rules for combining and scaling transforms, a very substantial amount of Fourier transform analysis can be carried out without any explicit integration at all— the integrations are prepackaged within the set of rules and pairs.

The aim of this book is to present again the rules-and-pairs approach to Fourier transforms, first defined systematically by Woodward [1], and to

illustrate its use. The rules and pairs, and notation, are given in Chapter 2, and the remaining chapters employ the technique in a number of areas of application. These are mainly in the field of signal or waveform processing (though not Chapter 8), but the technique is general, of course, and this choice should certainly not imply that other users of the Fourier transform should not also find the technique of interest and value.

The aim is not to provide a handbook of solutions to particular problems in the areas covered, though some results may be found particularly interesting and useful. More specifically, it is to show how such problems might be tackled and how the technique can be used with ingenuity in a variety of ways. These produce results that would be more difficult and tedious to obtain by integration and may not be so easy to interpret and understand. In fact an important advantage of the method, aided by the notation used, is the greater clarity regarding the nature of the transforms, obtained by keeping attention on the functions rather than on the mechanics of integration. While the illustrations given may not include a reader's particular problem, some examples may well be close enough to suggest how the problem could be tackled by the rules-and-pairs method and perhaps solved more easily than otherwise. Once the user has become familiar with the method, many results can be obtained remarkably easily and concisely, and the complexity of problems to which this method can be applied is surprising.

1.2   Origin of the Rules-and-Pairs Method for Fourier Transforms

With the arrival of the technology of electronics, early in the last century, the possibilities for handling information—sending, receiving, and processing it—expanded immensely over that possible with the mechanical technology, however ingenious, of the nineteenth century. The need to understand the limits of performance, whatever the technology available, and the dependence of performance on various parameters, such as bandwidth and signal-to-noise ratio, led to the rise of the subject of information theory. Under the stimulus of war, a new application of electronics, radar, developed rapidly in the 1930s and 1940s and again theoretical analysis followed. In 1953, P. M. Woodward's monograph, *Probability and Information Theory with Applications to Radar* [1] appeared. The topics of radar detection, accuracy, resolution, and ambiguity, in the later chapters are generally the reasons for the references to this book in modern radar textbooks, but, leading up to his conclusions, Woodward needed results in the field of waveform analysis, and this is the subject of his Chapter 2, in which his rules and pairs are introduced.

Waveforms and spectra are connected, of course, by a Fourier transform relationship, and this technique is the principal tool of the time-and-frequency analysis that Woodward implies is the basis of much of the mathematical study of information theory, radio, and radar.

It is not claimed that Woodward's rules and pairs in themselves are particularly original. The pairs are well known and, as Woodward says, the rules are "known by heart by most circuit mathematicians." What is perhaps new is the careful specification of the set of rules and the committed and consistent use of them to obtain transforms very directly and concisely. In addition to the results required for the mathematical study of radar, Woodward derives very neatly important general results (again, already known) such as Parseval's theorem, sampling theorems, and Poisson's formula, using this approach. What is more clearly new and valuable is Woodward's contribution to notation, including the rect and sinc functions, the comb function, and the rep operator. The term *sinc function* has since become more widely accepted and used, although, regrettably, there is ambiguity, with some writers using $\operatorname{sinc} x$ to mean $\sin x / x$ instead of, as here, $\sin \pi x / \pi x$. (We follow Woodward's definition here; in this form sinc is a more natural and more elegant function, with expressions less cluttered with factors of π, particularly in the Fourier transform application.) The comb function and the rep operator are used for describing sampled or repetitive waveforms and their spectra, and hence enable the whole field of Fourier series to be incorporated, in principle, into the field of Fourier transforms, as shown in Chapter 4. Thus, Fourier series can now be seen as particular forms of the Fourier transform, rather than the Fourier transform seen just as a limiting case of the Fourier series. For suitable waveforms, this enables the Fourier series coefficients to be obtained without explicit integration.

1.3   Outline of the Rules-and-Pairs Method

To use the method, the function to be transformed must first be expressed carefully in the notation in which the rules and pairs are expressed (i.e., in terms of the basic functions included in the table of Fourier transform pairs). This table gives the transforms of these functions, and the table of rules provides the relationships between these transforms (sums, products, convolutions, and appropriate scaling factors, for example) as determined by the relationships between the input basic functions.

The notation is specific and specialized, but is reasonably natural and quickly absorbed, and is given in Chapter 2 with the tables of the rules and pairs. Having obtained the transform using the rules and pairs, the resulting

expression requires interpretation and may benefit from rearranging and sim-
plifying. Sketches of the functions can be useful to bring to life a mathemati-
cal expression, and illustrations of functions and their transforms have been
provided fairly generously in Chapters 2, 3, and 4, particularly.

A feature of the notation is that a given function (or waveform) can
sometimes be correctly described in more than one way, leading to more than
one expression for its transform (or spectrum), though of course these expres-
sions must be equivalent. One of these expressions will be more appropriate
and convenient for the particular case under study than another, so there is
an art, based on experience and imagination (such as required for solving cer-
tain differential equations or some problems in integration) in choosing the
description of the waveform that will yield the spectrum represented in the
required form. This alternative description approach is particularly effective
in producing general results or theorems, as Woodward shows. A good ex-
ample is in Woodward's proof of the sampling theorem in the time domain,
given in Chapter 5, where, by expressing the spectrum of a waveform in two
different ways, the equivalence of a continuous waveform and its sampled
form is established.

1.4   The Fourier Transform and Generalized Functions

The concept of the Fourier series seems intuitively very reasonable—that any
periodic function can be represented by a sum of elementary periodic func-
tions, either sine and cosine functions, or, equivalently, complex exponentials.
The frequencies of the elementary functions are integer multiples (including
zero, giving a constant function) of the repetition frequency of the periodic
function. The sum may turn out to be infinite, but users of this mathematical
tool are generally content to let mathematicians justify such a sum, determin-
ing the conditions under which it converges; however, for problems arising
in practice, in physics or engineering, for example, it is obvious that such a
sum does converge. Thus we can put, for f a real or complex function of a real
variable x, with period X,

$$f(x) = \sum_{n=0}^{\infty} a_n \cos(2\pi nx/X) + \sum_{n=1}^{\infty} b_n \sin(2\pi nx/X) = \sum_{n=-\infty}^{\infty} c_n \exp(2\pi inx/X) \quad (1.1)$$

(By expressing the trigonometric functions as complex exponentials we can
relate c_n to a_n and b_n. From now on, we restrict our attention exclusively to

the complex exponential series, other than in Chapter 4.) The coefficients of the series are found by integration over one cycle of the function, so that, for example,

$$c_n = \frac{1}{X} \int_{x_0 - X/2}^{x_0 + X/2} f(x) \exp(-2\pi i n \, x / X) dx \qquad (1.2)$$

The Fourier transform can be obtained as the limiting case of the Fourier series when the period is increased toward infinity and the fundamental frequency falls to zero. In this case, as $X \to \infty$ we put $n/X \to y$, $1/X \to dy$, $c_n \to g(y)dy$, where g is a continuous function replacing the discrete series c_n, and the summations in (1.1) become integrals. Thus (1.1) and (1.2) become, respectively,

$$f(x) = \int_{-\infty}^{\infty} g(y) \exp(2\pi i x y) dy \qquad (1.3)$$

and

$$g(y) = \int_{-\infty}^{\infty} f(x) \exp(-2\pi i x y) dx \qquad (1.4)$$

Here $g(y)$ is the Fourier transform of $f(x)$. Even the practical user, not concerned about problems of convergence, knowing that he has a well-behaved continuous function with no poles, for example, and believing that there is a well-behaved solution for his problem, will find there is a difficulty here. Whereas it is clear that the integral in (1.2) converges (has a finite value) because it is over a finite interval, the same does not necessarily hold for the integral in (1.4), which is over an infinite interval. (The former is absolutely integrable for such a function—that is, the integral of the modulus of the integrand is finite—and the latter is not necessarily so.) The simplest function for which this difficulty arises is the constant function, and it is clear that the value of this mathematical tool would be severely limited if it could not handle even this case.

An approach to finding the Fourier transform of a constant function, say $f(x) = 1$, for all real x, is to find a sequence of functions that do have transforms as given by (1.4) and that approach f in the limit of some parameter. For example, we could choose $f_n(x)$ to be the function $\exp(-\pi x^2/n^2)$. Putting this into (1.4), we find that its transform is $g_n(y) = n\exp(-\pi n^2 y^2)$. We see that in the limit as $n \to \infty$, $f_n(x) \to f(x) = 1$, in that however small we choose the positive number ε, for any x we can find a value of n such that $f_n(x) > 1 - \varepsilon$. Also $g_n(y) \to g(y)$, where $g_n(0) \to \infty$, and $g_n(y) \to 0$; otherwise, as, for any

nonzero y and positive ε, however small, we can always find a value of n such that $g_n(y) < \varepsilon$. The limiting function g is the Dirac δ-function, which plays an important part in this theory. It is not strictly a function in the ordinary sense, but is a generalized function in Lighthill's terminology [2].

The fact that there is some difficulty in using (1.4) where $f(x)$ is a constant function (and also if it is periodic) does not mean that such functions do not have Fourier transforms. This problem has been tackled formally, and the subject of Fourier transforms put on a rigorous basis by Laurent Schwarz. However, to do this it was necessary to generalize the idea of a function to include the δ-function, and indeed the term *generalized function* has been introduced by Temple and presented clearly and accessibly by Lighthill [2]. It is shown in this text that, in general, ordinary functions satisfy the definition of generalized functions (as a limiting sequence of suitable functions). This means, in practice, that we can confidently accept and include δ-functions (and rows of delta-functions, in the case of a line spectrum) with ordinary functions for the purpose of Fourier transform operations and analysis.

The δ-function has been obtained as the limit of a series of Gaussian functions (as also in Woodward [1], on pp. 15 and 28), of a series of triangular functions and also in Figure 2.3 of Chapter 2, of a series of rectangular functions and of sinc functions. The fact that different sequences can be used is included in Lighthill's definition, though his functions should be differentiable everywhere, which actually rules out the series of triangular and rectangular functions.

There is no reference to generalized function theory by Woodward; Schwarz's work was published in 1950–51, only shortly before Woodward's book (1953), and the further spreading of these ideas by Temple (1955) and Lighthill (1958) followed later. The Dirac delta-function is an example of the not uncommon case where physics and engineering have required a new mathematical tool. This has been devised and given a very reasonable justification (e.g., as the limit of a series of triangular functions), only later to be given a more rigorous mathematical definition.

1.5   Complex Waveforms and Spectra in Signal Processing

The method uses the complex Fourier transform, by which a waveform, real or complex, is expressed as a sum or integral of complex exponentials (see Equation (1.3)), which are elementary complex waveforms. The idea of a complex waveform should not be seen as only a mathematical convenience, with the real-world waveform taken to be just the real part. The elementary

complex waveform exp$2\pi ift$ can be represented as the pair of real waveforms cos$2\pi ft$ and sin$2\pi ft$ in two channels, which must be handled appropriately (i.e., according to the rules of complex arithmetic). We recall that a complex number can be represented as an ordered pair of real numbers (i.e., $z = x + iy$ can be written as (x,y), satisfying the rules $(x_1,y_1) + (x_2,y_2) = (x_1 + x_2, y_1 + y_2)$ and $(x_1,y_1) \times (x_2,y_2) = (x_1 x_2 - y_1 y_2, x_1 y_2 + x_2 y_1)$). This avoids the explicit use of the imaginary constant i, if this worries the practical user, but we need only consider that i acts as a form of switch that moves a waveform from channel 1 ("real") to channel 2 ("imaginary"), or from channel 2 to channel 1, with a sign change in this case. We note that by using complex waveforms, meaning is given to the idea of negative frequency. Compared with the positive frequency form, this corresponds to an inversion of the waveform in the second channel (i.e., the pair (cos$2\pi ft$,-sin$2\pi ft$)).

In signal processing, it is convenient to use the analytic signal, which is the complex waveform corresponding to the real waveform that is present, as received, for example, from a radio or radar antenna or sonar sensor. Thus, if the waveform is expressed as $a(t)$cos$(2\pi f_0 t + \phi(t))$, that is, a carrier at intermediate frequency (IF) or radio frequency (RF) f_0, modulated (time varying) in both amplitude and phase, in the general case, then we form the complex form $a(t)$exp$i(2\pi f_0 t + \phi(t))$, which is the pair {$a(t)$cos$(2\pi f_0 t + \phi(t))$, $a(t)$sin$(2\pi f_0 t + \phi(t))$}. The second member of this pair is obtained from the first by a Hilbert transform, which in effect performs a wideband –90° phase shift. (Thus all cosine components in the signal, whatever their frequencies, become sines, and sines become –cosines.) In practice this can be achieved with a high degree of fidelity (for moderate fractional bandwidths) by a 3-dB hybrid directional coupler. The two (real) outputs of this coupler can be considered the required (complex) waveform pair. The advantage of using the analytic signal is that (at least when on a carrier) the spectrum is "one-sided," with only positive frequency components, in contrast to the two-sided spectrum of the real waveform. If the complex waveform is then mixed down to complex baseband, using the complex local oscillator (LO) exp$(-2\pi i f_0 t)$, we obtain the complex waveform $a(t)$exp$(i\phi(t))$, which is the part of the waveform (the modulation) containing the information of interest. At baseband, the spectrum will contain both positive and negative frequencies from the components of the incoming signal with frequencies above and below the LO frequency, respectively. The spectrum is not necessarily symmetrical, in general.

If the two real baseband waveforms are sampled (simultaneously) and digitized, the pairs of samples are available as complex numbers for any processing computation required. The two signal channels are commonly referred to as I and Q, for *in phase* and in (phase) *quadrature*, with respect to

the IF or RF form. This is rather clumsy, as the I refers to the real channel, rather than the imaginary. A more elegant terminology would be P and Q for in *p*hase and in *q*uadrature.

1.6   Outline of the Contents

The rules and pairs themselves are presented in Chapter 2, but, before they are given, the notation in which they are expressed is defined and illustrated. Four examples using the technique are then taken, which provide an introduction to the method and show how easily some useful and important results can be obtained. Two appendices, of material effectively in parenthesis, are added; one gives an outline of the derivations of the rules and pairs, and the other obtains the properties of the extremely useful sinc function, the transform of the rectangular pulse, using the rules.

The remaining chapters provide examples and illustrations of the use of the technique. It will be seen that the results have all been obtained without any (explicit) integration whatsoever, and indeed, except for some expressions that are used to define the problem in terms of Fourier transforms, there are few symbols of integration to be seen. The first of these, Chapter 3, on pulse spectra, covers one of the most natural applications of the technique. For readers new to the method, Chapters 2 and 3 should provide a relatively straightforward introduction to its use. Of the following chapters, while Chapters 4 and 5 may be of more interest theoretically than practically, Chapters 6 through 8 show the method applied in practical areas, giving some impressive results relatively easily.

In Chapter 4 the application of the method to periodic waveforms, as an alternative to the usual Fourier series approach using integration is shown. In particular, the common case of the analysis of real waveforms is taken, with a number of illustrations. The application to discrete waveforms is included here. Although the discrete Fourier transform (DFT) is not necessarily periodic, the very valuable fast Fourier transform (FFT) method is (generally implicitly), and the method shows clearly the forms of these waveforms and spectra.

Sampling, particularly relevant for digital signal processing, is studied in Chapter 5. The basic sampling theorems are given (following Woodward's examples), which give the minimum sampling rate necessary to retain all the information in a waveform of finite bandwidth. Some further forms of sampling are also analyzed, which again may be of more theoretical than practical interest. These results are certainly obtained more easily than in the earlier

papers on these sampling methods, which did not use Woodward's method and notation.

The question of deriving a series of samples offset in time from the original series is considered in Chapter 6. These interpolated samples correspond to the samples that would have been obtained by sampling the waveform with the time offset. The ability to do this, when the waveform is no longer available, is important, as it provides a sampled form of the delayed waveform. If the waveform is sampled at the minimum rate to retain all the waveform information, accurate interpolation requires combining a substantial number of input samples for each output value. It is shown that oversampling—sampling at a higher rate than actually necessary—can reduce this number very considerably, to quite a low value. The user can compare the disadvantage, if any, of sampling slightly faster with the saving on the amount of computation needed for the interpolation. One example (from a simulation of clutter in a radar MTI system) is given where the reduction in computation can be very great indeed.

The problem of compensating for spectral distortion is considered in Chapter 7. Compensation for delay (a phase error linear in frequency) is achieved by a similar technique to interpolation, but amplitude compensation is interesting in that it requires a new set of transform pairs, including functions derived by differentiation of the sinc function and defined here. The compensation is seen to be very effective for the problems chosen, and again oversampling can greatly reduce the complexity of the implementation. The problem of equalizing the response of a wideband antenna array used for a radar application is used as an illustration, showing the technique to be remarkably effective.

Finally in Chapter 8 we take advantage of the fact that there is a Fourier transform relationship between the illumination of a linear aperture and its beam pattern. In fact, rather than a continuous aperture, we concentrate mostly on the regular linear array, which is a sampled aperture, and mathematically has a correspondence with the sampled waveforms considered in earlier chapters. Two forms of the problem are considered—the low sidelobe directional beam and a much wider sector beam, covering an angular sector with uniform gain. Similar results could be achieved, in principle, for the continuous aperture, but it would be difficult in practice to apply the required aperture weighting (or tapering). The question of generating a required pattern from an irregular linear array is also considered, in particular for a sector beam.

We note that some of Chapter 3 and much of Chapters 5 through 8 analyze periodic waveforms (with line spectra) or sampled waveforms (with

periodic spectra), implying a requirement for Fourier series analysis rather than the nonperiodic Fourier transform. However, it would not make the problems any easier to turn to conventional Fourier series analysis. As remarked earlier, the classical Fourier series theory is now, as Lighthill states on p. 66 of [2], included in the more general Fourier transform approach. Using Woodward's notation, the ease with which the method applies (without requiring integration) to nonperiodic functions applies also to periodic ones, and no distinction, except in notation, is needed.

Finally, the included disk of MATLAB programs should be of interest and use to the reader. This contains the programs for all the main figures, giving results and illustrations in the form of graphical plots. The program names are those of the figures (with, for example, Fig608 or Fig614, being the files of the program for Figure 6.8 or 6.14). The preambles include definitions of all the parameters required as well as at least one example MATLAB statement for running the program. A statement can be pasted into the MATLAB command window and run to reproduce the figure. The user can then change parameters to obtain other results, according to his or her interest or requirements. Some of the programs require the sinc derivative functions, which are defined in Chapter 7 and called snc_r for the rth derivative. A program $snc(r,x)$ is included on the disk, which returns values for arguments x and order r (with r set to zero for the sinc function itself).

References

[1]   Woodward, P. M., *Probability and Information Theory, with Applications to Radar*, London, UK: Pergamon Press, 1953, reprinted at Norwood, MA: Artech House, 1980.

[2]   Lighthill, M. J., *Fourier Analysis and Generalised Functions*, Cambridge, UK: Cambridge University Press, 1960.

2

Rules and Pairs

2.1   Introduction

In this chapter we present the basic tools and techniques for carrying out Fourier transforms of suitable functions without using integration. In the rest of the book, the definitions and results given here will be used to obtain useful results relatively quickly and easily. Some of these results are well established, but these derivations will serve as valuable illustrations of the method, indicating how similar or related problems may be tackled.

   The method has already been outlined in Chapter 1. First, the function to be transformed is described formally in a suitable and precise notation. This defines the function in terms of some very basic, or elementary, functions, such as rectangular pulses or δ-functions, which are combined in various ways, such as by addition, multiplication, or convolution. Each of these elementary functions has a Fourier transform, the function and its transform forming a transform pair. Next, the transform is carried out by using the known set of pairs to replace each elementary waveform by its transform and by using a set of established rules that relate how the transforms are combined to the way the input functions were combined. For example, addition, multiplication, and convolution of functions transform to addition, convolution, and multiplication of transforms, respectively. Finally, the transform expression needs interpretation, possibly after rearrangement. Diagrams of the functions and transforms can be helpful and are widely used here.

We begin by defining the notation used. Some of these terms, such as rect and sinc, have been adopted more widely to some extent, but rep and comb are less well known. We include a short discussion on convolution, as this operation is important in this work. It is the operation in the transform domain corresponding to multiplication in the original domain (and vice versa). This is followed by the rules relating to Fourier transforms and a set of Fourier transform pairs. We then include four illustrations as examples before the main applications in the following chapters.

2.2 Notation

2.2.1 Fourier Transform and Inverse Fourier Transform

Let u and U be two (generalized) functions related by

$$u(x) = \int_{-\infty}^{\infty} U(y)e^{2\pi ixy}\,dy \tag{2.1}$$

and

$$U(y) = \int_{-\infty}^{\infty} u(x)e^{-2\pi ixy}\,dx \tag{2.2}$$

U is the Fourier transform of u, and u is the inverse Fourier transform of U. We have used a general pair of variables, x and y, for the two transform domains, but in the very widespread application of these transforms in spectral analysis of time dependent waveforms, we choose t and f, associated with time and frequency. We take the transforms in this form, with 2π in the exponential (so that in spectral analysis, for example, we use the frequency f, rather than the angular frequency $\omega = 2\pi f$) in order to maintain a high degree of symmetry between the definitions; otherwise, we need to introduce a factor of $1/2\pi$ in one of the expressions for the transform or $1/\sqrt{2\pi}$ in both. We find it convenient to keep generally to a convention of using lowercase letters for the waveforms, or primary domain functions, and uppercase for their transforms, or spectra. We indicate a Fourier transform pair of this kind by

$$u \Leftrightarrow U \tag{2.3}$$

with $\Rightarrow$ implying the forward transform and $\Leftarrow$ the inverse.

We note that there remains a small asymmetry between the expressions; the forward transform (deriving U from u) has a negative exponent and the

inverse has a positive exponent. Many functions used are symmetric, and for these the forward and inverse transform operations are identical. However, when this is not the case, it may be important to note just which transform is needed in a given application.

2.2.2 rect and sinc

The rect function is defined by

$$\operatorname{rect} x = \begin{cases} 1 & \text{for } -1/2 < x < +1/2 \\ 0 & \text{for } x < -1/2 \text{ and } x > +1/2 \end{cases} \quad (x \in \mathbb{R}) \tag{2.4}$$

(and $\operatorname{rect}(\pm\frac{1}{2}) = \frac{1}{2}$). This is a very commonly encountered gating function. This pulse is of unit width, unit height and is centered at zero (Figure 2.1(a)). A pulse of width T, amplitude A and centered at time t_0 is given by $A\operatorname{rect}((t - t_0)/T)$, shown in Figure 2.1(b). In the frequency domain, a rectangular frequency band of width B, centered at f_0, is defined by $\operatorname{rect}((f - f_0)/B)$. A pulse, or a filter, with this characteristic is not strictly realistic (or realizable) but may be sufficiently close for many investigations.

The Fourier transform of the rect function is the sinc function, given by

$$\operatorname{sinc} x = \begin{cases} \sin(\pi x)/\pi x & \text{for } x \neq 0 \\ 1 & \text{for } x = 0 \end{cases} \quad (x \in \mathbb{R}) \tag{2.5}$$

This is illustrated in Figure 2.2(a) and a shifted, scaled form is shown in Figure 2.2(b). This follows Woodward's definition [1] and is a neater function than $\sin x/x$, which is sometimes (confusingly) called $\operatorname{sinc} x$ (or the unscaled sinc function). It has the properties:
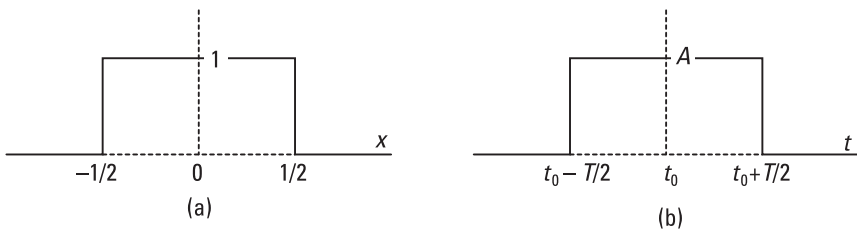
Figure 2.1 rect functions. (a) rect(*x*), and (b) *A*rect[*t* − *t*₀/*T*].
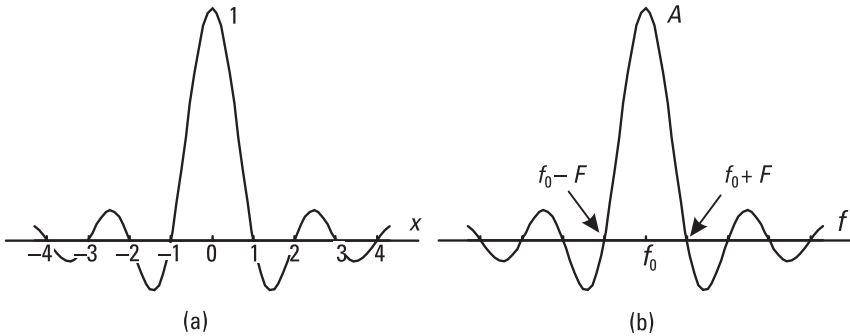
Figure 2.2   sinc functions. (a) sinc(x), and (b) Asinc$((f - f_0)/F$.

1. sinc$n = 0$, for n a non-zero integer;
2. $\int_{-\infty}^{\infty} \text{sinc}\, x\, dx = 1$;
3. $\int_{-\infty}^{\infty} \text{sinc}^2\, x\, dx = 1$;
4. $\int_{-\infty}^{\infty} \text{sinc}(x - m)\text{sinc}(x - n)\, dx = \delta_{mn}$, where m and n are integers and δ_{mn} is the Kronecker-δ ($\delta_{mn} = 1$ if $m = n$, $\delta_{mn} = 0$ if $m \neq n$);
5. sinc$\,ax \otimes \text{sinc}\,bx = (1/a)\text{sinc}\,bx$ $(a, b \in \mathbb{R},\ a \geq b > 0)$, where $\otimes$ indicates convolution, defined in Section 2.2.5.

For the function sinx/x the results are more untidy, with π or π^2 appearing. Property 4 can be stated in the following form: the set of shifted sinc functions $\{\text{sinc}(x - n) : n \in \mathbb{Z}, x \in \mathbb{R}\}$ is an orthonormal set on the real line. These results are easily obtained by the methods presented here, and are derived in Appendix 2A. In proving properties 3 and 4, we used the useful general result

$$\int_{-\infty}^{\infty} u(x)\, dx = U(0) \tag{2.6}$$

which follows from the definition of the inverse Fourier transform in (1.4) on putting $y = 0$. Thus, if a function u can be expressed in terms of the functions given in the list of pairs (Table 2.2), we can obtain the definite integral of u (over the range $-\infty$ to ∞) without actually doing any integration, but just setting the value of the variable in the transform of u to zero.

Despite the $1/x$ factor, this function is analytic on the real line. The only point where this property may be in question is at $x = 0$. However, as

$$\lim_{x \to +0} \text{sinc}\, x = \lim_{x \to -0} \text{sinc}\, x = 1,$$

by defining sinc(0) = 1 we ensure that the function is continuous and differentiable at this point. Useful facts about the sinc function are that its 4-dB beam width (i.e., the width of the beam at 4 dB below the peak) is almost exactly equal to half the width at the first zeros (at ± 1 in the basic function and at $\pm F$ in the scaled version of Figure 2.2(b)), the 3-dB width is 0.886 and the first sidelobe peak is at the rather high level of -13.3 dB relative to the peak of the main lobe.

2.2.3 δ-function and Step Function

The δ-function is not a proper function but can be defined as the limit of a sequence of functions that have integral unity, the sequence converging pointwise to zero everywhere on the real line except at zero. Suitable sequences of functions f_n such that $\lim_{n \to \infty} f_n(x) = \delta(x)$ are $n\,\mathrm{rect}\,nx$, $n\exp(-\pi n^2 x^2)$, $n\,\mathrm{tri}\,nx$ (see (3.6)), and $n\,\mathrm{sinc}\,nx$, illustrated in Figure 2.3. This function consequently has the properties
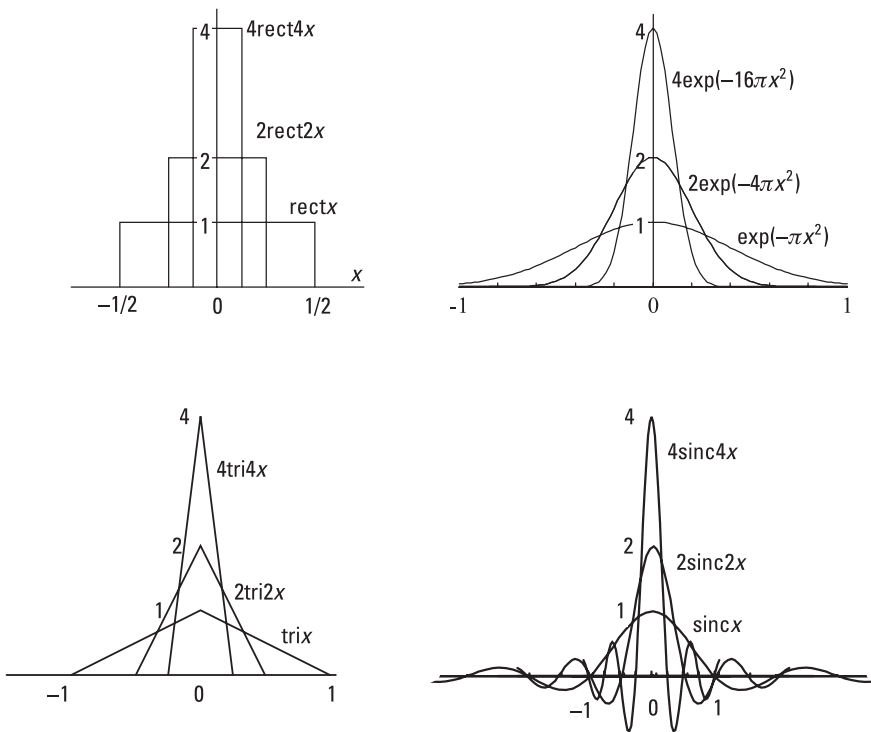
Figure 2.3 Four series approximating δ-functions.

$\delta(x - x_0)u(x)$

$$\delta(x) = \begin{cases} \infty & \text{for } x = 0 \\ 0 & \text{for } x \neq 0 \end{cases} \qquad (x \in \mathbb{R}) \qquad (2.7) \text{ and}$$

$$\int_{-\infty}^{\infty} \delta(x)dx = 1 \qquad (2.8)$$

In fact the generalized function defined by Lighthill [2] requires the members of the sequence to be differentiable everywhere; this actually rules out the rect and tri function sequences. From (2.7) we note that we can put

$$\delta(x - x_0)u(x) = \delta(x - x_0)u(x_0) \qquad (2.9)$$

(assuming u is bounded) as the product on the left is zero everywhere except at x_0. In particular, we note $\delta(x)u(x) = \delta(x)u(0)$. From (2.8) and (2.9) we deduce the useful property

$$\int_I \delta(x - x_0)u(x)dx = u(x_0) \qquad (2.10)$$

where I is any interval containing x_0. Thus the convolution (defined in Section 2.2.5) of a function u with a δ-function at x_0 is given by

$$u(x) \otimes \delta(x - x_0) = \int_{-\infty}^{\infty} u(x - x')\,\delta(x' - x_0)dx' = u(x - x_0) \qquad (2.11)$$

(i.e., the waveform is shifted so that its previous origin becomes the point x_0, the position of the δ-function). The function u itself could be a δ-function; for example,

$$\delta(x - x_1) \otimes \delta(x - x_2) = \int_{-\infty}^{\infty} \delta(x - x' - x_1)\delta(x' - x_2)dx' = \delta(x - (x_1 + x_2))$$

$$(2.12)$$

Thus, convolving δ-functions displaced by x_1 and x_2 from the origin gives a δ-function at $(x_1 + x_2)$.

The δ-function in the time domain represents a unit impulse occurring at the time when the argument of the δ-function is zero (i.e., $\delta(t - t_0)$), which represents a unit impulse at time t_0. In the frequency domain, it represents a spectral line of unit power (see Section 4.2.1). A scaled δ-function, such as

$A\delta(x - x_0)$, is described as being of strength A. In diagrams, such as Figure 2.6, this is represented by a vertical line of height A at position x_0.

The unit step function $h(x)$, shown in Figure 2.4(a), is here defined by

$$h(x) = \begin{cases} 1 & \text{for } x > 0 \\ 0 & \text{for } x < 0 \end{cases} \qquad (x \in \mathbb{R}) \qquad (2.13)$$

(and $h(0) = \frac{1}{2}$). It can also be defined as the integral of the δ-function:

$$h(x) = \int_{-\infty}^{x} \delta\ (\xi) d\ \xi, \qquad (2.14)$$

and the δ-function is the derivative of the step function.

The step function with the step at x_0 is given by $h(x - x_0)$ (Figure 2.4(b)).

2.2.4   rep and comb

The rep operator produces a new function by repeating a function at regular intervals specified by its suffix. For example, if $p(t)$ is a description of a pulse, an infinite sequence of pulses at the repetition interval T is given by $u(t)$, shown in Figure 2.5, where

$$u(t) = \text{rep}_T\ p(t) = \sum_{n=-\infty}^{\infty} p(t - nT) \qquad (2.15)$$

The shifted waveforms $p(t - nT)$ may be overlapping. This will be the case if the duration of p is greater than the repetition interval T. Any repetitive waveform can be expressed as a rep function—any section of the waveform one period long can be taken as the basic function and this is then repeated (without overlapping) at intervals of the period.
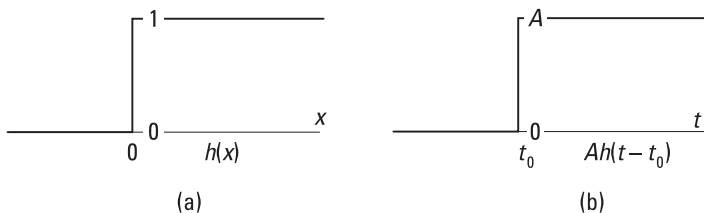
Figure 2.4   Step functions. (a) Unit step, and (b) scaled and shifted step.
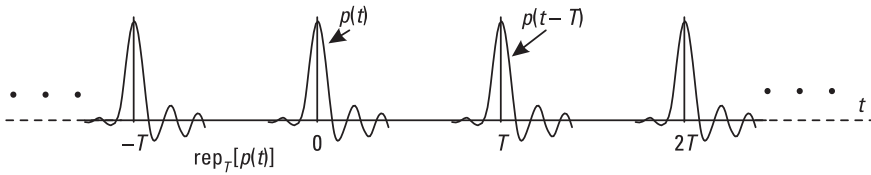
Figure 2.5 The rep operator.

The comb function derived from a continuous function replaces the function by δ-functions at regular intervals, specified by the suffix, with strengths given by the function values at those points; that is,

$$\mathrm{comb}_T\, u(t) = \sum_{n=-\infty}^{\infty} u(nT)\, \delta(t - nT) \qquad (2.16)$$

In the time domain, this represents an ideal sampling operation. In the frequency domain, the comb version of a continuous spectrum is the line spectrum corresponding to the repetitive form of the waveform, which gave the continuous spectrum.

The function $\mathrm{comb}_T u(t)$ is illustrated in Figure 2.6, where $u(t)$ is the underlying continuous function, shown dotted, and the comb function is the set of δ-functions.

2.2.5 Convolution

We denote the linear convolution of two functions u and v by $\otimes$, so that

$$u(x) \otimes v(x) = \int_{-\infty}^{\infty} u(x - x')v(x')dx' = \int_{-\infty}^{\infty} u(x')v(x - x')dx' \quad (2.17)$$

One reason for requiring such a function is to find the response of a linear, time-invariant system to an input $u(t)$ when the system's response to a unit impulse (at time zero) is $v(t)$. The response at time t to an impulse at time
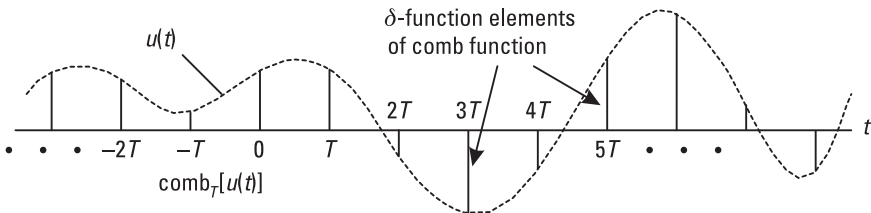
Figure 2.6 The comb function.

t' is thus $v(t - t')$. We divide u into an infinite sum of impulses $u(t')dt'$ and integrate, so that the output at time t is

$$\int_{-\infty}^{\infty} u(t')v(t - t')dt' = u(t) \otimes v(t) \qquad (2.18)$$

The reason for the reversal of the response v (as a function of t') is because the *later* the impulse $u(t')dt'$ arrives, the *earlier* in the impulse response is its contribution to the total response at time t.

It is clear, from the linear property of integration, that convolution is distributive and linear so that we have

$$u \otimes (av + bw) = au \otimes v + bu \otimes w \qquad (2.19)$$

where a and b are constants. It is also the case that convolution is commutative (so $u \otimes v = v \otimes u$) and associative, so that

$$u \otimes (v \otimes w) = (u \otimes v) \otimes w, \qquad (2.20)$$

and we can write these simply as $u \otimes v \otimes w$ without ambiguity. Thus we are free to rearrange combinations of convolutions within these rules and evaluate multiple convolutions in different sequences, as shown in (2.20).

It is useful to have a feel for the meaning of the convolution of two functions. The convolution is obtained by sliding one of the functions (reversed) past the other and integrating the point-by-point product of the functions over the whole real line. Figure 2.7(a) shows the result of convolving two rect functions, $\text{rect}(t/T_1)$ and $\text{rect}(t/T_2)$, with $T_1 < T_2$, and Figure 2.7(b) shows that the value of the convolution at the point $-t_0$ is given by the area of overlap of the functions, when the "sliding" function, $\text{rect}(t/T_1)$, shown dashed, is centered at $-t_0$. We note that overlap begins when $t = -(T_1 + T_2)/2$ and increases linearly until the smaller pulse is within the larger, at $(T_1 - T_2)/2$. The magnitude of the flat top is just T_1, the area of the smaller pulse, for these unit height pulses. This is equal to the area of overlap when the narrower pulse is entirely within the wider one. For pulses of magnitudes A_1 and A_2 the level would be $A_1 A_2 T_1$, and for pulses centered at t_1 and t_2 the convolved response would be centered at $t_1 + t_2$.

In many cases we will be convolving symmetrical functions such as rect or sinc, but if we have a nonsymmetric one it is important to note from (2.17) that $u(x - x')$, considered as a function of x', is not only shifted by x (the sliding parameter) but is reversed with respect to $u(x')$. In Figure 2.8(a) we show the result of convolving an asymmetric triangular
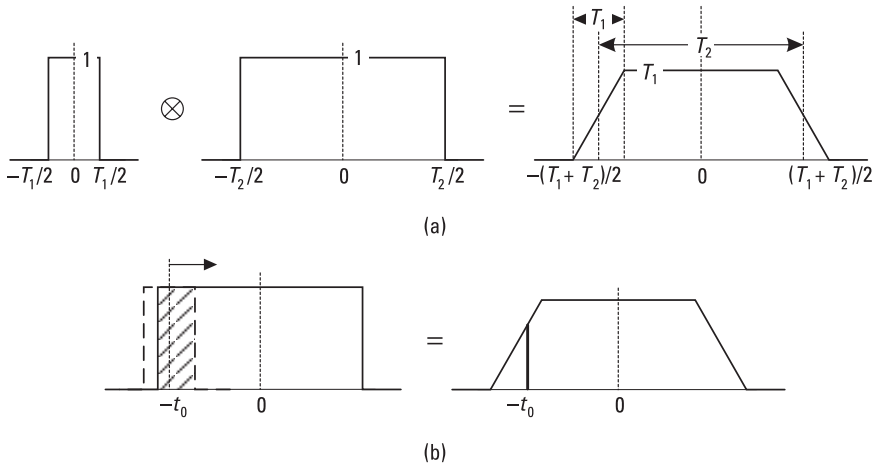
Figure 2.7   Convolution of two rect functions. (a) Full convolution, and (b) value at a single point.

pulse with a rect function, and in Figure 2.8(b) we show, on the left, that the reversed triangular pulse is used when it is the sliding function; on the right, we show that, because of the commutativity of convolution, we could equally well use the rect function as the moving one, which, being symmetric, is unchanged when reversed, of course.

2.3   Rules and Pairs

The rules and pairs, which are at the heart of this technique of Fourier analysis, are given in Table 2.1. The rules are relationships that apply generally to all functions (u and v in the table) and their transforms (U and V). The pairs are certain specific Fourier transform pairs. All these results are proved or derived in outline in Appendix 2.2.

In this table, the rules labelled b are derivable from those labelled a using other rules, but it is convenient for the user to have both a and b versions. We see that there is a great deal of symmetry between the a and b versions, with differences of sign in some cases.

To illustrate such a derivation, we derive Rule 6b from Rule 6a. Let U be a function of x with transform V, then from Rule 6a

$$U(x - x_0) \Longleftrightarrow V(y)\exp(-2\pi i x_0 y)$$
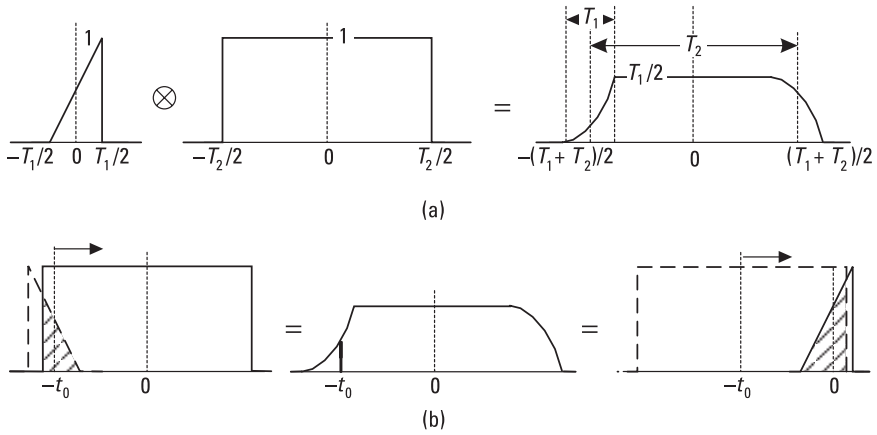
Figure 2.8 Convolution with a nonsymmetric function. (a) Full convolution, and (b) value at a single point.

From Rule 4, if $u(x) \Leftrightarrow U(y)$, then $U(x) \Leftrightarrow u(-y)$, so in this case we have

$$U(x) \Leftrightarrow V(y) = u(-y)$$

and so

$$U(x - x_0) \Leftrightarrow u(-y)exp(-2\pi i x_0 y) \qquad (2.21)$$

Now we use Rule 4 again, in reverse (i.e., if $Z(x) \Leftrightarrow z(-y)$, then $z(x) \Leftrightarrow Z(y)$), so that (2.21) becomes

$$u(x)exp(2\pi i y_0 x) \Leftrightarrow U(y - y_0)$$

on renaming the constant x_0 as y_0, and this is Rule 6b. However, in this case, the result is easily obtained from the definition of the Fourier transform in (2.2), as shown in Appendix 2B.

In Table 2.2, not only are pairs 1b, 2b, and 3b derivable from the corresponding a form, but the pairs 7 through 11 are all derivable from other pairs using the rules, and these are indicated by the P and R notation, which will be used subsequently. Although they are not fundamental, these results are included for convenience, as they occur frequently.

Table 2.1
Rules for Fourier Transforms

Rule	Function	Transform	Notes
_	$u(x)$	$U(y)$	See (2.1), (2.2)
1	$au + bv$	$aU + bV$	a, b constants (a, b $\in$, $-\mathbb{C}$ in general)
2	$u(-x)$	$U(-y)$	
3	$u^*(x)$	$U^*(-y)$	* indicates complex conjugate
4	$U(x)$	$u(-y)$	
5	$u(x/X)$	$\|X\|U(Xy)$	$X \in \mathbb{R}$, X constant
6a	$u(x - x_0)$	$U(y)\exp(-2\pi i x_0 y)$	$x_0 \in \mathbb{R}$, x_0 constant
6b	$u(x)\exp(2\pi i x y_0)$	$U(y - y_0)$	$y_0 \in \mathbb{R}$, y_0 constant
7a	uv	$U \otimes V$	(2.17)
7b	$u \otimes v$	UV	
8a	$\text{comb}_X u$	$\|Y\|\text{rep}_Y U$	(2.16), (2.15), $Y = 1/X$, constant
8b	$\text{rep}_X u$	$\|Y\|\text{comb}_Y U$	
9a	$u'(x)$	$2\pi i y U(y)$	Prime indicates differentiation
9b	$-2\pi i x u(x)$	$U'(y)$	
10a	$\int_{-\infty}^{x} u(\xi)d\xi$	$\dfrac{U(0)\delta(y)}{2} + \dfrac{U(y)}{2\pi i y}$	
10b	$\dfrac{u(0)\delta(x)}{2} - \dfrac{u(x)}{2\pi i x}$	$\int_{-\infty}^{y} U(\eta)d\eta$	

An important point follows from Rule 3. For a real waveform we have

$$u(t) = u(t)^*$$

so, from R3,

$$U(f) = U(-f)^* \tag{2.22}$$

or

$$U_R(f) + iU_I(f) = U_R(-f) - iU_I(-f), \tag{2.23}$$

where U_R and U_I are the real and imaginary parts of U.

We see from (2.22) that for a real waveform, the negative frequency part of the spectrum is simply the complex conjugate of the positive frequency

Table 2.2
Fourier Transform Pairs

Pair	Function	Transform	Notes
1a	1	$\delta(y)$	(2.7)
1b	$\delta(x)$	1	
2a	$h(x)$	$\dfrac{\delta(y)}{2} + \dfrac{1}{2\pi iy}$	(2.13)
2b	$\dfrac{\delta(x)}{2} - \dfrac{1}{2\pi ix}$	$h(y)$	
2c	$\mathrm{sgn}(x)$	$\dfrac{1}{\pi iy}$	
3a	$\mathrm{rect}(x)$	$\mathrm{sinc}(y)$	(2.4), (2.5)
3b	$\mathrm{sinc}(x)$	$\mathrm{rect}(y)$	
4	$\mathrm{tri}(x)$	$\mathrm{sinc}^2 y$	(3.6)
5	$\exp(-x)$	$\dfrac{1}{1+2\pi iy}$	$(x \geq 0)$ Laplace transform
6	$\exp(-\pi x^2)$	$\exp(-\pi y^2)$	
7a	$\delta(x-x_0)$	$\exp(-2\pi ix_0 y)$	P1b, R6a
7b	$\exp(2\pi iy_0 x)$	$\delta(y-y_0)$	P1a, R6b
8a	$\cos 2\pi y_0 x$	$(\delta(y-y_0) + \delta(y+y_0))/2$	P7b, P1a
8b	$\sin 2\pi y_0 x$	$(\delta(y-y_0) - \delta(y+y_0))/2i$	P7b, P1a
9a	$u(x)\cos 2\pi y_0 x$	$(U(y-y_0) + U(y+y_0))/2$	R6b
9b	$u(x)\sin 2\pi y_0 x$	$(U(y-y_0) - U(y+y_0))/2i$	R6b
10	$\exp(-ax)$	$1/(a+2\pi iy)$	$(a>0,\ x\geq 0))$ P5, R5
11	$\exp(-x^2/2\sigma^2)$	$\sigma\sqrt{2\pi}\exp(-2\pi^2\sigma^2 y^2)$	P6, R5
12	$\mathrm{comb}_X(1)$	$|Y|\mathrm{comb}_Y(1)$	$Y=1/X$
13a	$\mathrm{ramp}_r x$	$\check{r}\mathrm{snc}_r y$	(7.11), (7.17)
13b	$\mathrm{snc}_r x$	$\check{r}\mathrm{ramp}_r y$	P13a, R4

a, x_0, y_0, X, Y, σ all real constants and also $x,y \in \mathbb{R}$

part and contains no extra information. It follows (see (2.23)) that the real part of the spectrum of a real function is always an even function of frequency and the imaginary part is an odd function. (Often spectra of simple waveforms are either purely real or imaginary—see P8a and P8b, for example).

Thus, for real waveforms we need only consider the positive frequency part of the spectrum, remembering that the power at a given frequency is twice the power given by this part because there is an equal contribution from the negative frequency component. (A short discussion and interpretation of negative frequencies is given in Section 1.5.)

2.4 Four Illustrations

2.4.1 Narrowband Waveforms

The case of waveforms modulated on a carrier is described by P9a or P9b (which could be considered rules as much as pairs). Although these relations apply generally, we consider the frequently encountered narrowband case, where the modulating or gating waveform u has a bandwidth that is small compared with the carrier frequency, f_0. We see that the spectrum, in this case, consists of two essentially distinct parts—the spectral function U, centered at f_0 and at $-f_0$. Again, for a real waveform, the negative frequency part of the waveform contains no extra information and can safely be neglected (apart from the factor of two when evaluating powers). However, strictly speaking, the function U centered at $-f_0$ may have a tail that stretches into the positive frequency region, and in particular it may stretch to the region around f_0 if the waveform is not sufficiently narrowband. In that case, the contribution of $U(f + f_0)$ in the positive frequency range must not be neglected.

　　Figure 2.9 shows how the spectrum $U(f)$ of the baseband waveform $u(t)$ is centered at frequencies $+f_0$ and $-f_0$ when modulating (or multiplying, in the mathematical representation) a carrier. When applied to the carrier $2\cos 2\pi f_0 t$ we see, from P8a, that we just have U shifted to these frequencies. When applied to $2\sin 2\pi f_0 t$ we obtain, from P8b, $-iU$ centered at f_0 and iU at $-f_0$. We have chosen a real baseband waveform $u(t)$, so that its spectrum is shown with a symmetric, or even, real part and an antisymmetric, or odd, imaginary part, as shown earlier for real waveforms. We see that this property holds for the spectra of the real waveforms $u(t)\cos 2\pi f_0 t$ and $u(t)\sin 2\pi f_0 t$.

2.4.2 Parseval's Theorem

Another result, Parseval's theorem, follows easily from the rules. Writing out Rule 8a using the definitions of Fourier transform, on the left side, and convolution on the right, ((2.1) and (2.17)), gives
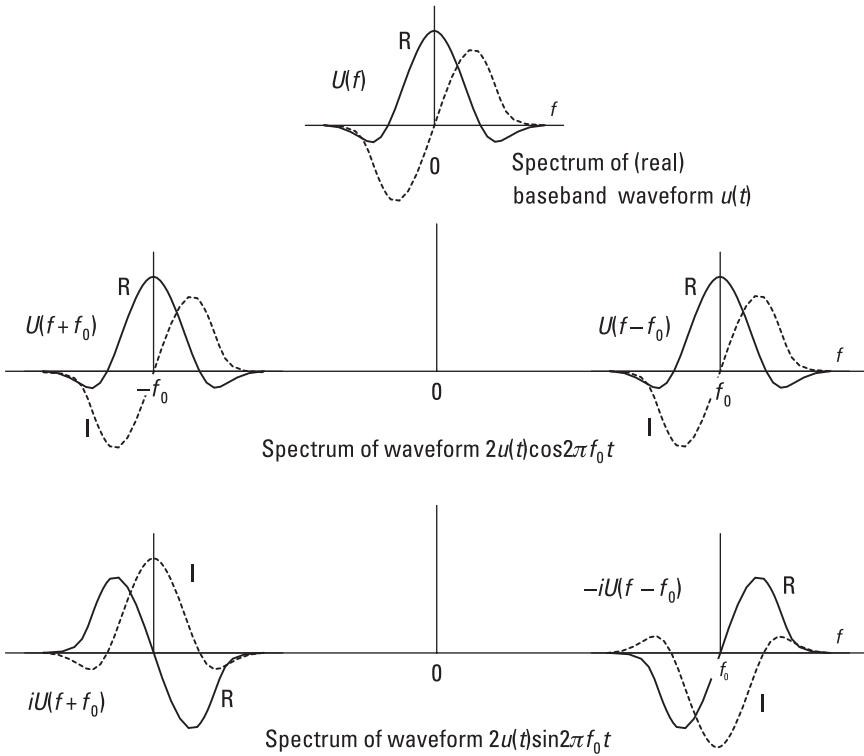
Figure 2.9 Spectra of modulated carrier, (real) narrowband waveforms.

$$\int_{-\infty}^{\infty} u(x)v(x)e^{-2\pi i x y}\,dx = \int_{-\infty}^{\infty} U(\psi)V(y-\psi)\,d\psi \qquad (2.24)$$

Putting $y = 0$ in this equation and then replacing the variable of integration ψ by y gives

$$\int_{-\infty}^{\infty} u(x)v(x)\,dx = \int_{-\infty}^{\infty} U(y)V(-y)\,dy \qquad (2.25)$$

Replacing v by v^* and using R3, gives Parseval's theorem:

$$\int_{-\infty}^{\infty} u(x)v(x)^*\,dx = \int_{-\infty}^{\infty} U(y)V(y)^*\,dy \qquad (2.26)$$

Taking the particular case of $v = u$ then gives

$$\int_{-\infty}^{\infty} |u(x)|^2\,dx = \int_{-\infty}^{\infty} |U(y)|^2\,dy \qquad (2.27)$$

This simply states that the total energy in a waveform is equal to the total energy in its spectrum. For a real waveform we have

$$\int_{-\infty}^{\infty} u(x)^2 dx = 2\int_{0}^{\infty} \left|U(y)\right|^2 dy \tag{2.28}$$

using $U(y) = U(-y)^*$ for the spectrum of a real waveform.

2.4.3   The Wiener-Khinchine Relation

This states that the autocorrelation function of a waveform is given by the (inverse) Fourier transform of its power spectrum. For a waveform u with (amplitude) spectrum U, the power spectrum is $|U|^2$ and, from R2 and R3 we see that $U^*(f)$ is the transform of $u^*(-t)$, so we have

$$u(t)\otimes u^*(-t) \Longleftrightarrow U(f) \times U^*(f) = |U(f)|^2 \tag{2.29}$$

Writing out the convolution we have

$$u(t) \otimes u*(-t) = \int_{-\infty}^{\infty} u(t-t')u*(-t')dt' = \int_{-\infty}^{\infty} u(s)u*(s-t)ds = r(t) \tag{2.30}$$

where $s = t - t'$ and $r(t)$ is the autocorrelation function for a delay of t. The delay, or time shift between the correlating waveforms, is generally given the symbol τ, rather than t, used for the usual time variable. Thus we have, from (2.29) and (2.30),

$$r(\tau) \Longleftrightarrow |U(f)|^2, \tag{2.31}$$

which is the Wiener-Khinchine relation, obtained very concisely by this method.
     Note the difference between (2.30)—correlation—and (2.17)—convolution. In (2.30) the sliding function is not time reversed, and also (if complex) its conjugate is required.

2.4.4   Sum of Shifted sinc Functions

In this section, we derive two interesting results using the rules-and-pairs technique. First we find an expression for the spectrum of a finite train of evenly spaced δ-functions (or equivalently an expression for the sum of a set

of regularly spaced complex exponentials). Let the N δ-functions be spaced about the time origin at intervals T; then, we have a waveform u given by

$$u(t) = \frac{1}{N} \sum_{k=-(N-1)/2}^{(N-1)/2} \delta(t + kT) \tag{2.32}$$

and so, from P1b and R6a, its spectrum is

$$U(f) = \frac{1}{N} \sum_{k=-(N-1)/2}^{(N-1)/2} \exp(2\pi i k f T) \tag{2.33}$$

Now we take the identity

$$\operatorname{rect} \frac{t}{NT} = \operatorname{rect} \frac{t}{T} \otimes \sum_{k=-(N-1)/2}^{(N-1)/2} \delta(t + kT) = N \operatorname{rect} \frac{t}{T} \otimes u(t) \quad (2.34)$$

where the rect pulse of length NT has been divided into N contiguous pulses of length T, as shown in Figure 2.10. Taking the Fourier transforms we have, using R5, R7b, P3a

$$NT \operatorname{sinc} NfT = NT \operatorname{sinc}(fT).U(f)$$

so that

$$U(f) = \frac{\operatorname{sinc} NfT}{\operatorname{sinc} fT} = \frac{\sin N\pi fT}{N \sin \pi fT} \tag{2.35}$$

This neat result can also be obtained, with little more effort, by noting that the set of complex exponentials in (2.33) forms a finite geometric series, with ratio between the terms of $\exp(2\pi i fT)$. However, the following result, expressing the sum of an infinite series of shifted sinc functions in closed form, would be more difficult to obtain by an alternative method.
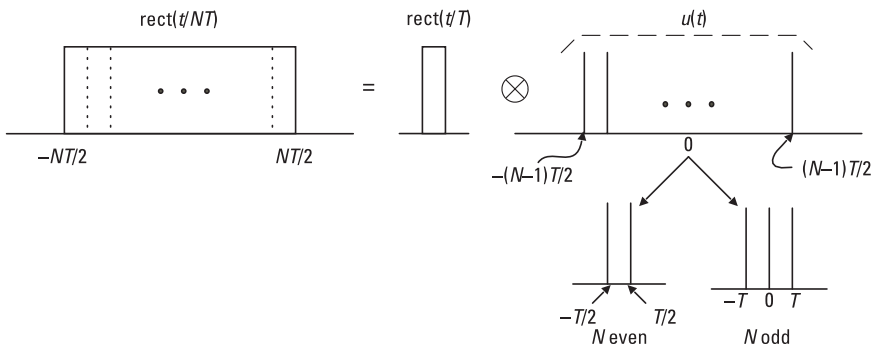
Figure 2.10 Alternative forms of rect function.

We can also put u in (2.32) in the form (for N odd)

$$u(t) = \frac{1}{N} \mathrm{comb}_T (\mathrm{rect}\, \frac{t}{NT}) \tag{2.36}$$

with transform

$$U(f) = \frac{1}{NT} \mathrm{rep}_F (NT \,\mathrm{sinc}\, NfT) = \sum_{k=-\infty}^{\infty} \mathrm{sinc}\, N(f - kF)T$$

$$= \sum_{k=-\infty}^{\infty} \mathrm{sinc}\, N(fT - k), \tag{2.37}$$

where $F = 1/T$.

If we plot these expressions for U we find that (2.37) gives a series of main lobes with value $+1$, while (2.35) gives the identical series when N is odd, but when N is even the lobes alternate in sign. (To evaluate (2.35) at integer multiples of F we need L'Hôpital's Rule, as the denominator is zero at these points. Taking the differentials, and using $FT = 1$, we obtain $U(kF) = \cos kN\pi / \cos k\pi = (-1)^{k(N-1)}$, for k an integer. For N odd (and hence $(N - 1)$ and $k(N - 1)$ even) we have $U(kF) = 1$ for all k, which is also the result given by (2.37). However, for N even (and $N - 1$ odd), the parity of $k(N - 1)$ will be that of k, so we have alternations in sign.)

The discrepancy is because the derivation of (2.37) is only valid for odd N. For even N we do not have a line in u at 0, but at $\pm T/2, \ldots$ (as shown in Figure 2.10), so to use the comb function, which has lines at $0, \pm T, \ldots$, we need to shift the rect function by $T/2$, before applying the comb operation, and then we need to shift the result back by $-T/2$. Thus, for N even we have

$$u(t) = \frac{1}{N} \delta(t + T/2) \otimes \mathrm{comb}_T \left(\mathrm{rect}\, \frac{t - T/2}{NT} \right) \tag{2.38}$$

with transform, using P1b, P3a, R5, R6a, R7b, R8a,

$$U(f) = \frac{F}{N} e^{\pi i f T} (\mathrm{rep}_F (NT e^{-\pi i f T} \,\mathrm{sinc}\, NfT))$$

$$= e^{\pi i f T} \sum_{k=-\infty}^{\infty} e^{-\pi i (f - kF)T} \,\mathrm{sinc}\, N(f - kF)T \tag{2.39}$$

$$= \sum_{k=-\infty}^{\infty} e^{\pi i k} \,\mathrm{sinc}\, N(f - kF)T = \sum_{k=-\infty}^{\infty} (-1)^k \,\mathrm{sinc}\, N(fT - k) \,(N \text{ even})$$

From (2.35) and combining (2.37) and (2.39) we have (for all N, k integral)

$$U(f) = \frac{\sin N\pi fT}{N \sin \pi fT} = \sum_{k=-\infty}^{\infty} (-1)^{(N-1)k} \operatorname{sinc} N(fT - k) \qquad (2.40)$$

References

[1]   Woodward, P. M., *Probability and Information Theory, with Applications to Radar*, Norwood, MA: Artech House, 1980.

[2]   Lighthill, M. J., *Fourier Analysis and Generalised Functions*, Cambridge, UK: Cambridge University Press, 1960.

Appendix 2A: Properties of the sinc Function

1. $\operatorname{sinc} n = 0$ (n a non-zero integer).

    When $n \neq 0$, as $\sin n\pi = 0$, we have $\operatorname{sinc} n = \sin n\pi / n\pi = 0$. Also, for x small,

$$\operatorname{sinc} x = \frac{\sin \pi x}{\pi x} = 1 - \frac{(\pi x)^2}{3!} + \dots$$

so, as $x \to \pm 0$, $\operatorname{sinc} x \to 1$.

2. $\int_{-\infty}^{\infty} \operatorname{sinc} x \, dx = 1.$

We can write

$$\int_{-\infty}^{\infty} \operatorname{sinc} x \, dx = \int_{-\infty}^{\infty} \operatorname{sinc} x e^{2\pi i x y} \, dx \bigg|_{y=o} = \operatorname{rect} y \big|_{y=0} = 1$$

Here we have converted the integral into an inverse Fourier transform (though the variable in the transform domain here has the value zero), and used P3.

3. $\int_{-\infty}^{\infty} \operatorname{sinc}^2 x \, dx = 1.$

We have, using R7 and P3,

$$\int_{-\infty}^{\infty} \text{sinc}^2 \, x dx = \int_{-\infty}^{\infty} \text{sinc}\, x \times \text{sinc}\, x \; e^{2\pi i x y} dx \bigg|_{y=o} = \text{rect}\, y \otimes \text{rect}\, y\big|_{y=0} = 1$$

rect$y \otimes$ rect$y$ is a triangular function, with peak value 1 at $y = 0$. (This convolution is shown in Figure 3.4 in Chapter 3, with $A = 1$ and $T = 1$ in this case.)

4. $\int_{-\infty}^{\infty} \text{sinc}(x - m)\text{sinc}(x - n)dx = \delta_{mn}$.

If $m = n$ the integral is

$$\int_{-\infty}^{\infty} \text{sinc}^2(x - n)dx = \int_{-\infty}^{\infty} \text{sinc}^2 \, x dx = 1$$

using the result for property 3.
If $m \neq n$ then

$$\int_{-\infty}^{\infty} \text{sinc}(x - m)\text{sinc}(x - n)dx = \int_{-\infty}^{\infty} \text{sinc}(x - m)\text{sinc}(x - n)e^{2\pi i x y} dx \bigg|_{y=0}$$

$$= e^{-2\pi i m y} \, \text{rect}(y) \otimes e^{-2\pi i n y} \, \text{rect}(y) \big|_{y=0}$$

on using R7a, R6a, and P3b. Forming the convolution integral this becomes

$$\int_{-\infty}^{\infty} e^{-2\pi i m y'} \, \text{rect}(y')e^{-2\pi i n(y-y')} \, \text{rect}(y - y')dy' \bigg|_{y=0}$$

$$= \int_{-\infty}^{\infty} e^{2\pi i(n-m)y'} \, \text{rect}(y')\text{rect}(-y')dy'$$

$$= \int_{-\infty}^{\infty} e^{2\pi i(n-m)y'} \, \text{rect}(y')dy' = \text{sinc}(n - m) = 0,$$

on using rect$(-y') = $ rect(y'), rect$^2(y') = $ rect(y'), P3a and Property 1.

5. $\text{sinc}\, ax \otimes \text{sinc}\, bx = (1/a)\text{sinc}\, bx \quad (a, b \in \mathbb{R}, \; a \geq b > 0)$

We give two proofs of this, as a further example of the benefit of using the integration-free rules-and-pairs technique. The first is via the Fourier transform, using this method, and the second requires contour integration. The first is very simple and concise, while the second requires considerably more effort.

(i) Proof using the Fourier transform

The Fourier transform of $\operatorname{sinc} ax \otimes \operatorname{sinc} bx$ is given, from P3b, R5 and R7b, by

$$\operatorname{sinc} ax \otimes \operatorname{sinc} bx \Rightarrow (1/ab)\operatorname{rect}(y/a)\operatorname{rect}(y/b)$$

The product of the rect functions, centered on zero, and of different width gives a rect function of width equal to the narrower one, as illustrated in Figure 2A.1. In this case, with $a \geq b$,

$$(1/ab)\operatorname{rect}(y/a)\operatorname{rect}(y/b) = (1/ab)\operatorname{rect}(y/b)$$

Taking the inverse transform, using P3b and R5 again, we have

$$(1/a)\operatorname{sinc} bx \Leftarrow (1/ab)\operatorname{rect}(y/b)$$

(ii) Proof using contour integration.

Writing out the convolution, and then expressing the sines in exponential form, we have

$$\operatorname{sinc} ax \otimes \operatorname{sinc} bx = \int_{-\infty}^{\infty} \frac{\sin \pi a(x-x')}{\pi a(x-x')} \cdot \frac{\sin \pi b x'}{\pi b x'} dx' = \ldots = \frac{1}{(2\pi i)^2 ab}(I^* + I)$$

where

$$I = e^{-i\pi ax} \int_{-\infty}^{\infty} \frac{e^{i\pi(a-b)x'} - e^{i\pi(a+b)x'}}{x'(x-x')} dx'$$

We now consider the integral K of $e^{ikz}/z(u-z) = e^{k(ix-y)}/z(u-z)$ ($k \geq 0$, $z = x + iy$) round the rectangular contour C shown in Figure 2A.2. On the vertical sides we have $x = \pm\infty$, $y \geq 0$, so, as e^{ix} is bounded, the denominator dominates and the integrand is zero for all values of y. On the top side $y = \infty$
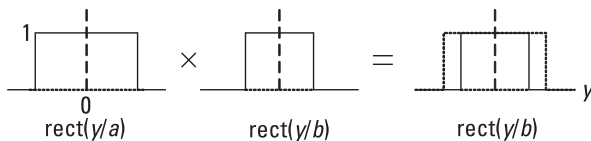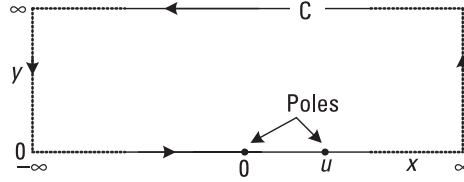

1      $\times$ $=$

rect(y/a)   rect(y/b)   rect(y/b)

Figure 2A.1 Product of rect functions.

Figure 2A.2   Contour for integral in sinc convolution.

so again the integrand is zero (with $k \geq 0$) for all values of x. Thus, the only side along which it is not zero is along the real axis where $y = 0$ and $z = x$, so that we have

$$K = \int_C \frac{e^{ikz}}{z(u-z)}dz = \int_{-\infty}^{\infty} \frac{e^{ikx}}{x(u-x)}dx = \int_{-\infty}^{\infty} \frac{-e^{ikx}}{x(x-u)}dx \quad (k > 0)$$

We now use the contour integral result

$$\int_C f(z)dz = 2\pi i(\text{residues within the contour } C)$$

$$+ \pi i(\text{residues on the contour } C).$$

where $f(z)$ has simple singularities. (The residue for a singularity at p, for example, if $f(z)$ is put in the form $f(z) = g(z)/(z - p)$, is $g(p)$.) The singularities in this case are at 0 and u, on the contour, so with this result we have

$$K = \pi i\left(\frac{1}{u} - \frac{e^{iku}}{u}\right)$$

Using this result in I (with x' for x, x for u and $\pi(a - b)$ or $\pi(a + b)$ for k) we obtain

$$I = \frac{\pi i e^{-i\pi a x}}{x}(1 - e^{\pi i(a-b)x} - 1 + e^{\pi i(a+b)x}) = \frac{\pi i(e^{i\pi bx} - e^{-i\pi bx})}{x}$$

$$= \frac{2\pi i^2 \sin \pi bx}{x} = I^*$$

and putting this into the sinc convolution above we have

$$\text{sinc } ax \otimes \text{sinc } bx = \frac{1}{(2\pi i)^2 ab}\left(\frac{4\pi i^2 \sin \pi bx}{x}\right) = \frac{\sin \pi bx}{ab\pi x} = \frac{1}{a}\text{sinc } bx$$

(The point where we used the condition $a \geq b$ is when we required k to be nonnegative in the contour integration. This is required to make the integrand zero on the $y = \infty$ part of the contour.)

Appendix 2B: Brief Derivations of the Rules and Pairs

2B.1 Rules

- R1: This follows from the linearity of integration.

- R2: $\int_{-\infty}^{\infty} u(-x)\exp(-2\pi ixy)dx = \int_{-\infty}^{\infty} u(z)\exp\left(-2\pi iz(-y)\right)dz$

$$= U(-y) \quad (z = x)$$

- R3: $\int_{-\infty}^{\infty} u^*(x)\exp(-2\pi ixy)dx = \left(\int_{-\infty}^{\infty} u(x)\exp(2\pi ix(y))dz\right)^*$

$$= \left(\int_{-\infty}^{\infty} u(x)\exp\left(-2\pi ix(-y)\right)dz\right)^* = U^*(-y)$$

- R4: $\int_{-\infty}^{\infty} U(x)\exp(-2\pi ixy)dx = \int_{-\infty}^{\infty} U(x)\exp 2\pi ix(-y)dx$

$$= u(-y)$$

  (using the inverse transform, as in (2.1)).

- R5(a): $X > 0$, $z = x/X = x/|X|$

$$\int_{-\infty}^{\infty} u(x/X)\exp(-2\pi ixy)dx = X\int_{-\infty}^{\infty} u(z)\exp(-2\pi iz\, Xy)dz$$

$$= XU(Xy) = |X|U(Xy)$$

- R5(b): $X < 0$, $z = x/X = -x/|X|$

$$\int_{-\infty}^{\infty} u(x/X)\exp(-2\pi ixy)dx = -|X|\int_{\infty}^{-\infty} u(z)\exp(2\pi iz|X|y)dz$$

$$= |X|\int_{-\infty}^{\infty} u(z)\exp(-2\pi iz(-|X|y))dz = |X|U(-|X|y) = |X|U(Xy)$$

- R6a: $\int_{-\infty}^{\infty} u(x - x_0)\exp(-2\pi ixy)dx = \int_{-\infty}^{\infty} u(z)\exp(-2\pi i(z + x_0)y)dz$

$$= U(y)\exp(-2\pi ix_0 y) \quad (z = x - x_0)$$

- R6b: $\displaystyle\int_{-\infty}^{\infty} u(x)\exp(2\pi ixy_0)\exp(-2\pi ixy)dx$

$$= \int_{-\infty}^{\infty} u(x)\exp(-2\pi ix(y-y_0))dx$$

$$= U(y-y_0)$$

- R7a: $\displaystyle\int_{-\infty}^{\infty} u(x)v(x)\exp(-2\pi ixy)dx$

$$= \int_{-\infty}^{\infty}\int_{-\infty}^{\infty} U(z)\exp(2\pi ixz)v(x)\exp(-2\pi ixy)dxdz$$

$$= \int_{-\infty}^{\infty}\int_{-\infty}^{\infty} U(z)v(x)\exp(-2\pi ix(y-z))dxdz$$

$$= \int_{-\infty}^{\infty} U(z)V(y-z)dz = U(y)\otimes V(y)$$

- R7b: The transform of $u(x)\otimes v(x)$ is, using $x-z=t$,

$$\int_{-\infty}^{\infty}\int_{-\infty}^{\infty} u(z)v(x-z)\exp(-2\pi ixy)dxdz$$

$$= \int_{-\infty}^{\infty}\int_{-\infty}^{\infty} u(z)v(t)\exp(-2\pi i(z+t)y)dtdz$$

$$= \int_{-\infty}^{\infty}\int_{-\infty}^{\infty} u(z)\exp(-2\pi izy)v(t)\exp(-2\pi ity)dtdz$$

$$= U(y)\int_{-\infty}^{\infty} v(t)\exp(-2\pi ity)dt$$

$$= U(y)V(y)$$

- R8a: Let $v(x)=\mathrm{comb}_X\, u(x)= \displaystyle\sum_{n=-\infty}^{\infty} u(nX)\delta(x-nX)$, then the transform is (from P1b and R6a)

$$V(y)= \sum_{n=-\infty}^{\infty} u(nX)\exp(-2\pi inXy)$$

This is in the form of a Fourier series, with period $1/X = Y$, and the coefficients are given by integration of V (weighted with a complex exponential) over one period:

$$u(nX) = \frac{1}{Y}\int_0^Y V(y)\exp(2\pi in\, y/Y)dy$$

Also, from the Fourier transform,

$$u(nX) = \int_{-\infty}^{\infty} U(z)\exp(2\pi inXz)dz = \sum_{m=-\infty}^{\infty} \int_{mY}^{(m+1)Y} U(z)\exp(2\pi inz/Y)dz,$$

on dividing the range of integration into units of length Y. Putting $y = z - mY$ for each value of m,

$$u(nX) = \int_0^Y \sum_{m=-\infty}^{\infty} U(y+mY)\exp\big(2\pi in(y+mY)/Y\big)dy$$

$$= \int_0^Y \sum_{m=-\infty}^{\infty} U(y+mY)\exp(2\pi iny/Y)dy$$

Comparing the two expressions for $u(nX)$ we see that

$$V(y) = Y\sum_{m=-\infty}^{\infty} U(y+mY) = Y\,\mathrm{rep}_Y\, U(y)$$

(This is in line with Woodward's comment [1], following his list of rules and pairs, that the transform relationship between comb and rep "can be justified by resorting to a Fourier series representation." NB: The rule actually uses $|Y|$ rather than Y; however, from the definitions it is clear that $\mathrm{rep}_{-x}u = \mathrm{rep}_X u$ and $\mathrm{comb}_{-x}u = \mathrm{comb}_X u$, so $|Y|$ can replace Y.)

- R8b: Let $v(x) = \mathrm{rep}_X u(x) = \sum_{m=-\infty}^{\infty} u(x - mX)$, which is periodic, with period X, so we can put v as a Fourier series:

$$v(x) = \sum_{n=-\infty}^{\infty} a_n \exp(2\pi inx/X)$$

with the coefficients given by

$$a_n = \frac{1}{X}\int_0^X v(x)\exp(-2\pi inx/X)dx$$

Substituting for v in rep form, the coefficients are given by

$$a_n = \frac{1}{X}\int_0^X \sum_{m=-\infty}^{\infty} u(x-mX)\exp(-2\pi inx/X)dx$$

and then putting $z = x + mX$, we have

$$a_n = \frac{1}{X}\sum_{m=-\infty}^{\infty}\int_{mX}^{(m+1)X} u(z)\exp\left(-2\pi in(z-mX)/X)\right)dz$$

$$= \frac{1}{X}\sum_{m=-\infty}^{\infty}\int_{mX}^{(m+1)X} u(z)\exp\left(-2\pi inz/X\right)dz$$

as $\exp(2\pi inm) = 1$. This gives

$$a_n = \frac{1}{X}\int_{-\infty}^{\infty} u(z)\exp\left(-2\pi inz/X\right)dz = \frac{1}{X}U(n/X)$$

Then, substituting for the a_n in v,

$$v(x) = \frac{1}{X}\sum_{n=-\infty}^{\infty} U(n/X)\exp(2\pi inx/X)$$

and, taking the Fourier transform,

$$V(y) = \frac{1}{X}\sum_{n=-\infty}^{\infty} U(n/X)\delta(y-n/X) = \frac{1}{X}\mathrm{comb}_{1/X}\,U(y)$$

$$= Y\,\mathrm{comb}_Y\,U(y)$$

(from the definition of the comb function) where $Y = 1/X$.

- R9a: $u(x) = \int_{-\infty}^{\infty} U(y)\exp(2\pi ixy)dy$

  $$u'(x) = \int_{-\infty}^{\infty} 2\pi iy U(y)\exp(2\pi ixy)dy$$

so $u'(x)$ is the inverse Fourier transform of $2\pi iy U(y)$ where u' is the derivative of u.

- R9b: $U(y) = \int_{-\infty}^{\infty} u(x)\exp(-2\pi ixy)dx$

  $$U'(y) = \int_{-\infty}^{\infty} -2\pi ix u(x)\exp(-2\pi ixy)dx$$

so $U'(y)$ is the Fourier transform of $-2\pi i x u(x)$ where U' is the derivative of U.

- R10a: $\int_{-\infty}^{x} u(\xi)d\xi = \int_{-\infty}^{\infty} u(\xi)h(x-\xi)d\xi = u(x) \otimes h(x)$

Taking the transform (using R7b and P2a) gives

$$\int_{-\infty}^{x} u(\xi)d\xi \rightarrow U(y)\left(\frac{\delta(y)}{2} + \frac{1}{2\pi iy}\right) = \frac{U(0)\delta(y)}{2} + \frac{U(y)}{2\pi iy}$$

where we have also used (2.9).

- R10b: $\int_{-\infty}^{y} U(\eta)d\eta = \int_{-\infty}^{\infty} U(\eta)h(y-\eta)d\eta = U(y) \otimes h(y)$

Taking the inverse transform gives

$$u(x)\left(\frac{\delta(x)}{2} - \frac{1}{2\pi ix}\right) \Leftarrow \int_{-\infty}^{y} U(\eta)d\,\eta$$

where we have used R7a and P2b.

2B.2 Pairs

- P1a: A derivation, using P6 (and R5), is given in Section 1.4.
- P1b: This follows from P1a, with R4 and using $\delta(-y) = \delta(y)$.
- P2a and P2c: Defining the signum function by

$$\text{sgn}(x) = \begin{cases} 1 & \text{for } x > 0 \\ -1 & \text{for } x < 0 \end{cases} \qquad (x \in \mathbb{R})$$

(and sgn$(0) = 0$) the unit step function $\overset{\circ}{h}$ can be written as

$$2h(x) = 1 + \text{sgn}(x)$$

We now require the transform of sgn which can be given by expressing the signum function as the limit of an antisymmetric decaying exponential function, with the form $-\exp(\lambda x)$ for $x < 0$ and $\exp(-\lambda x)$ for $x > 0$ (and $\lambda > 0$):

$$\lim_{\lambda \to 0}\left(\int_{-\infty}^{0} -\exp(\lambda x)\exp(-2\pi ixy)dx + \int_{0}^{\infty} \exp(-\lambda x)\exp(-2\pi ixy)dx\right)$$

$$= \lim_{\lambda \to 0} \left(-\frac{\exp(\lambda x - 2\pi i x y)}{\lambda - 2\pi i y} \Big|_{-\infty}^{0} - \frac{\exp(-\lambda x - 2\pi i x y)}{\lambda + 2\pi i y} \Big|_{0}^{\infty} \right)$$

$$= \lim_{\lambda \to 0} \left(-\frac{1}{\lambda - 2\pi i y} - \frac{-1}{\lambda + 2\pi i y} \right) = \lim_{\lambda \to 0} \left(\frac{-4\pi i y}{\lambda^2 - 4\pi^2 i^2 y^2} \right)$$

$$= \frac{1}{\pi i y}$$

With this result the Fourier transform of $h(x)$ is now found to be, using P1a,

$$h(x) \Rightarrow \frac{1}{2} \left(\delta(y) + \frac{1}{\pi i y} \right)$$

- P2b: From P2a and R4 the transform of $\frac{1}{2} \left(\delta(x) + \frac{1}{\pi i x} \right)$ is $h(-y)$, then we use R2, with $\delta(-x) = \delta(x)$.

- P3a: $\int_{-\infty}^{\infty} \text{rect}(x) \exp(-2\pi i x y) dx = \int_{-1/2}^{1/2} \exp(-2\pi i x y) dx$

$$= \frac{\exp(-2\pi i x y)}{-2\pi i y} \Big|_{-1/2}^{1/2}$$

$$\frac{\exp(-\pi i y) - \exp(\pi i y)}{-2\pi i y} = \frac{-2i\sin(\pi y)}{-2\pi i y} = \text{sinc}(y)$$

- P3b: From P3a and R4, with $\text{rect}(-y) = \text{rect}(y)$.
- P4: See (3.7) and (3.8), using P3a and R7b.
- P5: The transform of $\exp(-x) h(x)$ (or $\exp(-x)$ for $x \geq 0$) is

$$\int_{0}^{\infty} \exp(-x) \exp(-2\pi i x y) dx = -\frac{\exp(-(1 + 2\pi i y)x)}{1 + 2\pi i y} \Big|_{0}^{\infty} = +\frac{1}{1 + 2\pi i y}$$

- P6: $\int_{-\infty}^{\infty} \exp(-\pi x^2) \exp(-2\pi i x y) dx = \int_{-\infty}^{\infty} \exp\left(-\pi(x + iy)^2 - \pi y^2\right) dx$

$$= \exp(-\pi y^2) \int_{-\infty+iy}^{\infty+iy} \exp(-\pi z^2) dz$$

where $z = x + iy$. We perform a contour integration round the contour shown in Figure 2B.1; as there are no poles within the contour the contour integral is zero, and as the contributions at $z = \pm\infty + i\eta$ ($0 \leq \eta \leq y$) are zero, we have

$$\int_{-\infty+iy}^{\infty+iy} \exp(-\pi z^2)dz + \int_{-\infty}^{\infty} \exp(-\pi z^2)dz = 0,$$

so the required integral is equal to the real integral $\int_{-\infty}^{\infty} \exp(-\pi x^2)dx$, which has the value 1.

- P7– P11: These are all found using the earlier pairs and the rules, as indicated.
- P12: From the definitions, ((2.15) and (2.16)) we can express the comb function for a constant as a rep function:

$$\text{comb}_X(1) = \sum_{n=-\infty}^{\infty} \delta(x - nX) = \text{rep}_X \delta(x)$$

and then, by P1b and R8b, the transform is $|Y|\text{comb}_Y(1)$ where $Y = 1/X$.

A more rigorous approach is taken in Lighthill [2], particularly for the derivations of the transform of the δ-function, P1b, the transform of the signum function, used in obtaining P2a, and the comb and rep transforms.

- P13a: See Section 7.3 in Chapter 7.
- P13b: From P13a and R4 we have

$$i^r \text{snc}_r x \Longleftrightarrow \text{ramp}^r(-y) = (-1)^r \text{ramp}^r(y)$$

On multiplying by $(-i)^r$ we have

$$\text{snc}_r x \Longleftrightarrow i^r \text{ramp}^r(y)$$
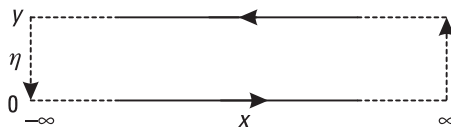

Figure 2B.1   Contour for integral required for P5.

3

Pulse Spectra

3.1   Introduction

In this chapter we consider the spectra of pulses and pulse trains. Signals used in radar, sonar, and radio and telephone communications often turn out to be combinations of certain quite simple basic waveforms or of variations on them. For example, the rectangular pulse is an almost universal feature of radar waveforms, and although the perfect pulse is a mathematical idealization, it is often closely realized in practice, and the approximation is good enough for an analysis based on the idealization to give very useful results very simply in some cases.

One reason for studying the spectrum of a pulse, or pulse train, can be to investigate the interference that the pulse transmission will generate outside the frequency band allocated. The sharp-edged rectangular pulse is particularly poor in this respect, producing quite high interference levels at frequencies several times the radar bandwidth away from the radar operating frequency. The interference levels can be lowered quite considerably by reducing the sharp, vertical edges in various ways. Giving the edges a constant finite slope, so that the pulse becomes trapezoidal, produces a considerable improvement, as shown later in Section 3.2. The triangular pulse (Section 3.3) is a limiting case of the trapezoidal, with the flat top reduced to zero. The asymmetric trapezoidal and triangular pulses (with sides of different magnitude slope) are considered in Section 3.4 and Section 3.5. While the practical

use of such pulses is not obvious, these are interesting exercises in the use of the rules-and-pairs method, showing that this gives solutions for the spectrum quite easily and concisely, once a suitable approach has been found. Another form of pulse, smoother than the rectangular pulse, is the raised cosine, and this is shown to have considerably improved spectral sidelobes (Section 3.6). The trapezoidal pulse still has sharp corners, and rounding these is the subject of Section 3.7 and Section 3.8. Finally the spectra of pulse trains, as might be used in radar, are studied in the next three sections.

3.2 Symmetrical Trapezoidal Pulse

The rectangular pulse, with zero rise and fall times, may be a reasonable approximation in many cases but for short pulses the rise and fall times may not be negligible compared with the pulse width and may need to be taken into account. The symmetrical trapezoidal pulse is particularly easily analyzed by the methods used here. We noted in Chapter 2 (Figure 2.7) that such a pulse of width T between the half amplitude points and with rise and fall times of τ can be expressed as the convolution of rect functions (illustrated in Figure 3.1):

$$u(t) = (1/\tau)\operatorname{rect}(t/\tau) \otimes A\operatorname{rect}(t/T) \qquad (3.1)$$

The scaling factor $1/\tau$ keeps the peak height the same, as the narrow pulse now has unit area, though often we are not interested in the scaling factors as much as the shapes and relative levels of the waveforms and spectra. The rise and fall times of the edges is τ and the pulse is of width T at the half amplitude points. The spectrum (from R7b, P3a and R5) is

$$U(f) = AT\operatorname{sinc}(f\tau)\operatorname{sinc}(fT) \qquad (3.2)$$
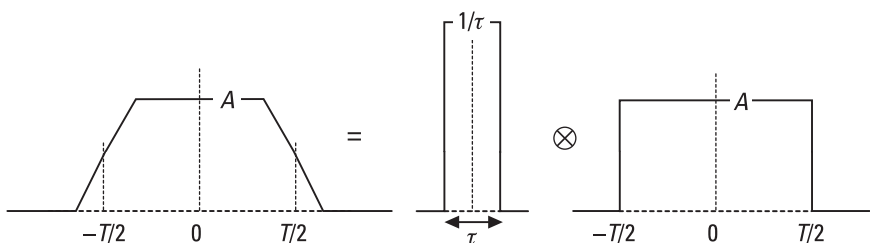
Figure 3.1 Symmetrical trapezoidal pulse.
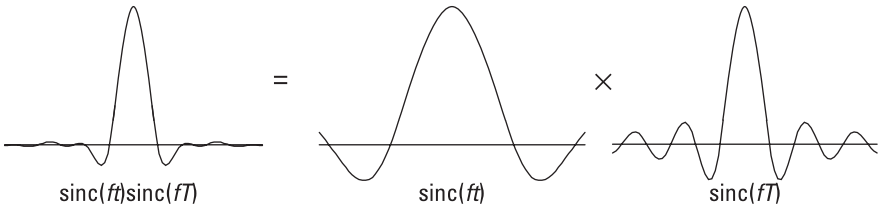
Figure 3.2 Product of sinc functions.

Thus, the spectrum is that of the pulse of length T multiplied by the broader sinc$f\tau$ function, the transform of the shorter pulse. This will narrow slightly the width of the main lobe of the spectrum and also reduce the sidelobe levels, as shown in Figure 3.2, where $\tau = 0.4T$ in this example.

   An application of this result would be to answer (approximately) the question of what rise time, relative to the half-amplitude width, will minimize the first sidelobes of the spectrum. We note that the function sincfT has its first zeros at $\pm 1/T$ and $\pm 2/T$ and the first sidelobes peak at about $\pm 3/2T$. Clearly, we will be very close to minimizing the first sidelobes if we make the first zeros of the sinc$f\tau$ function occur at these points. Thus, we require

$$1/\tau = 3/2T, \text{ or } \tau = 2T/3 \tag{3.3}$$

This is not of course the precisely optimized solution, but this approximate result is close to optimum and is very easily solved by these methods. In fact, the peak spectral sidelobes are 28.8 dB below the peak in this case, compared with only 13.3 dB for the rectangular pulse. If we chose $\tau = 0.6992T$, corresponding to placing the first null of the wide sinc more precisely at the position of the first peak of the narrow sinc (at $\pm 1.4303/T$), then we improve the sidelobe discrimination slightly to 30.7 dB. This spectrum is illustrated in Figure 3.3, with the spectrum of the rectangular pulse shown by dotted lines, for comparison. (The frequency axis is in units of $1/T$.)
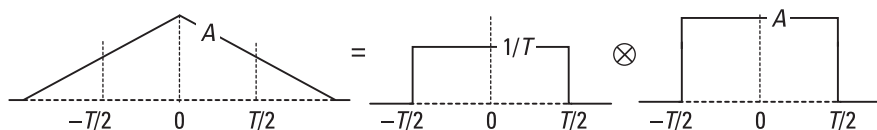
3.3   Symmetrical Triangular Pulse

A pulse of this shape may arise in practice as a result of convolving rectangular pulses of equal width in the process of demodulating a spread spectrum waveform (e.g., Figure 3.4). It is the limiting version of the trapezoidal pulse and is given (with $\tau = T$) by

$$u(t) = (1/T)\,\text{rect}(t/T) \otimes A\,\text{rect}(t/T) \tag{3.4}$$

(a)

(b)
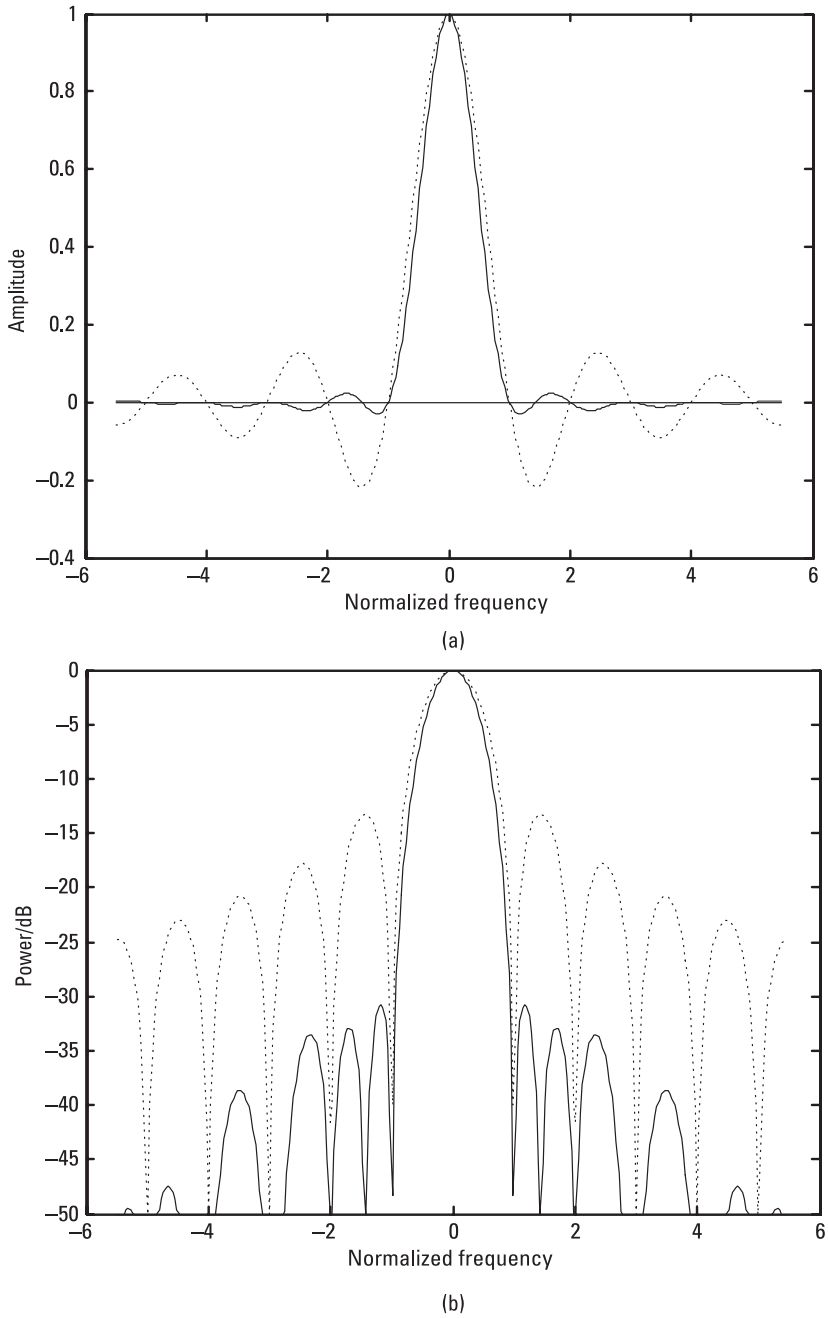
**Figure 3.3**   Spectrum of low sidelobe trapezoidal pulse. (a) Linear form, and (b) logarithmic form.

Figure 3.4   Symmetrical triangular pulse.

with spectrum, from (3.2)

$$U(f) = AT \operatorname{sinc}^2(fT) \tag{3.5}$$

This is the amplitude spectrum. The power spectrum is a sinc[4] function and is shown in logarithmic form in Figure 3.5, with the rect pulse spectrum for comparison shown dotted. The frequency is in units of $1/T$ as before. This spectrum has its 3-dB points at $\pm0.32/T$, its value at $\pm1/2T$ is nearly 8 dB below the peak value, and the maximum sidelobes are 26.5 dB below the peak.
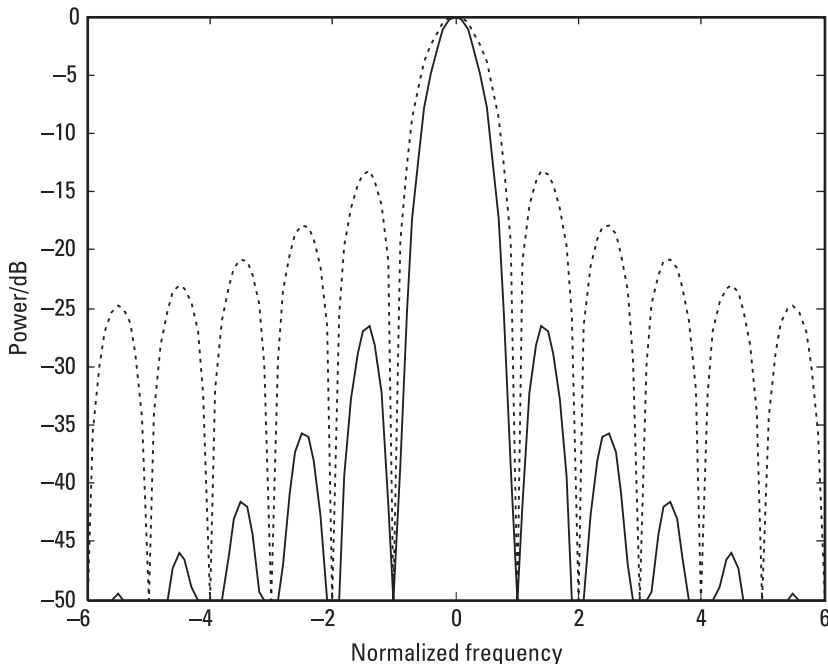
Figure 3.5   Spectrum of triangular pulse.

In a case where triangular pulses are used frequently, it could be useful to define a triangular function tri such that

$$\text{tri}(x) = \begin{cases} 1 + x & \text{for } -1 < x \le 0 \\ 1 - x & \text{for } \;\; 0 \le x < 1 \\ 0 & \text{otherwise} \end{cases} \tag{3.6}$$

and then we have

$$\text{tri}(x) = \text{rect}(x) \otimes \text{rect}(x) \tag{3.7}$$

and the transform pair

$$\text{tri}(x) \Leftrightarrow \text{sinc}^2(y) \tag{3.8}$$

We note that tri(x/X) extends from $-X$ to X, with half-amplitude width X.

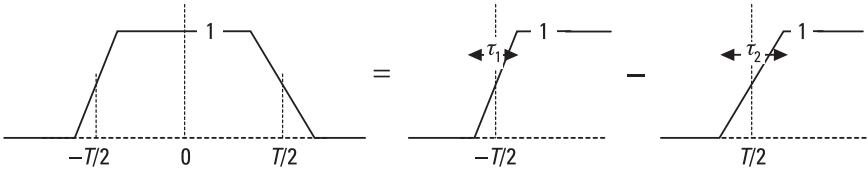## 3.4 Asymmetric Trapezoidal Pulse

A linear rising edge of duration τ is given by the convolution of a step function and a pulse of duration τ (Figure 3.6).

If the height of the edge is to remain at the same level as the step function, then the convolving pulse must have a height of $1/\tau$. With these results we can define the asymmetric trapezoidal pulse of unit height, centered (at its half amplitude points) at the origin, with width T at this level, and with rise and fall times of τ_1 and τ_2, by the difference of two such modified step functions (Figure 3.7). These have rising and falling edges of the required durations and are centered at $-T/2$ and $+T/2$. The waveform is given by

$$u(t) = \frac{1}{\tau_1}\text{rect}\left(\frac{t}{\tau_1}\right) \otimes h\left(t + \frac{T}{2}\right) - \frac{1}{\tau_2}\text{rect}\left(\frac{t}{\tau_2}\right) \otimes h\left(t - \frac{T}{2}\right) \tag{3.9}$$
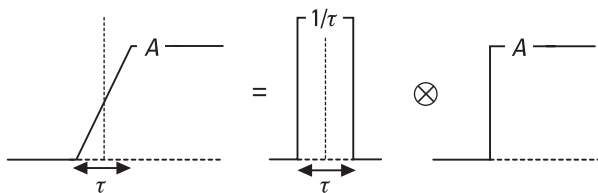
Figure 3.6   Rising edge of width τ.

Figure 3.7 Asymmetrical trapezoidal pulse.

The Fourier transform of this waveform is given, using P2a, R6a in addition to the now more familiar P3a and R5, by

$$U(f) = \text{sinc}(f\tau_1)\left(\frac{\delta(f)}{2} + \frac{1}{2\pi if}\right)e^{\pi ifT} - \text{sinc}(f\tau_2)\left(\frac{\delta(f)}{2} + \frac{1}{2\pi if}\right)e^{-\pi ifT}$$

(3.10)

As the δ-function is zero except at 0, we can put $\text{sinc}(f\tau_1)\delta(f)e^{\pi ift} = \text{sinc}(0)\delta(f)e^0 = \delta(f)$, as in (2.9), and similarly for the $\text{sinc}(f\tau_2)\delta(f)$ term so that the δ-function terms cancel and we have

$$U(f) = \frac{\text{sinc}(f\tau_1)e^{\pi ifT} - \text{sinc}(f\tau_2)e^{-\pi ifT}}{2\pi if}$$

(3.11)

We note that the spectrum for the unit height symmetrical pulse, given by putting $\tau_1 = \tau_2 = \tau$ in this expression, is

$$U(f) = \frac{\text{sinc}(f\tau)(e^{\pi ifT} - e^{-\pi ifT})}{2\pi if} = \frac{\text{sinc}(f\tau)\sin(\pi fT)}{\pi f} = T\text{sinc}(f\tau)\text{sinc}(fT)$$

which is the result given in (3.2) (with $A = 1$ in this case). Equation (3.11) is a neat and compact expression for the spectrum of this asymmetric function and is very easily found by these methods.

Two examples of the spectrum of an asymmetric pulse are given in Figure 3.8. Only the positive frequency side is given, as these power spectra, of real waveforms, are symmetric about zero frequency, as discussed at the end of Section 2.3. The frequency scale is in units of $1/T$, where T is the half amplitude pulse width. For comparison, the spectra of the symmetric pulses, with rise and fall times equal to the mean of those of the asymmetric pulses, are shown by dotted curves. This mean width in the second example, shown in Figure 3.8(b), is $0.7T$. This is very close to the value found in Section 3.2, which places the null due to the slope at the peak of the first sidelobe of the underlying rectangular pulse spectrum, with the result given in
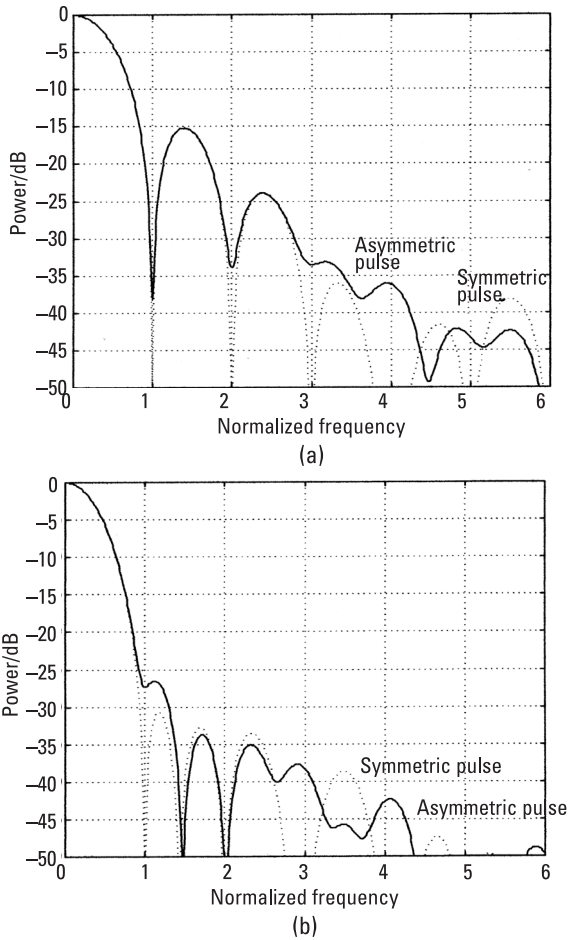
Figure 3.8   Asymmetric trapezoidal pulse spectra. (a) Edges 0.2T and 0.3T, and (b) edges 0.6T and 0.8T.

Figure 3.3(b). We see, in Figure 3.8(b), that the asymmetry has raised the low first sidelobe about 4 dB, while with the sharper edges and higher sidelobes of Figure 3.8(a) the effect of asymmetry is not seen until considerably further out in the pattern.

3.5   Asymmetric Triangular Pulse

We can consider the asymmetrical triangular pulse as a limiting case of the trapezoidal pulse. We note that the flat top of the trapezoidal pulse

(Figure 3.7) is of length $T - (\tau_1 + \tau_2)/2$, so if we set $T = (\tau_1 + \tau_2)/2$, we have a flat top of zero width, and we have a triangular pulse with rising edge of length τ_1 and falling edge of length τ_2 (Figure 3.9(a)).

Its spectrum is given by (3.11) with T, the half-amplitude width, replaced by $(\tau_1 + \tau_2)/2$. However, this pulse has the time origin at the midpoint between the half-amplitude points and the peak at $\Delta\cdot = (\tau_1 - \tau_2)/4$, while it may be preferred to have the origin at the peak position of the pulse. Thus, if $u(t)$ is the pulse in Figure 3.9(a), then $v(t) = u(t + \Delta\tau)$ is the required pulse, shown in Figure 3.9(b) with the peak at 0. From R6a, this time shift multiplies the spectrum by $2\pi i f \Delta\tau$. Applying this to (3.11), and substituting for T and $\Delta\tau$ gives

$$V(f) = \frac{\mathrm{sinc}(f\tau_1)e^{\pi i f \tau_1} - \mathrm{sinc}(f\tau_2)e^{-\pi i f \tau_2}}{2\pi i f} \tag{3.12}$$
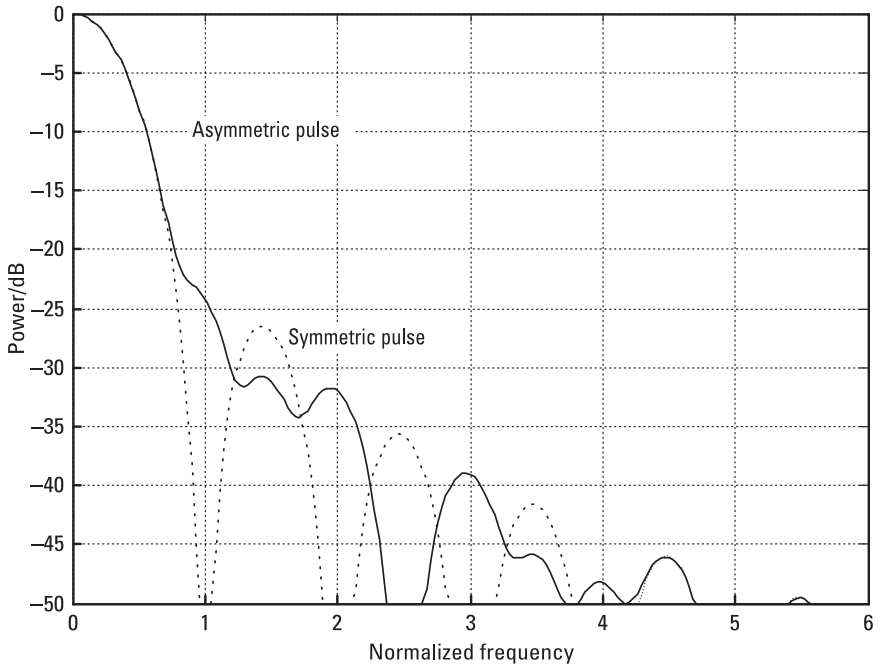
as the spectrum of the triangular pulse with its peak at $t = 0$. This result is also obtainable, alternatively, by centering the edges at $-\tau_1/2$ and $\tau_2/2$, instead of $\pm T/2$, and by placing the steps of the step functions of Figure 3.7 at these points. Then (3.9) is replaced by

$$v(t) = \frac{1}{\tau_1}\mathrm{rect}\left(\frac{t}{\tau_1}\right) \otimes h\left(t + \frac{\tau_1}{2}\right) - \frac{1}{\tau_2}\mathrm{rect}\left(\frac{t}{\tau_2}\right) \otimes h\left(t - \frac{\tau_2}{2}\right) \tag{3.13}$$

and this leads to (3.12) in the same way that (3.9) leads to (3.11).
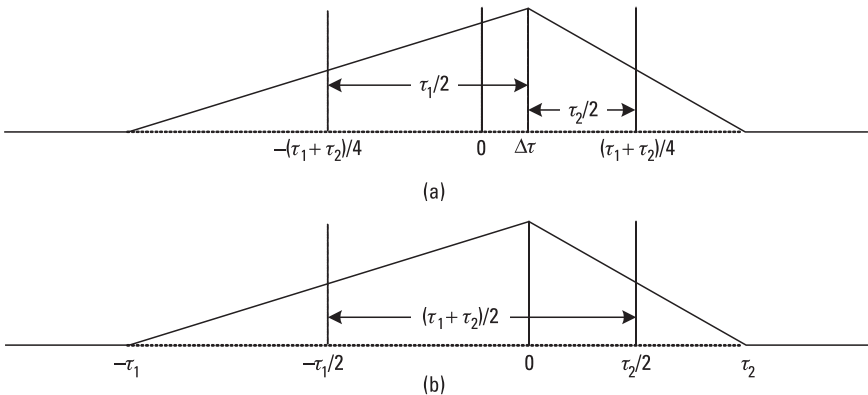
Figure 3.9 Asymmetric triangular pulse. (a) Half-amplitude points centered about time origin, and (b) peak at time origin.

Figure 3.10   Asymmetric triangular pulse spectrum, ratio of rise and fall times 2/3.

We note that, as the pulse width at the half-amplitude points is $T = (\tau_1 + \tau_2)/2$, the rise and fall times relative to T are $2\tau_1/(\tau_1 + \tau_2)$ and $2\tau_2/(\tau_1 + \tau_2)$, which sum to 2. Unlike the trapezoidal pulse, only one parameter is needed to define the shape of this pulse; we could choose T_1, the relative rise time, in which case the relative fall time is $T_2 = 2 - T_1$, or the ratio of the two edge times, $r = \tau_1/\tau_2$, in which case $T_1 = 2r/(r + 1)$ and $T_2 = 2/(r + 1)$.

An example of the spectrum of an asymmetric triangular pulse is given in Figure 3.10. The normalized frequency is again $1/T$, where T is now $(\tau_1 + \tau_2)/2$. The ratio r was 2/3, giving rise and fall times relative to the half-amplitude width of 0.8 and 1.2. The symmetric pulse, with $r = 1$, is shown dotted, for comparison.

3.6   Raised Cosine Pulse

We define this pulse as being of width T at the half amplitude points, which is consistent with the definitions of the earlier triangular and trapezoidal pulses. Then a unit amplitude pulse is part of the waveform $(1 + \cos 2\pi f_0 t)/2$, where

$f_0 = 1/2T$ (i.e., $2T$ is the duration of a cycle of the cosine). This waveform is gated for a time $2T$ so the pulse is given by

$$u(t) = \text{rect}(t/2T)(1 + \cos 2\pi f_0 t)/2 \qquad (3.14)$$

The unit amplitude pulse is shown in Figure 3.11(a), with the time axis in units of T.

The spectrum is thus, using P3a, P1a, P8a, and R5

$$U(f) = 2T \text{ sinc } 2fT \otimes \left(\delta(f) + \tfrac{1}{2}\left[\delta(f - f_0) + \delta(f + f_0)\right]\right)/2$$

$$= T\left(\text{sinc}(f/f_0) + \tfrac{1}{2}[\text{sinc}(f/f_0 - 1) + \text{sinc}(f/f_0 + 1)]\right), \quad (3.15)$$

as convolution with a δ-function corresponds to a shift in the position of the δ-function.

This spectrum is seen to consist of three closely overlapping sinc functions. These are shown as dotted lines in Figure 3.11(b), with the pulse spectrum as the solid line. The frequency axis is in units of f_0 or $1/2T$. These sum to give a spectral shape with first zeros at $\pm 2f_0$ or $\pm 1/T$ (and zeros in general at $n/2T$ for n integral, $|n| \geq 2$) with quite low spectral sidelobes. These are shown more clearly in logarithmic form in Figure 3.12, with the spectrum of the gating pulse for comparison. The highest spectral sidelobes are 31 dB below the peak. These lower sidelobes could be expected from the much smoother shape of this pulse, compared with the rectangular or triangular pulses, the highest sidelobes of which are 13 dB and 27 dB below the peak, respectively. We note that the cost of lower sidelobes is a broadening of the main lobe, relative to the spectrum of the gating pulse of width $2T$. The broadening is by a factor of 1.65 at the 4-dB points.

As an aside, it is interesting to note how similar the two shapes in Figure 3.11 are. In fact they are both close to the Gaussian shape, the function that is the same shape as its transform (P6). These three shapes are illustrated in Figure 3.13.

Pulse shapes of the form $(1 - a - b) + a\cos \pi t/T + b\cos 2\pi t/T$ (gated from $-T$ to T) are easily transformed by the method used here. These include the Hamming window and the Blackman window as well as the Hann window (the raised cosine function considered here) with $a = \tfrac{1}{2}$, $b = 0$.

The transform of this more general form is easily seen to be an extension of (3.15):

$$T\left(2(1 - a - b)\text{sinc}(f/f_0) + a\left(\text{sinc}(f/f_0 - 1) + \text{sinc}(f/f_0 + 1)\right)\right)$$
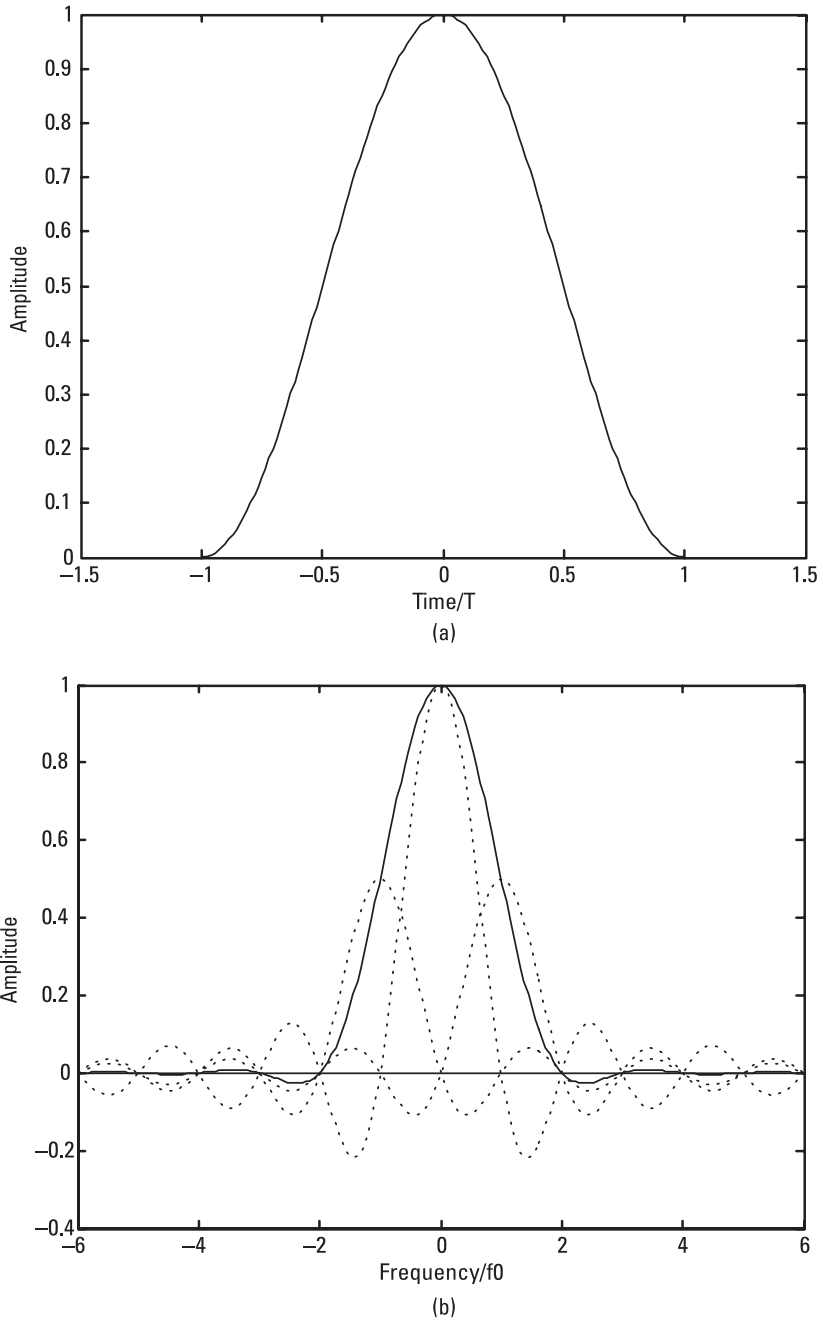
**Figure 3.11**   Raised cosine pulse. (a) Normalized waveform, and (b) normalized spectrum.
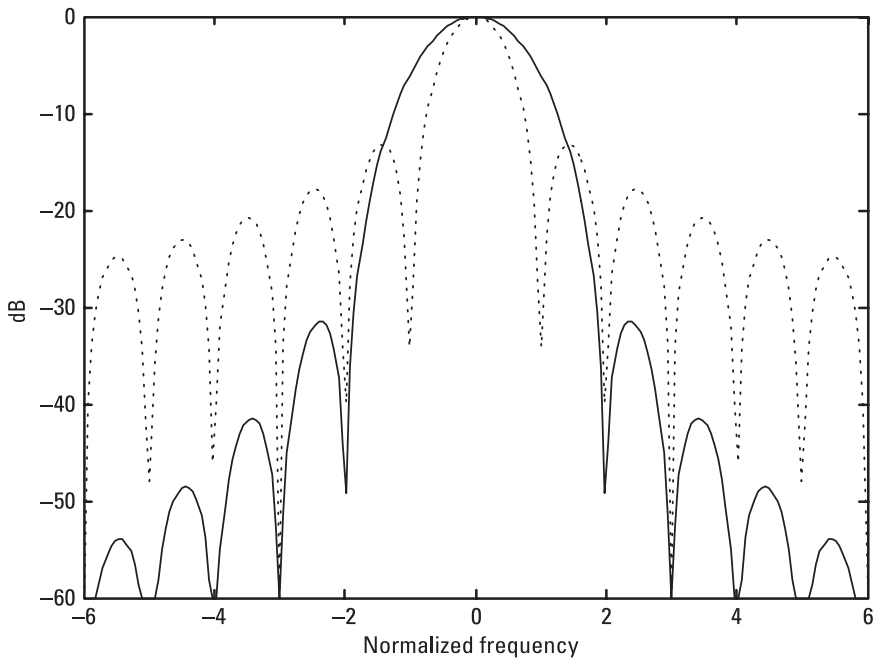
Figure 3.12   Raised cosine pulse spectrum, log scale.

$$+b\big(\operatorname{sinc}(f/f_0 - 2) + \operatorname{sinc}(f/f_0 + 2)\big) \qquad (f_0 = 1/2T)$$

If a base of width T is preferred, we replace T by $T/2$.

3.7   Rounded Pulses

The step discontinuity of rectangular pulses is the cause of the poor spectrum with high sidelobes. This discontinuity in level is removed by generating rising and falling edges of finite slope. In the case of the symmetric trapezoidal pulse, this is achieved by the convolution of the rectangular pulse with another, shorter rectangular pulse, as shown in Section 3.2. This reduction in discontinuity improves the sidelobe levels. There are still discontinuities in slope for these pulses, and these can be removed by another convolution, with a further reduction in sidelobe levels. The convolution need not, in principle, be with a rectangular pulse, but this is perhaps the simplest and is the example taken here.
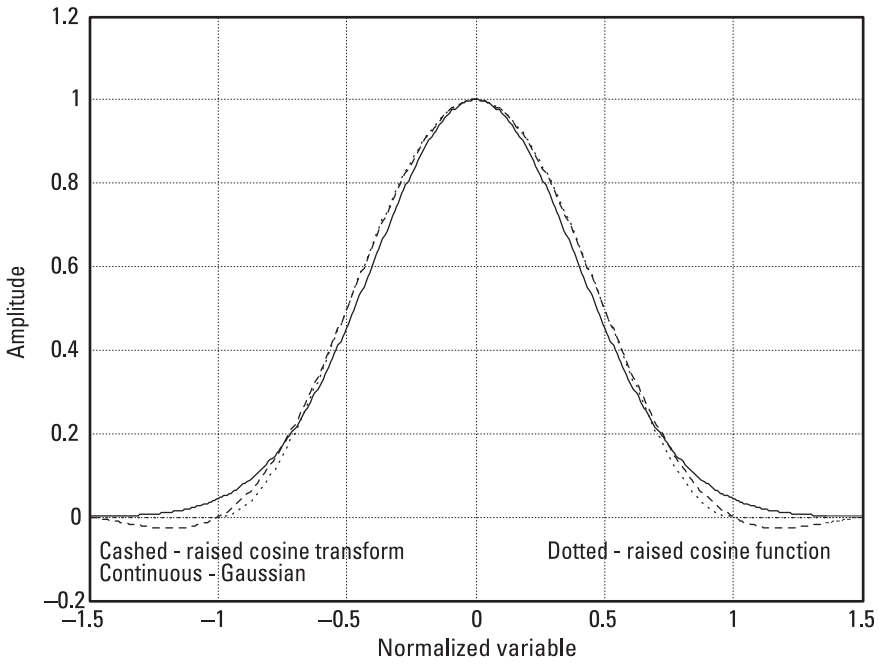
Figure 3.13 Comparison of raised cosine function, its transform, and the Gaussian function.

Figure 3.14 illustrates the effect of convolution with a rectangular pulse on one of the corners of the trapezoidal pulse. The pulse is of length T and over the region $-T/2$ to $+T/2$ relative to the position of the corner the waveform rises as t^2, returning to a constant slope (rising as t) after this interval.

Convolving the trapezoidal pulse with this rectangular pulse will round all four corners in a similar manner. If $f(t)$ describes the trapezoidal pulse waveform and $F(f)$ is its spectrum, then for the rounded waveform we have (from R7b, P3a and R5)

$$f(t) \otimes (1/T)\,\mathrm{rect}(t/T) \Leftrightarrow F(f)\,\mathrm{sinc}\,fT, \qquad (3.16)$$
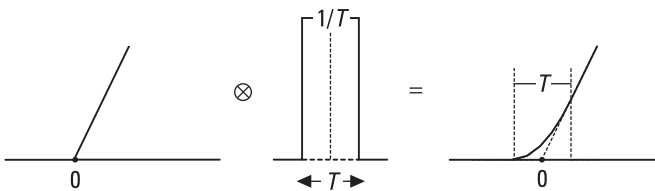
Figure 3.14 Rounded corner of width T.

that is, the spectrum is multiplied by the spectrum of the short pulse, which lowers the sidelobes further.

In practice, a pulse is likely to be rounded by stray capacitance, which could be modeled by the circuit shown in Figure 3.15. In electrical engineering notation the frequency response of this network is given by

$$A(\omega) = \frac{(1/R_2 + j\omega C)^{-1}}{R_1 + (1/R_2 + j\omega C)^{-1}} = \frac{1}{1 + R_1/R_2 + j\omega C R_1} \qquad (3.17)$$

where $j^2 = -1$ and ω is the angular frequency $2\pi f$. In the notation we use here this becomes

$$A(f) = \frac{1}{1 + R_1/R_2 + 2\pi i f C R_1} = \frac{R_2}{R_1 + R_2} \cdot \frac{1}{1 + 2\pi i f \tau} \qquad (3.18)$$

where

$$\tau = \frac{C R_1 R_2}{R_1 + R_2} \qquad (3.19)$$

The product of capacitance and resistance has the dimension of time, so τ represents a time constant for the circuit, and the factor $R_2/(R_1 + R_2)$ is the limiting attenuation to low frequency signals (approaching DC or $f = 0$).

The impulse response $a(t)$ of this circuit is the (inverse) Fourier transform of the frequency response, and from P5 and R5, we have (apart from the scaling factor $R_2/[R_1 + R_2]$)
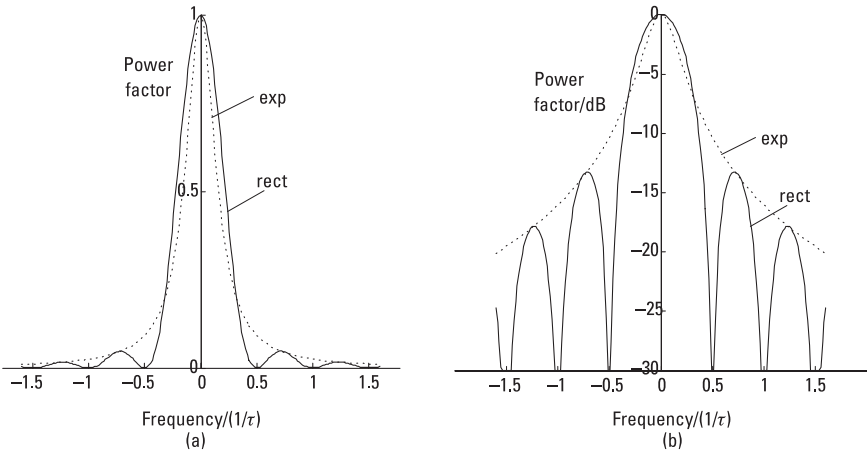
$$a(t) = \frac{1}{\tau} e^{-t/\tau} \; (t \geq 0) \text{ or } a(t) = \frac{1}{\tau} e^{-t/\tau} h(t) \qquad (3.20)$$

where h is the step function. The response of the circuit to a pulse is given by the convolution of the pulse and the impulse response. We look first at
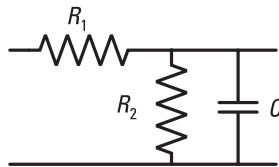
**Figure 3.15** Model for stray capacitance.

Figure 3.16   Power spectra for rect and exponential impulse responses. (a) Linear form, and (b) logarithmic form.

the effect on the rising edge of the trapezoidal pulse, given by $g(t) = kt \cdot h(t)$ (i.e., $g(t) = kt$ for $t>0$). This is

$$a(t) \otimes g(t) = \int_{-\infty}^{\infty} \frac{1}{\tau} e^{-(t-t')/\tau} h(t-t')kt'h(t')dt' = \int_{0}^{t} \frac{k}{\tau} t' e^{-(t-t')/\tau} dt'$$

$$= k\left(t - \tau(1 - e^{-t/\tau})\right) \qquad (t > 0) \qquad (3.21)$$

For large t/τ the exponential term becomes small and we see that the response approaches $k(t - \tau)$, instead of kt, corresponding to a delay of τ. With a similar effect on the falling edge, we see that this delay applies to the pulse as a whole (in addition to the rounding distortion), assuming τ is small compared with the pulse duration. We note that if we move the rectangular rounding pulse of Figure 3.14 so that it starts, like the exponential impulse response, at time zero, rather than at $- T/2$, then this rectangular "impulse response" causes a delay of $T/2$, so this pulse with length $T = 2\tau$ will give the same delay as the exponential impulse and will be approximately equivalent. Figure 3.16 shows the spectral power factors (in both linear and logarithmic form) multiplying the original pulse spectrum in the two cases, $\mathrm{sinc}^2 2f\tau$ for the rectangular pulse and $1/(1 + (2\pi f\tau)^2)$ for the stray capacitance. The power spectrum of the smoothed pulse is that of the spectrum of the original pulse multiplied by one of these spectra. Assuming the smoothing impulse response is fairly short compared with the pulse length, the spectrum of the pulse will be mainly within the main lobe of the impulse response spectrum. We see that the sidelobe pattern of the pulse will be considerably reduced
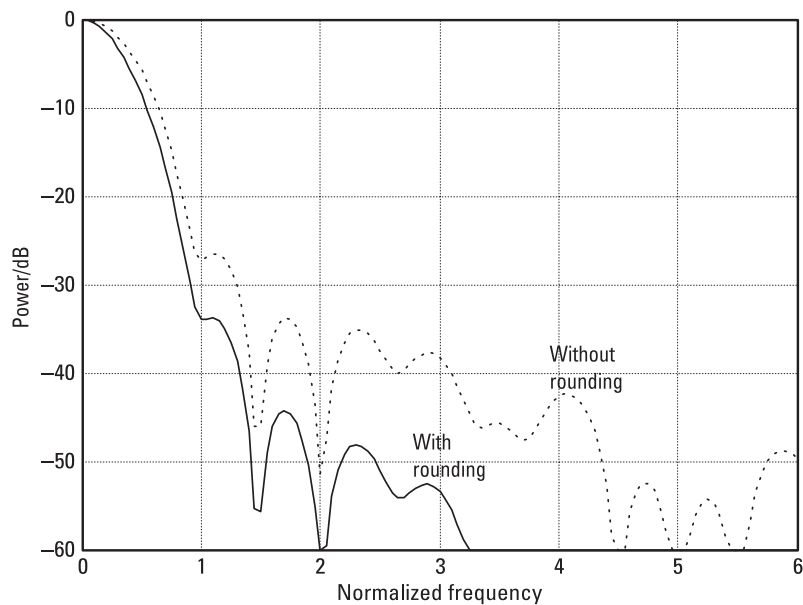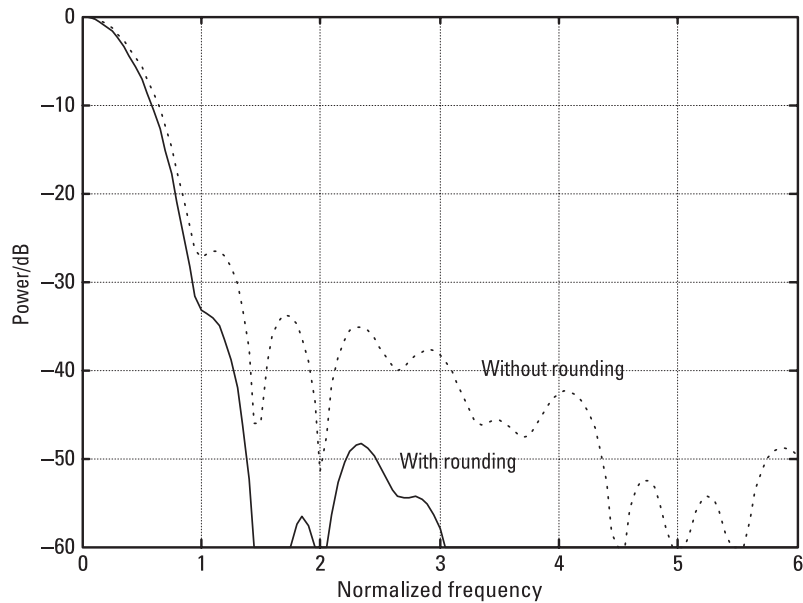
Figure 3.17   Effect of rounding on trapezoidal pulse spectrum. (a) Exponential (capacitative) rounding, (b) rectangular pulse rounding.

by the smoothing (e.g., by about 10 dB at $\pm 0.4/\tau$ from center frequency). We also see that the rect pulse of width 2τ gives a response fairly close to the stray capacitance filter with time constant τ, as expected by the earlier argument considering delay.

We show the effect of these forms of rounding on the spectrum of the asymmetric trapezoidal pulse used for Figure 3.8, with the time constant $\tau = 0.3T$. In Figure 3.17(a), we see the effect of rounding by the exponential impulse response of (3.20), due to capacitance, as in Figure 3.15. The sidelobes are lowered considerably, as should be expected. The response with rectangular rounding, with a pulse width of 2τ, in Figure 3.17(b) is very similar, *except* near the frequency $3/2T$ (normalized frequency 1.5), which corresponds to the position of the first null of the rect spectrum.

3.8 General Rounded Trapezoidal Pulse

Here we consider the problem of rounding the four corners of a trapezoidal pulse independently (i.e., over *different* time intervals, with rect pulses or even with different rounding functions). This may not be a particularly likely problem to arise in practice in connection with radar, but the solution to this awkward case is interesting and illuminating, and may be of use in some other application.

The problem of the asymmetrical trapezoidal pulse was solved in Section 3.4 by forming the pulse from the difference of two step-functions, each of which was convolved with a rectangular pulse to form a rising edge. By
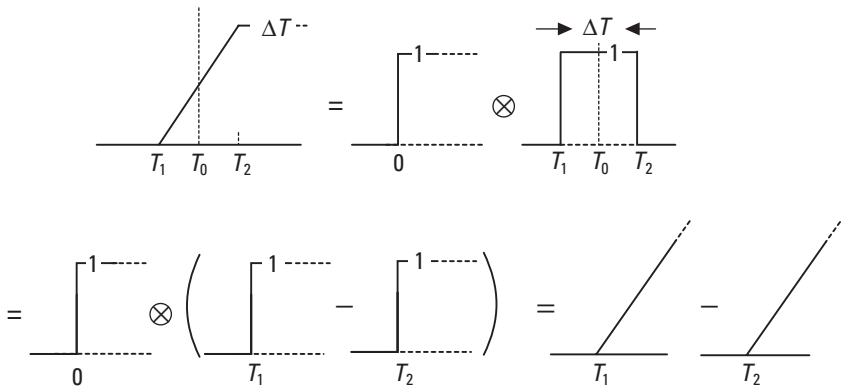
Figure 3.18 Rising edge as the difference of two Ramp functions.
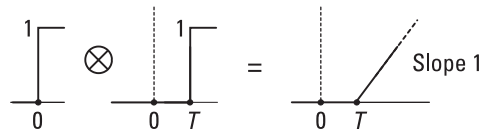
Figure 3.19 Ramp function.

using different width rectangular pulses, we were able to obtain different slopes for the front and back edges of the pulse.

In this case, we extend this principle by expressing the convolving rect pulses themselves as the difference of two step functions. The (finite) rising edge can then be seen to be the difference of two infinite rising edges, as shown in Figure 3.18. Each of these, which we call Ramp functions, is produced by the convolution of two unit step functions, as shown in Figure 3.19 and defined in (3.22).

We define the Ramp function, illustrated in Figure 3.19, by

$$\text{Ramp}(t - T) = h(t) \otimes h(t - T), \tag{3.22}$$

so that

$$\text{Ramp}(t) = \begin{cases} 0 & \text{for } t \le 0 \\ t & \text{for } t > 0 \end{cases} \qquad (t \in \mathbb{R}) \tag{3.23}$$

(A different, finite, ramp function is required in Chapter 7; this is called ramp.) Having now separated the four corners of the trapezoidal pulse into the corners of four Ramp functions, they can all be rounded separately by convolving the Ramp functions with different width rect functions (or other rounding functions, if required) as in Figure 3.14, before combining to form the smoothed pulse. Before obtaining the Fourier transform of the rounded pulse, we obtain the transform of the trapezoidal pulse in the form of the four Ramp functions (two for each of the rising and falling edges).

In mathematical notation, the rising edge of Figure 3.18 can be expressed in the two ways

$$h(t) \otimes \text{rect}\left(\frac{t - T_0}{\Delta T}\right) = h(t) \otimes \left(h(t - T_1) - h(t - T_2)\right)$$

$$= \text{Ramp}(t - T_1) - \text{Ramp}(t - T_2) \tag{3.24}$$

(T_0 is the midpoint of the rect function, at $(T_2 + T_1)/2$, and $\Delta T = T_2 - T_1$ is its width.) The Fourier transform of the left side is, from P2a, P3a, R7b, R5, and R6a,

$$\left(\frac{\delta(f)}{2} + \frac{1}{2\pi i f} \right) \Delta T \operatorname{sinc} f \Delta T \exp(-2\pi i f T_0)$$

$$= \Delta T \left(\frac{\delta(f)}{2} + \frac{\operatorname{sinc} f \Delta T \exp(-2\pi i f T_0)}{2\pi i f} \right), \qquad (3.25)$$

where we have used $\delta(f - f_0)u(f) = \delta(f - f_0)u(f_0)$ in general (see (2.9)), so $\delta(f)\operatorname{sinc} f\Delta T \exp(-2\pi i f T_0) = \delta(f)$. The transform of the difference of the Ramp functions on the right side is, using (3.22), P2a, R7b, and R6a,

$$\left(\frac{\delta(f)}{2} + \frac{1}{2\pi i f} \right) \left[\left(\frac{\delta(f)}{2} + \frac{1}{2\pi i f} \right) \left(\exp(-2\pi i f T_1) - \exp(-2\pi i f T_2) \right) \right] \quad (3.26)$$

Using $T_0 = (T_1 + T_2)/2$ and $\Delta T = T_2 - T_1$, as in Figure 3.18, the difference of the exponential terms becomes $\exp(-2\pi i f T_0)\left(\exp(\pi i f \Delta T) - \exp(-\pi i f \Delta T) \right)$ or $2i\sin(\pi f\Delta T)\exp(-2\pi i f T_0)$ so, again using (2.9), (3.26) becomes

$$\left(\frac{\delta(f)}{2} + \frac{1}{2\pi i f} \right) \left[\left(\frac{\delta(f)}{2} + \frac{1}{2\pi i f} \right) 2i \sin(\pi f \Delta T) \exp(-2\pi i f T_0) \right]$$

$$= \left(\frac{\delta(f)}{2} + \frac{1}{2\pi i f} \right) \frac{\sin(\pi f \Delta T) \exp(-2\pi i f T_0)}{\pi f}$$

$$= \left(\frac{\delta(f)}{2} + \frac{1}{2\pi i f} \right) \Delta T \operatorname{sinc}(f \Delta T) \exp(-2\pi i f T_0) \qquad (3.27)$$

$$= \Delta T \left(\frac{\delta(f)}{2} + \frac{\operatorname{sinc}(f \Delta T) \exp(-2\pi i f T_0)}{2\pi i f} \right),$$

which is the same as (3.25), as expected.

We are now in a position to find the spectrum of the trapezoidal pulse shown in Figure 3.20, with different roundings of each corner. This pulse is separated, as shown, into four Ramp functions and has rising and falling edges of width ΔT_r and ΔT_s, centered at T_r and T_s, respectively. The edges, formed from pairs of Ramp functions, are normalized to unity by dividing by
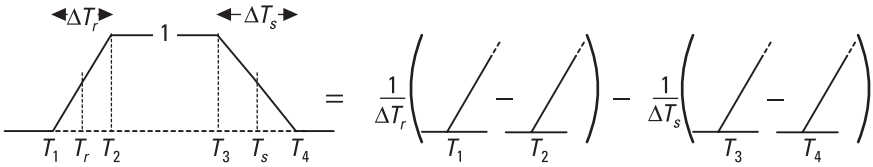
Figure 3.20 Unit height trapezoidal pulse.

the width, ΔT_r or ΔT_s. (They certainly have to be scaled to the same height if the initial and final levels are to be the same.) Thus, this pulse is given by

$$\frac{1}{\Delta T_r}\left(\mathrm{Ramp}(t - T_1) - \mathrm{Ramp}(t - T_2)\right) - \frac{1}{\Delta T_s}\left(\mathrm{Ramp}(t - T_3) - \mathrm{Ramp}(t - T_4)\right)$$

$$(3.28)$$

To round a corner we replace $\mathrm{Ramp}(t - T_k)$ with $r_k(t) \otimes \mathrm{Ramp}(t - T_k)$, where $r_k(t)$ is a rounding function of unit integral (such as the rect pulse in Figure 3.14). For a function with this property, it follows (see (2.6)) that $R(0) = 1$, where R is the Fourier transform of r.

The rounded rising edge, given by $e_r(t) = \left(r_1(t) \otimes \mathrm{Ramp}(t - T_1) - r_2(t) \otimes \mathrm{Ramp}(t - T_2)\right)/\Delta T_r$, can be written, from the definition of Ramp in (3.22),

$$e_r(t) = h(t) \otimes \left(r_1(t) \otimes h(t - T_1) - r_2(t) \otimes h(t - T_2)\right)/\Delta T_r \qquad (3.29)$$

with transform

$$E_r(f) = \frac{1}{\Delta T_r}\left(\frac{\delta(f)}{2} + \frac{1}{2\pi i f}\right)$$

$$\left[\left(\frac{\delta(f)}{2} + \frac{1}{2\pi i f}\right)\left(R_1(f)\exp(-2\pi i f T_1) - R_2(f)\exp(-2\pi i f T_2)\right)\right]$$

$$= \left(\frac{\delta(f)}{2} + \frac{1}{2\pi i f}\right)\left[\frac{\left(R_1(f)\exp(\pi i f \Delta T_r) - R_2(f)\exp(-\pi i f \Delta T_r)\right)}{2\pi i f \Delta T_r}\right]\exp(-2\pi i f T_r)$$

$$= \frac{\delta(f)}{2} + \left[\frac{\left(R_1(f)\exp(\pi i f \Delta T_r) - R_2(f)\exp(-\pi i f \Delta T_r)\right)}{(2\pi i f)^2 \Delta T_r}\right]\exp(-2\pi i f T_r),$$

$$(3.30)$$

following the approach of the nonrounded case of (3.25) to (3.27). (The last two lines again use the result $\delta(f)g(f) = \delta(f)g(0)$, from (2.9). We note that the

term in square brackets at $f = 0$ in the second line becomes sinc(0) = 1.) Combining the two edges, the δ-functions disappear, as in forming the spectrum of the asymmetric trapezoidal pulse in Section 3.4 (equations (3.10) and (3.11)), to give the final result for the spectrum of the generally rounded trapezoidal pulse:

$$-\frac{\left(R_1(f)e^{\pi i f \Delta T_r} - R_2(f)e^{-\pi i f \Delta T_r}\right)}{(2\pi f)^2 \Delta T_r}e^{-2\pi i f T_r}$$

$$+\frac{\left(R_3(f)e^{\pi i f \Delta T_s} - R_4(f)e^{-\pi i f \Delta T_s}\right)}{(2\pi f)^2 \Delta T_s}e^{-2\pi i f T_s} \qquad (3.31)$$

As a check, we note that if we used a single rounding function, r, with transform R, the expression in (3.31) reduces to

$$R(f)\left[\frac{\operatorname{sinc} f \Delta T_r}{2\pi i f}e^{-2\pi i f T_r} - \frac{\operatorname{sinc} f \Delta T_s}{2\pi i f}e^{-2\pi i f T_s}\right], \qquad (3.32)$$

which (with $T_r = -T/2$, $T_s = T/2$, $\Delta T_r = \tau_1$, and $\Delta T_s = \tau_2$) is seen from (3.11) to be exactly the result of smoothing the asymmetrical trapezoidal pulse with the function r.

3.9 Regular Train of Identical RF Pulses

This waveform could represent, for example, an approximation to the output of a radar transmitter using a magnetron triggered at regular intervals. The waveform is defined by

$$u(t) = \operatorname{rep}_T \left\{\operatorname{rect}(t/\tau)\cos 2\pi f_0 t\right\} \qquad (3.33)$$

where the pulses of length τ of a carrier at frequency f_0 are repeated at the pulse repetition interval T and shown in Figure 3.21.
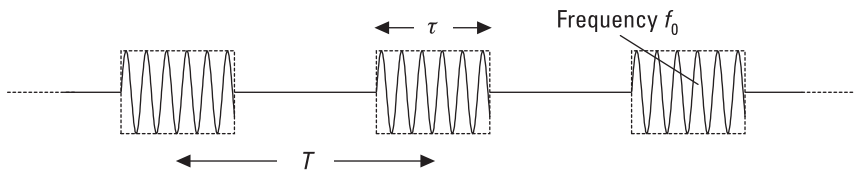
**Figure 3.21** Regular train of identical RF pulses.

We note that the rep operator in (3.33) applies to a product of two functions, so the transform will be (by R8b and R7a) a comb version of a convolution of the transforms of these functions. We could express the cosine as a sum of exponentials, but more conveniently we use P9a in which this and the convolution have already been done. Thus (from P3a, P9a, R8b, and R5) we obtain

$$U(f) = (\tau/2T)\text{comb}_{1/T}\left\{\text{sinc}\,(f - f_0)\tau + \text{sinc}\,(f + f_0)\tau\right\} \quad (3.34)$$

This spectrum is illustrated (in the positive frequency region) in Figure 3.22.

Thus, we see that the spectrum consists of lines (which follows from the repetitive nature of the waveform) at intervals $1/T$, with strengths given by two sinc function envelopes centered at frequencies f_0 and $-f_0$. As discussed in Chapter 2, the negative frequency part of the spectrum is just the complex conjugate of the real part, for a real waveform, and provides no extra information. (In this case the spectrum is real, so the negative frequency part is just a mirror image of the real part.) However, as explained in Section 2.4.1, the contribution of the part of the spectrum centered at $-f_0$ in the positive frequency region can only be ignored if the waveform is sufficiently narrowband (i.e., if $f_0 \gg 1/\tau$), the approximate bandwidth of the two spectral branches.

An important point about this spectrum, which is very easily made evident by this analysis, is that, although the envelope of the spectrum is centered at f_0, there is, in general, no spectral line at f_0. This is because the lines are at multiples of the pulse repetition frequency (PRF) $(1/T)$ and only if f_0 is an exact multiple of the PRF will there be a line at f_0. Returning to the time domain, we would not really expect power at f_0 unless the carrier of one pulse was exactly in phase with the carrier of the next pulse.
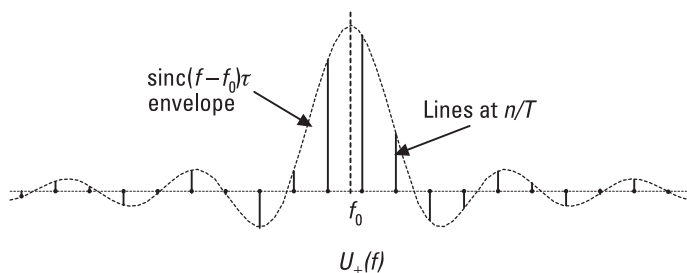
Figure 3.22 Spectrum of regular RF pulse train.

For there to be power at f_0, there should be a precisely integral number of wavelengths of the carrier in the repetition interval T (i.e., the carrier frequency should be an exact multiple of the PRF). This is the case in the next example.

3.10   Carrier Gated by a Regular Pulse Train

This waveform would be used, for example, by a pulse Doppler radar. A continuous stable frequency source is gated to produce the required pulse train (Figure 3.23). Again we take T for the pulse repetition interval τ for the pulse length and f_0 for the carrier frequency. The waveform is given by

$$u(t) = (\text{rep}_T(\text{rect } t/\tau))\cos 2\pi f_0 t \qquad (3.35)$$

and its transform, shown in Figure 3.24, (using R7a, R8b, P3a, and P8a) is

$$U(f) = (\tau/2T)\text{comb}_{1/T}(\text{sinc } f\tau) \otimes (\delta(f - f_0) + (\delta(f + f_0)) \qquad (3.36)$$

Denoting the positive frequency part of the spectrum by U_+ and assuming the waveform is narrowband enough to give negligible overlap of the two parts of the spectrum, we have

$$U_+(f) = (\tau/2T)\text{comb}_{1/T}(\text{sinc} f\tau) \otimes \delta(f - f_0) \qquad (3.37)$$

The function $\text{comb}_{1/T}\text{sinc} f\tau$ is centered at zero and has lines at multiples of $1/T$, including zero. Convolution with $\delta(f - f_0)$ simply moves the center of this whole spectrum up to f_0. Thus, there are lines at $f_0 + n/T$ (n integral, $-\infty$ to ∞), including one at f_0. In general there is not a line at $f = 0$; this is only the case if f_0 is an exact multiple of $1/T$. Unlike the previous case, we would expect the waveform to have power at f_0 as the pulses all consist of samples of the same continuous carrier at this frequency.
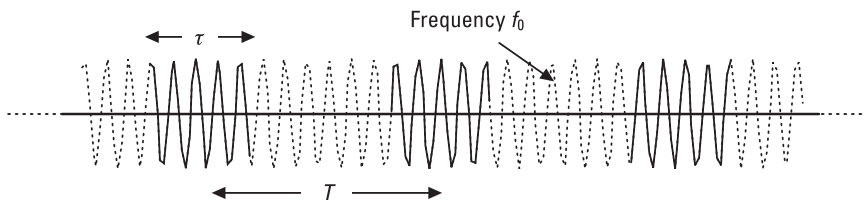
Figure 3.23   Carrier gated by a regular pulse train.
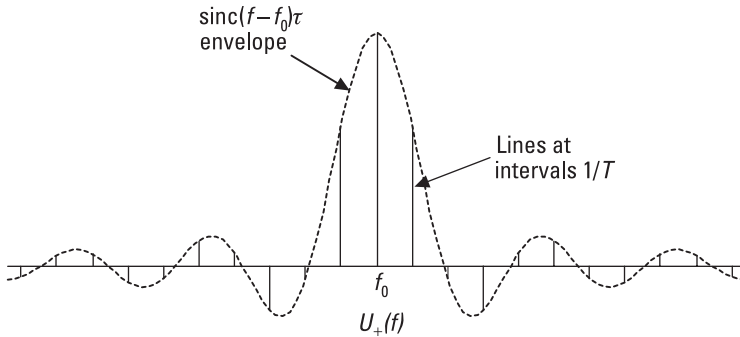
Figure 3.24 Spectrum of regularly gated carrier.

3.11 Pulse Doppler Radar Target Return

In this case we take the model for the target echo received by a pulse Doppler radar to be a number of coherent pulses with their amplitudes modulated by the beam shape of the radar as it sweeps past the target. (The echo is actually modulated twice, on transmission and on reception, so the beam shape is applied squared.) Here, for simplicity, we approximate this modulation first by a rectangular function of width θ (i.e., θ is the time on target). A more general case will be taken later. The pulse train is given by u in (3.35) so the waveform received from a stationary point target is given, apart from an amplitude scaling factor, but with the modulation imposed by the beam, by

$$x(t) = \text{rect } (t/\theta)u(t) \tag{3.38}$$

(as $\text{rect}^2 = \text{rect}$). The spectrum (from R7a, P3a, and R5) is

$$X(t) = \theta\text{sinc}f\theta \otimes U(f) \tag{3.39}$$

where U is given in (3.36). The convolution effectively replaces each δ-function in the spectrum U by a sinc function. This is of width $1/\theta$ (at the 4-dB points), which is normally very small compared with the envelope sinc function of the spectrum, which has width $1/\tau$, and also is small compared with the line spacing $1/T$ if $\theta \gg T$ (i.e., many pulses are transmitted in the time on target). In fact, there will also be a Doppler shift on the echoes, if the target is moving relative to the radar. If it has a relative approaching radial velocity v, then the frequencies in the received waveform should be scaled by the factor $(c + v)/(c - v)$, where c is the speed of light. This gives an approximate overall spectral shift of $+2vf_0/c$ (assuming $v \ll c$, and the spectrum is narrowband, so
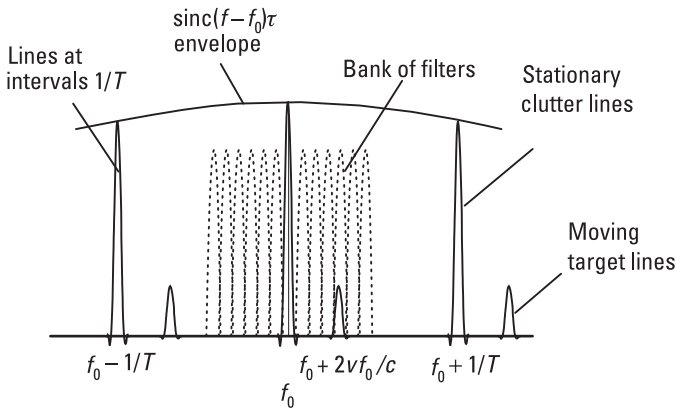
Figure 3.25   Spectrum of pulse Doppler radar waveform.

that all significant spectral energy is close to f_0 or $-f_0$). Figure 3.25 illustrates the form of the spectrum of the received signal. Stationary objects (or "clutter") produce echoes at frequency f_0 and at intervals n/T about f_0, all within an envelope defined by the pulse spectrum (as in Figure 3.25). The smaller, moving target echoes produce lines offset from the clutter lines, so that such targets can be seen, as a consequence of their relative movement, in the presence of otherwise overwhelming clutter.

Figure 3.25 is diagrammatic; the filter bank may be at baseband ($f_0 = 0$) or a low IF and may be realized digitally. By suitable filtering, not only can the targets be seen, but an estimate is obtained of the Doppler shift, and hence of the target radial velocity.

As indicated by (3.39), all the lines are broadened by the spectrum of the beam modulation response (squared) but a rectangular beam, as taken earlier, is not realistic, except as a very rough approximation. In Chapter 8 we see that, for a linear aperture, the beam shape is essentially the inverse Fourier transform of the aperture illumination function, and with a constant angular rotation rate this becomes the (one-way) beam modulation. (We require the small angle approximation $\sin\theta \approx \theta$, which is generally applicable in the radar case, near broadside.) If the aperture function is $\text{rect}(x/X)$, where X is the width of the aperture in wavelengths, then the beam shape is of the form $\text{sinc}(\alpha X)$, where α is the azimuth angle (in radians). If the beam scans at constant speed say $\alpha = kt$, then the received pulse train is modulated by a function of the form $(\text{sinc}\,kXt)^2$ and the target echo spectrum is the transform of this (i.e., it is the triangular function, $\text{tri}(f/kX)$, from P4,R4,R5). The

width of this function (given by $f_0 = kX$ at the half-amplitude, or 6 dB points) determines the width of the filters and hence the velocity resolution.

To put in some reasonable values, let $X = 30$ wavelengths, for a 3m aperture at S-band (3 GHz), and if the rotation period is 3 seconds, then $k = 2\pi/3$ rad/sec and $kX = 60\pi/3$, or approximately 60 Hz. At this carrier frequency, a target with a radial velocity of 1m/s will give a Doppler shift of 20 Hz so the line broadening is only equivalent to about 3 m/s wide.

If we put the weighting function in the form $a(x)\text{rect}(x/X)$, the beam shape is $\left(A(\alpha) \otimes \text{sinc}(\alpha X)\right)^2$ and the two-way response is $(A(\alpha)\otimes\text{sinc}(\alpha X))^2$. The echo modulation is $\left(A(kt) \otimes \text{sinc}(kXt)\right)^2$ and the line shape, broadened by this modulation, is $a(f/k)\text{rect}(f/kX)\otimes a(f/k)\text{rect}(f/kX))$. Because of the mixture of convolution and multiplication, this expression is not easily simplified for typical functions a, though it may be possible to obtain estimates of the line shape and its width by making approximations. In general, weighting functions that give desirable low-sidelobe responses produce broader main lobes, reducing the resolution by a factor of up to two.

3.12   Summary

The spectra of a number of pulses and of pulse trains have been obtained in this chapter using the rules-and-pairs method. As remarked earlier, the aim is not so much to provide a set of solutions on this topic as to illustrate the use of the method so that users can become familiar with it and then solve their own problems using it. Thus, whether all the examples correspond demonstrably to real problems (e.g., finding the spectra of the asymmetric trapezoidal pulse and, particularly, this pulse with different roundings of each corner) is not the question—the variety of possible user problems cannot be anticipated, after all—but rather the examples are meant to demonstrate various ways of applying the method to yield solutions neatly and concisely without any explicit integration.

4

Periodic Waveforms, Fourier Series, and Discrete Fourier Transforms

4.1 Introduction

In this section, we consider some aspects of periodic waveforms, using the rules-and-pairs method. First we note that these waveforms do not have finite energy, so that the result following Parseval's Theorem (2.27), equating the waveform energy with an equivalent form based on the spectrum, cannot be applied. Instead, it is shown in Section 4.2 that the relevant quantity in this case is power, rather than energy, and expressions for the powers of the waveforms and spectra are derived using the rules and pairs.

Periodic waveforms can be represented as Fourier series, of course. A periodic waveform has a line spectrum, given in the rules-and-pairs approach by a set of δ-functions whose strengths give the coefficients of the series obtained by the standard method, using integration. If we express a periodic function u, with repetition interval T, in the form

$$u(t) = \sum_{n=-\infty}^{\infty} c_n \exp 2\pi i n F t \qquad (4.1)$$

as in (1.1), then by P1a and R6b the spectrum is given by

$$U(f) = \sum_{n=-\infty}^{\infty} c_n \delta(f - nF),$$ (4.2)

where $F = 1/T$ is the fundamental frequency of the waveform. The coefficients are found, using the orthogonality of the complex exponential functions over one period. That is,

$$\int_{I_T} \exp(-2\pi imt/T)\exp(2\pi int/T)dt = T\delta_{nm},$$

where I_T is an interval of length T, and δ_{mn} is the Kronecker-δ. Thus, we have

$$c_n = 1/T \int_{I_T} u(t)\exp(-2\pi inFt)dt$$ (4.3)

Equations (4.1) and (4.3) would normally define a Fourier series relationship. Equation (4.2) gives the spectrum formally as a function of frequency, but usually only the coefficients c_n are needed. Equivalent equations can be obtained for the expressions in trigonometric form, using sine and cosine series, using the orthogonality of the sine and cosine functions over one period.

In the case of a regular train of pulses of finite duration, the spectrum is simply a sampled form of the continuous spectrum of a single pulse. This is shown very simply by the rules-and-pairs method—if $s(t)$ is the pulse waveform, repeated with period T, then the pulse train is represented by $\text{rep}_T s(t)$, which has transform $F\text{comb}_F S(f)$, where $F = 1/T$ and S is the spectrum of the pulse, the transform of s. We see that we replace the continuous function S by a discrete function, consisting of δ-functions (or spectral lines) at multiples of F and of strength $FS(nF)$, F times the value of S at these frequency points. Thus, if we have a train of pulses of one of the forms already analyzed in Chapter 3 (Section 3.2 through Section 3.8) we obtain the spectrum of the pulse train immediately by sampling the pulse spectrum at the points nF (and multiplying by F).

However, the Fourier transform obtained here, by the rules-and-pairs method, expresses the waveform in terms of complex exponential functions of frequency (cisoids)—as an integral over a frequency continuum in the non-

periodic case, or as a sum over discrete frequencies in the periodic case. (So, for example, c_n is the coefficient of $\exp 2\pi i n F t$, the component at frequency nF, in the Fourier series of (4.1)) This expansion in terms of complex exponentials may not be the most convenient for the user. Fourier series analysis can be applied, of course, to real-valued or complex-valued functions, expressing them in terms of either real functions (possibly with complex coefficients) or complex functions. However, generally the main area of application is to real functions, expressed more naturally as a sum of real functions (sines and cosines) rather than as a sum of complex exponentials. In Section 4.3, we show how to obtain the Fourier series coefficients for this case, using the rules-and-pairs approach, without having to perform any of the usual integration. To illustrate the method, we take as examples a rectangular pulse train, a sawtooth waveform, periodic triangular waveforms (symmetric and asymmetric), and rectified sinewaves (half-wave and full-wave.)

The discrete Fourier transform (DFT) differs from the other Fourier transforms in this book. For these other transforms, the input waveforms are mathematical functions, which may describe, with varying degrees of accuracy, actual physical quantities. For the DFT, considered in Section 4.4, the input of the transform is a set of data samples, without necessarily any explicit mathematical description. Thus, the waveform is discrete, rather than continuous, though it may be considered to be a sampled form of an implicit underlying continuous function. The case of general discrete waveforms is taken initially. If the data is considered to be from a regularly sampled waveform (described by a comb function), its spectrum, from the comb-rep pair, is a repetitive, or periodic, function of frequency. This has the advantage that only a single period is needed to define the spectrum. However, in general this spectrum is continuous, and the question arises of how to sample it suitably in order to describe it in finite terms. If we sample it regularly (and take the condition that the sampling interval is an integer submultiple of the repetition interval), then we find that this spectrum is both periodic and regularly sampled, and its inverse transform is a waveform that is also both periodic and regularly sampled. The number of samples in one period of the spectrum is found to be equal to the number of input samples, the number in one period of the supposed periodic waveform. This is the basis for the fast Fourier transform (FFT), which is an efficient implementation of this DFT. We show how the DFT is implemented—in particular, we derive the coefficients relating the spectral components to the input data samples, using the rules-and-pairs technique, and give an example, using the MATLAB FFT as an illustration of the principles.

4.2   Power Relations for Periodic Waveforms

4.2.1   Energy and Power

If $u(t)$ represents the voltage at an instant t across a resistor with resistance R, then $|u(t)|^2/R$ is the rate of conversion of electrical energy into heat at time t, and the integral of this over some time interval gives the heat energy generated during this interval. In general, ignoring R, as a fixed scaling factor we consider $\int |u(t)|^2\, dt$ to be the *energy* in the waveform in appropriate units. It may be convenient to keep to this terminology even when u does not represent a physical quantity, such as voltage or the amplitude of a wave, and we simply mean the integrated square modulus of the function.

In the discussion of Parseval's theorem in Section 2.4.2 we have assumed that the waveform u in (2.27) is a finite energy waveform (i.e., that the infinite integral on the left side of this equation [and consequently also that on the right] converges). For this to be the case, we must have $u(t) \rightarrow 0$ as $t \rightarrow \pm\infty$. (This is a necessary but not sufficient condition. For example, as $|u|^2$ is monotonic, at large values of t its value must also fall faster than t^{-1}.) For the repetitive waveforms considered in this chapter, this condition is not met, and (2.27) is not applicable. Instead we can consider the mean energy per unit time, or *power*, and this is the appropriate measure, rather than energy, for these waveforms. The mean power in a waveform u over an interval of length T is given by $\dfrac{1}{T}\int_T |u(t)|^2\, dt$ (where $\int_T$ indicates integration over this interval) and for a (statistically stationary) random waveform we could estimate the power level by taking the limit as $T \rightarrow \infty$. However, for a periodic function, there is a natural time interval to choose, which is its period of repetition. This approach is used to obtain results equivalent to (2.27) for both the case of a periodic waveform, which has a spectrum of discrete lines, and a sampled waveform, which has a periodic spectrum. The equivalent result for a waveform that is both sampled and repetitive, as used for the DFT, is given in Section 4.4.

4.2.2   Power in the δ-Function

We know that the integral of the δ-function is unity, but what is the value of $\int \delta(f)^2 df$? In order to tackle this question, we return to the definition of the δ-function (given in Section 2.2.3) as the limit of a suitable sequence of functions of unit integral, such that the limiting function is nonzero only

at a single point. In this case, we take the sinc function as the basis for our sequence.

Consider first the waveform

$$u_n(t) = \operatorname{rect} t/n,$$

a rectangular pulse of length n, with spectrum

$$U_n(f) = n \operatorname{sinc} nf$$

The energy in the waveform is given by

$$E_n = \int_{-\infty}^{\infty} |u_n(t)|^2 dt = \int_{-\infty}^{\infty} \operatorname{rect}^2(t/n) dt = \int_{-\infty}^{\infty} \operatorname{rect}(t/n) dt = n, \quad (4.4)$$

as $\operatorname{rect}^2 = \operatorname{rect}$. The spectral energy is

$$\int_{-\infty}^{\infty} |U_n(f)|^2 df = \int_{-\infty}^{\infty} n^2 \operatorname{sinc}^2(nf) df = \int_{-\infty}^{\infty} n \operatorname{sinc}^2(nf) d(nf) = n. \quad (4.5)$$

using property 3 of the sinc function (Section 2.2.2). The equality of the waveform and spectral energies is in agreement with Parseval's Theorem (see (2.27)). Now we consider the limit of the sequences of the functions u_n and U_n. We have

$$\lim_{n \to \infty} u_n(t) = \lim_{n \to \infty} (\operatorname{rect} t/n) = 1$$

and

$$\lim_{n \to \infty} U_n(f) = \lim_{n \to \infty} (n \operatorname{sinc} nf) = \delta(f),$$

using the definition of the δ-function given in Section 2.2.3. We now see from (4.4) and (4.5) that the energy in these functions $\lim_{n \to \infty} (E_n)$ is infinite. (This answers the question at the start of this section.) However, the *power* in each waveform u_n is given by dividing by the pulse length n, so is given by $p_n = E_n/n = 1$. As this is independent of n, it is clear that this is also the power of the limiting waveform, the constant function $u(t) = 1$, which has transform $\delta(f)$ (i.e., the power represented by a δ-function of unit strength is unity,

and the power in a δ-function of strength a is thus $|a|^2$). It seems reasonable to suppose that a more complex function, with a spectrum of many lines, will have power given by the sum of the powers in the spectral lines, and this is proved in the next section (see (4.14)). This is also true of shifted δ-functions, as $U(f) = \delta(f - f_0)$ has transform $u(t) = \exp 2\pi i f_0 t$ and $|u(t)|^2 = 1$.

4.2.3   General Periodic Function

A periodic waveform is not one of finite energy, but if we take one period of it then we have a finite energy waveform, for which the energy equation of (2.27) holds, following directly from Parseval's Theorem. Let the periodic function be u with repetition interval T and let v be a single period of u, obtained by gating (see Figure 4.1). Then we have

$$v(t) = \text{rect}(t/T)u(t) \text{ and also } u(t) = \text{rep}_T\, v(t) \qquad (4.6)$$

Their spectra are given by

$$V(f) = T\,\text{sinc}(fT) \otimes U(f) \text{ and } U(f) = F\,\text{comb}_F\, V(f). \quad (F = 1/T) \quad (4.7)$$

Writing out the comb function we can put U in the form

$$U(f) = F\sum_n V(nF)\delta(f - nF) = \sum_n U_n\delta(f - nF), \qquad (4.8)$$

where $U_n = FV(nF)$ is the strength of the δ-function at frequency nF in the spectrum of U.
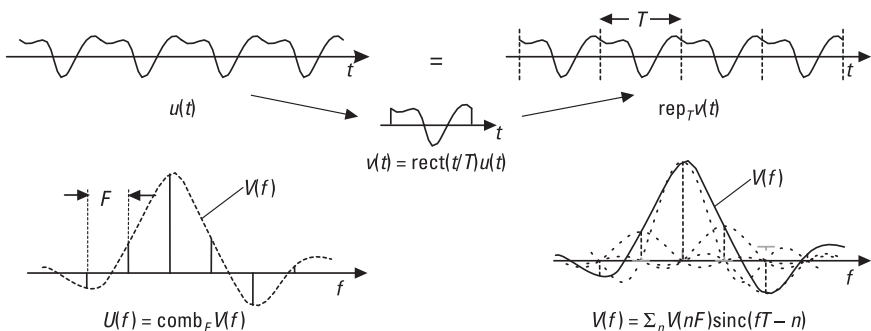
Figure 4.1   Waveforms and spectra for a periodic function.

From the two spectral expressions in (4.7) we have

$$V(f) = \operatorname{sinc}(fT) \otimes \operatorname{comb}_F V(f) \qquad (4.9)$$

$$= \operatorname{sinc} fT \otimes \sum_n V(nF)\delta(f - nF) = \sum_n V(nF)\operatorname{sinc}((f - nF)T)$$

$$= \sum_n V(nF)\operatorname{sinc}(fT - n) \qquad (4.10)$$

$\sum_n$ here means summation over all n, from $-\infty$ to ∞. This shows that the spectrum V can be represented by its samples at intervals $F = 1/T$, interpolated using sinc functions. This result holds for any spectrum V as long as the corresponding waveform v is within the interval $[-T/2, T/2]$. It is the converse of the waveform interpolation result given in (5.2). These waveforms and spectra are illustrated diagrammatically in Figure 4.1.

As v is now a finite energy waveform, we can use the result (2.27) from Parseval's Theorem. In this case, the energy in v and hence in one period of u is E_v, given by

$$E_v = \int_{-\infty}^{\infty} |v(t)|^2 \, dt = \int_T |u(t)|^2 \, dt \qquad (4.11)$$

Strictly, from the definition of v, $\int_T$ should mean integration over the interval $-T/2$ to $T/2$, the range over which the rect function has value unity, but in fact it could be over any interval of length T, which would contain one whole period of u.

Using (4.10) we have

$$\int_{-\infty}^{\infty} |V(f)|^2 \, df = \int_{-\infty}^{\infty} \sum_n V(nF)\operatorname{sinc}(fT - n)\sum_m V(mF)^* \operatorname{sinc}(fT - m)df$$

$$= 1/T \int_{-\infty}^{\infty} \sum_n \sum_m V(nF)V(mF)^* \operatorname{sinc}(fT - n)\operatorname{sinc}(fT - m)d(fT)$$

$$= F\sum_n \sum_m V(nF)V(mF)^* \delta_{nm} = F\sum_n |V(nF)|^2, \qquad (4.12)$$

where we have used property 4 of the sinc function (see Section 2.2.2), the orthonormal property of the set of shifted sinc functions. Here δ_{nm} is the Kronecker-δ, unity if $m = n$ and zero if $m \neq n$.

Equation (4.12) is an interesting result in itself: for a spectrum V, where the waveform v is within the interval $[-T/2,+T/2]$, the integral of the continuous function $|V|^2$ is F times the sum of samples of $|V|^2$ taken at intervals $F=1/T$.

The power in waveform u is thus given by p_u where

$$p_u = \frac{E_v}{T} = \frac{1}{T}\int_{-\infty}^{\infty}|v(t)|^2\,dt = \frac{1}{T}\int_{-\infty}^{\infty}|V(f)|^2\,df = F^2\sum_n|V(nF)|^2 \quad (4.13)$$

using (2.27) and (4.12). From (4.8) we have $U_n = FV(nF)$, and so, from (4.11) and (4.13), we have finally, for the power in u,

$$\frac{1}{T}\int_T|u(t)|^2\,dt = \sum_n|U_n|^2 \quad (4.14)$$

This confirms that the power in the periodic waveform u is equal to the sum of the square moduli of the δ-function strengths in its line spectrum (i.e., the powers of the frequency components) as proposed in Section 4.2.2.

If u is the repeated form of a known pulse waveform s, then from $u(t) = \text{rep}_Ts(t)$ we have

$$\int_T|\text{rep}_T\,s(t)|^2\,dt = F\sum_n|S(nF)|^2 \quad (4.15)$$

(NB: In general one period of $\text{rep}_Ts(t)$ is not necessarily equal to $s(t)$ because of the overlapping of repeated versions when the duration of s is greater than T. Only if s is time limited, with value zero outside the interval $-T/2$ to $+T/2$, can we replace $\text{rep}_Ts(t)$ by $s(t)$ in (4.15).)

We can present this result in a form rather closer to the Parseval result for finite energy waveforms (2.27) by integrating the sampled form of the power spectrum:

$$\int_{-\infty}^{\infty}\text{comb}_F|S(f)|^2\,df = \int_{-\infty}^{\infty}\sum_n|S(nF)|^2\,\delta(f-nF)df = \sum_n|S(nF)|^2$$

as the integrals of the δ-functions are unity. Thus (4.15) becomes

$$\int_T|\text{rep}_T\,s(t)|^2\,dt = F\int_{-\infty}^{\infty}\text{comb}_F|S(f)|^2\,df \quad (4.16)$$

This result shows that the energy in one period of a repetitive waveform is given by the integral of the sampled power spectrum times the sampling interval (in the frequency domain).

4.2.4 Regularly Sampled Function

If u is sampled regularly at intervals τ, then its spectrum is repetitive at intervals $\phi = 1/\tau$. In this case, we take the same approach as in Section 4.2.3, except that we gate out one period of the spectrum instead of one period of the waveform. Defining $V(f) = \text{rect}(f/\phi)U(f)$, we obtain results such as

$$\int |V(f)|^2\, df = \int_\phi |U(f)|^2\, df$$

and

$$v(t) = \sum_n v(n\tau)\,\text{sinc}(\phi t - n),$$

leading to

$$\int |v(t)|^2\, dt = \tau \sum_n |v(n\tau)|^2,$$

corresponding to (4.11), (4.10), and (4.12) respectively, and to $u_n = \tau v(n\tau)$. Using these results in (2.27) gives:

$$\frac{1}{\tau}\sum_n |u_n|^2 = \int_\phi |U(f)|^2\, df$$

to obtain (as $\phi\tau = 1$) the equivalent of (4.14):

$$\sum_n |u_n|^2 = \frac{1}{\phi}\int_\phi |U(f)|^2\, df \tag{4.17}$$

If u is the sampled form of a pulse waveform s, so that $u(t) = \text{comb}_\tau\, s(t)$ and $U(f) = \phi\,\text{rep}_\phi\, S(f)$, we have, corresponding to (4.15),

$$\tau \sum_n |s(n\tau)|^2 = \int_\phi |\text{rep}_\phi\, S(f)|^2\, df \tag{4.18}$$

4.2.5 Note on Dimensions

In this section we justify the energy and power expressions in dimensional terms, as it is not always evident what forms the expressions represent. The notation here is that $[u]$ represents the dimension of a waveform, $[U]$ that of a spectrum, and $[T]$ and $[F]$ are the dimensions of time and frequency. We also use the symbol $\sim$ to mean "has the same dimension as." Thus, we have $[F] \sim [T]^{-1}$. We will also take, as a convention, $[u^2]$ to have the dimension of power so that $[u^2][T] \sim$ energy (as in Section 4.2.1).

From the definitions (1.3) and (1.4), we see that $[u] \sim [U][F]$ and $[U] \sim [u][T]$, then in (2.27) the left side has dimension $[u^2][T]$, or energy, and the right side has dimension $[U^2][F] \sim [u^2][t]^2[F] \sim [u^2][T]$, again an energy expression. Thus, this equation does equate the waveform and spectral energy for a finite energy waveform.

It is important to notice that for sampled waveforms and spectra, the samples, as δ-function strengths, do not have the same dimension as the sampled function. In (4.8), for example, we note that integrating over a frequency interval I_n including only the line at frequency nF, we have $\int_{I_n} U(f)df = U_n$ so that U_n has the dimension $[U][F]$ (*not* $[U]$). (In fact $[U_n] \sim [u]$.) Similarly, for a sampled waveform, we find that the samples u_n have dimension $[u][T]$, or $[U]$. We see that the left side of (4.14) has dimension $[u^2]$, or power, and so has the right side, given that $[U_n] \sim [u]$, as required. The left side of (4.17) has dimension $[U]^2/[T]$, and the right side has dimension $[U]^2[F]$, and these are both energy expressions, so this equation matches the energy in one period of the spectrum with the sum of the square magnitudes of the waveform samples divided by the sample interval. Finally, for the regularly sampled periodic function of Section 4.4.3, we see that the two sides of (4.59) have the dimension of energy, so this effectively equates the energy in one period of the waveform with that in one period of the spectrum.

4.3 Fourier Series of Real Functions Using Rules and Pairs

4.3.1 Fourier Series Coefficients

The rules-and-pairs method, as used here, is a fully complex method, giving the complex spectra of both real and complex waveforms. Thus, even for a real waveform, the waveform is expressed as a sum, or integral, of complex

exponential functions of the form $\exp 2\pi ift$. In general (though not necessarily), Fourier series analysis is applied to periodic real waveforms, which are expressed as sums of real functions (sines and cosines) with real coefficients. In this section, we show how these coefficients are obtained from the spectrum given by the rules-and-pairs method, in the case of periodic real waveforms, and in the following three sections examples are given for square, sawtooth, triangular, and rectified sinewave waveforms.

Given that u is periodic, with repetition interval T, the spectrum U is a comb function and so can be put in the form

$$U(f) = \sum_{n=-\infty}^{\infty} c_n \delta(f - nF) \tag{4.19}$$

where $F = 1/T$. The waveform can be expressed, from the inverse transform, as

$$u(t) = \sum_{n=-\infty}^{\infty} c_n \exp 2\pi inFt, \tag{4.20}$$

and we see that the coefficients c_n weight both the δ-functions in the spectrum and also the complex exponentials in the expansion of the waveform. We now want to express u as a Fourier series in the form

$$u(t) = a_0 + \sum_{n=1}^{\infty} (a_n \cos 2\pi nFt + b_n \sin 2\pi nFt) \tag{4.21}$$

as in (1.1), and now we need the coefficients a_0, a_n, and b_n. From (4.20) we have

$$u(t) = \sum_{n=-\infty}^{\infty} c_n e^{2\pi inFt} = \sum_{n=-\infty}^{\infty} c_n (\cos 2\pi nFt + i \sin 2\pi nFt)$$

$$= c_0 + \sum_{n=1}^{\infty} c_n (\cos 2\pi nFt + i \sin 2\pi nFt) + \sum_{n=1}^{\infty} c_{-n} (\cos 2\pi nFt - i \sin 2\pi nFt)$$

$$= c_0 + \sum_{n=1}^{\infty} (c_n + c_{-n}) \cos 2\pi nFt + i(c_n - c_{-n}) \sin 2\pi nFt$$

Now for real waveforms we have $U(-f) = U(f)^*$ for any frequency f (see (4.2.1)), so, in (4.19), $c_{-n} = c_n^*$ and

$$c_n + c_{-n} = c_n + c_n^* = 2\operatorname{Re} c_n$$

and

$$c_n - c_{-n} = c_n - c_n^* = 2i\operatorname{Im} c_n$$

so finally we have

$$u(t) = c_0 + \sum_{n=1}^{\infty} (2\operatorname{Re} c_n \cos 2\pi nFt - 2\operatorname{Im} c_n \sin 2\pi nFt) \qquad (4.22)$$

where c_0 is also real. Comparing (4.21) and (4.22) we have

$$a_0 = c_0, a_n = 2\operatorname{Re} c_n \text{ and } b_n = -2\operatorname{Im} c_n \qquad (4.23)$$

Thus, to find the Fourier series coefficients for a real periodic waveform, we obtain the spectrum U by the rules-and-pairs method, which gives the coefficients c_n, then use (4.23). This method is illustrated in the following sections.

4.3.2 Fourier Series of Square Wave

A square wave of period T is given by a regular train of rectangular pulses of length $T/2$, so can be represented in the form

$$u(t) = \operatorname{rep}_T \left(\operatorname{rect} \frac{2t}{T} \right) \qquad (4.24)$$

with transform

$$U(f) = F\operatorname{comb}_F \left(\frac{T}{2} \operatorname{sinc} \frac{fT}{2} \right) = \frac{1}{2} \operatorname{comb}_F \left(\operatorname{sinc} \frac{fT}{2} \right)$$

$$= \frac{1}{2} \sum_{n=-\infty}^{\infty} \operatorname{sinc} \frac{nFT}{2} \delta(f - nF) \qquad (4.25)$$

where $F = 1/T$. Now we note that

$$c_n = \frac{1}{2}\text{sinc}\frac{nFT}{2} = \frac{1}{2}\text{sinc}\frac{n}{2} \quad (n \in \mathbb{Z}) \tag{4.26}$$

$$= \frac{\sin(n\pi/2)}{n\pi} = (-1)^{(n-1)/2}\frac{1}{n\pi} \quad (n \text{ odd})$$

when n is odd, and is zero when n is even $(n \neq 0)$. (c_n is defined as in Section 4.3.1, such that $U(f) = \sum_{n=-\infty}^{\infty} c_n\delta(f - nF)$). As c_n is real, we have, from Section 4.3.1, $a_n = 2c_n = (-1)^{(n-1)/2}2/n\pi$ (n odd) or 0 (n even), and $b_n = 0$, for $n = 1$ to ∞, and we see also from (4.26) that $a_0 = c_0 = 1/2$, as expected, as this is the mean level of the waveform. Thus, the Fourier series for the square wave u is

$$u(t) = \frac{1}{2} + \frac{2}{\pi}\sum_{n=1}^{\infty}\frac{(-1)^{(n-1)/2}}{n}\cos 2\pi nFt, \tag{4.27}$$

agreeing with the result given by conventional Fourier analysis and obtained without using any integration.

This is for the case illustrated in Figure 4.2(a), where the pulse train is centered on zero, giving an even function, which would be expected to give an expansion in terms of even functions (i.e., cosines) only. It is interesting to take the case shown in Figure 4.2(b), where the function (apart from the mean level) is an odd function and should give a sine series only.

In this case, the pulses are offset by $T/4$, so the waveform is given by

$$v(t) = \text{rep}_T\left(\text{rect}\frac{(t - T/4)}{T/2}\right) \tag{4.28}$$

and its transform, using R6a, is

$$V(f) = F\text{comb}_F\left(\frac{T}{2}\text{sinc}\frac{fT}{2}\exp\frac{-2\pi if T}{4}\right) = \frac{1}{2}\text{comb}_F\left(\text{sinc}\frac{fT}{2}\exp\frac{-\pi if T}{2}\right)$$

$$= \frac{1}{2}\sum_{n=-\infty}^{\infty}\text{sinc}\frac{nFT}{2}\exp\frac{-\pi inFT}{2}\delta(f - nF) = \frac{1}{2}\sum_{n=-\infty}^{\infty}\text{sinc}\frac{n}{2}\exp\frac{-in\pi}{2}\delta(f - nF)$$
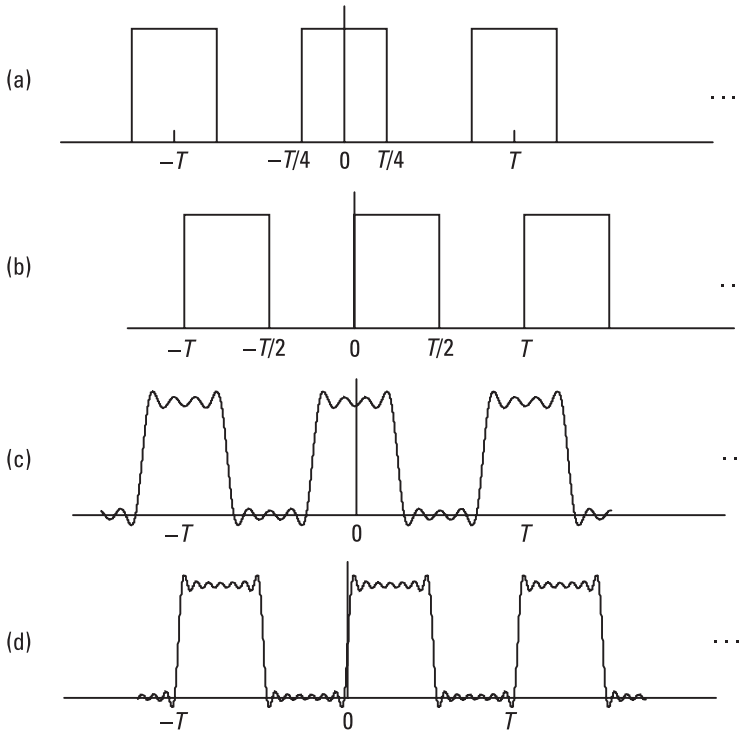
Figure 4.2   Square wave synthesis from Fourier series. Square wave with (a) pulse cen-
tered at time zero, (b) pulse starting at time zero; waveform formed using (c)
four terms of even series, and (d) seven term of odd series.

Thus we have $c_n = \dfrac{1}{2}\operatorname{sinc}\dfrac{n}{2}\exp\dfrac{-in\pi}{2} = \dfrac{1}{2}\dfrac{\sin n\pi/2}{n\pi/2}\left(-i\sin\dfrac{n\pi}{2}\right) = \dfrac{-i}{n\pi}$, for
n odd, and $c_n = 0$ for n even $(n > 0)$. In this case the Fourier series coefficients
are $a_0 = c_0 = 1/2$, $a_n = 2\operatorname{Re}c_n = 0$ $(n > 0)$, and $b_n = -2\operatorname{Im}c_n = 2/n\pi(n$ odd$)$.
Thus, the Fourier series for this square wave is

$$v(t) = \frac{1}{2} + \frac{2}{\pi}\sum_{n=1}^{\infty}\frac{1}{n}\sin 2\pi nFt \quad (n \text{ odd}) \tag{4.29}$$

The approximations to the square waves, taking the constant term plus
the first N sinusoidal terms using these series for u and v, are given in Figure
4.2(c) (for $N = 4$, or $n = 1$ to 7) and (d) ($N = 7$).
    For a regular pulse train (centered on zero in this case) with a duty ratio
r ($r < 1$), the pulses are of length rT and the waveform is given by

$$u(t) = \mathrm{rep}_T \left(\mathrm{rect} \, \frac{t}{rT} \right) \tag{4.30}$$

The spectrum is

$$U(f) = F\mathrm{comb}_F\,(rT \sin c \, frT) = r\mathrm{comb}_F\,(\mathrm{sinc} frT)$$

$$= r \sum_{n=-\infty}^{\infty} \mathrm{sinc}(rnFT)\delta(f - nF) = r \sum_{n=-\infty}^{\infty} \mathrm{sinc}(rn)\delta(f - nF) \tag{4.31}$$

Thus, $a_0 = c_0 = r$, $c_n = \dfrac{\sin rn\pi}{n\pi}$, $a_n = 2\,\mathrm{Re}\,c_n = \dfrac{2\sin rn\pi}{n\pi}$, and $b_n = 0$. We note the value of the constant term is r, the mean level, as expected. Putting $r = 1/2$ gives the square wave case.

4.3.3   Fourier Series of Sawtooth

A sawtooth waveform of period T, of amplitude 2, mean level zero, and centered at the time origin is shown in Figure 4.3(a). This is an odd function, so its Fourier series will be given by a sum of sinewaves only. This waveform can be represented in the form

$$u(t) = \mathrm{rep}_T \left(\mathrm{ramp}\!\left(\frac{t}{T} \right) \right) \tag{4.32}$$

where we define $\mathrm{ramp}(x) = 2x\mathrm{rect}(x)$, as in Section 7.3 in Chapter 7, where this function is discussed further, and is illustrated in Figure 7.2. The transform, using the pair given in (7.18) is given by

$$U(f) = F \, \mathrm{comb}_F\,(iT \, \mathrm{snc}_1 \, fT) = i \sum_{n=-\infty}^{\infty} \mathrm{snc}_1(nFT)\delta(f - nF)$$

where $F = 1/T$ and $\mathrm{snc}_1 x = d(\mathrm{sinc}\,x)/\pi dx$ (see (7.17)). As $\mathrm{snc}_1 0 = 0$ we have $a_0 = c_0 = 0$, and as c_n is imaginary we have $a_n = 0$, and

$$b_n = -2\,\mathrm{Im}\,c_n = -2\,\mathrm{snc}_1\,n = \frac{2(-1)^{n+1}}{n\pi} \quad (n > 0) \tag{4.33}$$
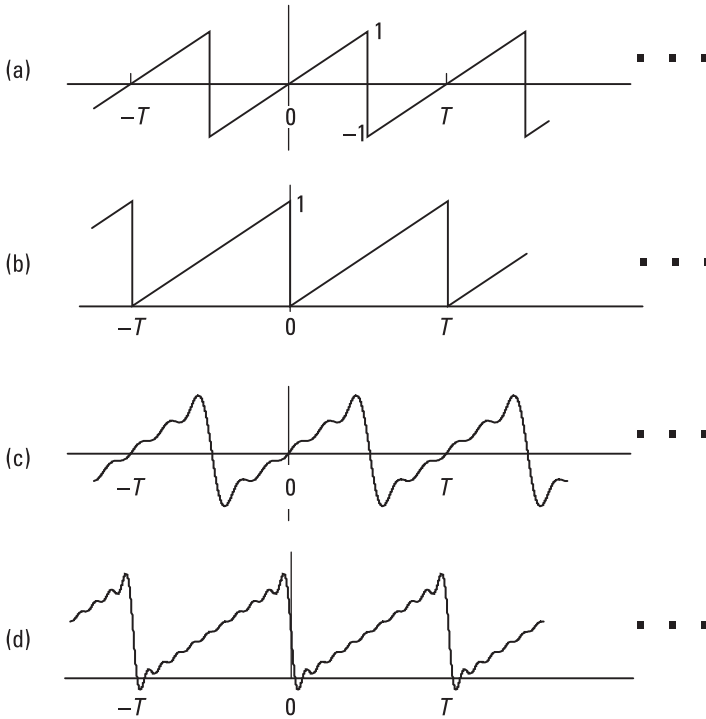
Figure 4.3 Sawtooth wave synthesis from Fourier series. Sawtooth (a) centered at time zero, (b) with ramp starting at time zero; waveform formed using (c) five terms, and (d) ten terms.

(From (7.20) we have $\mathrm{snc}_1 n = (\cos\pi n - \mathrm{sinc} n)/n\pi = (-1)^n/n\pi$ $(n > 0)$.) The Fourier series for the sawtooth u is thus

$$u(t) = \frac{2}{\pi}\sum_{n=1}^{\infty}(-1)^{n+1}\frac{\sin 2\pi nFt}{n} = \frac{2}{\pi}\left(\sin 2\pi Ft - \frac{\sin 4\pi Ft}{2} + \frac{\sin 6\pi Ft}{3} - \cdots\right)$$

(4.34)

The sawtooth shown in Figure 4.3(b) is given by

$$v(t) = \frac{1}{2} + \frac{1}{2}\mathrm{rep}_T\left(\mathrm{ramp}\left(\frac{t - T/2}{T}\right)\right)$$

(4.35)

and after Fourier transforming as before we have

$$c_n = i\,\mathrm{snc}_1\,n\exp(-in\pi)/2 = i(-1)^n\,\mathrm{snc}_1\,n/2 = i/2n\pi$$

(using $\text{snc}_1 n$ from earlier). Thus, $a_0 = c_0 = 1/2$, $a_n = 2\,\mathrm{Re}\,c_n = 0$, and $b_n = -2\,\mathrm{Im}\,c_n = -1/n\pi$. In this case, the sawtooth is given by

$$v(t) = \frac{1}{2} - \frac{1}{\pi} \sum_{n=1}^{\infty} \frac{\sin 2\pi nFt}{n} \tag{4.36}$$

The approximate sawtooth waveforms obtained by taking terms up to $n = 5$ in (4.34) and $n = 10$ in (4.36) are shown in Figure 4.3(c) and (d), respectively.

4.3.4   Fourier Series of Triangular Waves

The symmetrical triangular wave shown in Figure 4.4(a), with period T, can be written

$$u(t) = \text{rep}_T \, \text{tri}\!\left(\frac{t}{T/2}\right) \tag{4.37}$$

where the function tri(x) is defined in (3.6). From R5 and P4 the transform is
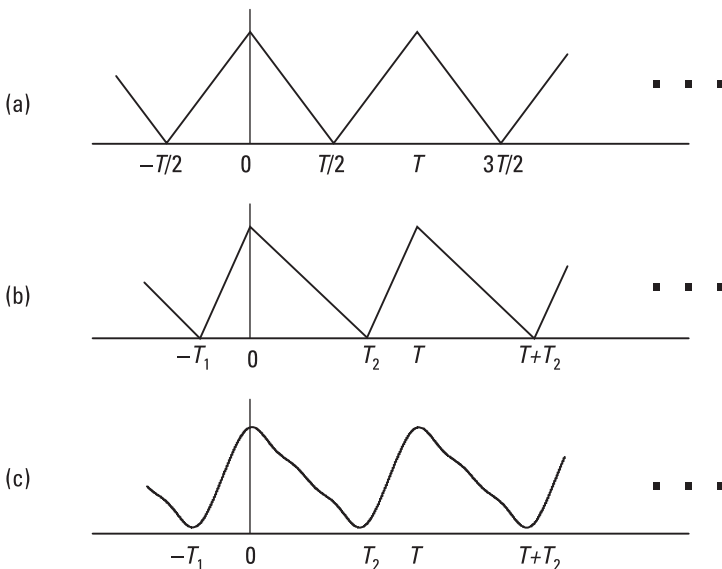
Figure 4.4   Triangular waves. (a) Symmetric, (b) asymmetric, and (c) asymmetric wave synthesized using four terms.

$$U(f) = F \operatorname{comb}_F \left(\frac{T}{2} \operatorname{sinc}^2 \frac{fT}{2} \right) = \frac{1}{2} \sum_{n=-\infty}^{\infty} \operatorname{sinc}^2 \frac{n}{2} \delta(f - nF) \quad (4.38)$$

Thus, $c_n = \frac{1}{2} \operatorname{sinc}^2 \frac{n}{2}$, so $a_0 = \frac{1}{2}$, $a_n = 2 \operatorname{Re} c_n = \left(\frac{\sin(n\pi/2)}{n\pi/2} \right)^2$, or $\left(\frac{2}{n\pi} \right)^2$ for n odd and 0 for n even, and $b_n = 0$ for all n. In this case the Fourier series coefficients are found very directly, without integration, by the rules-and-pairs method.

For the asymmetrical triangular wave, shown in Figure 4.4(b), we can use the asymmetric triangular pulse of Section 3.5 (with peak at $t = 0$) formed as the differences of two step functions convolved with different width rect pulses. Taking this pulse, the triangular wave is given by

$$u(t) = \operatorname{rep}_T \left(v(t) \right)$$

where $v(t)$ is given in (3.13), and this has the transform given in (3.12), so that the spectrum of the triangular wave of Figure 4.4(b) is given by

$$U(f) = F \operatorname{comb}_F \left(\frac{\operatorname{sinc}(fT_1)e^{\pi i f \tau_1} - \operatorname{sinc}(fT_2)e^{-\pi i f \tau_2}}{2\pi i f} \right)$$

$$= -i \sum_{n=-\infty}^{\infty} \frac{\operatorname{sinc} nFT_1 e^{\pi i n F \tau_1} - \operatorname{sinc} nFT_2 e^{-\pi i n F \tau_2}}{2\pi n} \delta(f - nF)$$

$$= -i \sum_{n=-\infty}^{\infty} \frac{\operatorname{sinc} nr_1 e^{\pi i n r_1} - \operatorname{sinc} nr_2 e^{-\pi i n r_2}}{2\pi n} \delta(f - nF) \quad (4.39)$$

where $r_k = T_k/T = FT_k$ (so $r_1 + r_2 = 1$ as $T_1 + T_2 = T$).

To first order, as $n \to 0$ (for n real), we have

$$c_0 = \lim_{n \to 0} \left(\frac{-i}{2\pi n} (1 + \pi i n r_1 + \ldots - (1 - \pi i n r_2 + \ldots) \right) = \lim_{n \to 0} \frac{\pi n(r_1 + r_2)}{2\pi n} = \frac{1}{2}$$

so $a_0 = c_0 = 1/2$, as expected. Also,

$$a_n = 2 \operatorname{Re} c_n = \frac{\operatorname{sinc} nr_1 \sin \pi n r_1 + \operatorname{sinc} nr_2 \sin \pi n r_2}{n\pi} \quad (4.40)$$

$$= r_1 \operatorname{sinc}^2 nr_1 + r_2 \operatorname{sinc}^2 nr_2$$

and

$$b_n = -2\operatorname{Im} c_n = \frac{\operatorname{sinc} nr_1 \cos \pi nr_1 - \operatorname{sinc} nr_2 \cos \pi nr_2}{n\pi} \qquad (4.41)$$

Except for certain particular values of r_1 and r_2, these expressions do not simplify further. Using these coefficients up to $n = 4$ with $r_1 = 0.3$ and $r_2 = 0.7$ gives the waveform shown in Figure 4.4(c).

If we put $r_1 = r_2 = 0.5$ (giving the symmetrical case) then we find

$$a_n = \frac{1}{2}\operatorname{sinc}^2 \frac{n}{2} + \frac{1}{2}\operatorname{sinc}^2 \frac{n}{2} = \operatorname{sinc}^2 \frac{n}{2}$$

and $b_n = 0$, which are the coefficients for the symmetric triangular wave found earlier. Also, if we put $r_1 = 1$ and $r_2 = 0$, we have $\operatorname{sinc} nr_1 = 0$, so that $a_n = 0$ ($n > 0$), and $\operatorname{sinc} nr_2 = 1$, so that $b_n = -1/n\pi$, as found in Section 4.3.3 for the sawtooth waveform of Figure 4.3(b).

We could, alternatively, form the asymmetric triangular pulse as the difference of two ramp functions. In this case, we define the wave shown in Figure 4.4(b) by

$$u(t) = \frac{1}{2}\big(1 + v(t)\big)$$

where

$$v(t) = rep_T\left(\operatorname{ramp}\left(\frac{t + T_1/2}{T_1}\right) - \operatorname{ramp}\left(\frac{t + T_2/2}{T_2}\right)\right)$$

(We note that $v(t)$ ranges from -1 to $+1$ so $u(t)$ ranges from 0 to 1, as required.) Following through the analysis, using the pair $\operatorname{ramp} x \Leftrightarrow i \operatorname{snc}_1 y$, gives

$$a_n = 2\operatorname{Re} c_n = -(r_1 \operatorname{snc}_1 nr_1 \sin \pi nr_1 + r_2 \operatorname{snc}_1 nr_2 \sin \pi nr_2)$$

$$b_n = -2\operatorname{Im} c_n = r_2 \operatorname{snc}_1 nr_2 \cos \pi nr_2 - r_1 \operatorname{snc}_1 nr_1 \cos \pi nr_1$$

Putting $\operatorname{snc}_1 x = (\cos \pi x - \operatorname{sinc} x)/\pi x$, and using $r_1 + r_2 = 1$, we can show that these expressions for a_n and b_n reduce to those in (4.40) and (4.41).

4.3.5   Fourier Series of Rectified Sinewaves

We consider first the half-wave rectified waveform, shown in Figure 4.5(a). This can be represented as a repetitive form of the first half-cycle of the sine-wave, obtained by gating. Thus, for a sinewave of frequency F and period $T = 1/F$ this waveform is given by

$$u_{\frac{1}{2}}(t) = \text{rep}_T \left\{ \sin 2\pi Ft \, \text{rect}\left(\frac{t - T/4}{T/2} \right) \right\} \tag{4.42}$$

with transform

$$U_{\frac{1}{2}}(f) = F\,\text{comb}_F \left(\frac{\delta(f-F) - \delta(f+F)}{2i} \otimes \frac{T}{2}\text{sinc}\frac{fT}{2} e^{-2\pi i f T/4} \right) \tag{4.43}$$
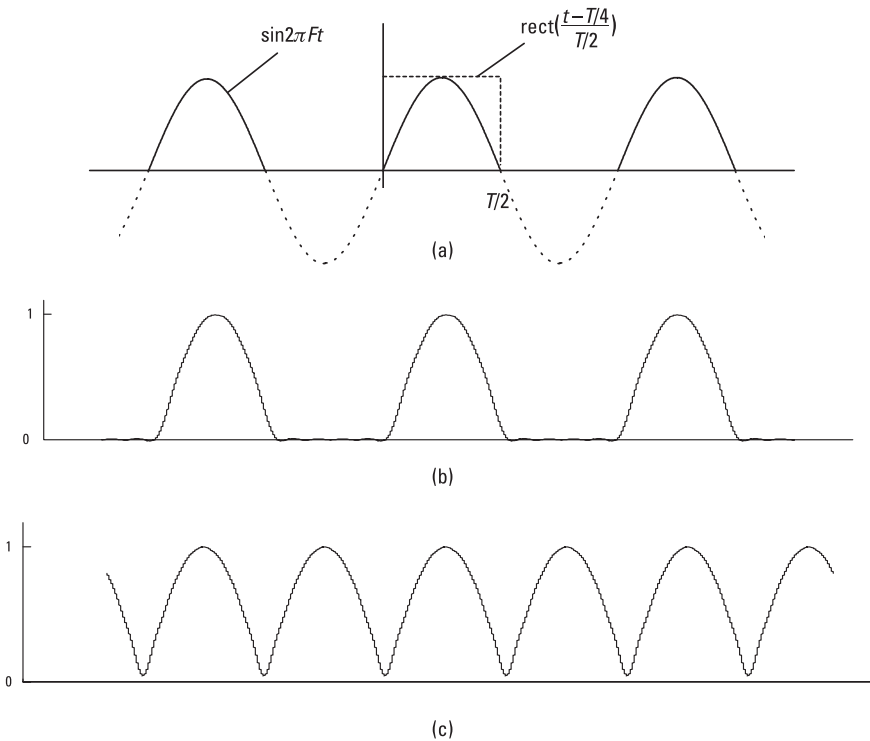
Figure 4.5   Rectified sinewaves. (a) Half-wave rectified sinewave, (b) half-time rectified sinewave synthesized using four cosine terms, and (c) full-wave rectified sinewave synthesized using seven cosine terms.

(We have used P8b, P3a, R8b, R7a, R5, and R6a.) Performing the convolutions with the δ-functions, we obtain

$$U_{1/2}(f) = \frac{-i}{4}\text{comb}_F\left(\text{sinc}\frac{(f-F)T}{2}e^{-2\pi i(f-F)T/4}\right.$$
$$\left. -\text{sinc}\frac{(f+F)T}{2}e^{-2\pi i(f+F)T/4}\right)$$

Writing out the comb function (defined in (2.19)) we obtain (using $FT = 1$)

$$U_{1/2}(f) = \frac{-i}{4}\sum_{-\infty}^{\infty}\left(\text{sinc}\frac{(n-1)}{2}e^{-\pi i(n-1)/2}-\text{sinc}\frac{(n+1)}{2}e^{-\pi i(n+1)/2}\right)\delta(f-nF)$$

Thus, the coefficients c_n (putting $\exp(\pi i/2) = i$) are given by

$$c_n = \frac{(-i)^n}{4}\left(\text{sinc}\frac{(n-1)}{2}+\text{sinc}\frac{(n+1)}{2}\right)$$

Then,

$$a_0 = c_0 = \frac{1}{2}\text{sinc}\frac{1}{2} = \frac{\sin(\pi/2)}{2(\pi/2)} = \frac{1}{\pi} \tag{4.44}$$

We note c_n is real for n even and imaginary for n odd, so, putting $n = 2m$,

$$a_{2m} = 2\,\text{Re}\,c_{2m} = \frac{(-1)^m}{2}\left(\frac{\sin(2m-1)\pi/2}{(2m-1)\pi/2}+\frac{\sin(2m+1)\pi/2}{(2m+1)\pi/2}\right)$$

Noting $\sin(2m-1)\pi/2 = (-1)^{m+1}$ and $\sin(2m+1)\pi/2 = (-1)^m$, we obtain

$$a_{2m} = \frac{1}{\pi}\left(\frac{-1}{2m-1}+\frac{1}{2m+1}\right) = \frac{-2}{\pi(4m^2-1)} \tag{4.45}$$

For n odd we see that $(n-1)/2$ and $(n+1)/2$ are integers so that (by sinc property 1) $\text{sinc}(n-1)/2 = \text{sinc}(n+1)/2 = 0$, except for $n = 1$, so we have

$$b_1 = -2\,\mathrm{Im}\,c_1 = 1/2 \text{ and } b_n = 0 \ (n \text{ odd}, \ n > 1) \tag{4.46}$$

We can now write the Fourier series of the half-wave rectified sinewave using (4.44), (4.45), and (4.46), as

$$u_{\frac{1}{2}}(t) = \frac{1}{\pi} + \frac{1}{2}\sin 2\pi Ft - \frac{2}{\pi}\sum_{m=1}^{\infty}\frac{\cos 4\pi mFt}{(4m^2 - 1)} \tag{4.47}$$

The half-wave rectified waveform of (4.42), generated using only four cosine terms is shown in Figure 4.5(b), with slight rounding of the corners at the edges of the half-cycles, and a little residual ripple. If we had begun with a cosine waveform, and gated a half-cycle centered on $t = 0$, the expressions would have been simpler (with no exponential factors) and, being a symmetrical function, there would be only cosine contributions, as the reader might confirm.

The full-wave rectified waveform is based on the same gated half-cycle as the half-wave, but repeated at intervals $T/2$, so is given by

$$u_1(t) = \mathrm{rep}_{T/2}\left(\sin 2\pi Ft\,\mathrm{rect}\left(\frac{t - T/4}{T/2}\right)\right) \tag{4.48}$$

and its spectrum is

$$U_1(f) = 2F\,\mathrm{comb}_{2F}\left(\frac{\delta(f - F) - \delta(f + F)}{2i} \otimes \frac{T}{2}\mathrm{sinc}\frac{fT}{2}e^{-2\pi ifT/4}\right) \tag{4.49}$$

which leads to

$$U_1(f) = \frac{-i}{2}\sum_{-\infty}^{\infty}\left(\mathrm{sinc}\frac{(2n-1)}{2}e^{-\pi i(2n-1)/2} - \mathrm{sinc}\frac{(2n+1)}{2}e^{-\pi i(2n+1)/2}\right)$$
$$\delta(f - 2nF),$$

and we see that the spectrum contains frequencies that are only multiples of $2F$. Putting $\exp(\pi i/2) = i$ and $\exp(\pi i) = -1$, the coefficients of the complex spectrum are

$$c_{2n} = \frac{(-1)^n}{2}\left(\mathrm{sinc}\frac{(2n-1)}{2} + \mathrm{sinc}\frac{(2n+1)}{2}\right) \tag{4.50}$$

Thus,

$$a_0 = c_0 = \mathrm{sinc}\,\frac{1}{2} = \frac{\sin(\pi/2)}{(\pi/2)} = \frac{2}{\pi} \tag{4.51}$$

and

$$a_{2n} = \frac{(-1)^n}{2}\left(\frac{\sin(2n-1)\pi/2}{(2n-1)\pi/2} + \frac{\sin(2n+1)\pi/2}{(2n+1)\pi/2}\right) = \frac{(-1)^n}{\pi}\left(\frac{(-1)^{n+1}}{2n-1} + \frac{(-1)^n}{2n+1}\right)$$

$$= \frac{-2}{\pi(4n^2 - 1)} \tag{4.52}$$

As the coefficients c_{2n} are real, $b_{2n} = 0$ for all n, and the Fourier series for this waveform is

$$u_1(t) = \frac{2}{\pi} - \frac{2}{\pi}\sum_{n=1}^{\infty}\frac{\cos 4\pi nFt}{4n^2 - 1} \tag{4.53}$$

The full-wave rectified waveform of (4.53) using seven cosine terms is shown in Figure 4.5(c). The sharp corners between successive half-cycles are slightly rounded, in this approximation.

4.4 Discrete Fourier Transforms

4.4.1 General Discrete Waveform

In Section 4.4, we see how we can use the rules-and-pairs technique to understand the spectra of discrete time waveforms, leading in particular to the DFT and realized in practice in the FFT. The waveforms are finite data sets of values taken at specific instants—discrete points in time—and may be samples from a known function or may be a set of experimental values, for which the underlying, or implicit, function is not known.

As usual, we need first to express the data as a function of time. As this function has nonzero values only at discrete points in the time domain, it is represented by δ-functions at these points. (Thus, the function is in fact a generalized function, as discussed in Section 1.4 in Chapter 1.) Initially we

take the most general case where we have N data values s_n taken at N instants t_n, and we write the waveform function as

$$s(t) = \sum_{n=1}^{N} s_n \delta(t - t_n) \qquad (4.54)$$

The spectrum is given (from P1b, R6a) by

$$S(f) = \sum_{n=1}^{N} s_n \exp(-2\pi i f t_n) \qquad (4.55)$$

Given the data set $\{(s_n, t_n) : n = 1 \text{ to } N\}$, we can evaluate (4.55) for any frequency. If the times t_n are irregular (in particular, if the intervals are not rationally related), then there is no definite structure to S, which is an infinite spectrum (i.e., there are no frequency values, positive or negative, beyond which the spectrum is zero). In general any finite waveform has an infinite spectrum, as shown in Appendix 4A. Furthermore, the spectrum does not die away as $f \to \pm\infty$, but maintains the same general level, averaged over a sufficient interval. Figures 4.6(a) and (b) show an example of a finite discrete waveform and its spectrum. (The modulus of the complex spectrum is plotted.) We note that the waveform, consisting of δ-functions, has infinite energy and so also has the spectrum. However, the infinite spectrum would only be needed to reconstitute the waveform s perfectly. If we limited the spectrum to the frequency range $-F/2$ to $F/2$, we see, by taking $S'(f) = S(f)\,\text{rect}\,f/F$, that this gives the waveform $s'(t) = s(t) \otimes F \,\text{sinc}\,t/T$ (putting $T = 1/F$), shown in Figure 4.6(c). The δ-functions are replaced by sinc functions, which could be an acceptable approximation if these were narrow enough (i.e., if T, which defines their width, were small compared with the separation of the closest samples). In this example, F is 15 times the reciprocal of the mean separation, which is one time unit, so T is one fifteenth the mean separation of the samples. If the samples were uniformly spaced this would give a spectrum repeating at intervals of one frequency unit. Clearly, the approximation will become better as the amount of spectral energy within the gate increases. In this case, both the spectrum and the waveform have finite energy. If we took a triangular spectral window, with a sinc^2 transform, the sidelobe levels would be lower. This can be seen by running the program Fig406. We note that the power spectrum (or the modulus of the amplitude, as plotted here) will be essentially the same wherever the gate is placed; the effect of shifting the gate from the frequency origin is to apply a progressive phase factor (by R6b),

(a)

(b)

(c)
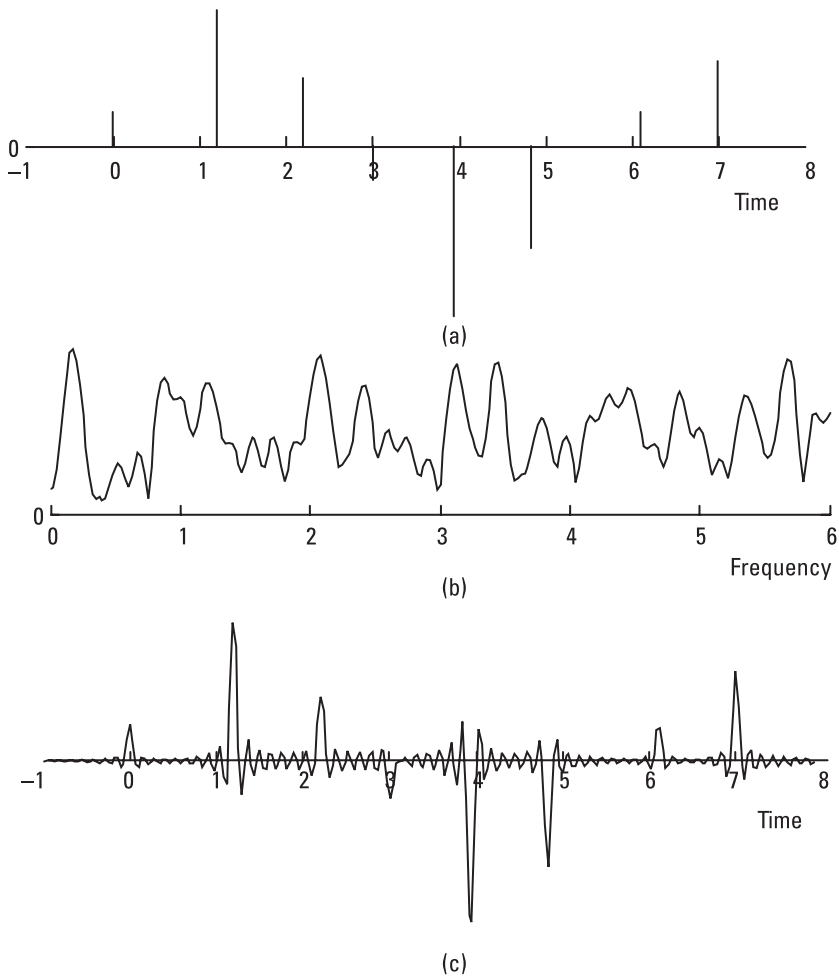
Figure 4.6   Spectrum and waveforms of general finite discrete time series. (a) Finite ir-
regular time series, (b) infinite spectrum, and (c) waveform of gated spectrum.

which will have no substantial effect on the peaks, though the sidelobe details
will change with the sidelobe patterns from the peaks interfering differently.

Another example of a transform of a discrete function of this kind is
given in Chapter 8, applied to the case of an irregular linear array of antennas.
The samples, in this case taken in space rather than in time, are of a finite, or
gated, sinc function, giving a (nearly) rectangular response in the transform
domain, near the origin (Figure 8.10(a)). However we see that the response
is not strictly periodic, because of the irregular spacing of the samples, which

are roughly regularly spaced in this example (i.e., the elements are slightly displaced randomly form regular positions), with "repetitions" becoming more degraded on moving further away from the origin.

4.4.2 Transform of Regular Time Series

In this case we take the data to be from N samples spaced in time at equal intervals τ, so, taking the time relative to the first sample, the waveform is given by

$$s(t) = \sum_{n=0}^{N-1} s_n \delta(t - n\tau) \tag{4.56}$$

The spectrum is given by

$$S(f) = \sum_{n=0}^{N-1} s_n \exp(-2\pi i n f \tau) \tag{4.57}$$

We see that the exponentials in (4.57) are unchanged on replacing f by $f + \phi$, where $\phi = 1/\tau$, so that $S(f) = S(f + \phi)$ (i.e., S is periodic in the *frequency* domain) at intervals ϕ. It follows, from the orthogonality of the complex exponential functions over one period, (i.e., $\int_{I_\phi} \exp(2\pi i n f / \phi) \exp(-2\pi i m f / \phi) df = \phi \delta_{nm}$, where δ_{nm} is the Kronecker-δ), that

$$s_n = \frac{1}{\phi} \int_{I_\phi} S(f) \exp(2\pi i n f \tau) df \tag{4.58}$$

where I_ϕ is an interval of length ϕ, the repetition period. By comparing (4.57) and (4.58) with the Fourier series expressions (using complex exponentials) in (4.1) through (4.3), we see that these equations represent what may be called an inverse Fourier series (finite, in this case). In the case of the Fourier series (4.1), we expand a periodic waveform as a series of complex exponentials, the spectrum being a set of δ-functions whose strengths are the coefficients of the series (which may be finite or infinite). In the case of the discrete time series, we find that this series gives the coefficients of the expansion of the periodic spectrum as a series of complex (negative) exponentials. In the first case, the exponentials are functions of time, and in the second case (equation (4.57)) they are functions of frequency. These two cases are illustrated diagrammatically in Figure 4.7.

(a)

(b)
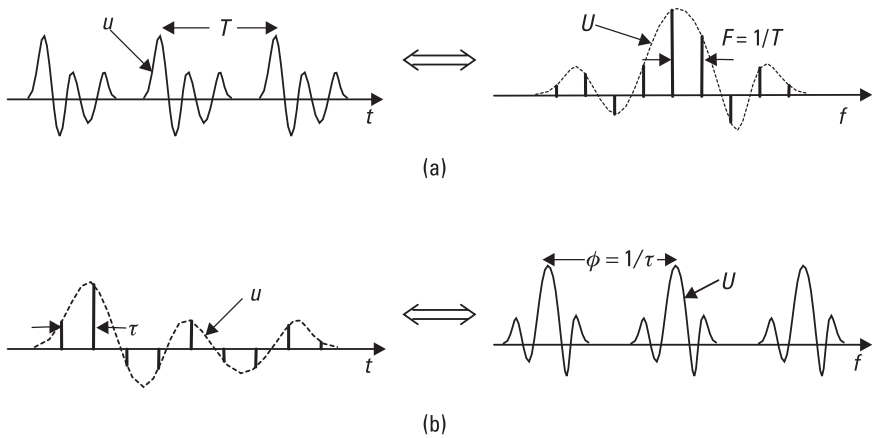
Figure 4.7   (a) Fourier series and (b) "inverse" Fourier series (transform of discrete waveform).

If we were given a periodic spectrum S (one cycle being sufficient to define it) and wanted to find out what time series this spectrum represented, our procedure would depend on how S is presented. If it has the form of a repeated known function, expressible in terms of functions in the table of Fourier transform pairs, then we could use the rules-and-pairs method as in Section 4.2 (using the inverse transform). If it were given only as a set of values, then one approach would be to carry out the integral in (4.58) numerically, over any interval of one period I_ϕ. However, a more satisfactory alternative is given in the next section.

4.4.3   Transform of Sampled Periodic Spectrum

In the last section the question arose of how to define a continuous spectrum, such as S in (4.58), which is not described by a known function. The only obvious solution is to specify it by a set of values taken across the spectrum, and most suitably by equally spaced samples. This gives an approximation but could, in principle, be made as accurate as required by sampling finely enough. If we choose the spectral sampling interval F so that there is an integral number N of these intervals in one spectral period ϕ, then the samples will occur at the same relative points in each period, as illustrated in Figure 4.8. (See Appendix 4B. It is also shown there that, with this condition, rep and comb are commutative.) In this case, we only need these N values to represent the spectrum in sampled form.
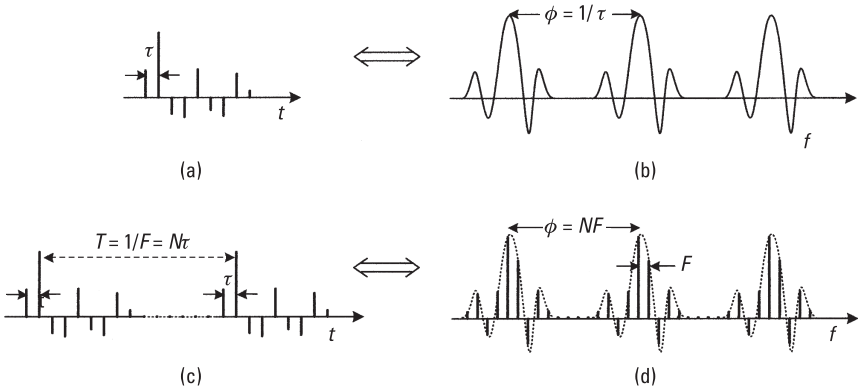
Figure 4.8   Discrete waveforms and spectra.

Let S' be the sampled form of S, then we have

$$S'(f) = \text{comb}_F\, S(f) \tag{4.59}$$

with inverse transform

$$s'(t) = T\,\text{rep}_T\, s(t) \tag{4.60}$$

where $T = 1/F$. We see that the regularly sampled form of S is actually the spectrum of a repeated form of the regular time series s, Figure 4.8(c). We also see that the original finite series waveform $s(t)$ is obtained correctly as one period of $s'(t)/T$.

Putting $\phi = NF$, with N an integer, we also find, taking reciprocals, that $\tau = T/N$, so that there are N time sample intervals in the repetition period T. Then, expanding the comb function, (4.59) gives

$$S'(f) = \sum_{m=-\infty}^{\infty} S(mF)\delta(f - mF) = \sum_{m=-\infty}^{\infty} S_m\delta(f - mF)$$

where $S_m = S(mF)$ are the strengths of the δ-functions in the comb (or sampled) form of S. From (4.57) we have

$$S_m = S(mF) = \sum_{n=0}^{N-1} s_n \exp(-2\pi inmF\tau)$$

Using $F\tau = FT/N = 1/N$ we have

$$S_m = \sum_{n=0}^{N-1} s_n \exp(-2\pi inm/N) \quad (m = 0 \text{ to } N-1) \qquad (4.61)$$

As remarked earlier, we only need the N values of S_m within one period of S, as these will be the same in other periods. (We see from (4.61) that $S_{m+kN} = S_m$ for all integers k, using $\exp(2\pi ikn) = 1$, with k and n integer.) In principle we could take any N successive values of m to define a period of S, but it seems most satisfactory to begin at zero frequency, with $m = 0$.

The inverse transform is given by

$$s_n = \frac{1}{N} \sum_{m=0}^{N-1} S_m \exp(2\pi imn/N) \qquad (4.62)$$

This can be shown by a similar approach or quite easily by the matrix representation of Section 4.4.6 in (4.67).

Two comments may be made on (4.61) and (4.62). First, if we prefer to number the time and frequency samples as 1 to N, rather than 0 to $N-1$, but make the first sample correspond to the zero time or zero frequency sample, respectively, then the mn product in the exponentials is replaced by $(m-1)(n-1)$. Second, if the number of time samples n_t in the given data set is less than N, the desired number of samples in one spectral period, then we add $N - n_t$ zero values to make up the number. This is not an arbitrary choice but follows from the inverse transform. If the continuous spectrum of the single discrete waveform $s(t)$, of length n_t samples, is sampled at rate $F = \phi/N$, the inverse transform of this sampled spectrum gives a repeated waveform, with repetitions at intervals of N samples, and hence there must be $N - n_t$ zero values in between.

The derivation of (4.62), other than from the matrix form of the transform and its inverse, is similar to that of (4.61) but a little more complex. We provide it here for interest. As the sampled form S' of the spectrum S is also periodic, we can put, from (4.58),

$$s_n' = \frac{1}{\phi} \int_{I_\phi} S'(f) \exp(2\pi inf\,\tau) df$$

where I_ϕ is a frequency interval of length ϕ. We now substitute for S' using (4.59), putting S_m for $S(mF)$, taking the interval to include $m = 0$ to $m = N - 1$, and, using the δ-function property given in (2.10),

$\int \exp(2\pi imf\,\tau)\delta(f - nF)df = \exp(2\pi imnF\tau)$ (where the range of integration includes the δ-function, as here) to obtain

$$s'_n = \frac{1}{\phi} \sum_{m=0}^{N-1} S_m \exp(2\pi imnF\tau)$$

Then, from (4.60), we have, using $\phi T = NFT = N$ and $F\tau = FT/N = 1/N$ again,

$$s_n = s'_n/T = \frac{1}{\phi T} \sum_{m=0}^{N-1} S_m \exp(2\pi imnF\tau) = \frac{1}{N} \sum_{m=0}^{N-1} S_m \exp(2\pi imn/N)$$

and this is (4.62).

4.4.4 Fast Fourier Transform

At first sight it appears in (4.61) that many coefficients (approaching $N^2/2$) are required to give all the S_m from the data values s_n. In fact, as $\exp 2\pi i = 1$, we could take integer multiples of N from the product mn and replace mn by $mn \bmod N$. This leaves only N distinct values for the coefficients. However, there are still N^2 products of data samples with coefficients in (4.61), which may be very large for a DFT of large order (given by N). Fast DFT algorithms (FFTs) take advantage of any available factorization of N to order the multiplications efficiently to reduce the number required. (In the limit, when N is a power of 2 only, say 2^k, this is reduced to Nk, a reduction by a factor of over 100 when k is 10.)

The MATLAB function *fft* for the transform of order N gives the values of S_m, for m from 0 to $N-1$, which shows a whole period beginning at zero frequency (the constant, or DC component). However, if it is preferred to show the spectrum centered near zero frequency, the program *fftshift* shifts the solution given by *fft* by half a period of the periodic spectrum to give a solution equivalent to a single period centered on zero frequency. Thus the first half is moved forward half a period and the second half moved back, to give the solution centered on zero. This is illustrated in Figure 4.9. When N is even (Figure 4.9(a)) the values of $m = 0$ to $N/2 - 1$ are moved ahead of the values $N/2$ to $N - 1$. These last values, because of the periodicity of the spectrum (over N frequency intervals) are the same as the values from $-N/2$ to -1, so we now have values for one period from $-N/2$ to $N/2 - 1$, as il-
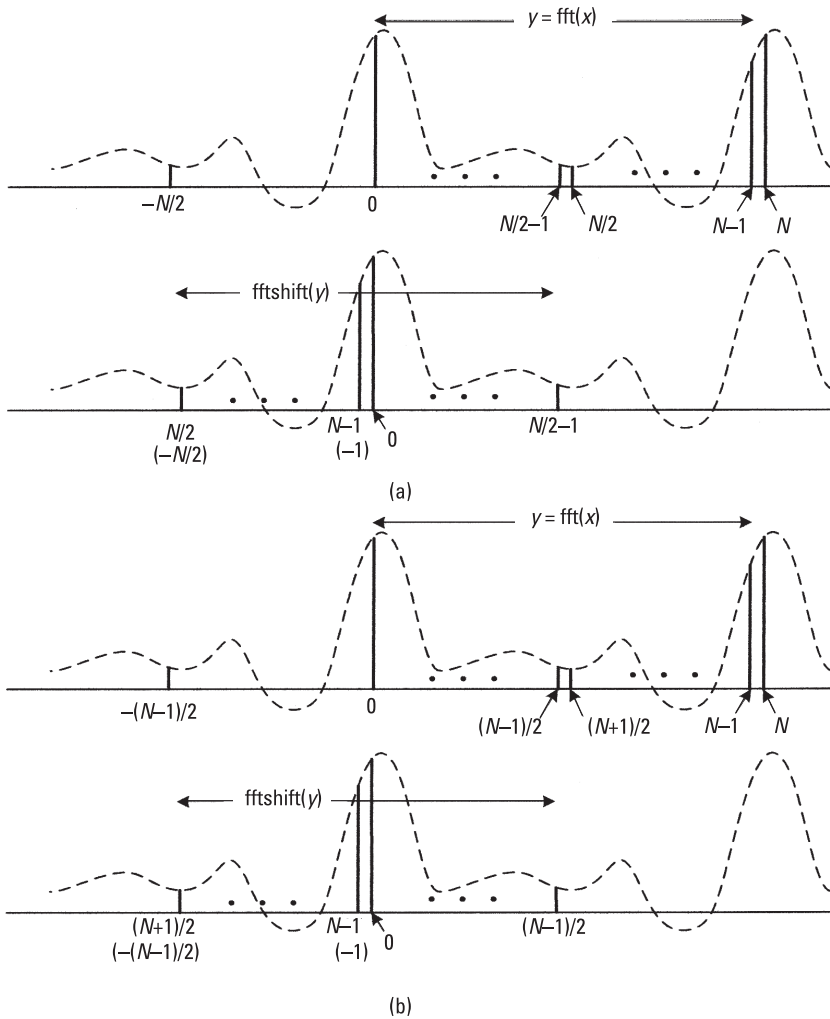
Figure 4.9 Use of *fftshift* to center spectrum near zero. (A) *N* even, and (b) *N* odd.

lustrated. When N is odd (Figure 4.9(b)) the first element is for the m value $(N+1)/2$, which is equivalent, on subtracting N, to $-(N-1)/2$.

4.4.5   Examples Illustrating the FFT and DFT

To illustrate these ideas and expressions, in this section we take the case of a symmetric triangular pulse with a low-order DFT. The pulse is shown, as

the real time series [0 1 2 3 2 1 0 0 0], in Figure 4.10(a), with its spectrum in Figure 4.10 (b). The FFT order is 9, and this is the length of the vectors of the time series and the spectral coefficients. First we note that the spectrum has the symmetric real part and antisymmetric imaginary part given by a real waveform. Also, from (4.61), the FFT gives $S_0 = \sum_{n=0}^{N-1} s_n$, which is seen to be 9 in this case.
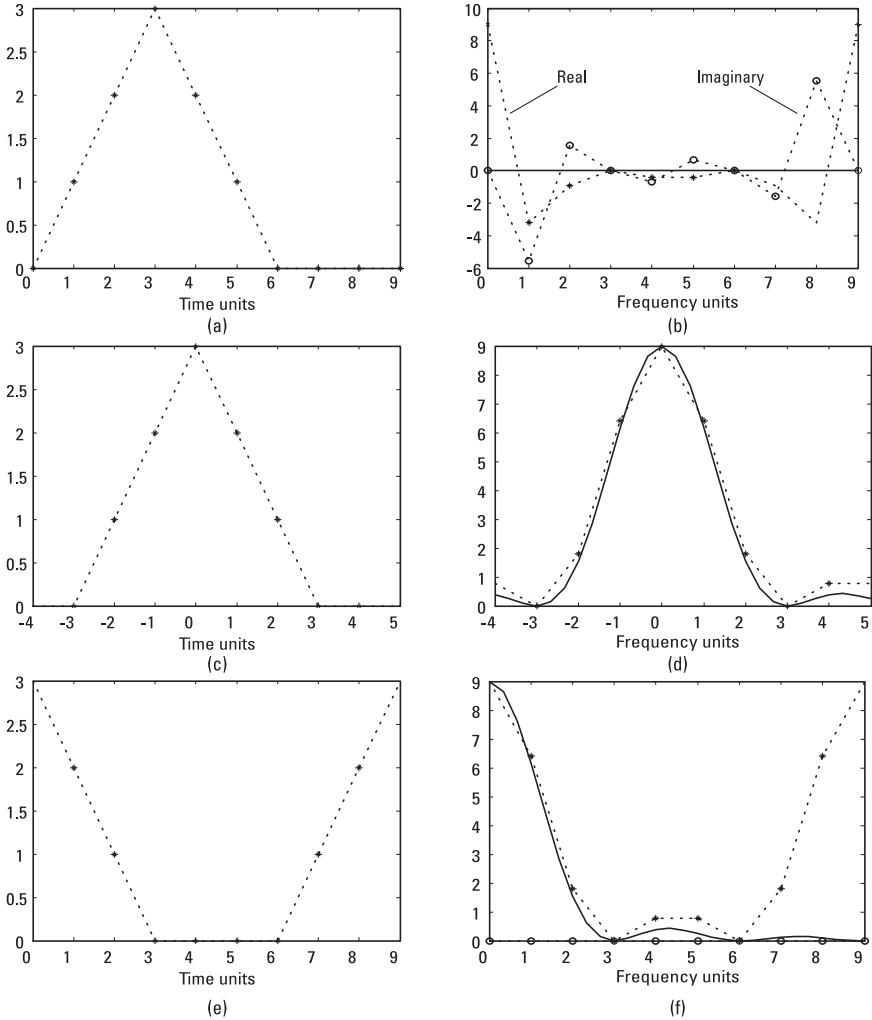
Figure 4.10   Triangular pulse and spectrum (FFT order 9).

If we take the triangular pulse to be centered at time zero, then it would extend from $m = -3$ to $+3$, as shown in part (c), but the FFT requires one period starting at zero, so the time series is [3 2 1 0 0 0 0 1 2], as shown in (e). This shows half the pulse centered at zero and half the next repetition of the pulse, centered at time sample 9. This real symmetric waveform gives a real symmetric spectrum, as expected from R2 and R3. If $u(t) = u(-t)$ then $U(f) = U(-f)$, and if $u(t) = u^*(-t)$ then $U(f) = U^*(f)$. The time and frequency sequences plotted in (c) and (d) are given from those of (e) and (f) by the *fftshift* function or the *ifftshift* function (so for (c) it is [0 1 2 3 2 1 0 0 0]).

We could obtain the waveform in (e) from that in (a) by shifting back three time samples, given by convolving the waveform with $\delta(t + 3\tau)$. From P1b and R6a, this multiplies the spectrum by $\exp(6\pi i f\tau)$. Putting $f = mF$, and $mF\tau = m/N = m/9$, in this case, we find that if we multiply the spectrum samples in (b) by $\exp 2m\pi i/3 (m = 0$ to $8)$, we correctly obtain the spectrum values shown in (f).

In Figure 4.10(d) and (f), we show the transform of the triangular pulse shown in (c) or (e) (*not* in repeated form and not sampled) as the continuous curve. As the pulse is given by $3\text{tri}(t/3\tau)$, its spectrum is $9\tau\text{sinc}^2(3f\tau)$ (from P4, R5), and this is what is plotted as the continuous curve. (The first zero of the sinc function is at $f = 1/3\tau = \phi/3 = NF/3 = 3F$, as $N = 9$ (i.e., at $m = 3$, as seen in the figure). Figure 4.10(d) shows that the FFT (dashed curve) does not give exactly the spectrum of the waveform that has been sampled (i.e., as the sampled waveform is an approximation, the spectrum is also an approximation). The inaccuracy is seen mainly in the tails of the spectrum (in the middle of (f) and at the sides of (d)) and is due to the overlapping of the repeated forms of the spectrum of the single pulse.

The tails of the spectrum are not improved by increasing the order of the FFT, as shown in Figure 4.11, where the order is 20. The waveform repetition interval is now 20 samples, with the basic waveform unchanged but with more zeros between repetitions, as shown in part (a). (We have chosen a sampling interval of 1/2 ms in this case, as a specific example.) The benefit of the higher order is only to increase the sampling density of the spectrum. In order to improve the approximation of the tails of the FFT spectrum to that of a single sampled pulse, we need to increase the pulse sampling rate. This represents the pulse more accurately, and in Fourier transform terms it increases the spectral repetition period. This is shown in Figure 4.11(b), where the sampling time is now ¼ ms, and the match up to the midpoint of 2 kHz is much better.
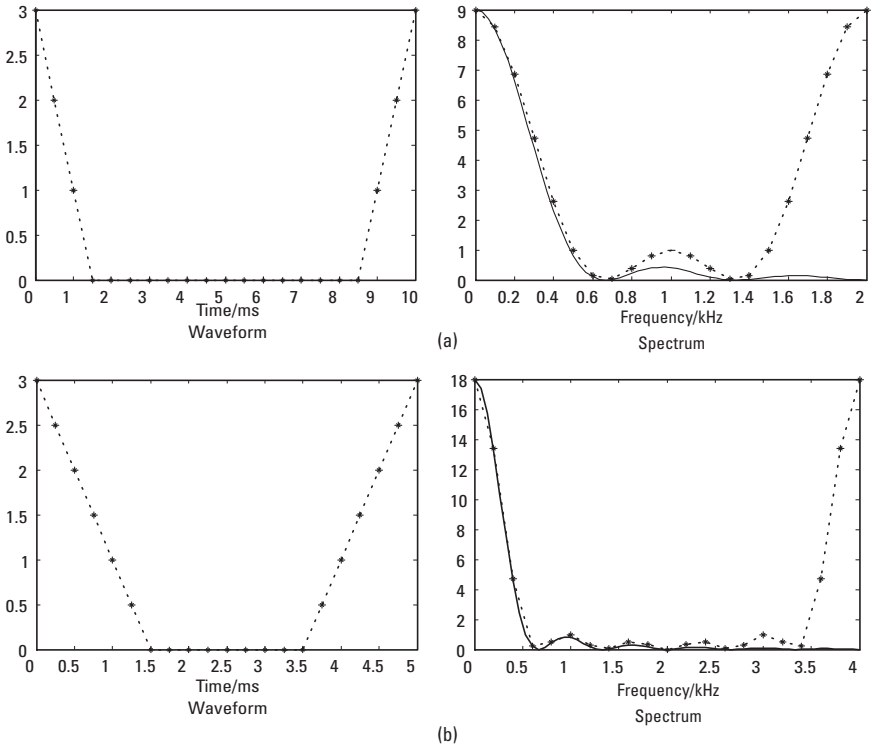
Figure 4.11   Triangular pulse and spectrum (FFT order 20).

4.4.6   Matrix Representation of DFT

We can express the DFT in a vector-matrix representation, writing (4.61) in the form

$$\mathbf{S} = \mathbf{T}\mathbf{s} \tag{4.63}$$

where $\mathbf{s} = [s_0 \quad s_1 \quad \ldots \quad s_{N-1}]^{\mathrm{T}}$ is an N-vector containing the input data and $\mathbf{S} = [S_0 \quad S_1 \quad \ldots \quad S_{N-1}]^{\mathrm{T}}$ contains the output data, the DFT spectrum sample values. (The raised suffix T indicates transposition.) The $N \times N$ matrix $\mathbf{T}$ represents the transform operation, and has components given, from (4.61), by

$$t_{mn} = \exp(-2\pi imn/N) \quad (m, n = 0 \text{ to } N-1) \tag{4.64}$$

As noted in Section 4.4.3, if we prefer to label the components of **s** and **S** from 1 to N, then we put $t_{mn} = \exp(-2\pi i(m-1)(n-1)/N)$ with $m,n = 1$ to N.

Now we note that component mn of the product $\mathbf{T}^H\mathbf{T}$ (H indicating complex conjugate transpose) is given by

$$(\mathbf{T}^H\mathbf{T})_{mn} = \sum_{k=0}^{N-1} t_{km}{}^* t_{kn} = \sum_{k=0}^{N-1} \exp 2\pi i \frac{(m-n)k}{N} \qquad (4.65)$$

If $n = m$ we have $(\mathbf{T}^H\mathbf{T})_{mm} = N$, but if $n \neq m$ we put $\alpha = \exp 2\pi i(m-n)/N$ and then

$$(\mathbf{T}^H\mathbf{T})_{mn} = \sum_{k=0}^{N-1} \alpha^k = \frac{1-\alpha^N}{1-\alpha} = 0$$

after summing the geometric series and noting that $\alpha^N = \exp 2\pi i(m-n) = 1$, as $m - n$ is integral. Thus,

$$\mathbf{T}^H\mathbf{T} = N\mathbf{I} \qquad (4.66)$$

where $\mathbf{I}$ is the $N \times N$ identity matrix. As $\mathbf{T}$ is symmetric ($t_{mn} = t_{nm}$) we have $\mathbf{T}^H = \mathbf{T}^*$ (with * representing complex conjugate), so from (4.66) we have $N\mathbf{T}^{-1} = \mathbf{T}^H = \mathbf{T}^*$, and so the inverse DFT is given, from (4.63) by

$$\mathbf{s} = \mathbf{T}^{-1}\mathbf{S} = \mathbf{T}^*\mathbf{S}/N \qquad (4.67)$$

or, in the form given in (4.62),

$$s_n = \frac{1}{N}\sum_{m=0}^{N-1} S_m \exp(2\pi imn/N) \qquad (n = 0 \text{ to } N-1)$$

The conjugate relation between the coefficients in the forward and inverse DFT parallels that of the Fourier transform definitions in (1.4) and (1.3).

From the vector-matrix representation, we can obtain directly the power relation for repetitive, sampled waveforms. From (4.63) we have

$$\sum_{n=0}^{N-1} \left|S_n\right|^2 = \mathbf{S}^H\mathbf{S} = \mathbf{s}^H\mathbf{T}^H\mathbf{T}\mathbf{s} = N\mathbf{s}^H\mathbf{s} = N\sum_{m=0}^{N-1}\left|s_m\right|^2 \qquad (4.68)$$

This result, apparently asymmetric between time and frequency components, can easily be confirmed for the MATLAB implementation. We also note that, if $\left|s_m\right|^2$ is the power in a line defined by a δ-function of strength s_m (see Section 4.2.2), then $\sum_{m=0}^{N-1}\left|s_m\right|^2$ represents the power in the waveform. Taking the power in the spectrum S to be the mean square value, this is given by averaging over one period, $\int_{I_\phi}\left|S(f)\right|^2 df \big/ \phi$. Equating the powers of the waveform and spectrum, and using (4.68), we have $\int_{I_\phi}\left|S(f)\right|^2 df \big/ \phi = \frac{1}{N}\sum_{n=0}^{N-1}\left|S_n\right|^2$, or, as $\phi = NF$,

$$\int_{I_\phi}\left|S(f)\right|^2 df = F\sum_{n=0}^{N-1}\left|S_n\right|^2$$

(where I_ϕ is an interval of one period, as before). This is very similar to the result in (4.12); under appropriate conditions, the integral of a continuous function can be replaced by a sum of regular samples of the function multiplied by the sampling interval.

4.4.7 Efficient Convolution Using the FFT

We can perform the convolution of two finite energy waveforms numerically by sampling these waveforms at suitable resolution and carrying out the procedure described in Section 2.2 (i.e., slide one waveform in time-reversed form past the other, multiply the two waveforms point by point, and sum the result. This is an approximation in the same way as numerical integration is an approximation, but the error can be made as low as desired by fine enough sampling. As a simple example, we take two waveforms with samples [1 3 2] and [1 3 5 6 4 2]. These arrays give the nonzero samples; the waveforms are implicitly infinite, with all the other samples having value zero. Taking the smaller sequence as the sliding waveform, and reversing it to become [2 3 1], we see that the first convolved value is given by $1 \times 1 = 1$, the second by $3 \times 1 + 1 \times 3 = 6$, and so on, to give [1 6 16 27 32 26 14 4]. If there are n_1 values in the first sequence and n_2 in the second, the length of the result of the convolu-

tion is $n_1 + n_2 - 1$ and the total number of (nonzero) multiplications required is $n_1 n_2$. (This is seen most easily by noting that each value in one sequence multiplies each of the values in the other sequence at some point.) While the computational load is trivial in this example, if we have two substantial sequences, of length 10000, for example, the number of multiplications becomes 10^8, which is more significant.

To reduce the computational work required we use rule 7b, the fact that the convolution of two waveforms, u and v, has a spectrum that is the product of the spectra of the waveforms. Thus, we transform the two waveforms, using the efficient FFT, multiply their spectra, U and V, point by point, and inverse transform the result UV, to obtain the result $u \otimes v$. However, we must consider the orders of the FFT and its inverse (IFFT) required. First, the waveforms used must be of the same length, so that the results of their FFTs are the same length and can be multiplied together. Second, we note that the length, $n_{12} = n_1 + n_2 - 1$, of the convolved sequence $w = u \otimes v$ is greater than that of u or v. Thus, the spectrum of w must be of length at least n_{12} to avoid overlapping, or aliasing, as we know from Section 4.4.3 that the discrete spectrum of length N transforms to a waveform periodic over N samples. In the earlier example, where $n_1 = 3$ and $n_2 = 6$, we need transforms of length at least 8, so we choose sequences $s_1 = [1\ 3\ 2\ 0\ 0\ 0\ 0\ 0]$ and $s_2 = [1\ 3\ 5\ 6\ 4\ 2\ 0\ 0]$. Using the following MATLAB statements, S1 = fft(s1); S2 = fft(s2); S12 = S1.*S2; s12 = ifft(S12), we obtain the result [1.0000 6.0000 16.0000 27.0000 32.0000 26.0000 14.0000 4.0000], agreeing with the previous result obtained directly. If we use FFTs of order 9, by adding another sample of zero to each of s_1 and s_2, we have the same result, except for another zero in the result sequence, and some added values of $\pm0.0000i$, indicating the existence of very small errors due to finite word lengths in the arithmetic.

In order to obtain maximum benefit from this approach, it is probably best to arrange the FFT orders to be a power of 2. Thus, we expand the sequences (by adding samples of zero) from lengths n_1 and n_2 to length $N = 2^m$, where m is the lowest power of 2 such that $N \geq (n_1 + n_2 - 1)$. We now have to carry out three transforms each of mN multiplications, plus a product of the N-point spectra, requiring N multiplications. Overall we have $N(3m + 1)$ multiplications, compared with $n_1 n_2$, performing the convolution directly. If we had $n_1 = n_2 = 2^{m-1}$ – that is, the lengths of the sequences for convolution are equal, and a power of 2, then $n_1 + n_2 = 2^m = N$, so the condition for N is satisfied, and the direct convolution requires $n_1 n_2 = 2^{2m-2} = N^2/4$ multiplications. Using the three Fourier transforms, the saving, in this aspect of the computation, is by a factor of $N/4(3m+1)$, or $2^{m-2}/(3m+1)$. If we take input

sequences of length 8192, so that $m = 14$, then this factor is over 95. For sequences 8 times longer, with $m = 17$, the factor is 630.

If we carry out the same procedure using discrete transforms of the same length as the given series (with one augmented with zeros, if necessary) we obtain the *circular* (or periodic) convolution of the series. Thus if we take $s_1 = [1\ 3\ 2\ 0\ 0\ 0]$ and $s_2 = [1\ 3\ 5\ 6\ 4\ 2]$, form S_1, S_2 and then S_{12} and s_{12}, we obtain the result [15.0000 10.0000 16.0000 27.0000 32.0000 26.0000]. This is what would be given if we shortened the full convolution given by the 8-point transform by taking the last two terms (14 and 4) and adding them to the first two (1 and 6). This is because the 6-point sampling of the product spectrum gives a waveform repetitive at six time intervals, so the result of the linear convolution of the two series will overlap itself. This result is also obtainable directly in the time domain, by convolving the series [1 3 2] with a repetitive form of s_2 and taking one period of the result.

4.5   Summary

We have looked at three aspects of periodic waveforms in this chapter using the rules-and-pairs technique. In Section 4.2, having noted that power, rather than energy, is the appropriate measure for these waveforms, we derived expressions for the power of periodic waveforms corresponding to the energy expression for finite energy waveforms given by Parseval's Theorem. We also obtained a corresponding result for a sampled finite energy waveform. The result for sampled, periodic functions, as used for the FFT, is obtained after finding the relation between the DFT spectrum to the input data.

Next we considered performing Fourier series analysis on periodic waveforms using the rules-and-pairs method. In its basic form this is quite straightforward, but it gives the function as a sum of complex exponential functions, which may not be the most convenient form. Fourier series are very often required for the case of real functions, expressing these as sums of real functions, sines, and cosines, rather than complex exponentials. In Section 4.3, we showed how to obtain the Fourier series coefficients of real periodic functions for this case, without explicit integration, and illustrated the method by analyzing square waves, sawtooth waveforms, triangular waveforms, and rectified sinewaves.

The third topic covered was that of the discrete Fourier transform, the Fourier transform of discrete waveforms. In the general case the transform is a continuous function, and in the case of a regularly sampled waveform it is

periodic. If we require a sampled spectrum, this is seen to be the transform of a periodic waveform, and this is the case for the FFT. The DFT theory is given, using the rules and pairs, and the relation between the spectrum sample values and the input data samples, is derived. Some results used in the theory are justified in an appendix. The use of the rules and pairs, by keeping attention on the waveforms, aided by figures for illustration, may help clarify the ideas used.

Appendix 4A: Spectrum of Time-Limited Waveform

We define a time-limited waveform $p(t)$ as one that has no energy outside some finite time interval. Thus, for this waveform there is some T such that p is zero outside the interval $[-T/2, T/2]$. For such a waveform, there is no over-lapping when the waveform is repeated at intervals T (or greater). It would be desirable if the spectrum were similarly limited (in frequency, in this case) because if the spectrum $P(f)$ is required but only $\text{rep}_\phi P(f)$ is available, then one period of $\text{rep}_\phi P(f)$ contains $P(f)$ precisely if there is no overlapping, but not otherwise. Unfortunately a time-limited waveform does not have a frequency-limited spectrum—there is no ϕ such that the spectrum has no energy outside $[-\phi/2, \phi/2]$. We can show this by writing the waveform identity

$$p(t) = \text{rect}(t/T)\,p(t)$$

which transforms to the spectral identity

$$P(f) = T\,\text{sinc}(fT) \otimes P(f) = \int_{-\infty}^{\infty} \text{sinc}\big((f - f')T\big)P(f')df' \quad (4A.1)$$

From the right-hand side of this equation we see that spectral component $P(f')df$ at frequency f' is spread over the whole frequency range, contributing $P(f')df\,\text{sinc}(f-f')T$ to the total convolution integral. Although the sinc function decreases in magnitude as $f \to \pm\infty$, there is no frequency beyond which there is no energy, and, although there may be single points at which the value of P is zero, there cannot be an interval over which P (on the left of (4A.1)) is zero without P (on the right) being zero everywhere. We conclude that a time-limited waveform has a frequency-unlimited spectrum which, when repeated, will always have some degree of overlap (or aliasing). However, as the spectrum always dies away at large enough frequency values

(positive and negative) there will be frequencies ϕ such that there can be negligible energy outside $\pm\phi/2$, and negligible overlap, for practical purposes.

Appendix 4B: Constraint on Repetition Period

Let the given time series, with sampling interval τ, be given by $\mathrm{comb}_\tau p(t)$ where p is the continuous function that has been sampled. (In the case of experimental data, p is an unknown, implicit function.) Then we define u as the waveform obtained by repeating this series at intervals T, so that $u(t) = \mathrm{rep}_T\left(\mathrm{comb}_\tau\, p(t)\right)$. The waveform, where $T = (m + \alpha)\tau$, with m an integer and $0 < \alpha < 1$, is illustrated in Figure 4B.1(a). We see that u is not a regularly sampled form of $\mathrm{rep}_T(p)$ in this case. The spectrum of u is given by $U(f) = F\phi\,\mathrm{comb}_F\left(\mathrm{rep}_\phi P(f)\right)$ (where $F = 1/T$ and $\phi = 1/\tau$), illustrated in Figure 4B.1(b). In this case we see that, though $\mathrm{rep}_\phi P$ is periodic, U is not periodic as the lines within the successive repetitions of P occur at different points in the waveform. (Strictly speaking, if α were a rational fraction, then U would be periodic, though not at intervals F.) We note, taking the reciprocal of the relation between T and τ, that $\phi = (m + \alpha)F$. If we want the spectrum to be really periodic, so that all intervals of length ϕ contain the same set of δ - functions, then we must have $\alpha = 0$ (i.e., the period of the spectrum must be an integer times the line spacing). Similarly, the period of

(a)

(b)
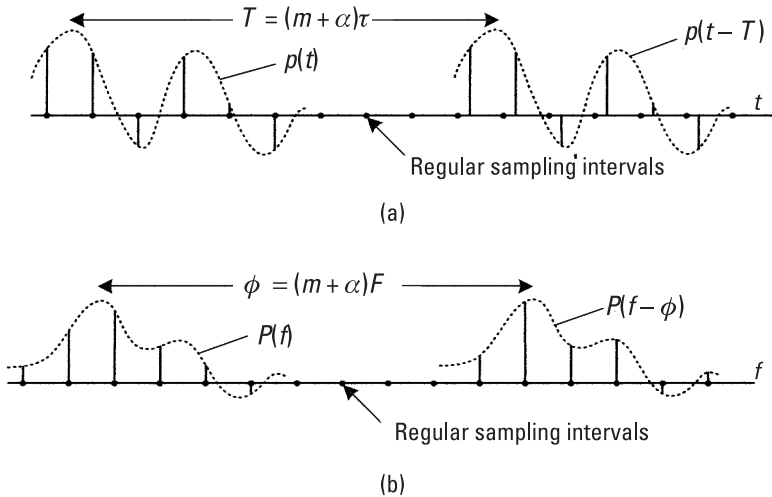
Figure 4B.1 Effect of nonintegral ratio of period to sample interval. (a) $\mathrm{rep}_T(\mathrm{comb}_T\, p(t))$ not a comb function, and (b) $\mathrm{comb}_\phi\,(\mathrm{rep}F(p(f)))$ not a rep function.

the waveform must be (the same) integer times the sampling interval so that the samples in each repetition lie on a single comb sequence.

If the period of the rep operator is an integer multiple of the sampling interval of the time series $\text{comb}_\tau p(t)$ then we obtain the same result whether we repeat the sampled waveform or sample the repeated waveform. (This is the case whether or not the repeated waveforms overlap.) Thus we have

$$\text{rep}_T\left(\text{comb}_\tau\ p(t)\right) = \text{comb}_\tau\left(\text{rep}_T\ p(t)\right)$$

This is *not* the case if T/τ is not integral, as shown in Figure 4B.1(a). On expanding the comb and rep functions, we see that the coefficient of $\delta(t-k\tau)$ (the line at $t = k\tau$) on each side of the equation is given (within a constant) by

$$\ldots +\ p\big((k+m)\tau\big) + p(k\tau) + p\big((k-m)\tau\big) + p\big((k-2m)\tau\big)$$

$$+\ \ldots, \text{ or } \sum_{n=-\infty}^{\infty} p\big((k+nm)\tau\big)$$

where $T = m\tau$.

Thus, if (and only if) the rep operator repeats at an interval that is an integer times the sampling interval of a comb function, then rep and comb are commutative.

5

Sampling Theory

5.1   Introduction

In this chapter, we use the rules-and-pairs notation and technique to derive several sampling theorem results, very concisely in some cases. In fact, the wideband (or baseband) sampling theorem and the Hilbert sampling theorem for narrowband (or RF and IF) waveforms are obtained here following the derivations of Woodward [1]. Two other narrowband sampling techniques, uniform sampling and quadrature sampling, have been analyzed by Brown [2], but these results have been obtained here much more easily using Woodward's approach and have been extended to show what sampling rates are acceptable, rather than just giving the minimum sampling rates presented by Brown.

Woodward's technique is to express the spectrum U of the given waveform u in a repetitive form, then gate it to obtain the spectrum again. The Fourier transform of the resulting identity shows that the waveform can be expressed as a set of impulses of strength equal to samples of the waveform, suitable interpolated. This is the converse of repeating a waveform to obtain a line spectrum: if a waveform is repeated at intervals T, a spectrum is obtained consisting of lines (δ-functions in the frequency domain) at intervals $F = 1/T$, with envelope U, the spectrum of u. Conversely if a spectrum U is repeated at intervals F, we obtain a waveform of impulses (δ-functions in the time domain) at intervals $T = 1/F$ with envelope u, the (inverse) transform of U. The problem in this case is to express the spectrum precisely as a gated repetitive

form of itself. In general, this can only be done by specifying that U should have no power outside a certain frequency interval, and that there should be no overlapping when U is repeated. (In one case, quadrature sampling overlapping is allowed, provided a condition is met, but this is for the case of a strictly band-limited spectrum.) This finite bandwidth condition is not a completely realizable one—it corresponds with an infinite waveform (see Appendix 4A)—but can be interpreted as the condition that U should have *negligible* power (rather than *no* power) outside the given band. The values that are considered negligible will depend on the system and are not analyzed here. However, the approach used here can be used to determine, or at least to estimate, the effect of spectral overlap, which is in fact aliasing.

Brown's approach is to express the waveform u as an expansion in terms of orthogonal time functions. In fact these orthogonal functions are just the set of displaced interpolating functions of the Woodward approach, the interpolating function being the Fourier transform of the spectral gating function. It is necessary to show that this set of functions, which varies with the sampling technique used, is complete. This method is rather complicated compared with Woodward's, which can use the standard results for Fourier series using sets of complex exponential, or trigonometrical, functions. Furthermore, the Woodward approach seems generally easier to understand and so to modify or apply to other possible sampling methods.

5.2   Basic Technique

First, we present the basic technique that is used in subsequent sections to derive the sampling theory results. Because a regularly sampled waveform, which is the ultimate target, has a repetitive spectrum, we repeat the spectrum U of the given waveform u at frequency intervals F, then gate (or filter) this spectrum to obtain U again. This identity is then Fourier transformed to produce an identity between the waveform and an interpolated sampled form of itself. Because this is an identity, it means that all the information in the original waveform u is contained in the sampled form. (The definition of the interpolating function is also needed if it is required to reconstitute the analogue waveform u.) In symbols, we write

$$U(f) = \left(\operatorname{rep}_F U(f) \right) G(f) \qquad\qquad (5.1)$$

$$u(t) = (1/F) \operatorname{comb}_{1/F} u(t) \otimes g(t) \qquad\qquad (5.2)$$

where $G(f)$ is the spectral gating function and $g(t)$ is its transform (i.e., the impulse response of a filter with frequency response G).

The comb function consists of a set of impulse responses (δ-functions) at intervals $T = 1/F$ of strength equal to the value of the function u at the instant of the impulse:

$$\text{comb}_T u(t) = \Sigma u(nT)\delta(t - nT) \tag{5.3}$$

The convolution of a function g with a δ-function simply transfers the origin of g to the position of the δ-function. Thus, equations (5.2) and (5.3) give, with $T = 1/F$,

$$u(t) = T\text{comb}_T u(t) \otimes g(t) = T\Sigma u(nT)\delta(t - nT) \otimes g(t)$$

$$= T\Sigma u(nT)g(t - nT) \tag{5.4}$$

This makes clear the identity between u and its sampled form, when correctly interpolated by the function g with the scaling factor T.

In the following sections of this chapter, the starting point is equation (5.1), choosing the appropriate sampling frequency F and spectral gating function G, in the different cases. The basic problem is to express U in terms of a gated repetitive form of itself, where the repetition frequency F is chosen so that no spectral overlapping occurs. We are primarily concerned with determining F, which is the required sampling rate (to retain all the information and reconstitute the signal if required), and are less concerned with the gating function G. Nevertheless G must be accurately defined to establish the identity (5.1). The transform of G, the interpolating function g, is obtained on transforming the waveform expressed in its gated form and could be used to reconstitute the waveform from its sampled form, in principle, but this is not usually required. In Sections 5.3 and 5.4 (wideband and uniform sampling), we simply repeat the spectrum of u. In Section 5.5 (Hilbert sampling), we also include the spectrum of $\hat{u}$, the Hilbert transform of u, and, in Section 5.6 (quadrature sampling), we include a quarter wave delayed form of u. The sampling techniques of Sections 5.4 and 5.6 are for narrowband waveforms—signals on a carrier.

5.3 Wideband Sampling

By a wideband waveform u, we mean here a waveform containing energy at all frequencies from zero up to some maximum W beyond which there
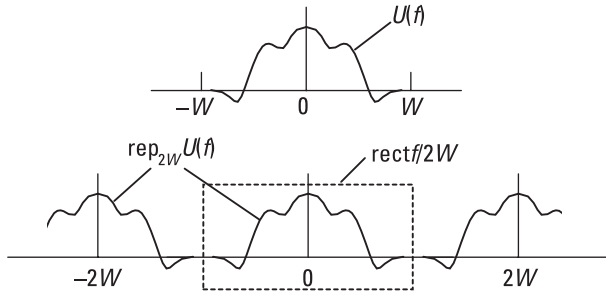
Figure 5.1 Gated repeated waveform.

is no spectral energy. A real waveform has a complex spectrum U that is conjugate symmetric about zero, so real waveforms of interest have spectra within the interval $[-W, W]$ (Figure 5.1). However, the analysis is not limited to real waveforms. If the waveform is complex, we still take the spectrum to have no energy outside this interval (i.e., W is the largest positive or negative frequency). If we repeat this spectrum at intervals $2W$ it will not overlap, as there is no spectral energy outside this interval, so we can write the identity

$$U(f) = \text{rep}_{2W} U(f) \text{rect}(f/2W) \tag{5.5}$$

where we have equated the spectrum to a gated portion of the repeated form of the spectrum itself (Figure 5.1) Taking the Fourier transform we obtain

$$u(t) = \text{comb}_{1/2W} u(t) \otimes \text{sinc} 2Wt \tag{5.6}$$

This is the particular form of (5.2) for this sampling case. This equation states that u is equal to itself sampled at a rate of $2W$ (i.e., at intervals $1/2W$) and correctly interpolated; the interpolating function in this case is $\text{sinc} 2Wt$. The equivalent form of (5.4) is

$$u(t) = \Sigma u(nT) \text{sinc}(t - nT) \tag{5.7}$$

and the equivalence of the waveform to its interpolated sampled form is illustrated in Figure 5.2.

It is clear (from Figure 5.1, for example) that if we repeat the spectrum at intervals $2W'$, where $W' > W$, we still obtain the spectrum U on gating
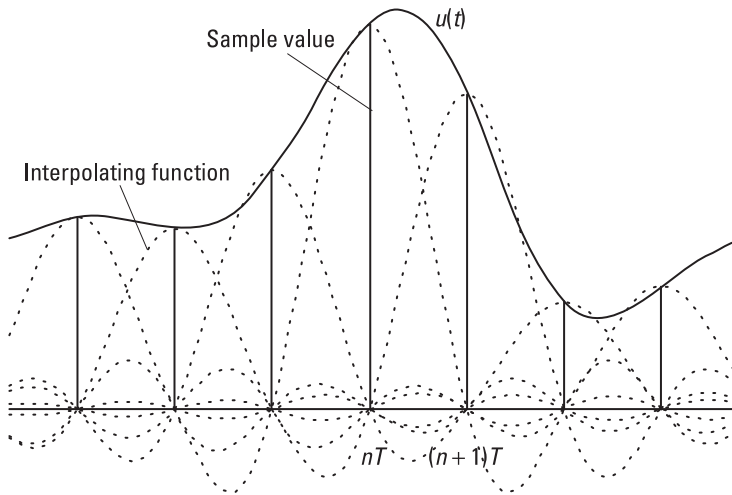
Figure 5.2 Sampled waveform with interpolating functions.

with either $2W$ or $2W'$ bandwidth. Thus, any sampling rate greater than $2W$ is also adequate.

Thus, we have the *wideband sampling theorem*:

If a real waveform has no spectral energy above a maximum frequency W, then all the information in the waveform is retained by sampling it at a rate $2W$ (or higher).

In principle, reconstituting the waveform in this case is achieved by driving a rectangular bandwidth low pass filter with impulses of strength proportional to the sample values and at the sample times. In practice, an approximation to u could be formed easily as a boxcar waveform from the sample values (simply holding the value $u(nT)$ constant over the interval $[nT,(n+1)T)$. Smoothing this with a low pass filter would give a better approximation to u.

One reason for specifying real waveforms in the statement of the theorem is that complex waveforms do not have symmetric spectra and may have different maximum values of positive and negative frequencies. We could omit "real" and replace W by |W| if required. However, of particular interest is the case of the one-sided spectrum of positive frequencies only. This is the Hilbert sampling case, discussed in Section 4.5.

5.4 Uniform Sampling

5.4.1 Minimum Sampling Rate

We define a real narrowband (or IF) waveform as one that has negligible power outside a frequency band W centered on a carrier frequency f_0, where $W/2 < f_0$. The complex spectrum of a real IF waveform consists of two bands centered at $\pm f_0$. We label these U_+ and U_- for convenience, as shown in Figure 5.3. For such a waveform, we find that it is not necessary to sample at twice the maximum frequency (i.e., at $2f_0 + W$ here) as in the case of a wideband waveform, but at approximately twice the bandwidth.

We initially restrict W so that the upper edge of the signal band f_u is an integer multiple of W (i.e., $f_u = f_0 + W/2 = kW$ for k integral). The lower edge of the band is then at $(k-1)W$. The spectrum can now be repeated at intervals $2W$ without overlap as $2f_0 = (2k-1)W$, so a displacement of $2kW$ or $2(k-1)W$ moves the spectral band U_-, centered at $-f_0$, adjacent to the band U_+ at f_0 without overlapping it (Figure 5.4). Thus we can write

$$U(f) = \mathrm{rep}_{2W}\, U(f) \left\{ \mathrm{rect}\left(\frac{(f-f_0)}{W} \right) + \mathrm{rect}\left(\frac{(f+f_0)}{W} \right) \right\} \qquad (5.8)$$

again representing U as a gated repeated form of itself. The transform of this equation is

$$u(t) = \frac{1}{2W} \mathrm{comb}_{1/2W}\, u(t) \otimes W\, \mathrm{sinc}\, Wt \left(e^{2\pi i f_0 t} + e^{-2\pi i f_0 t} \right) \qquad (5.9)$$

Thus, u is equal to itself sampled at a rate $2W$ and interpolated by the function $\mathrm{sinc}\, Wt \cos(2\pi f_0 t)$, which is the impulse response of an ideal rectangular bandpass filter of bandwidth W centered at frequency f_0.

We now remove the condition relating f_0 and W. We note that a spectrum within a band $(f_u - W, f_u)$ is also within the band $(f_u - W', f_u)$ if $W' \geq W$.
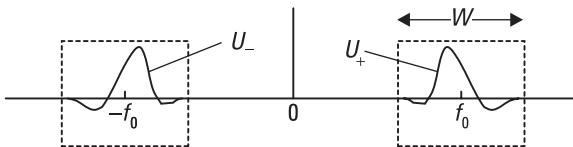
Figure 5.3 Narrowband spectrum.
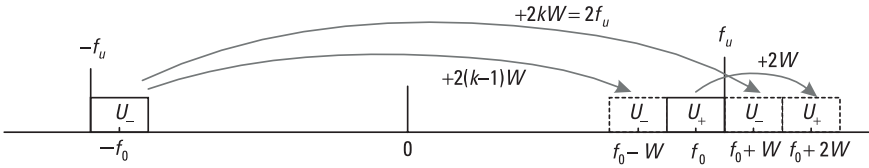
Figure 5.4 Allowed spectral shifts.

Thus, if W does not satisfy the condition $f_u = kW$ (k integral), we choose the smallest $W' > W$ that does satisfy it. More specifically, if $f_u = (k + \alpha)W$, where $0 \leq \alpha < 1$, we choose W' so that $f_u = kW'$, and we can write $k = [f_u/W]$, where $[x]$ means the largest integer contained in x. Then repeating the spectrum at intervals $2W'$ again produces a nonoverlapping spectrum (Figure 5.5), but this time with some gaps (of size $2(W' - W)$) due to the difference between W' and W.

It is clear that to regain U from the repeated form of the spectrum shown in Figure 5.5 it is only necessary to gate with the same gating function as before (given in (5.8)—gates of width W centered at $+f_0$ and $-f_0$) leading to the same interpolating function, $\text{sinc}\,Wt\cos(2\pi f_0 t)$. Brown [2] in effect uses the more complicated interpolating function $\text{sinc}(2W't)\cos 2\pi f_0' t$, where $f_0' = f_0 - (W' - W)/2$. This corresponds to using the gating function $\text{rect}((f - f_0')/W')$, which will also gate out U as required (Figure 5.6) but is more complicated than necessary.

5.4.2 General Sampling Rate

The minimum sampling rate $2f_u/k$, found in the previous section, is such that the band U_- shifted by $2kW'$ is just above U_+ when the repetitive spectrum is formed (Figure 5.5). If W' is increased above this value, this band will move up in frequency, and so will the band U_-, shifted by $2(k - 1)W'$, which will
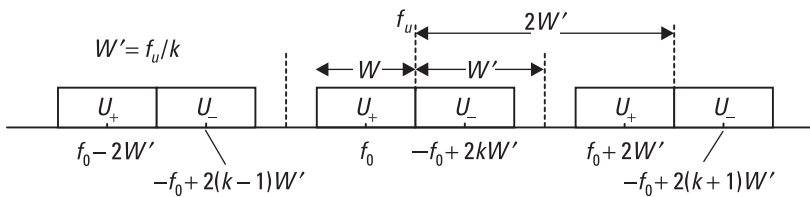
Figure 5.5 $\text{rep}_{2W}U(f)$ near $+f_0$.
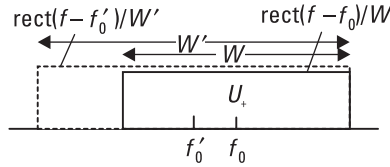
Figure 5.6 Selecting $U(f)$.

eventually start to overlap U_+. This will define a (local) maximum allowed sampling rate, and this occurs when $2(k-1)W' = 2f_l$, where f_l is the frequency at the lower edge of the signal band (Figure 5.7). Thus, the allowed sampling rate $2W'$ ranges from a minimum value $2f_u/k$ to a maximum $2f_l/(k-1)$. As k is defined here by $f_u = (k+\alpha)W$, we also have $f_l = f_u - W = (k-1+\alpha)W$, and we see that the range of allowed sampling rates $2W'$ is given by

$$2f_u/k = 2(k+\alpha)W/k \le 2W' \le 2(k-1+\alpha)W/(k-1) = 2f_l/(k-1) \qquad (5.10)$$

It is convenient to define a relative sampling rate r as the actual rate divided by the minimum value possible (to retain all the signal data) $2W$, so that the allowed relative rate $2W'/2W$ becomes

$$(k+\alpha)/k \le r \le (k-1+\alpha)/(k-1) \qquad (5.11)$$

or

$$1 + \alpha/k \le r \le 1 + \alpha/(k-1) \qquad (5.12)$$

If the sampling rate is increased above the "maximum" $2f_l/(k-1)$, we see from Figure 5.7 that U_- will overlap U_+ until the rate rises to $2f_u/(k-1)$ when we reach a new local minimum value for the allowed sampling rate. The rate can now be increased to a new local maximum $2f_l/(k-2)$ before
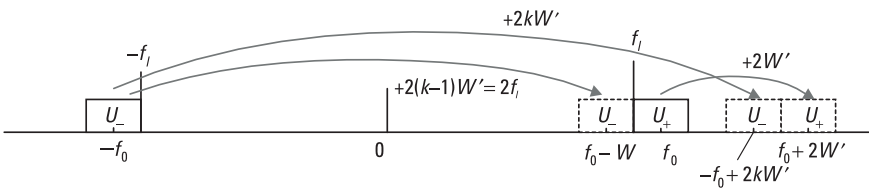
Figure 5.7 Maximum sampling rate.

overlap starts again. In general, we see that allowed relative sampling rates are given by

$$(k + \alpha)/n \le r \le (k - 1 + \alpha)/(n - 1) \quad (n = k, k-1, \dots, 1) \quad (5.13)$$

In the $n = 1$ case, we only have a minimum rate; the maximum rate in this case is unbounded. Putting $n = k$ gives the absolute minimum rate, $1 + \alpha/k$. The allowed relative sampling rates are given in the shaded regions of Figure 5.8 as a (multivalued) function of the center frequency normalized to the bandwidth. (We note $f_0 = f_u - W/2 = (k + \alpha - \frac{1}{2})W$, so its minimum normalized value is $\frac{1}{2}$, when $k = 1$ and $\alpha = 0$.)

We note from Figure 5.8 that the lowest range of allowed rates becomes very narrow at high values of f_0/W. This indicates that the sampling rate should be carefully chosen in this case, and perhaps should be synchronized to some frequency in the signal band. The minimum rate is in fact defined by f_u, but there is no actual signal power here (from the definition of W) so it would be more convenient to use f_0. The allowed band of relative rates, from (5.12), is between $1 + \alpha/k$ and $1 + \alpha/(k-1)$, so $1 + \alpha/(k - \frac{1}{2})$ would be near the mean of these. The actual rate, with this choice, is thus $2W(k + \alpha - \frac{1}{2})/(k - \frac{1}{2}) = 2f_0/(k - \frac{1}{2})$. This rate is indicated by the dashed lines and is very close to the minimum rate for higher values of f_0/W (e.g., above $3\frac{1}{2}$).
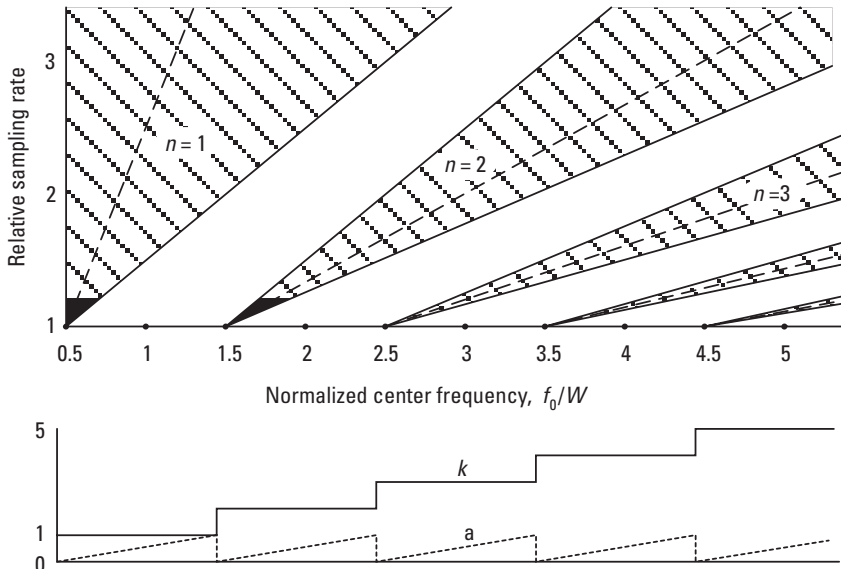
Figure 5.8 Relative sampling rates (uniform sampling).

We note that if $f_0/W = \frac{1}{2}$ we have effectively a wideband waveform of positive frequency bandwidth W (see Figure 5.3), and with positive frequencies extending from 0 to W. The minimum uniform sampling rate in this case is $2W$ (see Figure 5.8), which agrees with the result in Section 5.3 for a wideband waveform. We also note that the minimum rate is substantially different from $2W$ (when $r = 1$) only for large fractional bandwidths (W/f_0 large and so f_0/W small). For small fractional bandwidths of, for example, a few percent, which is often the case for radio and radar signals, whether at high frequency (HF), very high frequency (VHF), ultra-high frequency (UHF), or microwave frequency, the correct rate will be very close to $2W$, and setting it actually at $2W$ will generally give negligible degradation.

Finally, we state a simplified form of the *uniform sampling theorem* for narrowband waveforms, which is not as neatly defined as for the wideband case:

> If a real waveform has no spectral energy outside a frequency band of width W centered on a carrier of frequency f_0, then all the information in the waveform is retained by sampling it at a rate $2rW$, where r is given in (5.13). (k and α in (5.13) are given by $k + \alpha = f_0/W + \frac{1}{2}$, k integral and $0 \le \alpha < 1$; k is the largest integer in $f_0/W + \frac{1}{2}$).

We note that for small fractional bandwidths, we can sample at rate $2f_0/(k - \frac{1}{2})$, synchronizing to the center frequency, and this is very close to optimum.

5.5 Hilbert Sampling

Given a real waveform u, the complex waveform $v = u + i\hat{u}$ has a spectrum consisting of positive frequency components only, where $\hat{u}$ is the Hilbert transform of u, defined in Appendix 5A. (In effect, the Hilbert transform applies a wideband 90° phase shift, as shown in this appendix.) For narrowband waveforms, a 3-dB coupled line directional coupler is a very good approximation to a Hilbert transformer, which generates $\hat{u}$ from u. The two outputs of such a coupler are a Hilbert transform pair and may be considered to form a complex waveform, if the rules for complex arithmetic are observed when processing this two-channel waveform.

If W is the width of the bands, centered on $-f_0$ and f_0, outside which U has negligible power, then we can see that V is within a band of width W,
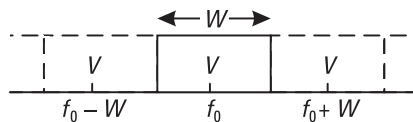
Figure 5.9 $\text{rep}_W V(f)$ near $+f_0$.

centered on $+f_0$ only, and so can be repeated at intervals W without overlapping (Figure 5.9).

Thus, we can write the identity

$$V(f) = \text{rep}_W \left(V(f) \right) \text{rect} \left((f - f_0)/W \right) \tag{5.14}$$

Performing the inverse Fourier transform using P3b, R8a, R6b, and R5, we obtain

$$v(t) = (1/W) \text{comb}_{1/W} \, v(t) \otimes (W \, \text{sinc} \, Wt \exp 2\pi i f_0 t) \tag{5.15}$$

Now u is the real part of v, so taking the real part of both sides we obtain

$$u(t) = \text{comb}_{1/W} \, u(t) \otimes (\text{sinc} \, Wt \cos 2\pi f_0 t)$$
$$- \text{comb}_{1/W} \, \hat{u}(t) \otimes (\text{sinc} \, Wt \sin 2\pi f_0 t) \tag{5.16}$$

We see that u is equal to a combination of samples of u and $\hat{u}$ appropriately interpolated, the samples being taken at intervals $1/W$ (i.e., at a rate W). We also note that by taking the imaginary part of v from (5.15) we obtain the sampled form of $\hat{u}$. If we repeat the spectrum at intervals $W' > W$, corresponding to sampling at the rate W', we still have a nonoverlapping spectrum. This could be gated with a rectangular window of any width from W to W' to obtain V again. Thus, we obtain the *Hilbert sampling theorem*, which is more simply stated than the uniform sampling theorem, for the same type of waveform:

> If a real waveform u has no spectral energy outside a frequency band of width W centered on a carrier of frequency f_0, then all the information in the waveform is retained by sampling it and its Hilbert transform $\hat{u}$ at a rate W (or higher). (The complex samples, with real and imaginary parts the samples of u and $\hat{u}$, respectively, are of the analytic waveform

corresponding to u. This has a spectrum of positive frequencies only, the positive side of the spectrum of u.)

We note that the sampling rate is independent of f_0, unlike the case for uniform sampling or quadrature sampling (an approximation to Hilbert sampling, described in Section 5.6). As pointed out by Woodward, a real waveform of duration T and bandwidth W requires (as a minimum) $2WT$ real values to specify it completely. Either we take real samples at a rate $2W$ (as given by wideband sampling, or as the minimum rate for uniform or quadrature sampling) or complex samples at the rate W (each containing two real values, in the real and imaginary parts) in the case of Hilbert sampling. The waveform can be said to require $2WT$ degrees of freedom for its specification.

5.6   Quadrature Sampling

5.6.1   Basic Analysis

If it is not convenient or practical to use a quadrature coupler, or any other method, to produce the Hilbert transform of a narrowband waveform, an approximation to the transformed waveform can be obtained by delaying the signal by a quarter cycle of its carrier frequency. This follows from the fact that the Hilbert transform is equivalent to a delay of $\pi/2$ radians (for all frequency components, as shown in Appendix 5.1) so the quarter cycle delay will be correct at the center frequency and nearly so for frequencies close to it. The smaller the fractional bandwidth, the better this approximation becomes. As this is an approximation to the Hilbert transform, it follows that sampling at the rate W (the Hilbert sampling rate) will not, in general, sample the waveform adequately to retain all the information contained in it. However, we will see that the method will in fact sample correctly, by compensating for the phase variation, but at the cost, compared with Hilbert sampling, of requiring an increased sampling rate, which depends on the ratio of bandwidth to center frequency (similarly to the case of uniform sampling).

If $u(t)$ is the basic waveform, with spectrum $U(f)$, then a delayed version $u(t - \tau)$ has spectrum $U(f)\exp(-2\pi i f \tau)$. If we repeat the spectrum of u at intervals W, corresponding to sampling at the rate W, we will obtain an overlapping spectrum which, when gated, is not equal to U in general. However, a suitable combination of the repeated spectra of u and its delayed version will give U after gating. We start by imposing the condition $2f_0 = kW$, where k is
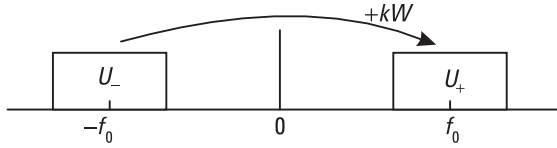
Figure 5.10   Basic quadrature sampling.

an integer, so that there is complete overlap of the two parts of the spectrum of u and also of the two parts of the spectrum of its delayed version, when repeated (Figure 5.10).

The appropriate identity for U is

$$U(f) = \tfrac{1}{2}\{\text{rep}_W U(f) + \exp(2\pi i f \tau)\text{rep}_W [U(f)\exp(-2\pi i f \tau)]\}$$

$$\times\{\text{rect}(f - f_0)/W + \text{rect}(f + f_0)/W\} \qquad (5.17)$$

if τ is correctly chosen. (We note that if the delay is ¼ cycle at the center frequency, $\tau = 1/4f_0$, then $U(f_0)\exp(-2\pi i f_0 \tau)$ is the 90° shifted, or Hilbert transform, component.) To check the identity in (5.17), we consider the output of the positive frequency spectral gate—for frequencies in the range $f_0 - W/2 < f < f_0 + W/2$. In this interval we have, as there is overlap of the negative frequency part of the spectrum, moved up by $2f_0$, or $2kW$, for some integer k,

$$\tfrac{1}{2}\{U(f) + U(f - 2f_0) + \exp(2\pi i f \tau)[U(f)\exp(-2\pi i f \tau) + U(f-2f_0)$$
$$\times \exp(-2\pi i(f - 2f_0)\tau)]\} = U(f) + \tfrac{1}{2}U(f - 2f_0)\{1 + \exp(4\pi i f_0 \tau)\}$$
$$(f_0 - W/2 < f < f_0 + W/2) \qquad (5.18)$$

This is simply $U(f)$, as required, if we choose τ such that $4f_0\tau = 1$, or, more generally, if $4f_0\tau = 2m + 1$, where m is an integer. The same condition results if we consider the output of the negative frequency gate—we simply replace f_0 by $-f_0$ throughout. Thus, the required delay is seen to be an odd number of quarter wavelengths of the carrier, or center frequency, f_0 (i.e., one quarter cycle in the simplest case). Taking the (inverse) Fourier transform of the identity for $U(f)$ in (5.17) we have

$$u(t) = \tfrac{1}{2}\{(1/W)\text{comb}_{1/W}u(t) + \delta(t + \tau)\otimes(1/W)\text{comb}_{1/W}u(t - \tau)\}\otimes 2W\phi(t)$$

$$= \text{comb}_{1/W}u(t)\otimes\phi(t) + \text{comb}_{1/W}u(t - \tau)\otimes\phi(t + \tau) \qquad (5.19)$$

where ϕ is the interpolating function. This is obtained from the (inverse) Fourier transform of the spectral gating function Φ, defined by

$$2W\Phi(f) = \text{rect}[(f - f_0)/W] + \text{rect}[(f + f_0)/W] \qquad (5.20)$$

Thus,

$$2W\phi(t) = W\text{sinc}(Wt)[\exp(2\pi i f_0 t) + \exp(-2\pi i f_0 t)]$$

or

$$\phi(t) = \text{sinc}(Wt)\cos(2\pi f_0 t) \qquad (5.21)$$

This interpolating function also appears in the uniform sampling case (see (5.9)) and the Hilbert sampling case (see (5.16)). Equation (5.19) states that the real waveform u is equal to the sum of the waveform obtained by sampling u at intervals $1/W$ (i.e., at rate W) and interpolating with the function ϕ and the waveform obtained by sampling a quarter-wave delayed version of u and interpolating with a quarter-wave advanced version of ϕ.

To remove the condition relating W and f_0, we choose $W' \geq W$ such that $2f_0 = kW'$, where $k = [2f_0/W]$, the largest integer in $2f_0/W$. We then repeat the spectrum at intervals W', which corresponds to sampling at the rate W', but we can keep the same spectral gating function and hence the same interpolating function. The minimum required sampling rate, relative to the minimum possible rate, equal to the bandwidth W, is $r = W'/W = 1 + \alpha/k$ if $2f_0/W = k + \alpha$. This minimum rate is plotted in Figure 5.11, and this is the rate given by Brown [2].

If W' is increased to higher values such that $2f_0 = nW'$ for n integral, $n < k$, we again obtain sampling rates which will retain the waveform information. These are shown by the dashed lines in Figure 5.11. The required sampling frequency could be obtained in practice by synchronizing W' to a submultiple of $2f_0$ (ideally the kth, for the minimum rate).

5.6.2   General Sampling Rate

Unlike the uniform sampling case, the required sampling rates determined so far are precise (Figure 5.11) instead of within bands (as in Figure 5.8). This is because the delay has been chosen to be a quarter cycle of f_0 (or an odd number of quarter cycles). In fact, on replacing $2f_0$ by kW' in (5.18), where
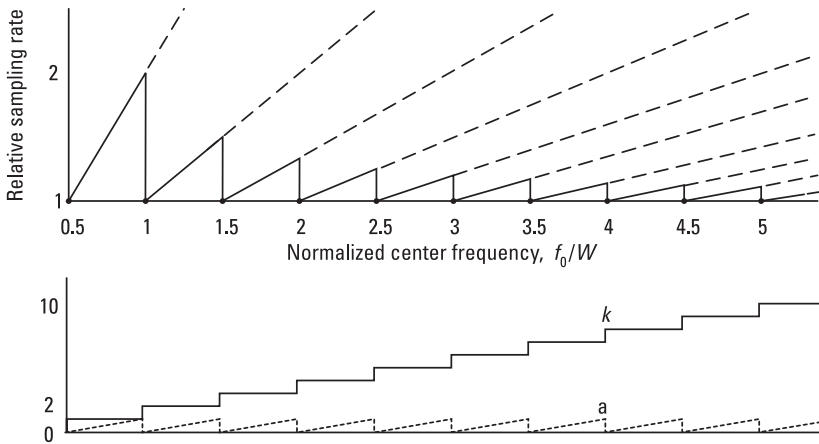
Figure 5.11 Relative sampling rates (basic quadrature sampling).

kW' is the frequency shift that takes U_-, centered at $-f_0$, onto U_+, centered at $+f_0$, we see that the condition to be satisfied is $2kW'\tau = 2m + 1$ (m an integer). If we relate the delay τ to the sampling rate W' instead of directly to f_0, then we have more freedom of choice of W'. In Figure 5.12(a) we see part of the function $\text{rep}_W U_-$, the signal band at $-f_0$ repeated at intervals W, in the region of $+f_0$ where $2f_0$ is *not* an integer multiple of W. If we consider the part of this spectrum that overlaps the band of width W, centered at $+f_0$, we see that there is a mixture of parts of U_- shifted by kW and by $(k+1)W$. If the delay is correct to make U_- disappear when shifted by kW, then it is not quite correct when shifted by $(k+1)W$, and a small amount of spectral overlap occurs.

The minimum repetition rate to avoid this is shown in Figure 5.12(b), where $W'(>W)$ is such that $(k+1)W'$ moves U_- just beyond the gated region (between f_l and f_u). Because $W' > W$, gaps of width $W' - W$ now occur between the repeated versions of U_-. The minimum required value of W' is given by $(k+1)W' = 2f_u$. (In fact, other local minimum rates are given by W' such that $(n+1)W' = 2f_u$, for n integral $n < k$.) We note, in Figure 5.12(b) that part of the signal band occupied by U_+ (between f_l and f_u) has no overlap, in which case there is no problem, and part has an overlap of $U-$ shifted by kW'. As stated earlier, putting kW' into (5.18) instead of $2f_0$, shows that the delay must satisfy $2kW'\tau = 1$. Thus, with the condition on W', we find that $\{4kf_u/(k+1) = 1\}\tau$ (i.e., the delay should be $(1 + 1/k)$ times a quarter cycle of the upper edge of the signal band, f_u, or an odd multiple of this).

If we increase the sampling rate further, we reach the condition shown in Figure 5.12(c), where the band U_- shifted by $(k-1)W'$ has just reached the
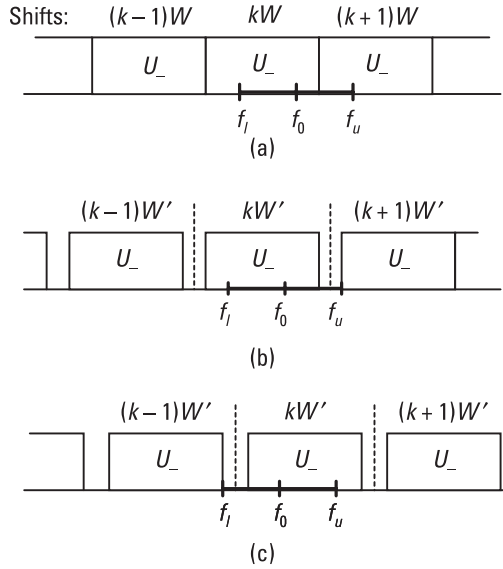
Figure 5.12   Shifted positions of U_-. (a) $2f_0 = (k + \alpha)W$ $(0 < \alpha < 1)$, (b) $2f_u = (k + 1)W'$, and $2f_1 = (k - 1)W'$.

lower edge of the gated band. This is when $(k - 1)W' = 2f_l$ (or, again, more generally when $(n - 1)W' = 2f_l$ for n an integer and $n \le k$). The delay required is $(1 - 1/k)$ times a quarter cycle of the lower edge of the signal band, f_l (or an odd multiple of this).

To summarize, the minimum and maximum relative sampling rates W'/W are given in general, (with $n \le k$) by $r_m = 2f_u/W(n + 1)$ and $r_M = 2f_l W(n - 1)$, where $f_u = f_0 + W/2$ and $f_l = f_0 - W/2$; a central rate (very close to the mean of these two) is $r_c = 2f_0/nW$. However, although these rates are valid, we are generally interested in keeping the sampling rate as low as conveniently possible, and this corresponds to taking the highest value of n (i.e., k). In fact $n < k$ corresponds to the continuations of lines from lower k values, as illustrated in Figure 5.13. Thus, taking the case giving the lowest sampling rates, we have

$$\frac{2f_u}{k + 1} \le W' \le \frac{2f_l}{k - 1} \text{ and } W' \approx \frac{2f_0}{k} \tag{5.22}$$

with corresponding delay values

$$\frac{k - 1}{4kf_l} \le \tau \le \frac{k + 1}{4kf_u} \text{ and } \tau \approx \frac{1}{4f_0} \tag{5.23}$$
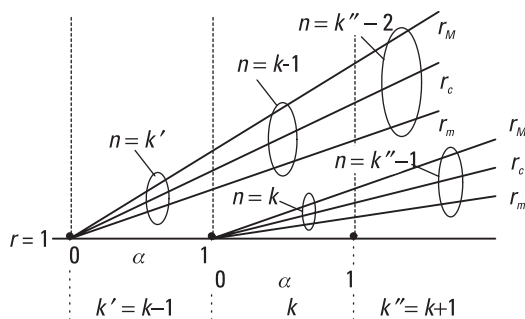
Figure 5.13 Lines of relative sampling rates.

The relative sampling rates, $r = W'/W$, are given, from (5.22) with $2f_0 = (k + \alpha)W$, and putting $2f_0 \pm W = (k + \alpha \pm 1)W$ for $2f_u$ and $2f_l$,

$$1 + \frac{\alpha}{k+1} \leq r \leq 1 + \frac{\alpha}{k-1} \text{ and } r \approx 1 + \frac{\alpha}{k} \tag{5.24}$$

We note that if $\alpha = 0$ (i.e., $2f_0/W$ is integral), then $r = 1$, and quadrature sampling is as good as Hilbert sampling in this case.

The allowed sampling rates relative to the bandwidth W are given in the shaded areas in Figure 5.14. The maximum and minimum rates r_M and r_m define the boundaries, and the central value r_c is shown as dashed lines in Figure 5.14. We note from Figure 5.14 that there are no unallowed sampling rates above $2W$. This is because when the interval between repetitions of U_- becomes $2W$, it is not possible to have parts of more than one repetition of U_- in the gating interval (see Figure 5.12(b) or (c) with $W' \geq 2W$), so if the delay is correctly chosen the U_- contribution in this interval can always be removed. (By putting $x = f_0/W = (k + \alpha)/2$ and equating r_m at k and r_M at $k + 1$, with $\alpha = 2x - k$, we find these lines meet at $x = k + \frac{1}{2}$ and the common value of r is 2, as shown in Figure 5.14).

Because the required delay for the actual minimum sampling rate $((k + 1)/4kf_u)$ is no longer exactly a quarter cycle (or an odd number of quarter cycles) of the carrier, this sampling has been termed *modified quadrature sampling* in the title of Figure 5.14. However, the general rates given in Figure 5.14 may not be very convenient in practice, as they require the delay to be proportional to a quarter of a cycle of f_u, which may not be as easy as choosing it to be $1/4f_0$, as assumed in Figure 5.11. In fact the central rate $2f_0/k$ (shown by the dashed lines in Figure 5.14) does require this more convenient delay,
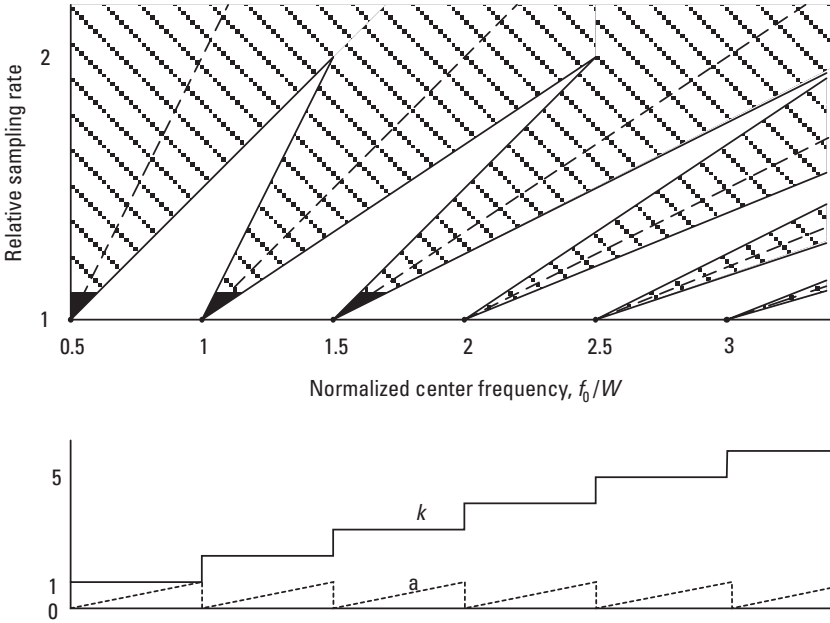
Figure 5.14   Relative sampling rates (modified quadrature sampling).

and for low fractional bandwidths (higher f_0/W values) we see that this is close to the minimum rate.

Thus we can now state a *quadrature sampling theorem*:

> If a real waveform u has no spectral energy outside a frequency band of width W centered on a carrier of frequency f_0, then all the information in the waveform is retained by sampling it, and a delayed version of it, is at a rate given by rW, where r is given in (5.24), and the delay (which is close to a quarter cycle of f_0), is given in (5.23). Complex samples, where the real parts are the samples of u and the imaginary parts are the samples of the delayed form, correspond to samples of the analytic waveform derived from u, equivalent to Hilbert sampling.

5.7   Low IF Analytic Signal Sampling

A signal $u(t)$, on a carrier at frequency f_0, can be written $u(t) = a(t)\cos\left(2\pi f_0 t + \phi(t)\right)$ and, at least in principle, we can derive its Hilbert transform, $\hat{u}(t) = a(t)\sin\left(2\pi f_0 t + \phi(t)\right)$ and hence the complex form $u(t) + i\hat{u}(t) = a(t)$

$\exp i\left(2\pi f_0 t + \phi(t)\right)$. The information in this signal is contained in the amplitude and phase functions $a(t)$ and $\phi(t)$, and what is required for digital signal processing is a digital form of the analytic signal $a(t)\exp i\phi(t)$. This is what is given by Hilbert sampling and quadrature sampling, discussed earlier, in particular from the point of view of finding the minimum sampling rate needed to preserve all the signal information. An alternative method of obtaining the sampled analytic, or complex baseband, signal is given in this section. This is simpler to implement in practice—not requiring the Hilbert transform or an accurate quarter cycle delay, and sampling in only a single channel, rather than in two—at the cost of requiring a higher sampling rate. At the minimum, this single sampling device, or analogue to digital converter (ADC), operates at just twice the rate of the two ADCs needed for the alternative methods.

The method requires bringing the signal carrier frequency down from the normally relatively high radio frequency (RF) to a low intermediate frequency (IF). To avoid the two parts of the spectrum overlapping, we see that we must have $f_0 \geq W/2$. The samples we require are those corresponding to the complex baseband waveform $V(f)$, given by

$$V(f) = 2U_+(f + f_0) \tag{5.25}$$

which is the positive frequency part of the spectrum (the spectrum of the equivalent complex waveform) centered at zero frequency (baseband) rather than at the IF carrier, f_0. We see that, given U, we can obtain V by first shifting U by $-f_0$, then gating it with $2\text{rect}(f/W)$ (Figure 5.15). In order to obtain the repetitive element in the spectrum, to give the δ-functions in the time domain corresponding to the sample values, we note that we can repeat this shifted U spectrum, without overlapping, at intervals $F \geq 2f_0 + W$, so that we have

$$V(f) = \text{rep}_F\left[2U(f + f_0)\right]\text{rect}\frac{f}{W} \tag{5.26}$$

Taking the (inverse) transform, using P3b, R8a, R6b, R5, and R7b we have
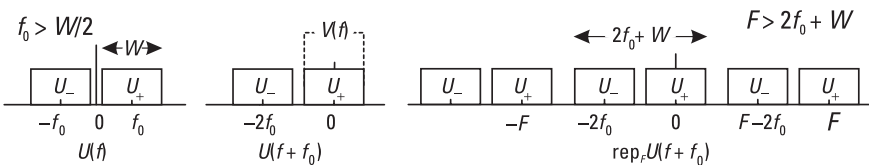
Figure 5.15 Low IF sampling spectra.

$$v(t) = \frac{2W}{F} \text{comb}_{1/F} \left[u(t) \exp(-2\pi i f_0 t) \right] \otimes \text{sinc}\, Wt \qquad (5.27)$$

Thus, the analytic, complex baseband waveform is given by sampling the real IF waveform u multiplied by the complex exponential $\exp(-2\pi i f_0 t)$—that is, after mixing down to baseband using a complex local oscillator (LO) at the signal's center frequency, f_0. (Again, in principle, to form this waveform we interpolate the samples obtained at intervals $1/F$, where the sampling rate F is $2f_0 + W$ or higher, with sinc functions.) In fact, we do not have to provide this LO waveform in continuous form, as we note that

$$\text{comb}_{1/F} \left[u(t) \exp(2\pi i f_0 t) \right] = \sum_{n=-\infty}^{\infty} u(n/F) \exp(-2\pi i n f_0 /F) \otimes \delta(t - n/F)$$

$$(5.28)$$

and we see that we multiply the samples of u by the sampled form of the complex exponential waveform. In the case where the IF carrier is $f_0 = W/2$ and the sampling rate F is the minimum $2W$, we see that F is just $4f_0$ and the sampled complex LO values are given by $\exp(-\pi i n/2)$ or $(-i)^n$ (i.e., we just multiply the real samples of u by 1, $-i$, -1, and i in turn, a particularly simple form of down-conversion). This gives a train of complex samples at rate $4f_0$, which are actually either real with imaginary part zero or imaginary with real part zero.

     If the IF is greater than $W/2$ (up to $3W/2$) then we can repeat the spectrum at the smaller interval of $2f_0 + W$, rather than $4f_0$, but in this case the complex down-conversion factors are not so simple, being given by $\exp\left(-\pi i n/(1+W/2 f_0)\right)$, leading to complex samples with both real and imaginary parts nonzero, in general. If the carrier frequency is not too high, then the $4f_0$ sampling rate may be preferred for its simplicity, even when it is not the very minimum rate.

     If the IF is considerably higher than the bandwidth, then lower sampling rates that avoid overlapping can be used, such as uniform sampling, as discussed in Section 5.4, of which this method is an example. Using the notation of Section 5.4, the lowest IF case corresponds to $f_u = W$ and $k = 1$. For higher IF values, we have $f_u = f_0 + W/2 = kW'$, where W' is the lowest value above (or equal to) W such that f_u/W' is an integer, k. Then the minimum required sampling rate is $2W' = (2f_0 + W)/k$, and the complex down-conversion factors are $\exp(-2\pi i f_0 n T)$, where $T = 1/2W'$ leading to the factors $\exp\left(-\pi i k n/(1+W/2 f_0)\right)$. Again this is an awkward form to apply, but if we chose the slightly higher sampling rate of $2f_0/(k - \frac{1}{2})$, as suggested in Section 5.4, then the down-conversion factors become simply $\exp(-\pi i n(k - \frac{1}{2}))$ or $-i^n$ for k odd and i^n for k even. However, sampling with a finite window

width on a high IF may require care, as discussed in the next section, and keeping the IF low would generally be preferable.

5.8   High IF Sampling

If we sample at a relatively high IF, the time taken to obtain a sample of the waveform may become significant compared with the period of the carrier. We take for our model a device that integrates the waveform over a short interval τ, the sample value recorded being the mean waveform value over this interval, the integral divided by τ. We see that this value is the same as would be given by a device that sampled instantaneously the waveform given by sliding a $(1/\tau)\mathrm{rect}(t/\tau)$ function across the waveform and integrating (i.e., forming the convolution of the waveform with the rect function). Thus, if u is the waveform, the samples actually correspond to the waveform v given by

$$v(t) = u(t)\otimes(1/\tau)\mathrm{rect}(t/\tau) \qquad (5.29)$$

The spectrum of this is

$$V(f) = U(f)\mathrm{sinc}(f\tau) \qquad (5.30)$$

Figure 5.16(a) shows the spectrum of V compared with that of U, shown as a rectangular band (in the positive frequency region only). With a low carrier frequency f_0, compared with $1/\tau$ (i.e., with τ a small fraction of the period of the carrier), in position "a," there is relatively modest distortion across the signal band. At a higher center frequency, position "b" (shown with a larger bandwidth), the distortion is more serious. At position "c," where the window is one cycle of f_0 ($f_0\tau = 1$), the distortion is severe and totally unacceptable. However in position "d," where the sinc function is near a stationary value, the distortion is very low. This is at $f_0\tau = 1.434$, so the window τ should be about 1.4 cycles of the carrier for a low-distortion result.

Although this may be interesting, it is probably not very practical. This is partly as the timing of 1.4 cycles may not in practice be accurate, moving the response to a more distorted part of the spectrum, but also the accuracy of the rect function may not be good, modifying the spectrum to a form that may have considerable slope at this point.

If we explore what window for integration would be ideal, we note that if we put $w(t)$ for the window shape, instead of the rect function in (5.29),

(a)

(b)
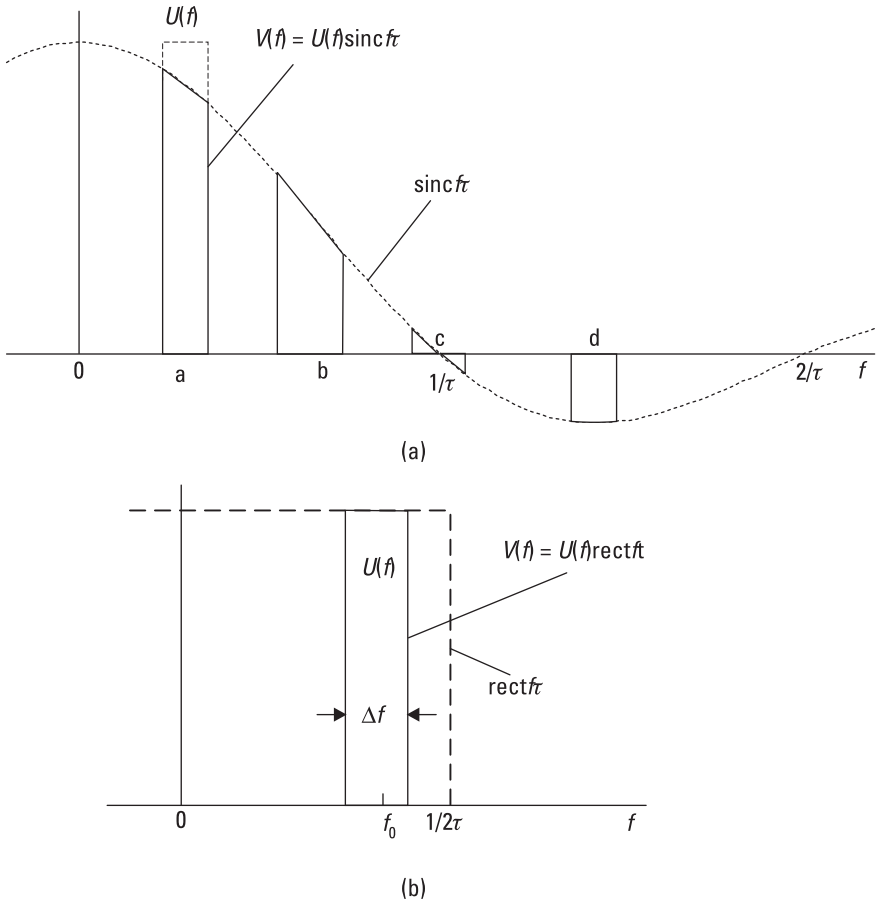
Figure 5.16   Spectrum of IF waveform sampled over a nontrivial interval. (a) Rectangular window, and (b) sinc window.

the signal spectrum would be multiplied by its transform $W(f)$, replacing the sinc function in (5.30). Ideally, we would like this to be flat over the band U, and this requires a rect function in the frequency domain and a sinc function window in the time domain. If we choose $w(t) = (1/\tau)\mathrm{sinc}\,t/\tau$ then $W(f) = \mathrm{rect}f\tau$. This has value 1 out to $1/2\tau$, which must be greater than $f_0 + \Delta f/2$, where Δf is the bandwidth, in order to cover the signal band, as shown in Figure 5.16(b).

Thus, we require $\tau \leq 1/(2f_0 + \Delta f)$, or rather less than half a cycle of the carrier. However the window, to give a reasonable approximation to the sinc function, would have to be many times τ in width or extend over several

cycles of the carrier. This would be a good distortionless way of sampling, but it is difficult to see how this could be implemented in practice.

5.9   Summary

In this chapter we have shown how the rules-and-pairs method can be used to obtain some sampling results very neatly and concisely. The main aim was to determine the minimum sampling rates that would retain the signal information, but in some cases the method was used to find what other rates would be acceptable (not necessarily all rates above the minimum). This was first applied to sampling wideband signals, with significant spectral power from some maximum W down to zero frequency. The information in a real waveform is all retained by sampling it at the rate $2W$ (or any higher rate). The second example, uniform sampling, applies to a narrowband signal, a signal on a carrier with a spectrum limited to a band of frequencies around the carrier. In this case, the rates acceptable are dependent on the ratio of the bandwidth W to the center frequency, f_0, being at least $2W$ and generally higher. This form of sampling is an example of the case where some higher sampling rates are not allowed if distortion is to be avoided.

A different approach is to convert the real waveform into the complex waveform that has the given waveform as its real part. This requires deriving the imaginary part from the real part by means of a Hilbert transform. In principle this is applicable to both wideband and narrowband waveforms, though it is more likely to be applied to the latter in practice (after downconversion to complex baseband). Given the complex waveform we find, very quickly, that we only have to sample (in the two channels, real and imaginary) at the rate W (or any higher rate) to obtain complex samples representing the waveform. It is this complex form that is normally required for digital signal processing.

Hilbert sampling seems a very satisfactory approach, but it does depend on the provision of a good Hilbert transform, which is equivalent to a wideband (all frequency) phase shift of 90°. A close approximation to Hilbert sampling, for narrowband waveforms, is quadrature sampling, where the Hilbert transform is replaced by a delay, essentially equal to a quarter of the carrier period. This provides the 90° shift of the carrier and close to 90° for frequencies close to the carrier. However, it is not exact—the signal envelope is delayed in the imaginary channel, which is a form of distortion, but in principle the waveform could be reconstituted by correct interpolation, with compensation for this delay. Nevertheless the analysis shows that all the data

in the signal can be retained by sampling at the correct rate and with the correct delay, but generally this rate is higher than for Hilbert sampling and, as with uniform sampling, depends on the ratio of W to f_0. Also, like the uniform sampling case, not all rates above the minimum are allowed.

The last method we consider is uniform sampling on a low IF, with down-conversion effectively achieved with the sampling. This includes the case of sampling at four times the carrier (IF) frequency and gives a particularly simple way of providing the complex baseband samples without the need for a Hilbert transformer or a quarter wave delay, so it is an attractive method to implement. The required sampling rate in a single channel is, at the minimum, twice that needed in the two channels for the other methods.

Finally, we consider the effect of trying to sample on too high an IF. If the sampling gate duration becomes a significant fraction of the carrier period, then there will be some spectral distortion. This is very easily shown using a simple model for the sampling analog-to-digital converter (ADC). However, it is also shown that the spectral distortion can be made low by careful choice of the ratio of the high IF period to the sampling gate width, using a rectangular window or by using, perhaps impractically, a window of near sinc function shape.

References

[1]   Woodward, P. M., *Probability and Information Theory, with Applications to Radar*, Norwood, MA: Artech House, 1980.

[2]   Brown Jr., J. L., "On Quadrature Sampling of Bandpass Signals," *IEEE Trans*. AES-15, No. 3, 1979, pp. 366–371.

Appendix 5A: The Hilbert Transform

A real waveform u has a spectrum U of positive and negative frequencies, with all the information about it contained in one half of the spectrum. (We have already seen, in Section 2.3, that the negative frequency components are just the complex conjugate of those of the corresponding positive frequencies.) We can define a complex function $v = u + i\hat{u}$ that has a positive frequency spectrum only, if we can form $\hat{u}$, with spectrum $\hat{U}$, such that $i\hat{U}$ is equal to U for positive frequencies and to $-\hat{U}$ for negative frequencies. Thus, given

$$v(t) = u(t) + i\hat{u}(t), \tag{5A.1}$$

with spectrum

$$V(f) = U(f) + i\hat{U}(f), \tag{5A.2}$$

if we choose

$$i\hat{U}(f) = \begin{cases} U(f) & \text{for } f > 0 \\ -U(f) & \text{for } f < 0 \end{cases} \tag{5A.3}$$

and $\hat{U}(0) = 0$) the spectrum of v is given by

$$V(f) = \begin{cases} 2U(f) & \text{for } f > 0 \\ 0 & \text{for } f < 0 \end{cases} \tag{5A.4}$$

and $V(0) = U(0)$). This is a spectrum of positive frequencies only, as required. To find $\hat{u}$, we note from (5A.4) that $V(f)$ can be written as $2U(f)h(f)$, so taking the inverse transform, using P2b, we have

$$v(t) = 2u(t) \otimes \left(\frac{\delta(t)}{2} - \frac{1}{2\pi it} \right) = u(t) + iu(t) \otimes \left(\frac{1}{\pi t} \right)$$

and so

$$\hat{u}(t) = u(t) \otimes \left(\frac{1}{\pi t} \right) = \frac{1}{\pi} \int_{-\infty}^{\infty} \frac{u(\tau)}{t - \tau} d\tau \tag{5A.5}$$

(We can also put, from (5A.3), $i\hat{U}(f) = U(f)\text{sgn}(f)$, so that, from P2c and R4 we have $i\hat{u}(t) = u(t) \otimes (-1/\pi it)$, leading directly to (5A.5)).

The Hilbert transform of $u(t) = \cos 2\pi f_0 t$ is $\hat{u}(t) = \sin 2\pi f_0 t$; this can be found using (5A.5) (treating τ as a complex variable and using contour integration) or, more simply, by choosing the function for $\hat{u}$ that converts the two-line spectrum (at $-f_0$ and $+f_0$) of u into the single line spectrum of v (at $+f_0$ only) (i.e., that makes v a single complex exponential). In this case $v(t)$ is given by

$$v(t) = \cos 2\pi f_0 t + i\sin 2\pi f_0 t = \exp 2\pi i f_0 t$$

and so $V(f) = \delta(f - f_0)$, which is a single line at $+f_0$. The spectra of u and $i\hat{u}$ are $\frac{1}{2}(\delta(f - f_0) + \delta(f + f_0))$ and $\frac{1}{2}(\delta(f - f_0) - \delta(f + f_0))$, respectively, which satisfy the form of (5A.3). Similarly, the Hilbert transform of $\sin 2\pi f_0 t$ is $-\cos 2\pi f_0 t$, so that in this case

$$v(t) = \sin 2\pi f_0 t - i\cos 2\pi f_0 t = -i\exp 2\pi i f_0 t$$

Both these Hilbert transforms correspond to a phase shift of $-\pi/2$ radians, as $\cos(2\pi f_0 t - \pi/2) = \sin 2\pi f_0 t$ and $\sin(2\pi f_0 t - \pi/2) = -\cos 2\pi f_0 t$. This is the case for all frequency components of a real waveform, so we see that the Hilbert transform is equivalent to a wideband (all-frequency) phase shift of $-\pi/2$.

6

Interpolation for Delayed Waveform Time Series

6.1 Introduction

Here we consider the question, given a time series obtained by regular sampling of some waveform, how do we form the time series of a delayed version of the waveform? Clearly there is no real problem for a delay that is a multiple of the sampling period—instead of the current sample from the undelayed waveform, we just take the correctly delayed sample. The required series could be obtained from a shift register clocked at the sampling rate. Thus, we are left with the problem of generating series corresponding to delays of less than a sampling period. We consider only sampled analytic signals (complex time series), and we show that considerable benefits, in terms of reduced computation, are given if the waveform is sampled at a rate above the minimum required to retain all its information (see Chapter 5)—the case of oversampling.

We first investigate, in Section 6.2, the weights on the taps of a transversal filter required to give the series for the delayed waveform, derived without reference to the waveform. This filter is thus suitable for the general case, where any waveform (subject to it being within a given bandwidth) may be taken and where its power spectrum is not necessarily known. We start with the case of the minimum sampling rate and then explore the gains possible

with an oversampled waveform. In Section 6.3, we find the weights that give the optimum series in the sense of the least mean square error (or error in power) between the interpolated series and the true series for the delayed waveform. The error arises because to achieve perfect interpolation in principle, ignoring practical problems of finite word lengths and sampling quantization, an infinitely long filter would be required, in general.

Two applications of interpolation are given in Sections 6.4 and 6.5. The first shows a remarkable reduction in computational load in generating simulated radar clutter, which is sampled at the pulse repetition frequency (PRF), typically a few kilohertz, and a much higher rate than the bandwidth of the clutter waveform (a few tens of hertz). The second shows how interpolation can be used for resampling—generating the sequence of samples that would have been obtained by sampling a signal at a rate different from that actually used.

6.2   Spectrum Independent Interpolation

In this section, we show how a finite impulse response (FIR) filter can be designed to achieve the required interpolation, with the coefficients easily obtained using the rules-and-pairs method. Generally, this requires quite a long filter if the interpolation is to be achieved with high fidelity when sampling at the minimum rate necessary to preserve the full information. More interestingly, we then consider the case where the waveform is sampled at a rate above this minimum—the oversampled case—and find that, by taking advantage of this higher rate, very considerable gains in terms of reducing the filter length, and so the required computation, can be achieved for comparable performance.

6.2.1   Minimum Sampling Rate Solution

Given a time series of samples of a continuous waveform, sample values of that waveform at other times can be calculated by taking a weighted combination of the given samples. A suitable set of weights will produce a time series corresponding to samples taken at a certain interval, or delay, after those of the input. This produces a time series corresponding to a delayed version of the waveform. The series itself is not delayed, except perhaps by a whole number of sample periods; it is otherwise synchronous with the input series. Figure 6.1 illustrates the structure, which is in fact a transversal, or finite
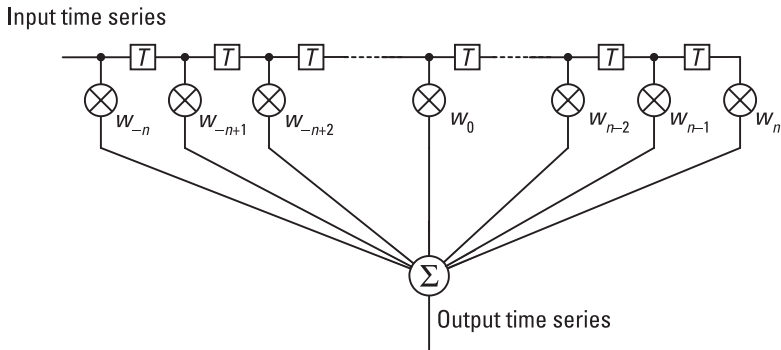
Figure 6.1 FIR filter for interpolation.

impulse response (FIR), filter. The delay T between taps is identical with the sampling period, and we note that the output of the center tap, with weight w_0, can be considered to be the undelayed waveform, if an overall delay of nT can be accepted. In this case, it is possible to obtain (relatively) negative delays as well as positive ones (e.g., if all the weights were zero except the first, w_{-n}, then the relative delay of the output series would be $-nT$). We take the time series to be that of a complex baseband waveform of finite bandwidth with spectrum in the band $-F/2$ to $+F/2$, corresponding to an RF or IF waveform of bandwidth F. The minimum sampling rate to retain the information in the waveform is F, and initially we take this to be the sampling rate for the time series, but subsequently we investigate the benefit, from the point of view of more efficient interpolation, of sampling at a higher rate. If the signal waveform is $u(t)$ and the spectrum is $U(f)$, then we can write the identity

$$U(f) = \mathrm{rect}(f/F)\,\mathrm{rep}_F\, U(f) \qquad (6.1)$$

This states that U is equal to a suitably gated portion of a repetitive form of itself (Figure 6.2).
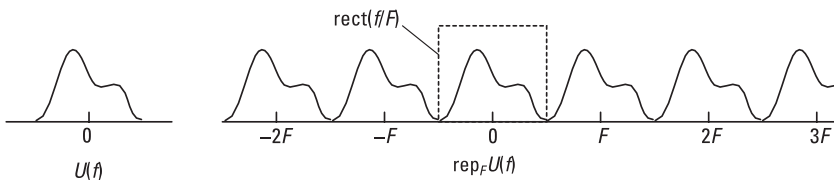
Figure 6.2 Equivalent forms of $U(f)$.

The inverse Fourier transform of this (from P3b, R5, R7b, and R8a) is

$$u(t) = F\operatorname{sinc}(Ft) \otimes \frac{1}{F}\operatorname{comb}_{1/F} u(t) = \operatorname{sinc}(t/T) \otimes \operatorname{comb}_T u(t) \quad (6.2)$$

where T is the sampling period and $T = 1/F$. The function $\operatorname{comb}_T u(t)$ is a set of δ-functions at intervals T of strengths given by the waveform values at the sampling point (as defined in (2.16)). Putting the comb function in this form we have, using (2.11) for the convolution with a δ-function,

$$u(t) = \operatorname{sinc}(t/T) \otimes \sum_{r=-\infty}^{\infty} u(rT)\delta(t - rT) = \sum_r u(rT)\operatorname{sinc}\left(\frac{t - rT}{T}\right) (6.3)$$

where we use Σ_r to imply summation over all integer r. This shows how to calculate $u(t)$ at any time t from the given set of samples at times $0, \pm T, \pm 2T, \ldots$ (i.e., $\{u(rT): r = -\infty \text{ to } +\infty\}$). We place a sinc function, scaled by the sample value, at each sample position and sum these waveforms (Figure 6.3). In particular, if $t = kT$, where k is an integer, then $\operatorname{sinc}((t - rT)/T) = \operatorname{sinc}(k - r) = \delta_k$, as $\operatorname{sinc}(x) = 0$ for x a nonzero integer and $\operatorname{sinc}(0) = 1$, and we have

$$u(kT) = \sum_r u(rT)\delta_{kr} = u(kT)$$

as required. (δ_{kr} is the Kronecker-δ; $\delta_{kr} = 0$ for $k \neq r$, $\delta_{kk} = 1$ for all k.)
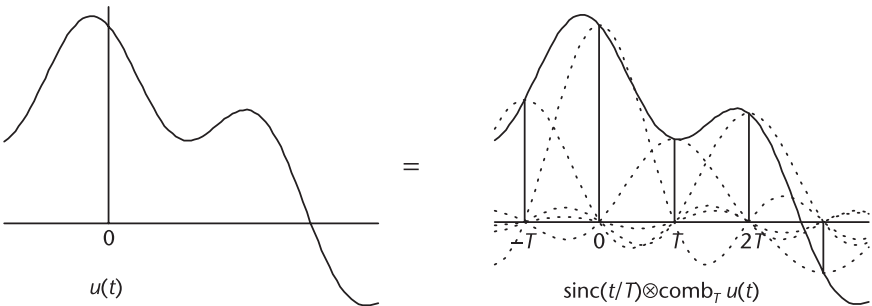
Figure 6.3 Equivalent forms of $u(t)$.

To determine the function value at time τ (where we only need to consider $|\tau| \leq T/2$) we have, from (6.3)

$$u(\tau) = \sum_r u(rT)\operatorname{sinc}\left(\frac{\tau - rT}{T}\right)$$

$$= u(0)\operatorname{sinc}\left(\frac{\tau}{T}\right) + u(T)\operatorname{sinc}\left(\frac{\tau - T}{T}\right) + \ldots$$

$$+ u(-T)\operatorname{sinc}\left(\frac{\tau + T}{T}\right) + \ldots = w_0 u(0) + w_1 u(T) + w_2 u(2T) + \ldots$$

$$+ w_{-1} u(-T) + w_{-2} u(-2T) + \ldots$$

$$(6.4)$$

In practice we cannot obtain $u(\tau)$ exactly, as this requires an infinite number of terms, but the weights applied generally fall (though not necessarily monotonically) for samples further away from the interpolated sample time (within $\pm T/2$ of the center), so we curtail the series when the weights become small. We note that the weights, given by $w_r = \operatorname{sinc}((\tau - rT)/T)$, are dependent on the delay required, τ. In fact, we consider them to be functions of $\rho = \tau/T$, the delay in units of the sampling interval, T. Thus, we have $w_r(\rho) = \operatorname{sinc}(\rho - r) = \operatorname{sinc}(r - \rho)$ (as the sinc function is symmetric). We assume that the delay has been matched as far as possible by shifts of a whole number of sampling intervals, so that the fractional interval ρ is between $-1/2$ and $+1/2$.

The worst case for interpolation is for delays of $\pm T/2$, at the maximum distance from a sample. The interpolation factor, or weight, applied to the output of tap r (i.e., to samples at time rT relative to the center tap output) in this case is

$$w_r(\tfrac{1}{2}) = \operatorname{sinc}(r - \tfrac{1}{2}) = \sin(\pi(r - \tfrac{1}{2}))/\pi(r - \tfrac{1}{2}) = (-1)^{r+1}/\pi(r - \tfrac{1}{2}) \qquad (6.5)$$

The tap weights are given in decibel form as the discrete points on the curve in Figure 6.4 for three delay values. For the case of a delay of $0.1T$ (with symbol +), the weight is close to unity for the zero delay tap and falls quite rapidly for the other weights. At a delay of $0.5T$, the weights (given by a dot symbol) are equal for the first two closest taps (numbers 0 and 1) and then fall away rather slowly. For a delay of $0.25T$, the weight pattern (symbol ×) is intermediate, but closer to the $0.5T$ case, falling away only slightly faster. If we take −30 dB as the weight level below which we will neglect the contributions, then we see that we need only about 7 taps for the $0.1T$ delay, but 14 at $0.25T$ and 20 at $0.5T$.
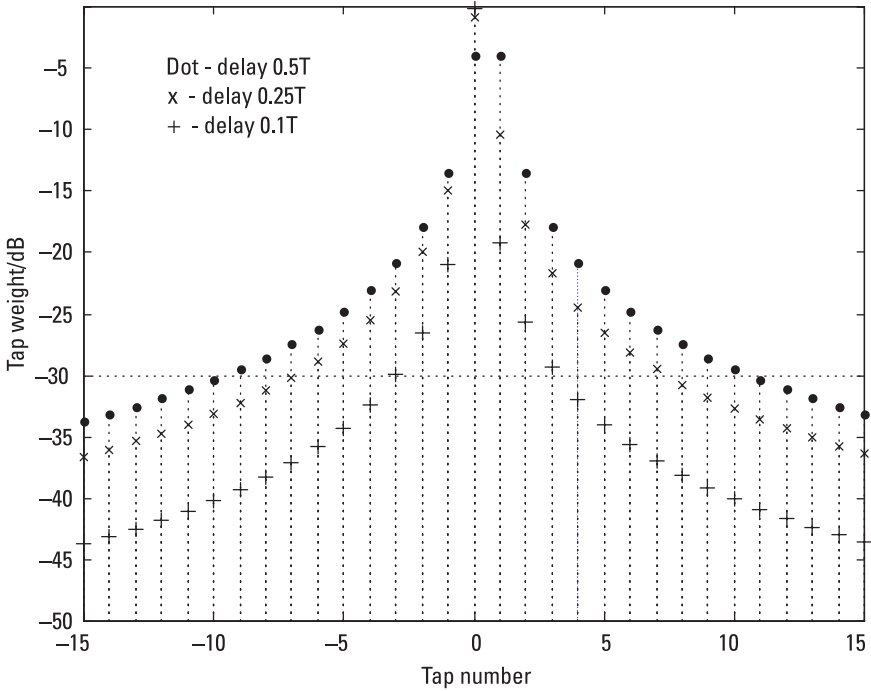
Figure 6.4　FIR filter weights for interpolation, at minimum sampling rate.

6.2.2　Oversampling and the Spectral Gating Condition

For a (complex) waveform of bandwidth F, the minimum sampling rate at which the waveform can be sampled without losing information is F. (This is the case using Hilbert sampling; see Chapter 5. With other forms of sampling, we may need slightly higher rates.) If we sample at a lower rate, then the repeating spectra will overlap, and the resulting set of samples would correspond to the result of sampling a slightly different waveform (a distorted form of the waveform) at this lower rate. This effect is known as *aliasing*. However if we sample at any rate higher than F, no spectral overlapping occurs; we retain all the waveform information and could reconstruct the waveform with correct interpolation. This is less efficient than sampling at the minimum rate in the sense that more work is done than is necessary, but we will see that it enables us to achieve much more efficient interpolation.

Let the sample rate be $F' = qF$, where $q > 1$, so that the interval between samples is now $T' = 1/F' = T/q$. In this case, the spectrum of the sampled waveform repeats at the interval F', which is greater than the width of the

basic spectrum, so there are gaps in the spectrum of the sampled waveform as shown in Figure 6.5. We see that we can put the identity for the waveform spectrum, corresponding to (6.1) for the minimum sampling rate, in the modified form

$$U(f) = G(f)\text{rep}_{F'}U(f) \tag{6.6}$$

where an example of the gating function G is shown in the figure. For (6.6) to be true, we see that there are two conditions that G must satisfy:

$$G(f) = 1 \text{ for } |f| < F/2 \quad \text{and} \quad G(f) = 0 \text{ for } |f| > F' - F/2 = (q - \tfrac{1}{2})F. \tag{6.7}$$

The first of these conditions is to ensure that there is no spectral distortion, and the second ensures that there is no aliasing (i.e., no energy is included from repeated parts of the spectrum). G is not defined in the regions $[-(q - \tfrac{1}{2})F, -F/2]$ and $[F/2, (q - \tfrac{1}{2})F]$ (except that it must remain finite) as there is no spectral power in these regions. Thus, we are free to choose G to be of any form as long as it satisfies the conditions (6.7). In the case of sampling at the minimum rate, F, we have $q = 1$, so the regions of free choice are of zero width and we are forced to make G the rect function, as in (6.1). We could note, as a more general form for the second condition in (6.7), that G should be zero only on all the intervals $|f - nF| < F/2$ ($n = -\infty$ to $+\infty$, $n \neq 0$) (i.e., for all bands of width F centered on all frequencies nF except $n = 0$). However, this will not generally be a useful relaxation of the condition.

From (6.6), taking the inverse Fourier transforms, we have

$$u(t) = (1/F')g(t) \otimes \text{comb}_{T'} u(t) = \phi(t) \otimes \text{comb}_{T'} u(t) \tag{6.8}$$

where the interpolating function is

$$\phi(t) = (1/F')g(t) = T'g(t) \tag{6.9}$$
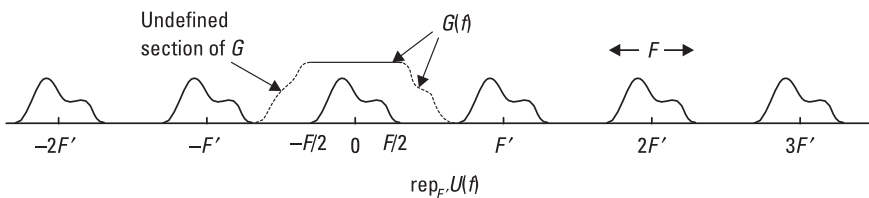
Figure 6.5   Spectrum of time series of u sampled at rate F'.

and g is the inverse Fourier transform of G. Expanding the comb function, we have

$$u(t) = \phi(t) \otimes \sum_r \delta(t - rT')u(rT')$$

$$= \sum_r \phi(t - rT')u(rT') = \sum_r w_r(t/T)u(rT')$$

Thus, the weights are given, for a delay $\tau = \rho T'$, by

$$w_r(\rho) = \phi\big((\rho - r)T'\big) \tag{6.10}$$

The samples in this case are at intervals T' so the worst-case delay is $T'/2$, smaller than the value at the minimum sampling rate, $T/2$, so there is some easing of the interpolation problem, but this is small compared with that obtainable from good choices of the gating function. Before considering these, we take the case of the simplest form of the gating function that takes advantage of oversampling (Figure 6.6). This is $G(f) = \text{rect}[f/(2F'-F)]$, or $\text{rect}[f/(2q-1)F]$, and the interpolating function is given, from (6.9) (and P3b, R5), by

$$\phi(t) = \frac{(2q-1)F}{qF}\text{sinc}\big((2q-1)Ft\big) = \frac{(2q-1)}{q}\text{sinc}\big((2q-1)t/T\big) \tag{6.11}$$

The characteristic width of this function, $T/(2q-1)$, is narrower than the sample separation, T/q, so we should be able to use fewer taps for a given lower limit to the tap weight magnitudes. The weights for a delay $\tau = \rho T' = \rho T/q$ (with $-0.5 < \rho \le 0.5$) are, from (6.10) and (6.11),

$$w_r(\rho) = \frac{2q-1}{q}\text{sinc}\left(\frac{(2q-1)(r-\rho)}{q}\right) = \left(\frac{2q-1}{q}\right)\text{sinc}(x+y) \tag{6.12}$$
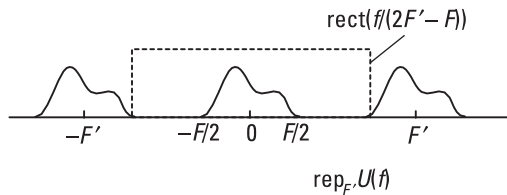
Figure 6.6 Optimum rectangular gate for oversampled time series.

where $x = (r - \rho)$ and $y = (q - 1)x/q$. (The variables x and y will be used in the weights required for the three further gating functions considered in Section 6.2.3.) We note from (6.12) that if ρ, and hence τ, is zero $w_r(0)$ is nonzero for all values of r, unlike the minimum sampling case illustrated in Figure 6.3, where $w_r(0) = 0$ except for $w_0(0)$, which is 1, so it is not immediately obvious how this sampling method produces the correct values at the sampling points, let alone between them. In particular $w_0(0) = (2q - 1)/q$, which approaches the value 2 for large q. Figure 6.7 illustrates the case where a flat part of the waveform, with constant value unity, has been sampled at an oversampling rate of $q = 3$. We see that at the sample points, the weight value is 5/3, but the contributions from the interpolating sinc functions from nearby sample points are negative, bringing the value down to the correct level of unity.

The weights given by (6.12) for oversampling factors of 2 and 3 are shown in Figure 6.8, for comparison with the values for the minimum sampling rate ($q = 1$) plotted in Figure 6.4. The same set of delays has been taken. These plots show that the weight for the tap nearest to the interpolation point (taken to be the center tap here) can be greater than unity, that the weight magnitudes do not necessarily fall monotonically as we move away from this point, and that much the same number of taps is required, above a given weight level, such as –30 dB. At first this last point might seem unexpected—there is no significant benefit from using the wider spectral gate that is possible with oversampling. However, the relatively slow falling off of the tap weight values is a result of the relatively slowly decaying interpolating sinc function, and this in turn is the result of using the rectangular gate, with its sharp, discontinuous edges. This is the case whether or not we have oversampling. The solution, if fewer taps are to be required, is to use a smoother spectral gating function, and this is the subject of the next section.
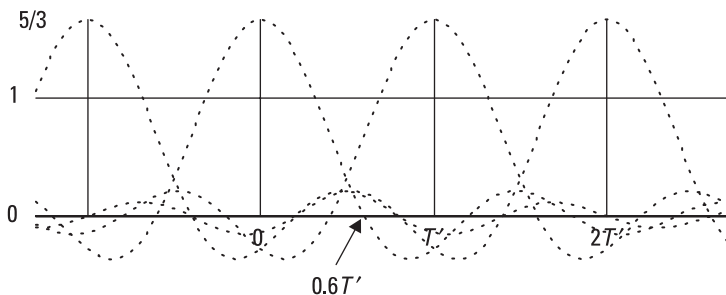
Figure 6.7 Flat waveform oversampled.
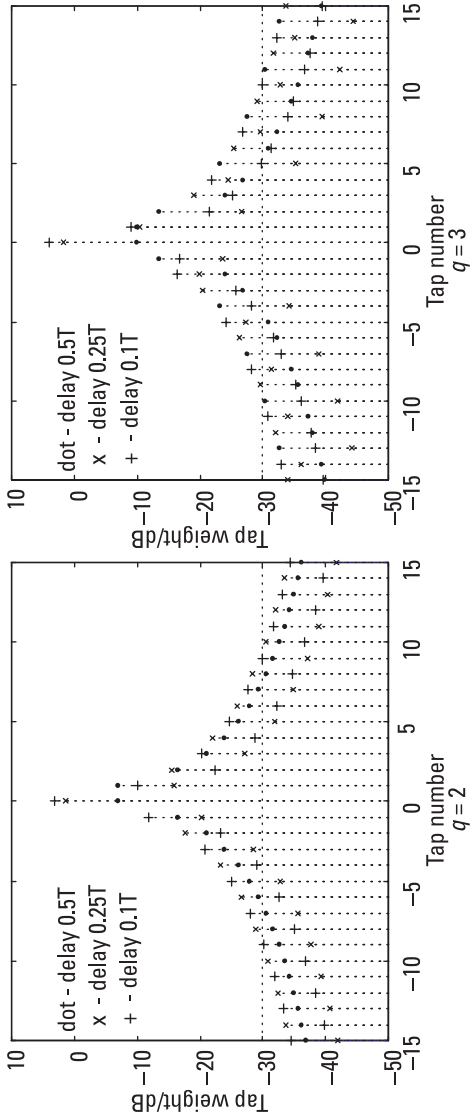
Figure 6.8 FIR interpolation weights with oversampling and rectangular gate.

6.2.3 Three Spectral Gates

Trapezoidal Gate

The first example of a spectral gate without the sharp step discontinuity of the rect function is given by a trapezoidal function (Figure 6.9). As illustrated, in this figure and also in Section 3.1, this symmetrical trapezoidal shape is given by the convolution of two rectangular functions with a suitable scaling factor. The widths of these rect functions has been chosen so that G, as in Figure 6.5, has the minimum flat top width necessary and slope of maximum length, extending to the edges of the repetitions of the spectrum centered at $+qF$ and $-qF$. The convolution of unscaled rect functions has a peak (plateau) level of $(q-1)F$, the area of the smaller rect function, so we define G by

$$G(f) = \frac{1}{(q-1)F} \operatorname{rect}\left(\frac{f}{qF}\right) \otimes \operatorname{rect}\left(\frac{f}{(q-1)F}\right) \tag{6.13}$$

Thus, on taking the transform, we have $g(t) = qF \operatorname{sinc}(qFt)\operatorname{sinc}\left((q-1)Ft\right)$, and the interpolating function is given, from (6.9) with $T' = 1/qF$, by

$$\phi(t) = \operatorname{sinc}(qFt)\operatorname{sinc}(q-1)Ft \tag{6.14}$$

From (6.8) we have

$$u(t) = \operatorname{sinc}(qFt)\operatorname{sinc}(q-1)Ft \otimes \operatorname{comb}_{1/F'}u(t) \tag{6.15}$$

The interpolating function ϕ is now a product of sinc functions, and this has much lower sidelobes than the simple sinc function (e.g., see Figure 3.2).
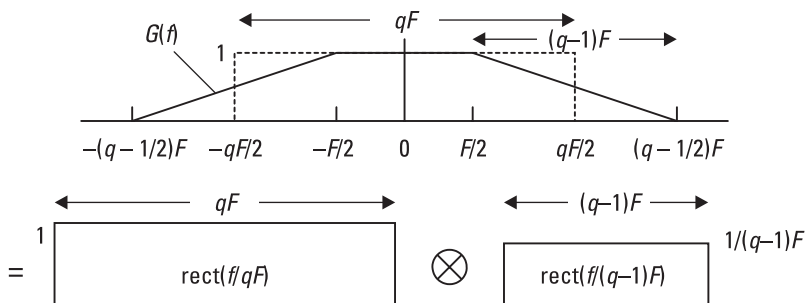
Figure 6.9 Trapezoidal spectral gate.

To interpolate at time $\tau = \rho T'$, where $-0.5 < \rho \leq 0.5$ (i.e., τ is a fraction of a tap interval), we consider the contribution from time sample r, giving

$$w_r(\rho) = \phi((\mathrm{r} - \rho)T') = \mathrm{sinc}(r - \rho)\,\mathrm{sinc}[(r - \rho)(q - 1)/q]. \quad (6.16)$$

Now let $x = r - \rho$ and $y = (q - 1)x/q$ (as in (6.12)), then

$$w_r(\rho) = \mathrm{sinc}x\,\mathrm{sinc}y = \sin X \sin Y / XY \quad (6.17)$$

where $X = \pi x$ and $Y = \pi y$. If we take the case of $\rho = 1/2$, the worst case, as in Section 6.2.1, we have $\sin X = \sin\pi(r - \frac{1}{2}) = (-1)^{r+1}$, and if we take $q = 2$ (sampling at twice the minimum rate), then $y = x/2$ and $\sin Y = \pm 1/\sqrt{2}$, for r integral, and so the magnitudes of the tap weights are

$$\left| w_r(\tfrac{1}{2}) \right| = \left| \phi((r - \tfrac{1}{2})T') \right| = \sqrt{2}\big/\pi^2(r - \tfrac{1}{2})^2 \quad (6.18)$$

Comparing this with (6.5), we see that the weight values now fall very much faster, and this is illustrated in Figure 6.10, for comparison with Figures 6.4 and 6.8. We see that the number of taps above any given level has been reduced dramatically—above -30 dB, for example, from 20, 15, and 7 for the three delays chosen, at $q = 1$, to 4, 3, and 3 at $q = 2$ and as few as 2, 3, and 2 at $q = 3$. Above the -40-dB level, the number of taps needed at $0.5\,T$ is found to be 65 at the minimum sampling rate, but only 8 for $q = 2$ and $q = 3$.

Trapezoidal Rounded Gate

The trapezoidal function of Figure 6.9 still has slope discontinuities, though not the step discontinuities that the rect function has. The corners of the trapezoid can be rounded by another rect convolution, to make three convolved rect functions in total. Equivalently, we can consider that the combination of the two narrower rect functions, one removing the steps and the other removing the abrupt slope changes, together form a trapezoidal pulse (see Figure 6.11), and this then rounds the largest rectangular pulse. As before, the main rect function is of width qF (as in Figure 6.9) and the overall rounding pulse is of base length $(q - 1)F$, as this is the space available for the rounding on each side. Let the two shorter rectangular pulses be of length $\alpha(q - 1)F$ and $(1 - \alpha)(q - 1)F$ where $0 < \alpha \leq 0.5$. Then their convolution will be of the required length $(q - 1)F$, as shown in the upper part of Figure 6.11. If these pulses are of unit height, then the trapezoidal pulse will be of height $\alpha(q - 1)F$, the area of the smaller pulse, so we need to divide by this factor to
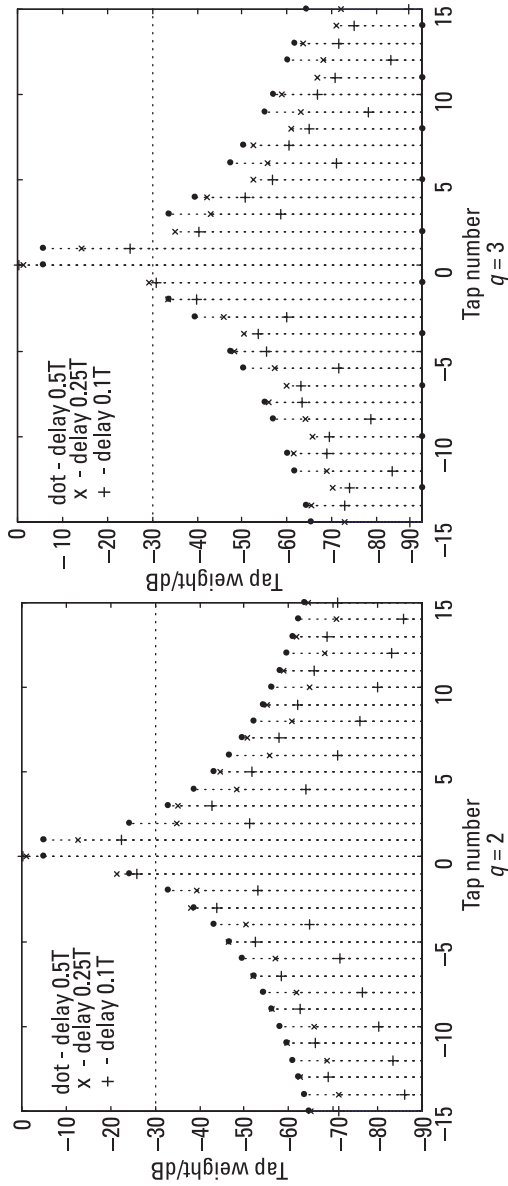
Figure 6.10 Filter weights with oversampling and trapezoidal spectral gate.
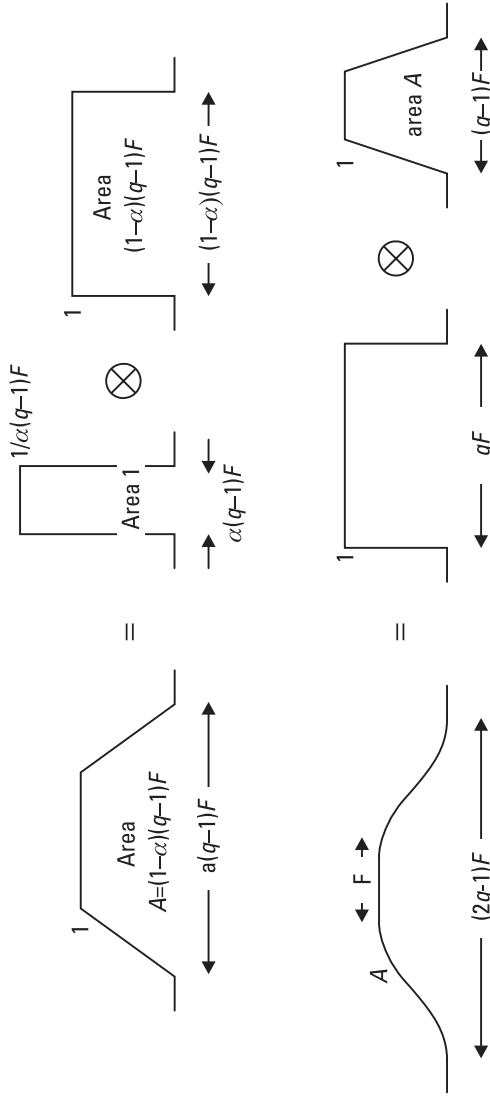
Figure 6.11   Trapezoidal rounding.

form a trapezoidal pulse of unit height. The area A of the (unit height) trapezoidal pulse is the same as that of the wider rectangle, $(1 - \alpha)(q - 1)F$, so we also have to divide by this factor when we perform the second convolution in order to make the height of G unity, as required. Thus, we have

$$G(f) = \frac{\text{rect}(f/qF) \otimes \text{rect}(f/\alpha(q-1)F) \otimes \text{rect}(f/(1-\alpha)(q-1)F)}{\alpha(1-\alpha)(q-1)^2 F^2} \quad (6.19)$$

The interpolating function ϕ is given by

$$\phi(t) = (1/qF)g(t) = \text{sinc } qFt \,\text{sinc}(\alpha(q-1)Ft)\,\text{sinc}\big((1-\alpha)(q-1)Ft\big) \quad (6.20)$$

Let $t = (r - \rho)T'$ as before (with $-0.5 < \rho \leq 0.5$), and also $x = qFt = r - \rho$ and $y = (q - 1)x/q$, as before, then

$$w_r(\rho) = \phi((r - \rho)T') = \text{sinc } x \,\text{sinc}(\alpha y)\,\text{sinc}((1 - \alpha)y)$$
$$= \text{sinc} x \,\text{sinc} y_1 \,\text{sinc} y_2 \quad (6.21)$$

where $y_1 = \alpha y$ and $y_2 = (1 - \alpha)y$. If we want the weights in terms of the sine function then

$$w_r(\rho) = \frac{\sin X \sin Y_1 \sin Y_2}{XY_1Y_2}$$

where $X = \pi x$, $Y_1 = \alpha \pi y$ and $Y_2 = (1 - \alpha)\pi y$.

If $\alpha = 0.5$ we have a triangular pulse for the rounding convolution, but this may make the edge too sharp. As we reduce α, we go through the trapezoidal rounding toward the rectangular case considered in Section 6.2.3. The weights for the same three delays as before are plotted in Figure 6.12 for oversampling factors of 2 and 3, and for a value for α of 1/3. Again, we see that very few taps are needed, compared with the rectangular case, and the weight values are seen to be falling away more rapidly than for the simple trapezoidal case, as expected.

Raised Cosine Rounded Gate

Here we use a raised cosine pulse for rounding instead of the trapezoidal pulse. This pulse is of the form $1 + \cos(af)$, so it has a minimum value of zero
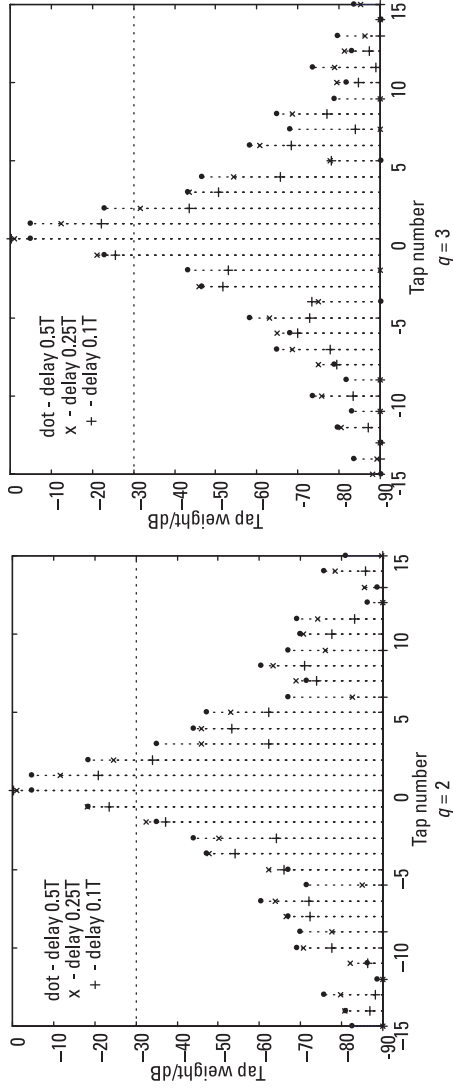
Figure 6.12   Filter weights with oversampling and trapezoidal rounded gate.

and is gated to one cycle width, which is the required value $(q-1)F$. If $2A$ is its peak value, then the pulse shape (in the frequency domain) is given by $A\,\text{rect}\left(f/(q-1)F\right)\left\{1+\cos\left(2\pi f/(q-1)F\right)\right\}$ (see Figure 6.13). This has integral $A(q-1)F$, due to the raised offset only, as the integral of the single cycle of the cosine function within the rect gate is zero. In order to make the area unity, we take $A = 1/(q-1)F$. Applying this to the main spectral gating rect function to give the smoothed form we have

$$G(f) = \text{rect}\frac{f}{qF} \otimes \left\{\text{rect}\left(\frac{f}{(q-1)F}\right)\frac{1+\cos(2\pi f/(q-1)F)}{(q-1)F}\right\} \quad (6.22)$$

and

$$g(t) = qF \operatorname{sinc} qFt \left\{\operatorname{sinc}(q-1)Ft \otimes \left(\delta(t) + \frac{\delta(t-\Delta t)+\delta(t+\Delta t)}{2}\right)\right\}$$

where $\Delta t = 1/(q-1)F$. On performing the δ-function convolutions, the interpolating function is

$$\phi(t) = \frac{1}{qF}g(t)$$

$$= \operatorname{sinc} qFt \left\{\operatorname{sinc}(q-1)Ft + \frac{1}{2}\operatorname{sinc}\left((q-1)Ft-1\right) + \frac{1}{2}\operatorname{sinc}\left((q-1)Ft+1\right)\right\}$$

$$(6.23)$$

The term in brackets (i.e., {}) has much lower sidelobes, though a wider main lobe, than the basic sinc function, as should be expected from the form
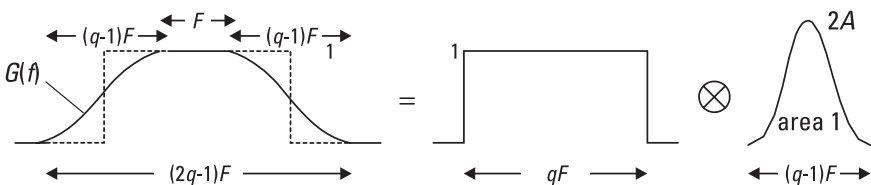
Figure 6.13 Raised cosine rounding.

of the gating, or windowing, function G (Hann weighting). With the same notation as used earlier, we have for the delay $\tau = \rho T'$,

$$w_r(\rho) = \phi\big((r-\rho)T'\big) = g\big((r-\rho)T'\big)/qF$$

$$= \operatorname{sinc} x \left\{ \operatorname{sinc} y + \frac{1}{2}\operatorname{sinc}(y-1) + \frac{1}{2}\operatorname{sinc}(y+1) \right\} \qquad (6.24)$$

where x and y are as before (in (6.17) and (6.21)).

We can simplify this slightly on putting

$$\operatorname{sinc}(y\pm 1) = \frac{\sin \pi(y\pm 1)}{\pi(y\pm 1)} = \frac{-\sin \pi y}{\pi(y\pm 1)} = \mp \frac{y\operatorname{sinc} y}{1\pm y}$$

so that

$$w_r(\rho) = \operatorname{sinc} x \operatorname{sinc} y \left(1 + \frac{y}{2(1-y)} - \frac{y}{2(1+y)} \right) = \frac{\operatorname{sinc} x \operatorname{sinc} y}{1-y^2} \qquad (6.25)$$

In terms of sine functions, this is

$$w_r(\rho) = = \frac{\sin X \sin Y}{XY(1-y^2)}$$

with X and Y as in (6.17)).

Compared with the case of the trapezoidal gate in equation (6.17), there is an extra factor in the denominator of $1 - y^2$, which is effective in reducing the magnitudes of w_r when r is large (and hence so are x and y). Figure 6.14 shows the weights for the same delays and oversampling factors as before, and we see that the weight values fall even faster than with trapezoidal rounding, as a result of the very smooth form of this rounding.

6.2.4   Results and Comparisons

In this section, we give the tap weights (in decibels) for the case $\rho = 1/2$ (i.e., for the worst-case interpolation, half-way between two taps). For smaller ρ the weight values will fall faster with r. For small delays (very much less than $T'/2$), oversampling may hardly be needed to keep down the number of taps
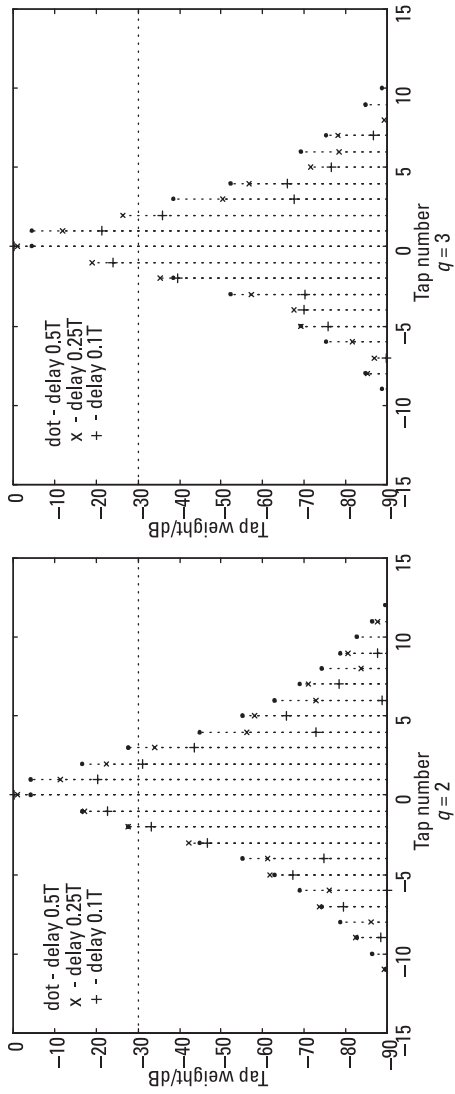
Figure 6.14   Filter weights with oversampling and raised cosine rounded gate.

while maintaining good signal fidelity, but in many applications a delay may be required, and here we evaluate the tap weights for the worst case.

Results for four different interpolation expressions are obtained, following the different spectral gating functions given earlier. These are, with ρ the required delay as a fraction of the sampling interval and q the factor by which the data is oversampled,

1. Maximum width rectangular gating (6.12)

$$w_r(\rho) = \left(\frac{2q-1}{q}\right)\mathrm{sinc}(x + y) \quad (x = r - \rho, y = (q-1)x/q)$$

2. Trapezoidal spectral gating (6.17)

$$w_r(\rho) = \mathrm{sinc}x\ \mathrm{sinc}y$$

3. Rectangular gate with trapezoidal rounding (6.21)

$$w_r(\rho) = \mathrm{sinc}x\ \mathrm{sinc}(1 - \alpha)y\ \mathrm{sinc}\alpha y \quad (0 < \alpha < 1)$$

4. Rectangular gate with raised cosine rounding (6.25)

$$w_r(\rho) = \frac{\mathrm{sinc}x\ \mathrm{sinc}y}{1 - y^2}$$

Figure 6.15 shows, in contour plot form, how the filter tap weights vary with oversampling rate, for the worst-case delay of $0.5T$. The tap weights are given in decibel form with tap number along the X axis and oversampling rate along the Y axis. The contours are at 10-dB intervals. Only integer values for the tap numbers are meaningful, of course, but these expressions are not restricted to integer values of r and so contour plots can be drawn.

The plots give a general impression of the benefit of oversampling and allow some comparison of gating functions. In general, the faster the weights fall with tap number, the better, so that when the values are below some low enough value, the taps are not required, and the filter length is limited. In these plots the lowest contour level is –70 dB, and we see there are considerable areas below this level in the cases of the trapezoidal rounded gate and the raised cosine rounded gate.
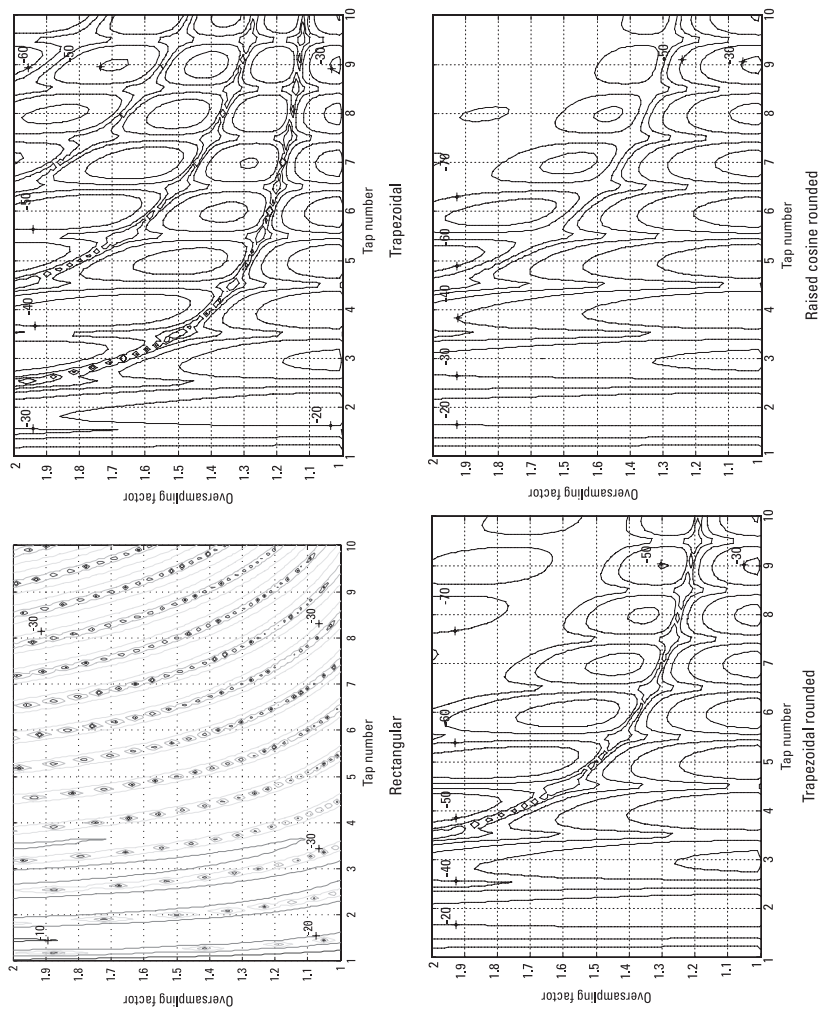
Figure 6.15 Tap weight variation with oversampling rate for four spectral gating functions, for delay of half a sampling interval.

These occur at quite modest oversampling rates and for reasonably short filter lengths (15 taps, for example, from $r = -7$ to $+7$, and $q = 1.5$). On the other hand, for the rectangular gate there are tap values at only -30 dB for the highest parameter values plotted, near $r = 10$ and $q = 2$, with only a very slow improvement as these increase.

We see how the weight values fall only slowly at $q = 1$ for all methods, but only a small increase to 1.2, for example, reduces the levels rapidly, except for the rectangular gate. The poor performance of the rectangular gate in rate of fall of coefficient strength with increasing sampling factor is consistent with the discussion of Figure 6.8 in Section 6.2.2.

6.3   Least Squared Error Interpolation

6.3.1   Method of Minimum Residual Error Power

In Section 6.2 we saw how to approximate the time series for the sampled delayed waveform, given the time series of a sampled waveform. The approximation is not exact because only a finite set of FIR filter taps can be used in practice. The error in curtailing the filter is not evaluated because this will depend on the actual waveform, and the approach of that section is independent of the waveform, given that it is of finite bandwidth. In this section a different approach is taken; the question tackled is: given a finite length filter, what is the set of tap weights that minimizes the error (in power) in the delayed waveform series? To answer this question, we do not need the actual waveform, but only its power spectrum, and some example spectral shapes are taken in Section 6.3.2 to illustrate the theory.

Figure 6.16 shows the FIR filter model, similar to Figure 6.1, with the waveforms x added. We do not distinguish between the continuous waveforms and the sampled forms, as we know that, correctly interpolated, the sampled series form will give the continuous one exactly for a band-limited signal. Let the required output waveform be delayed by ρT relative to the waveform $x(t)$ at the center tap, so it is given by $x(t - \rho T)$. T is the sampling period, and ρ (where $-0.5 < \rho < 0.5$) is the delay offset as a fraction of this interval. Although $x(t - \rho T)$ is indicated as the actual filter output in the figure, this could only be achieved with an infinite set of taps, correctly weighted; the actual output, with the tap weights derived next, is a least squared error approximation to this. The error waveform, the difference between the desired output and that given by the FIR filter, is $e(t)$, given by
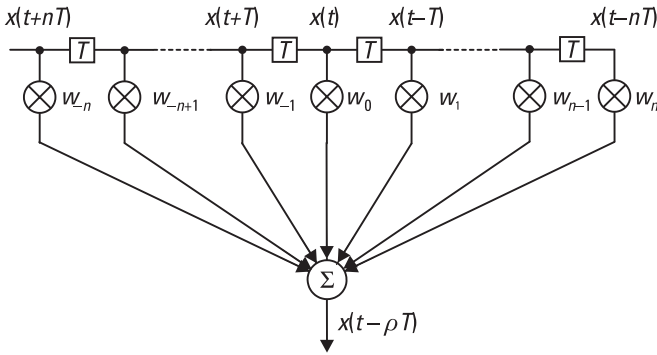
Figure 6.16 FIR filter for interpolation.

$$e(t) = x(t - \rho T) - \sum_{k=-n}^{n} x(t - kT)w_k \qquad (6.26)$$

Taking the Fourier transform of this equation we have

$$E(f) = X(f)\exp(-2\pi i f \rho T) - \sum_{k=-n}^{n} X(f)\exp(-2\pi i f k T)w_k = X(f)G(f)$$

$$(6.27)$$

where

$$G(f) = \exp(-2\pi i f \rho T) - \sum_{k=-n}^{n} \exp(-2\pi i f k T)w_k \qquad (6.28)$$

The error power p, considered to be a function of the set of weights, is given by

$$p = \int_{-\infty}^{\infty} |E(f)|^2 df = \int_{-\infty}^{\infty} |X(f)|^2 |G(f)|^2 df \qquad (6.29)$$

(Here the limits of the second integral could be $-F/2$ and $F/2$ as x is taken to be band limited, with no spectral power outside this interval.) We suppose that the waveform is of unit power so that $\int_{-\infty}^{\infty} |X(f)|^2 df = 1$. From (6.28) we have

$$|G(f)|^2 = 1 - 2\,\mathrm{Re}\left\{ \sum_{k=-n}^{n} \exp(2\pi i f(k-\rho)T)w_r{}^* \right\}$$

$$+ \sum_{k=-n}^{n}\sum_{h=-n}^{n} \exp(2\pi i f(k-h)T)w_k{}^* w_h, \tag{6.30}$$

Inserting this into (6.29) we can express the error power in a vector-matrix form by

$$p(\mathbf{w}) = 1 - 2\mathrm{Re}\{\mathbf{w}^H\mathbf{a}\} + \mathbf{w}^H\mathbf{B}\mathbf{w} \tag{6.31}$$

where we define

$$\mathbf{w} = [w_{-n}\ w_{-n+1}\ \ldots\ w_n]^T, \tag{6.32}$$

and the elements of the vector $\mathbf{a}$ and the matrix $\mathbf{B}$, of sizes $2n+1$ and $(2n+1) \times (2n+1)$, respectively, are given by

$$a_k = r\big((k-\rho)T\big) \quad \text{and} \quad b_{kh} = r\big((k-h)T\big) \tag{6.33}$$

where

$$r(\tau) = \int_{-\infty}^{\infty} |X(f)|^2 \exp(2\pi i f\tau)df \tag{6.34}$$

(The upper suffices T and H indicate matrix transpose and complex conjugate (Hermitian) transpose, respectively). We see that the components a_k and b_{kh} are values of the autocorrelation function of the waveform x, as r is the inverse Fourier transform of the power spectrum of x, and this gives the autocorrelation function, by the Wiener-Khintchine theorem (see Section 2.4.3).

By differentiating $p(\mathbf{w})$ with respect to $\mathbf{w}^*$ and setting the differential to zero (e.g., see Brandwood [1]) we find that p is a minimum when the weight vector is $\mathbf{w}_0$ given by

$$\mathbf{w}_0 = \mathbf{B}^{-1}\mathbf{a} \tag{6.35}$$

and the minimum error power is p_0, given by

$$p_0 = 1 - \mathbf{a}^H\mathbf{B}^{-1}\mathbf{a} \tag{6.36}$$

To calculate $\mathbf{w}_0$ and p_0 we only require $\mathbf{a}$ and $\mathbf{B}$, the components of which are all obtained from the autocorrelation function of the waveform. We do not need to postulate particular waveforms for x in order to calculate the optimum weight and the minimum residue, which will depend on the number of taps, the sampling interval, and the delay—only its spectral power function. Choosing some simple functions, which approximate likely spectra of real signals, it is possible to obtain values for the weights and the residues quite easily. In the next section, we use the rules-and-pairs technique to find the autocorrelation function for five spectral shapes, and in Section 6.3.3 we show some results.

6.3.2   Power Spectra and Autocorrelation Functions

Rectangular Spectrum

In this case, we take the power spectrum $|X(f)|^2$ to be given by $(1/F)\operatorname{rect}(f/F)$, the factor $1/F$ being required to normalize the total power to unity. The inverse Fourier transform of this is $r(\tau) = \operatorname{sinc}(F\tau)$, so we have, for the components of $\mathbf{a}$ and $\mathbf{B}$,

$$a_k = \operatorname{sinc}\bigl((k-\rho)FT\bigr) \quad \text{and} \quad b_{kh} = \operatorname{sinc}\bigl((k-h)FT\bigr) \tag{6.37}$$

The minimum sampling rate is equal to the bandwidth F so the sampling period is $T = 1/F$, but more generally if the sampling rate is qF then we have $T = 1/qF$, or $FT = 1/q$ so that (6.37) becomes

$$a_k = \operatorname{sinc}\bigl((k-\rho)/q\bigr) \quad \text{and} \quad b_{kh} = \operatorname{sinc}\bigl((k-h)/q\bigr) \tag{6.38}$$

Triangular Spectrum

A triangular shape of base width F can be formed as the convolution of two rectangular functions of width $F/2$, as in Section 3.3. This has a peak value of $F/2$, and so, with base width F, an area of $F^2/4$. In order to have a total area of unity, representing the total power in the power spectrum, we divide by this factor, so the spectrum and the autocorrelation function are given by

$$|X(f)|^2 = (4/F^2)\mathrm{rect}(2f/F) \otimes \mathrm{rect}(2f/F) \quad \text{and} \quad r(\tau) = \mathrm{sinc}^2(F\tau/2) \tag{6.39}$$

The required coefficients are thus

$$a_k = \mathrm{sinc}^2\big((k-\rho)/2q\big) \quad \text{and} \quad b_{kh} = \mathrm{sinc}^2\big((k-h)/2q\big) \tag{6.40}$$

Raised Cosine Spectrum

The raised cosine power spectrum of unit area is given by $(1/F)(1 + \cos(2\pi f/F))\mathrm{rect}(f/F)$.

The transform of the raised cosine, as in Section 3.6, gives the autocorrelation function $\mathrm{sinc}(F\tau) + 1/2(\mathrm{sinc}(F\tau - 1) + \mathrm{sinc}(F\tau + 1))$ and hence

$$a_k = \mathrm{sinc}\left(\frac{k-\rho}{q}\right) + \frac{1}{2}\mathrm{sinc}\left(\frac{k-\rho}{q}-1\right) + \frac{1}{2}\mathrm{sinc}\left(\frac{k-\rho}{q}+1\right) \tag{6.41a}$$

and

$$b_{kh} = \mathrm{sinc}\left(\frac{k-h}{q}\right) + \frac{1}{2}\mathrm{sinc}\left(\frac{k-h}{q}-1\right) + \frac{1}{2}\mathrm{sinc}\left(\frac{k-h}{q}+1\right) \tag{6.41b}$$

Gaussian Spectrum

The region of the domain over which the Gaussian, or normal, distribution function is nonzero (its support) is unbounded, so there is, strictly, no minimum sampling (or Nyquist) frequency F corresponding to sampling that will represent this function exactly. However, we can approximate the spectrum,

for practical purposes, by taking F to be the bandwidth at which the spectral power density has fallen to some low level, A decibels below the spectral peak, such that sampling at frequency F produces an acceptable low level of aliasing. This defines the variance of the spectrum as $\sigma^2 = F^2/1.84A$. The normalized spectrum is

$$\left|X(f)\right|^2 = \frac{1}{\sqrt{2\pi}\sigma}\exp(-f^2/2\sigma^2) \tag{6.42}$$

and its transform, from P6 with R5, is

$$r(\tau) = \exp(-2\pi^2\sigma^2\tau^2) \tag{6.43}$$

Expressing the variance in terms of the spectral limit level, A, we obtain (with $FT = 1/q$)

$$a_k = \exp(-2\pi^2(k-\rho)^2/1.84Aq^2) \quad \text{and} \quad b_{kh} = \exp(-2\pi^2(k-h)^2/1.84Aq^2) \tag{6.44}$$

Trapezoidal Spectrum

As in Section 3.2, we form a symmetrical trapezium with a base of width F and a top of width aF ($0 < a < 1$) by the convolution of two rect functions of width $(1-a)F/2$ and $(1+a)F/2$. These are the widths of the sloping edges and the half-height width, respectively (as in Figure 3.1). Using unit rect functions this gives a peak height of $(1-a)F/2$, which would give an area of $(1-a)(1+a)F^2/4$ so we have to divide by this factor to give the normalized spectrum:

$$\left|X(f)\right|^2 = (4/(1+a)(1-a)F^2)\mathrm{rect}(2f/(1-a)F)\otimes\mathrm{rect}(2f/(1+a)F) \tag{6.45}$$

The transform is

$$r(\tau) = \mathrm{sinc}\big((1-a)F\tau/2\big)\mathrm{sinc}\big((1+a)F\tau/2\big) \tag{6.46}$$

as shown in Figure 3.2, with $a = 3/7$. We note that taking $a = 1$ or $a = 0$ gives the result for the rectangular or triangular spectral case, respectively, as limiting cases of the trapezoidal form. Finally, we have

$$a_k = \mathrm{sinc}\big((1-a)(k-\rho)/2q\big)\,\mathrm{sinc}\big((1+a)(k-\rho)/2q\big) \qquad (6.47\mathrm{a})$$

and

$$b_{kh} = \mathrm{sinc}\big((1-a)(k-h)/2q\big)\,\mathrm{sinc}\big((1+a)(k-h)/2q\big) \qquad (6.47\mathrm{b})$$

6.3.3 Error Power Levels

The error power, given in (6.36) is shown, in contour plot form, in Figure 6.17, for two of these spectral shapes, the rectangular, using (6.38), and the raised cosine, using (6.41). The errors are for the worst case, a delay of half a sample period ($\alpha = 0.5$). These give the powers as a function of both the number of taps used and the oversampling factor. Although the contour lines, which are at 5-dB intervals, are continuous, only the values at integral tap numbers are meaningful, of course, and the error powers are only calculated at these abscissa values. These plots show that even modest oversampling rates are effective in reducing the number of taps for a given required mismatch level or alternatively greatly reducing the mismatch power for a fixed number of taps. For example, with nine taps, the mismatch power for the rectangular spectrum is reduced from above –15 dB to about –53 dB on increasing the rate from 1 to 1.5 (oversampling by 50 percent). The general patterns for these two spectra are quite similar, though the more compact raised cosine spectrum has lower mismatch power than the rectangular spectrum at the same parameter values, as might be expected. (For this spectrum and nine taps, the power falls from –30 dB with no oversampling to nearly –60 dB with 40 percent oversampling.) The results for the other spectral shapes are similar and generally between these two.

Figure 6.18 presents results for the rectangular spectrum with an expanded range of taps and a reduced range of oversampling factors. We see that even with 60 taps, the mismatch power when sampling at the minimum rate is about –22 dB, while with 10 percent oversampling this level is achieved using only eight taps, and at 25 percent only five taps are required. We also see that using 20 taps, the mismatch power at the minimum
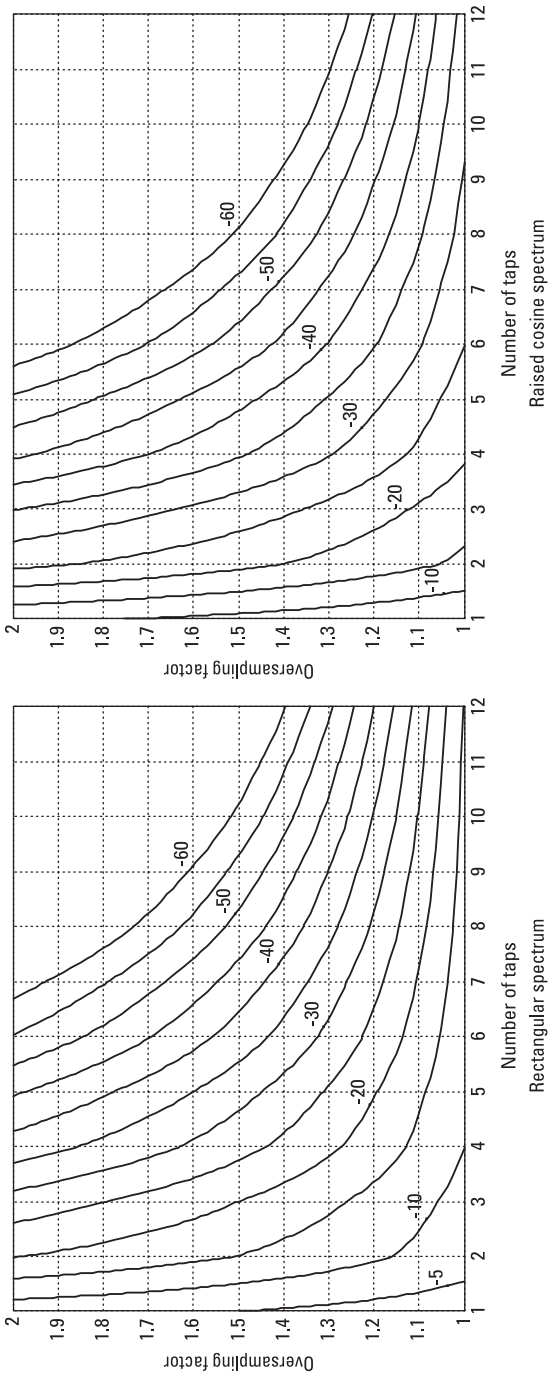
Figure 6.17 Mismatch powers for two power spectra.
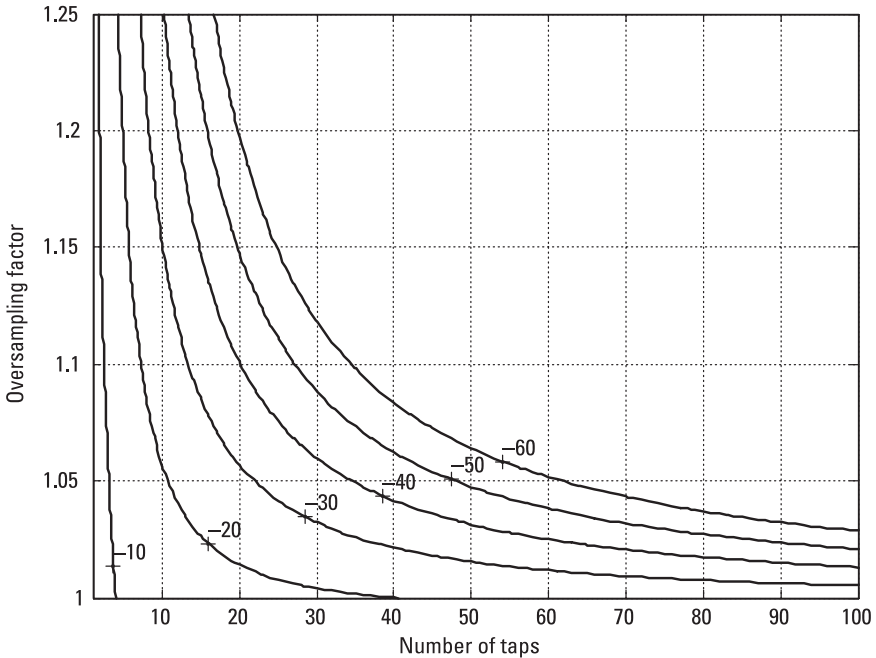
Figure 6.18   Mismatch power for rectangular spectrum.

sampling rate is about −17 dB but this falls to −50 dB at an oversampling rate of only 1.15. These figures show that even with quite low oversampling rates, considerable reductions in computation for a given performance level or considerable improvement in performance for a given computational effort is achievable.

6.4   Application to Generation of Simulated Gaussian Clutter

Here we take a particular example to show that that taking advantage of oversampling can give a very substantial saving in computation. The problem considered is to generate simulated clutter, as seen in a given range gate, for modeling radar performance. In this case, the clutter is taken to have a complex amplitude distribution that is normal (or Gaussian) and also has a Gaussian power spectrum. We show first, in Section 6.4.1, that the required waveform can be generated by an FIR filter fed with a sequence of pseudorandom samples from a normal distribution at the required sample rate, which

is the radar pulse repetition frequency (PRF). As the bandwidth of the clutter waveform is very much lower than the radar PRF, the clutter waveform is greatly oversampled, and the cost in computation is high. (Despite high speeds of computation, the large, complex simulations that require clutter in many range gates in this radar example can take significant times to carry out, and efficient computation is of value.) In Section 6.4.2, we show that the clutter waveform can be generated at a much lower sampling rate, though still oversampled, and then efficient interpolation is used to give the samples at the PRF, as required. This is shown to reduce the overall computation requirement by a very large factor. The parameters we use for this example are 10 kHz for the PRF and 10 Hz standard deviation for the spectrum of the clutter waveform.

6.4.1 Direct Generation of Gaussian Clutter Waveform

Any linear combination of independent normally distributed sequences will also be normally distributed (see Mardia et al. [2], for example). An FIR filter of length L fed with a sequence of samples from a normal distribution forms a linear combination of L samples and will produce output samples at intervals L, which are independent and normally distributed. The output samples that are at less than L sample intervals apart are not independent, as they are linear combinations of partially overlapping sets of samples, and the choice of FIR filter weights will determine the degree of dependence between successive samples (i.e., the rate of change of the values, or, equivalently, the frequency spectrum of the output sequence). If $|H(f)|^2$ is the power spectrum required, then the square root of this gives (within an arbitrary phase factor) the required amplitude spectrum and the inverse Fourier transform of this gives the required filter impulse response. In the case of an FIR filter, the filter weights, or tap coefficients, are set to the sampled values of the required impulse response (Figure 6.19). (It is clear that an impulse at the input will emerge at the output as a series of impulses scaled by the coefficients, and this is the filter impulse response.) If ϕ is the bandwidth of the spectrum, then we know, from Section 6.4, that the sampling rate must be ϕ or greater, and so the delay between taps in the FIR filter must be $1/\phi$ or less. The intervals at which the Gaussian impulses are generated and fed into the filter to give the output Gaussian sequence must match this delay, of course. (In this case, the sampling rate is the PRF F, which is very much greater than the bandwidth of the spectrum.)
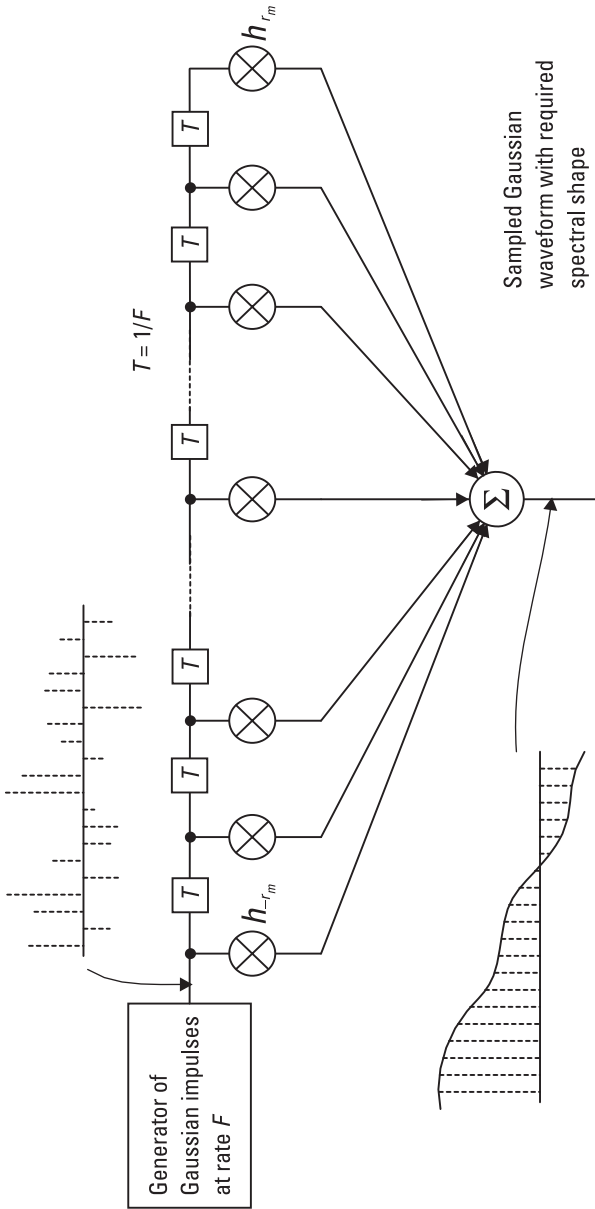
Figure 6.19   FIR filter for Gaussian waveform generation.

In the case of a Gaussian power spectrum of standard deviation σ and 3dB bandwidth 2.36σ we have

$$H(f)^2 \sim \exp(-f^2/2\sigma^2) \tag{6.48}$$

where we write ~ to indicate we are not concerned here with the particular scaling factor. As in Section 6.3.2, we have an infinite frequency region over which the spectral power density is finite, so we approximate the spectrum as being finite over the bandwidth $2r\sigma$ such that the density at $\pm r\sigma$ is small enough to allow us to neglect the spectral tails and hence the aliasing power. At these points, we have $H(\pm r\sigma)^2 = \exp(-r^2/2)$, and this has fallen to -35 dB, as a suitable low level below the peak, at $r = \sqrt{(7\ln 10)} \approx 4$. In this case the total bandwidth, outside which there is considered to be negligible spectral power, is 8σ. In this example this is 80 Hz, which is very low compared with the PRF of 10 kHz, and we see that the required clutter waveform is over-sampled by a factor of 125.

From (6.47) we have $H(f) \sim \exp(-f^2/4\sigma^2) = \exp(-\pi(f/2\sigma\sqrt{\pi})^2)$ and so, using P6 and R5, we obtain, for the required filter impulse response,

$$h(t) \sim \exp(-\pi(2\sigma\sqrt{\pi}t)^2) = \exp(-4\pi^2\sigma^2 t^2) \tag{6.49}$$

The FIR filter coefficients from the sampled impulse response are given by

$$h_r = h(rT) = \exp(-4\pi^2\sigma^2 r^2 T^2) \tag{6.50}$$

where $T = 1/F$ is the sampling interval. If we take coefficients to the -40 dB level, then we have $8\pi^2\sigma^2 r_m^2 T^2 = 4\ln 10$, or

$$r_m = \frac{\sqrt{\ln 10/2}}{\pi}\frac{F}{\sigma} = 0.342\frac{F}{\sigma} \tag{6.51}$$

where $\pm r_m$ are the indices of the first and last coefficients.

We can now estimate the amount of computation required to produce the simulated clutter directly. With $F = 10^4$ Hz and $\sigma = 10$ Hz, we see that $r_m = 342$, so there are 685 taps, and this is the number of complex

multiplications needed for each output sample (in addition to generating the inputs from a normal distribution).

6.4.2 Efficient Clutter Waveform Generation, Using Interpolation

In this case we generate Gaussian clutter with the required bandwidth but at a much lower sampling rate, f_s, and then interpolate to obtain the samples at the required rate F (Figure 6.20). Thus, we will need F/f_s times as many interpolations as samples. From Section 6.2, we know that with moderate oversampling rates, we can achieve good interpolation with very few taps. Let the number of taps in the interpolation filter be m, and the number in the Gaussian FIR filter is, from (6.51), $0.684\, f_s/\sigma$ (+1, which we neglect) so that the average number of complex multiplications per output sample is

$$v = m + (0.684\, f_s/\sigma)/(F/f_s) = m + 0.684\, f_s^2/\sigma F \qquad (6.52)$$

We have taken the effective bandwidth of the Gaussian spectrum (the width at the –35dB points) to be 8σ, and with an oversampling factor of q we have $f_s = 8\sigma q$, giving

$$v = m + 43.7\,\sigma q^2/F \qquad (6.53)$$
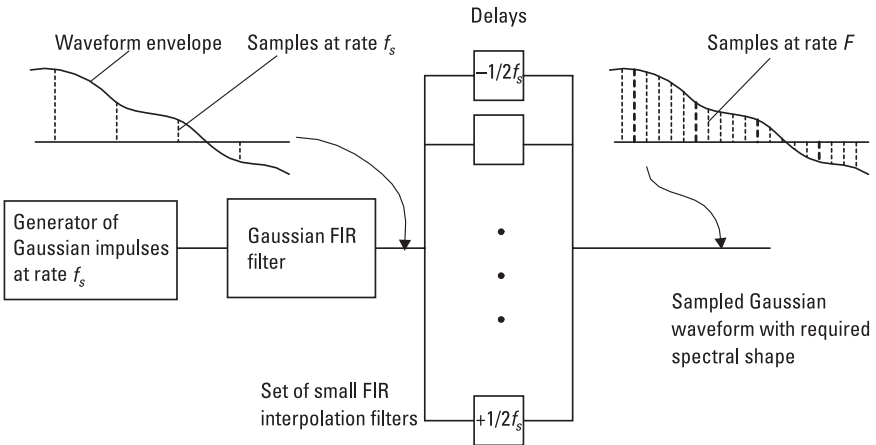
Figure 6.20   Gaussian waveform generation with interpolation.

In Figure 6.12 we see that with an oversampling factor of 3 we need only four taps, weighted above the −40-dB level, to interpolate up to the maximum time shift of half the sampling interval. Using these figures (i.e., $m = 4$, $q = 3$, $F = 10^4$ Hz, and $\sigma = 10$ Hz), in (6.53) we obtain $\nu = 4.4$, *a factor of over 150 lower* than in the direct sampling case. There will have to be $F/2f_s$ sets of four weights (or 21 sets in this example, as $f_s = 240$ Hz) to interpolate from $−1/2f_s$ to $+1/2f_s$ (for a symmetrical bank of F/f_s filters).

6.5 Resampling

An application of interpolation is to obtain a resampled time series. In this case, data has been obtained by sampling some waveform at one frequency, F_1, but the series that would have been obtained by sampling this waveform at a different frequency, F_2, is now required. We consider first the case where F_1/F_2 is rational and so can be expressed in the form n_1/n_2 with n_1 and n_2 mutually prime (with no common factor). Figure 6.21 illustrates the method, where we have take $n_1 = 4$ and $n_2 = 7$, and $F_1/F_2 = 4/7$. Over a time interval $T = n_1 T_1 = n_2 T_2$, the pattern repeats, where $T_1 = 1/F_1$ and $T_2 = 1/F_2$, and if the output sequence is timed so that some samples are at zero shift relative to the input, then there will be further time shifts of . . . −2, −1, 0, 1, 2, . . . in units of $\Delta T = T/n_1 n_2$. The input sample period is $T_1 = T/n_1 = n_2 \Delta T$, so n_2 delays are required, from 0 to $n_2 − 1$ in units of ΔT. Allowing negative relative delays, we require delays from $−(n_2−1)/2$ to $+(n_2−1)/2$ for n_2 odd, or $−n_2/2+1$ to $+n_2/2$ for n_2 even, keeping the delay magnitudes to within half a period of F_1. In Figure 6.21, the required time shifts for the different pulses are shown, in units of ΔT, with $F_1/F_2 = 4/7$, and we see the delays required are from $−3\Delta T$ to $+3\Delta T$. Over a period of four input pulse intervals, there are seven output pulses, with seven different delays, one of which is zero. We also see that if the frequency ratio were inverted in this figure, so that the input
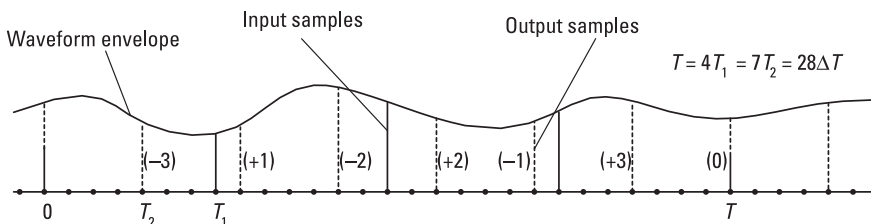
Figure 6.21 Resampling.

samples are shown by the dashed lines and the outputs by the continuous lines, then four time shifts, of -1, $+2$, $+1$ and zero only, relative to the nearest input sample, are required.

If the input sequence is oversampled, we can use the results of Section 6.3.2 to reduce the size of the sampling FIR filters and so achieve quite economical resampling, requiring only a few multiplications for each output sample. Only $n_2 -1$ time shifts are needed, and the number of distinct vectors defining the FIR filter coefficients is only $(n_2 - 1)/2$ (n_2 odd) or $n_2/2$ (n_2 even) (as the set coefficients are the same for positive and negative shifts, applied in reverse order, with a shift of the input sequence), and these can be precomputed and stored. The processing need not be in real time, of course—with the input and output pulses arriving and departing at the actual intervals specified. If the input data were stored, after sampling in real time, of course, the output sequence could then be generated at leisure, as these samples are the values that would have been obtained by real-time sampling at the new frequency. However, if real-time resampling is required (e.g., on continuous data), then economical computation could be particularly useful.

If the frequency ratio is not rational, some modifications are necessary. In the case of a block of stored data, it may be acceptable to find a good rational approximation to this ratio. As this is an approximation, the output frequency will not be exactly the specified frequency, and if the waveform is regenerated as if the samples were at this frequency (e.g., by a standard sound card, in the case of audio data), then there will be a slight frequency scaling of the whole signal. In the case of continuous, real-time data, this would require dropping, or inserting, a sample from time to time, generally causing an unacceptable distortion of the sound. An alternative would be to accurately calculate the required delay for each pulse and then the FIR filter tap weights, using equations from Section 6.2. Further, the calculated delay could be approximated to the nearest of a suitably fine set of values over the half output sample period (positive or negative) and the precalculated set of weights for this delay would be applied. (The topic of resampling is well covered in the literature, but the emphasis here is on the implementation and benefit of oversampling.)

6.6   Summary

In this chapter, we have shown how the rules-and-pairs method can be used to obtain results in the field of interpolation for a sampled time series, simply

and with insight into the underlying principles. The first main application was to find the FIR filter weights that would provide interpolation for any band-limited signal. In principle, this filter will be infinitely long for perfect interpolation, so in practice a finite filter will always give only an approximation to the correct interpolated waveform. However, a filter of suitable length will give as good an approximation as may be required. For waveforms sampled at the minimum rate, this could be quite long (perhaps one hundred or more taps, for good fidelity), but if the sampling is at a higher rate (i.e., the waveform is oversampled), the filter length for a given performance is found to fall quite dramatically. This saving in computation could be valuable in large simulations, or in providing real-time delayed waveforms in wide bandwidth systems, for example.

This first approach does not give a definite estimate of the accuracy of the interpolated waveform, which could be measured, for example, by comparing this waveform from the FIR filter with the exact delayed waveform. This will depend on the spectrum of the waveform, and no particular spectrum, within the specified finite bandwidth, is assumed. This is the subject of the second approach, which is to define the filter that will minimize the power in the error signal (i.e., the difference between the interpolated series and the exact series) for a given power spectrum. In this case, a few simple spectral shapes were taken to illustrate the technique. In practice, the actual signal spectrum could perhaps be considered a good approximation to one of these. In fact, the actual shape does not make a great deal of difference, given a reasonable degree of oversampling, with the rectangular spectrum being rather the poorest, but also not a likely form, in practice. Again, oversampling can be used to reduce greatly the filter length and the number of multiplications for each output sample.

Two applications of interpolation were studied. The first was for the case of generating a greatly oversampled Gaussian waveform. It was shown that generating the Gaussian waveform at a much lower oversampled rate and then interpolating could give a great reduction (two orders of magnitude) in the amount of computation needed. The second example was the case of resampling, where a sample sequence is required corresponding to having sampled a waveform at a different rate from that actually used. (The previous example is a special case of resampling, where the output frequency is a simple multiple of the input.) Again, this process could be made considerably more economical if the input sequence is oversampled. These examples may not solve any reader's actual problem, but they may provide indications of how to do so, in particular with the simplification and clarity given by the rules-and-pairs approach.

References

[1]   Brandwood, D. H., "A Complex Gradient Operator and Its Application in Adaptive Array Theory," *IEE Proc.* **133**, *Parts F and H*, 1983, pp.11–16.

[2]   Mardia, K. V., J. T. Kent, and J. M.Bibby, *Multivariate Analysis*, Academic Press, 1979.

7

Equalization

7.1   Introduction

In this chapter, we consider the problem of compensating for some known frequency distortion over a given band. One source of distortion is an unwanted delay and the resulting distortion is a phase variation, that is linear with frequency. This particular case, of delay mismatch, was the subject of Chapter 6 and the method of correction, or equalization, used in Section 7.5 here is basically the same as in Section 6.3. However we are also concerned with other forms of frequency distortion, so in this chapter the approach is more general and amplitude variation over the band is also included. In order to do this, a new Fourier transform pair is introduced in Section 7.3, the ramp function, which is a linear slope across the band, and its transform, the snc_1 function, which is a scaled first derivative of the sinc function. In fact, a set of transform pairs is defined. These are the integer powers of the linear variation across the band ($ramp^r$) and the scaled derivatives of corresponding order of the sinc function (snc_r). The sinc and rect functions are seen to be the first (or zeroth-order) members of these sets. With these results, any amplitude variation, expressed as a polynomial function of frequency across the band of interest, has a Fourier transform that is a sum of snc_r functions. A simple example of amplitude equalization is given in Section 7.4.

The method of equalization outlined in Section 7.2 is based on minimizing a weighted mean squared error across the band. The error at each

frequency is the (complex) amplitude mismatch between the equalized result (normally imperfect) and the ideal, or perfectly equalized, response. The weighting, as in Section 6.3, is given by the spectral power density function of the signal. This has the advantage that the equalization will tend to be best where there is most signal power and hence the effect of mismatch would be the most serious. If no weighting is required (e.g., if the signal spectrum is totally unknown and uniform emphasis across the band is considered most appropriate), then we simply replace the spectral function by the rect function. It is not likely that the spectrum needs to be accurately known and specified in practice, as a reasonable approximation to the spectral shape will give a result close to that given by an exact form and considerably better than the rather unrealistic unweighted (or constant) shape defined by the rect function, which gives full weight up to the very edges of the band, where normally the signal power will have fallen to a negligible level. Thus, as in Section 6.3, simplifying the spectrum to one of a few tractable forms should be satisfactory. Suitable forms to choose from include the normal (or Gaussian) shape, the raised cosine, or the (symmetric) trapezoidal shape.

In Sections 7.6 and 7.7, we apply the theory given in Sections 7.2 and 7.3 to a specific problem, that of forming broadband sum and difference beams as required for radars using monopulse. We take the simple example of a 16-element regular linear array to illustrate the application. It would not be difficult to extend the problem to larger, perhaps planar (two-dimensional) arrays—this would increase the number of channels to be equalized, each with its own compensation requirement, but the actual form of the equalization calculation is essentially the same in each case, with different parameters. Thus, although this simple array may not be particularly likely to be used in practice, it is quite adequate to illustrate the benefit of equalization in this application, showing a striking improvement obtained with quite modest computational requirements, given a moderate degree of oversampling.

The radar sum beam (i.e., its normal search beam, giving maximum signal to noise ratio) requires only delay compensation, and this could be provided for each element by the results of Section 6.3. However, Section 7.6 includes results for the full array response with equalization, not considered in Chapter 6, and also provides an introduction to Section 7.7, where the difference beam is considered. This beam, one form of which can be defined as a derivative (with respect to angle) of the sum beam, is used for fine angular position measurement. The required form should have a zero response in the radar look direction, for which the sum beam response is a maximum. For this example, we carry out equalization in each channel in amplitude as well as phase, and the results of Section 7.3 are now required.

7.2 Basic Approach

The problem to be tackled is that of compensating for a given frequency-dependent distortion in a communications channel, as illustrated in Figure 7.1. A waveform u with baseband spectrum U is received with some channel distortion G, such that at (baseband) frequency f the spectral component received is $G(f)U(f)$ instead of just $U(f)$. The signal is then passed through a filter with frequency response $K(f)$ such that the output spectrum, $K(f)G(f)U(f)$, is close to the undistorted signal spectrum, $U(f)$. Clearly the ideal required filter response at frequency f is simply $K(f) = 1/G(f)$, but in practice this filter may not be exactly realizable (e.g., if it is a finite impulse response digital filter, except in the unlikely case that K consists of a set of δ-functions corresponding to a number of delays at multiples of the sampling interval). In this case, we design the filter to give a best fit, in some sense, of $K(f)G(f)U(f)$ to $U(f)$ over the signal bandwidth. In fact the fit we choose is the least squared error solution, a natural and widely used criterion that has the advantage of yielding a tractable solution, at least in principle, and this is found to require the application of Fourier transforms. In order to compensate for G, we need to know the form of this function. This may be known from the nature of the system, as in the application in Sections 7.6 and 7.7, or a reasonable estimate may be available from channel measurements. In Figure 7.1 we show the incoming signal on a carrier, at frequency f_0, which is generally the case for radio and radar waveforms. This is down-converted to complex baseband (often in more than one mixing process) and, we assume, digitized for processing, including equalization and detection.

The amplitude error between the filter output and the desired response in an infinitesimal band δf at frequency f is given by $(K(f)G(f)U(f) - U(f))\delta f$, so the total squared error is

$$\int_{-\infty}^{\infty} \left| K(f)G(f) - 1 \right|^2 \left| U(f) \right|^2 df \tag{7.1}$$
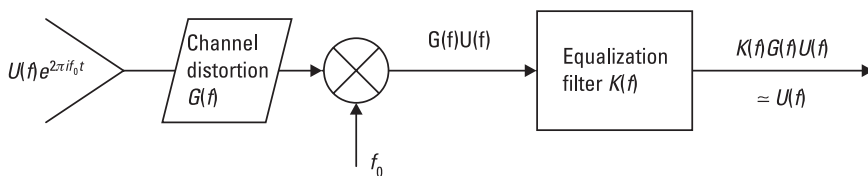
Figure 7.1 Equalization in a communications channel.

We note that as the signal spectrum U is included in the error expression, we will actually perform a *weighted* squared error match of KG to unity at all frequencies (the "equalized" solution), where the weighting function is the spectral power density function of the signal. This means that more emphasis is placed on compensating for distortion in regions where there is more signal power, which is generally preferable to compensating with uniform emphasis over the whole band, including parts where there may be little or no signal power.

The equalizing filter is of the form shown in Figure 6.1 or Figure 6.16, and if the filter coefficients are given by v_r for delay rT, where T is the sampling period, then the impulse response of the filter, of length $2n + 1$ taps, is

$$k(t) = \sum_{r=-n}^{n} v_r \delta(t - rT) \tag{7.2}$$

and its frequency response is the Fourier transform of this, which is (from P1b and R6a)

$$K(f) = \sum_{r=-n}^{n} v_r \exp(-2\pi irfT) \tag{7.3}$$

Thus, we can put

$$\left| K(f)G(f) - 1 \right|^2 = \left(\sum_{r=-n}^{n} v_r{}^* \exp(2\pi irfT)G^*(f) - 1 \right)$$

$$\times \left(\sum_{s=-n}^{n} v_s \exp(-2\pi isfT)G(f) - 1 \right) \tag{7.4}$$

$$= \sum_{r=-n}^{n} \sum_{s=-n}^{n} v_r{}^* v_s e^{2\pi i(r-s)fT} \left| G(f) \right|^2 - 2\,\mathrm{Re} \sum_{r=-n}^{r} v_r{}^* e^{2\pi irfT} G(f)^* + 1$$

The error power that is to be minimized, as a function of the weight vector $\mathbf{v}$ (where $\mathbf{v} = [v_{-n}\, v_{-n+1} \ldots \ldots v_n]^T$), is given from (7.1), on substituting for $KG - 1$ from (7.4) by

$$p(\mathbf{v}) = \int_{-\infty}^{\infty} |K(f)G(f) - 1|^2 |U(f)|^2 \, df = \sum_r \sum_s v_r^* v_s b_{rs} - 2\operatorname{Re} \sum_r v_r^* a_r + c$$

where the summations are from $-n$ to n. In vector-matrix form, this becomes

$$p(\mathbf{v}) = \mathbf{v}^H \mathbf{B} \mathbf{v} - 2\operatorname{Re}(\mathbf{v}^H \mathbf{a}) + c \qquad (7.5)$$

where the components of **a** and **B** are given by

$$a_r = \int_{-\infty}^{\infty} G(f)^* |U(f)|^2 \, e^{2\pi i f r T} \, df \qquad (7.6)$$

and

$$b_{rs} = \int_{-\infty}^{\infty} |G(f)|^2 |U(f)|^2 \, e^{2\pi i f (r-s)T} \, df, \qquad (7.7)$$

and c is $\int |U(f)|^2 df$. We can normalize the error power relative to the signal power by dividing by c or, equivalently, by normalizing U so that $c = 1$; we will take this to be the case. We note that (7.6) and (7.7) are in the form of inverse Fourier transforms. If $\rho_1(t)$ and $G(f)^*|U(f)|^2$ are a Fourier pair, and so are $\rho_2(t)$ and $|G(f)|^2|U(f)|^2$, then from (7.6) and (7.7) we have

$$a_r = \rho_1(rT) \quad \text{and} \quad b_{rs} = \rho_2\big((r-s)T\big) \qquad (7.8)$$

Here T is the sampling interval, so if there is oversampling by a factor q we have $T = 1/qF$. As in Section 6.3 we differentiate p in (7.5) with respect to **v** to find that the mismatch error is minimized at $\mathbf{v}_0$, given by

$$\mathbf{v}_0 = \mathbf{B}^{-1}\mathbf{a} \qquad (7.9)$$

and the minimum (normalized) squared error is

$$p(\mathbf{v}_0) = 1 - \mathbf{a}^H \mathbf{B}^{-1}\mathbf{a} = 1 - \mathbf{a}^H \mathbf{v}_0 \qquad (7.10)$$

We note that $\mathbf{a}^H \mathbf{B}^{-1} \mathbf{a}$ is real as, from (7.7), $\mathbf{B}$ is Hermitian (i.e., $b_{sr} = b_{rs}^*$). Thus, in order to find the tap weights for the equalization filter that are optimum (in the sense of giving least squared error), we need only $|U|^2$, the power spectrum of the signal and G, the complex channel response, and then we perform the Fourier transforms defined in (7.6) and (7.7) to give the components of $\mathbf{a}$ and $\mathbf{B}$, followed by some simple matrix processing. The derivation of $\mathbf{a}$ and $\mathbf{B}$ in the case of a simple delay mismatch has been given earlier in Section 6.3, but the cases of frequency-dependent amplitude mismatches as well are considered in Sections 7.4 and 7.7. The delay mismatch is a linear phase dependence on frequency, but we do not go on to cover the case of nonlinear phase correction, as the Fourier methods illustrated here are less convenient for handling phase functions rather than amplitude functions (which are normally, but not necessarily, real).

To summarize the method for equalization:

1. We need an expression for the distortion as a function of frequency, $G(f)$, and an expression for the spectral weighting across the band, $|U(f)|^2$, which is taken to be zero outside the signal band.

2. We obtain the functions of time $\rho_1(t)$ and $\rho_2(t)$ as the inverse Fourier transforms of $G(f)^*|U(f)|^2$ and $|G(f)|^2|U(f)|^2$ to obtain the components of $\mathbf{a}$ and $\mathbf{B}$ as in (7.8), where T is the sampling interval and filter tap spacing.

3. The optimum weight vector for the FIR filter is $\mathbf{v}_0$, given by (7.9).

A number of comments may be made on the rather concise summary here:

(a) If the distortion is given by (or approximated as) a polynomial function, often, but not necessarily, of low order (linear or quadratic), then the ramp and snc functions introduced later (and given as P13a and P13b in the pairs table) are generally necessary for the solution.

(b) In the simplest case, we take $|U(f)|^2$ to be rect(f/F). This corresponds to no weighting across the band and will give a useful degree of equalization.

(c) For some functions G and $|U|^2$ the products $G^*|U|^2$ and $|G|^2|U|^2$ may not be easy to transform. If their separate transforms are obtainable, then the convolution of these will give the required transforms of the products, by R7b. If $|U|^2$ can be approximated as a raised cosine function, then, as its transform includes three δ-functions

(see Section 3.6), this should give a solution in terms of the transform of G. If it is approximated as a trapezoidal (or triangular) shape, then the approach will be to split the transform into three (or two) intervals in the frequency domain.

7.3 ramp and snc_r Functions

Although the function G, describing the channel frequency response that is to be compensated, may be defined over the whole frequency domain, we are interested only in its form in the frequency interval containing significant signal energy. If, as we have generally assumed, the signal is limited (after down-conversion to complex baseband) to the band $(-F/2, F/2)$, then it will make no difference in the Fourier transform integrals of (7.6) and (7.7) if the function $\text{rect}(f/F)$ is included, as the factor $|U(f)|^2$ is taken to be zero anyway in the region outside the signal band. (We do not want to optimize the response over a band greater than that of the signal. This solution will generally be suboptimal for the given signal.) Thus, if we consider first the case where G is a linear function of frequency, to avoid the problem of the function $G(f) = af + b$ being unbounded as $f \to \pm\infty$, we can take, more conveniently, $G(f) = (af + b)\text{rect}(f/F)$. In order to handle polynomial functions of this kind, we introduce the function ramp defined by

$$\text{ramp}(x) = 2x\text{rect}(x) \tag{7.11}$$

and this is illustrated in Figure 7.2, with its squared and cubed forms.

Thus, $\text{ramp}(x) = 2x$ on $-1/2 < x < 1/2$, and $\text{ramp}(x) = 0$ for $x < -1/2$ and $x > 1/2$. For completeness, we can take $\text{ramp}(\pm 1/2) = \pm 1/2$. As the rect function has the property $\text{rect}^r(x) = \text{rect}(x)$, we see that

$$\text{ramp}^r(x) = (2x)^r\text{rect}(x), \tag{7.12}$$

so that we can express a polynomial in x on the interval $(-1/2, 1/2)$ as a polynomial in $\text{ramp}(x)$:

$$(a_0 + a_1x + a_2x^2 + \ldots)\text{rect}(x) = a_0\text{ramp}^0(x)$$
$$+ (a_1/2)\text{ramp}(x) + (a_2/4)\text{ramp}^2(x) + \ldots \tag{7.13}$$

To find the Fourier transform of ramp, we use rule R9b:

$$-2\pi ixu(x) \Longleftrightarrow U'(y) \tag{7.14}$$
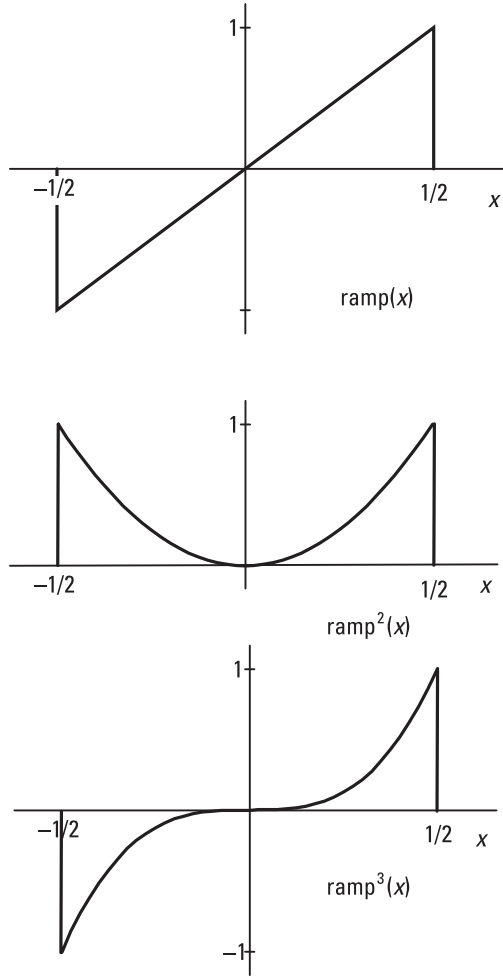
Figure 7.2 ramp functions.

where $u(x) \Longleftrightarrow U(y)$ and the prime denotes the derivative. If we define $V(y)$ as $U'(y)$, with inverse Fourier transform $v(x)$, then, from (7.14), $v(x) = -2\pi i x u(x)$ and also, by Rule 9b, $-2\pi i x v(x) \Longleftrightarrow V'(y)$. Substituting for v and V gives

$$(-2\pi i x)^2 u(x) \Longleftrightarrow U''(y)$$

and, in general, for any positive integer r,

$$(-2\pi i x)^r u(x) \Longleftrightarrow U^{(r)}(y) \tag{7.15}$$

where $U^{(r)}$ is the rth derivative of U. Now putting $u(x) = \text{rect}(x)$ and $U(y) = \text{sinc}(y)$, from Pair 3a, then substituting in (7.15), we obtain

$$(-\pi i)^r (2x)^r \text{rect}(x) \Longleftrightarrow \text{sinc}^{(r)}(y) \qquad (7.16)$$

If we introduce the notation

$$\text{snc}_r(y) = \frac{1}{\pi^r} \frac{d^r}{dy^r}(\text{sinc}(y)) \qquad (7.17)$$

then, from (7.12), (7.16) becomes

$$\text{ramp}^r(x) \Longleftrightarrow i^r \text{snc}_r(y) \qquad (7.18)$$

(Equation (7.18) is Pair 13a in Table 2.2.) We note, from (7.12) and (7.17) that we can write, formally,

$$\text{ramp}^0(x) = \text{rect}(x) \text{ and } \text{snc}_0(y) = \text{sinc}(y) \qquad (7.19)$$

From (7.17), carrying out the differentiation, we find

$$\text{snc}_1(y) = \frac{\cos(\pi y) - \text{snc}_0(y)}{\pi y} \qquad (7.20)$$

This holds for all real values of y except for $y = 0$, so we define $\text{snc}_1(0) = 0$, (the limiting value of $\text{snc}_1(y)$ as $y \to +0$ and $y \to -0$) to ensure that snc_1 is continuous and, in fact, analytic. Differentiating again we obtain

$$\text{snc}_2(y) = \frac{1}{\pi} \frac{d}{dy} \text{snc}_1(y) = -\text{snc}_0(y) - \frac{2\text{snc}_1(y)}{\pi y} \qquad (7.21)$$

with $\text{snc}_2(0) = -1/3$, obtained by taking the first two terms in the Taylor expansions of the functions sinc and cos with $y \to \pm 0$, or see (7.27). These three functions have been plotted in Figure 7.3. We note that the even order snc functions are even functions and the odd ones are odd functions.
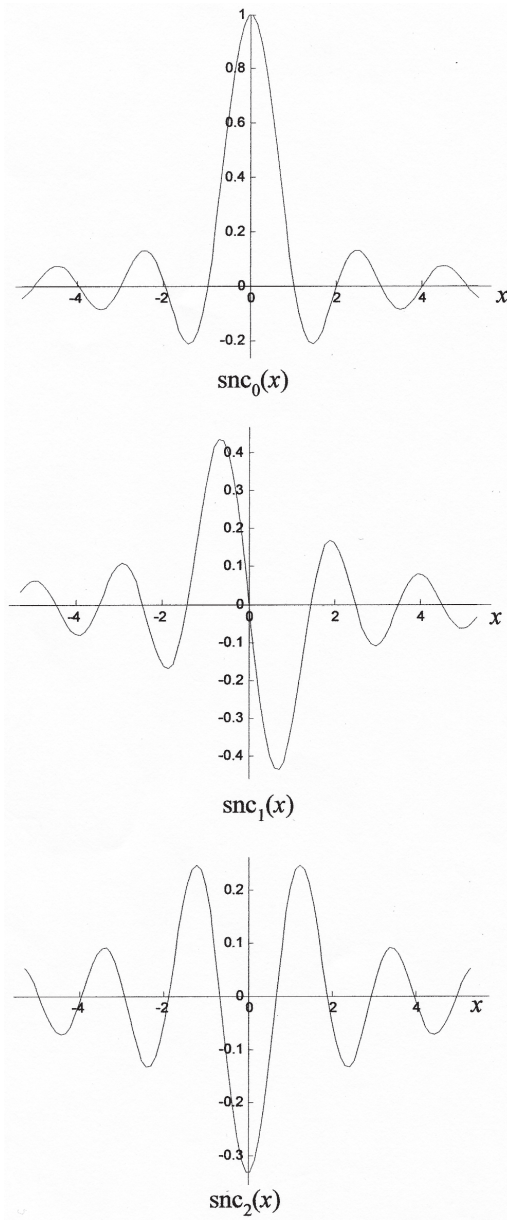
Figure 7.3   First three snc functions.

The peak magnitude (positive or negative) of the functions falls as the order rises.

We note that unlike (7.20), (7.21) contains all the trigonometric functions in snc functions only. By differentiating further, using (7.17) we can obtain a recursion formula, of which (7.21) is the first example, from which higher-order snc functions can be found:

$$\text{snc}_n(y) + \text{snc}_{n-2}(y) = -\frac{n\,\text{snc}_{n-1}(y) + (n-2)\text{snc}_{n-3}(y)}{\pi y} \quad (n \geq 2) \quad (7.22)$$

By expressing $\sin(\pi x)$ in its Taylor series form and differentiating term by term for snc_1 and snc_2, we find, for the first three snc functions,

$$\text{snc}_0(y) = \sum_{n=0}^{\infty} \frac{(-1)^n (\pi y)^{2n}}{(2n+1)!}, \quad (7.23)$$

$$\text{snc}_1(y) = \sum_{n=0}^{\infty} \frac{(-1)^n 2n(\pi y)^{2n-1}}{(2n+1)!} = \sum_{n=1}^{\infty} \frac{(-1)^n 2n(\pi y)^{2n-1}}{(2n+1)!}, \quad (7.24)$$

$$\text{snc}_2(y) = \sum_{n=1}^{\infty} \frac{(-1)^n 2n(2n-1)(\pi y)^{2n-2}}{(2n+1)!} \quad (7.25)$$

(The $n = 0$ term is dropped in (7.24), as it is zero. The next term dropped is for $n = 1$ in snc_3, which contains the factor $2n - 2$.) In general we can put

$$\text{snc}_r(y) = \sum_{n=\lfloor (r+1)/2 \rfloor}^{\infty} \frac{(-1)^n 2n!(\pi y)^{2n-r}}{(2n-r)!(2n+1)!} \quad (7.26)$$

where $\lfloor p \rfloor$ is the highest integer in p, so $\lfloor (r+1)/2 \rfloor = (r+1)/2$ for r odd and $\lfloor (r+1)/2 \rfloor = r/2$ for r even. The even-order series contain only even powers of y and so are even functions, and the odd series contain only odd powers and are odd functions. Thus, for all the odd-order snc functions, we have $\text{snc}_r(0) = 0$, while from (7.26) we see that for r even, say $r = 2s$, when $y = 0$ the only nonzero term is the first, for which $n = r/2 = s$, so that

$$\mathrm{snc}_{2s}(0) = \frac{(-1)^s \, 2s!}{0!(2s+1)!} = \frac{(-1)^s}{2s+1} \qquad (7.27)$$

We note that cosc has been used elsewhere to mean the derivative $d(\mathrm{sinc}y)/dy$, which would equal $\pi \mathrm{snc}_1 y$ as defined here. It seems that the derivative with the factor $1/\pi$ included, as in (7.17), is more consistent with the sinc function, as this derivative (and subsequent ones) can all be written as power series in πy as in (7.23) to (7.26).

A MATLAB program for evaluating snc_r functions (including snc_0 or sinc) is included in the disk provided with this book. It uses (7.22) for $n > 2$.

7.4 Example of Amplitude Equalization

It has already been remarked that the problem of delay equalization as considered here has been covered in Section 6.3 under the subject of sampled waveform delay, so no further illustrations are given here. However, the subject of amplitude equalization has not been illustrated before, so an example using the results of Section 7.3 is presented in this section, showing how effective the method is and with how little computation it is achieved if there is a degree of oversampling. We take the simple case of a linear amplitude distortion, with an unweighted squared error function over the bandwidth (equivalent to a rect function power spectrum). Following the program given at the end of Section 7.2, we note

1. The response to be matched is of the form $G(f) = 1 + af$ over the bandwidth (taken to be unity), and the weighting function is $|U(f)|^2 = \mathrm{rect}(f)$ [or $\mathrm{rect}(f/F)$ with $F = 1$].
2. Thus we have $G(f)^*|U(f)|^2 = \mathrm{rect}(f) + (a/2)\mathrm{ramp}(f)$ with inverse transform $\mathrm{snc}_0(t) - i(a/2)\mathrm{snc}_1(t)$. Also $|G(f)|^2|U(f)|^2 = \mathrm{rect}(f)(1 + 2af + a^2f^2) = \mathrm{rect}(f) + a\,\mathrm{ramp}(f) + (a^2/4)\mathrm{ramp}^2(f)$, with transform $\mathrm{snc}_0(t) - ia\,\mathrm{snc}_1(t) - (a^2/4)\mathrm{snc}_2(t)$. Putting t values rT and $(r-s)T$ for t into these expressions gives **a** and **B**.
3. Hence, we obtain the optimizing weights from (7.9).

We see that the Fourier transforms of G required for the components of **a** include a transform of the ramp function (i.e., a snc_1 function) as well

as a snc_0 from the rect function. As we require the transform of $G^2(f)$ to determine the elements of **B**, we also have a $ramp^2$ function, with its transform snc_2. There is an important detail to notice in that they are actually *inverse* Fourier transforms that are required—see (7.6) and (7.7). In many cases (using symmetric functions, in particular), there is no distinction between forward and inverse transforms, but here we have odd functions (ramp and snc_1). We see from (7.18) that $ramp^r$ (forward) transforms to $i^r snc_r$ so, from Rule 4, we have $i^r snc_r(x) \Leftrightarrow ramp^r(-y) = (-1)^r ramp^r(y)$, as ramp is an odd function. Multiplying by $-i^r$, we have (Pair 13b) $snc_r(x) \Leftrightarrow i^r ramp^r(y)$.

From this we see that the inverse transform of ramp is $-isnc_1$ and of $ramp^2$ it is $-snc_2$. These results are also used in this sum beam equalization in Section 7.6 and in the difference beam equalization in Section 7.7.

For Figure 7.4 we have taken a linear amplitude distortion for $G(f)$ of 10 dB across the band, from an amplitude of 0.48 to 1.52. Using a
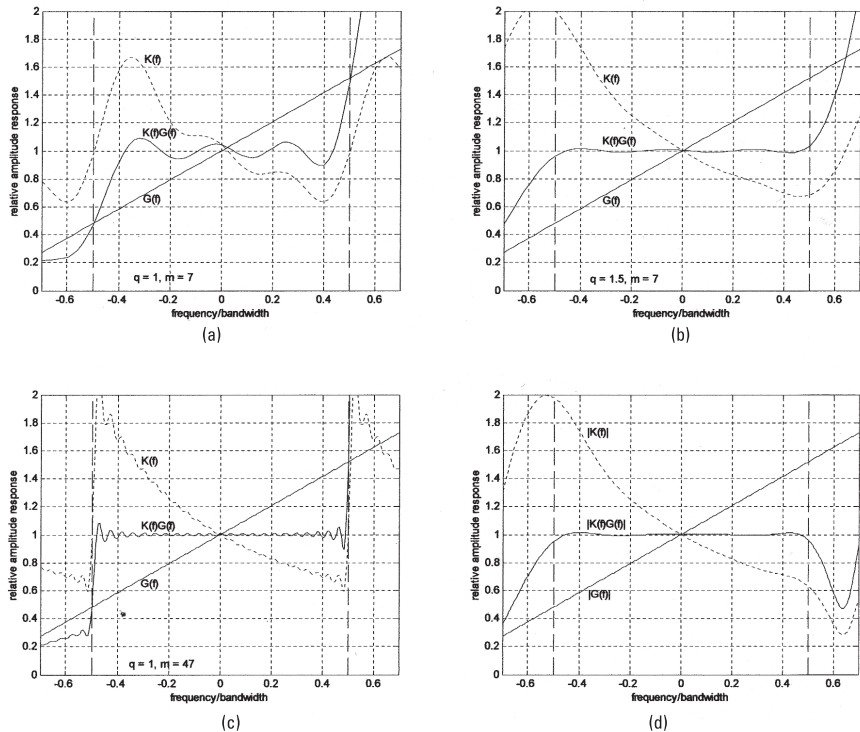
Figure 7.4 Equalization of linear amplitude distortion. (a) $m = 7$, $q = 1$, (b) $m = 7$, $q = 1.5$, (c) $m = 47$, $q = 1$, and (d) $m = 7$, $q = 1.5$, delay 0.5.

seven-element equalizing filter and a relative sampling rate of 1 (no oversampling), we get a useful degree of equalization (Figure 7.4(a)), using (7.6), (7.7) and (7.10). The figure shows the filter response K, which should ideally be the reciprocal of G over the band, as well as the equalized response, KG. If we increase the oversampling rate to 1.5, or 50 percent oversampling, the equalization becomes very good (Figure 7.4(b)). To get a comparable ripple performance at the basic sampling rate, we see that we have to increase the number of filter taps greatly—even at 47 taps (Figure 7.4(c)) the ripples are greater; the higher ripple frequency is due to the much greater time spread of the taps in this case.

Finally, for Figure 7.4(d), there was both amplitude variation and delay to be compensated. The same linear amplitude function was taken, with a delay error of 0.5 sampling interval, and the filter parameters are as for Figure 7.4(b). In this case, the functions have some residual phase variation so the modulus has been plotted, and we see that this has been very well equalized within the band—almost identically with the case of no delay error—but varies significantly (particularly on the positive frequency side) outside the band. The phases of K, G, and KG are also available from the program and show the phase has been accurately equalized (to zero) across the band.

The results of Figure 7.4 can be reproduced using MATLAB programs Fig704 and Fig704d on the accompanying disk, but this also contains an extra program Fig704X, showing excellent equalization of a quadratic amplitude distortion. In this case, the components of **a**, depending on G, the quadratic distortion, require snc_0 (or sinc), snc_1, and snc_2, but the components of **B**, dependent on G^2, also require values of snc_3 and snc_4, making considerable use of the program snc included on the disk. Again, oversampling is valuable in giving good performance from quite short filters.

7.5   Equalization for Broadband Array Radar

Many antennas for use in radio, radar, or sonar systems consist of an array of simple elements, rather than, in some radio cases, a single element, or, for radar and satellite communications, a large parabolic dish or even an exponential horn. For maximum signal-to-noise ratio (whether on transmission or reception) in a particular direction, the signals passing through the elements must be adjusted in phase so that they sum in phase at the frequency of operation. Of course, in practice all signals occupy a finite bandwidth so that in principle different phase shifts are needed across this band, as it is really a time difference, dependent on element position, that needs compensation. However, many signals are narrowband, in that the fractional bandwidth,

the ratio of the bandwidth to the center, or carrier, frequency is small. In this case the phase shift required across the band is close to that at the center frequency, and, as it is much easier to apply a simple (frequency-independent) phase shift than a delay, this approximation can be used. Whether or not this approximation is acceptable in a given system depends not only on the fractional bandwidth, but also on the size, or aperture, of the array. Thus, *narrowband* is a relative term, and perhaps the most appropriate definition of a narrowband signal in this context is that it can be termed narrowband if ignoring its finite bandwidth leads to negligible, or practically acceptable, errors. Conversely, a *broadband* signal as defined here is one where this is not the case, and allowance, or compensation, must be made for the different frequencies across its bandwidth to maintain the required performance. (There seems to be no standard definition of these terms, but this qualitative definition seems to be clearer in some ways than a quantitative one; for a very small array a 5 percent band may be "narrow" in this sense, while a 1 percent band may be "broad" in the context of a very large, and hence highly frequency-sensitive, aperture. We will use *wideband* for the case where the band of interest extends down to 0 Hz; this is the same as the 200 percent broadband case and is consistent with the use of the term in Section 5.3.)

The problem is illustrated in Figure 7.5 for a simple linear array. An element at distance d from the center of the array receives the signal from direction θ, relative to broadside, at time τ earlier than at the reference point, given by

$$\tau(\theta) = d\sin\theta/c \qquad (7.28)$$

where c is the velocity of light. Thus, in principle the output of this element should be delayed by $\tau(\theta)$ to steer the array in direction θ, but, as phase shifts
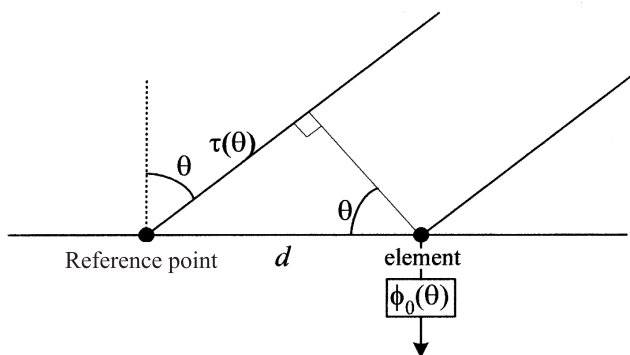
Figure 7.5 Array steering.

are much more easily implemented than delays, it is usual, using the narrow-band condition, to introduce the phase shift

$$\phi(\theta) = 2\pi f_0 \tau(\theta) = 2\pi(d/\lambda_0)\sin\theta \tag{7.29}$$

Here f_0 is the center frequency, λ_0 is the corresponding wavelength (such that $f_0\lambda_0 = c$), and d is the distance of the element from the reference point. (More generally, if the element position vector is $\mathbf{r}$, and the unit vector in the direction of interest is $\mathbf{e}(\alpha,\varepsilon)$ for azimuth α and elevation ε, then the required phase shift to steer in direction (α,ε) is $2\pi\mathbf{r}.\mathbf{e}(\alpha,\varepsilon)/\lambda_0$, where $\mathbf{r}.\mathbf{e}$ is the scalar product of these vectors). This phase shift is correct at the center frequency but is progressively in error for signal components at frequencies offset from the center, and for the broadband case, where this approximation is not acceptable, we need better matching of the delay.

Summing the element outputs in phase produces the peak response in the steered direction, and this form of response is known as the *sum beam*. (Strictly this is only the array factor; for the full response, this is multiplied by the element response, in the case of essentially identical elements). For high angular accuracy in radar a technique known as *monopulse measurement* is used. This requires a *difference beam*, which ideally has zero gain in the look direction, and a linear amplitude response near this direction. The angular offset of a target from the look direction is found by observing the level of its echo in the difference beam (normalized by the sum beam response) and dividing by the known slope of this beam. One form of difference beam, in the case of a regular linear or planar array, is obtained by dividing the array into two equal parts and subtracting the responses of the two halves (hence the origin of the name), but an alternative approach, which allows a difference beam to be formed with a more general geometry, is to form a beam that is the angular derivative of the sum beam. The form that will be considered in Section 7.7 is based on this. (We note that as there is no unique form of sum beam, as beams with different sidelobe patterns may be used, for example, so there is no unique form of difference beam. Thus, in Section 7.7 we *define* a suitable difference beam, basically as the derivative of the sum beam without the extra frequency sensitivity.)

7.6   Sum Beam Equalization

To steer a narrowband sum beam, we apply to the output of each array element a phase shift, corresponding at the carrier frequency to the relative delay

that is to be compensated. To steer a broadband sum beam, we need only to replace this simple phase shift by the delay itself. In fact, it is not easy in practice to provide flexible delays at RF, as would be required for a beam to be steered freely in various directions, but, for arrays with digital processing, we can provide a very close approximation to the required delays using the methods discussed here, which can be implemented rapidly. In fact, as the processing is carried out at baseband, after down-conversion and digitization, the delay is implemented at baseband. The phase shift on the carrier is still required and can be applied either at the RF stage, as for the narrowband application, or digitally, after down-conversion, but is independent of the equalization process. For the sum beam, considered here, the channel equalization is a simple delay, which can be approximated by the methods of Chapter 6 so this application of equalization requires essentially no new ideas. However, we show the benefit of this equalization with the example of a simple array, and in the next section we consider the equalization for the
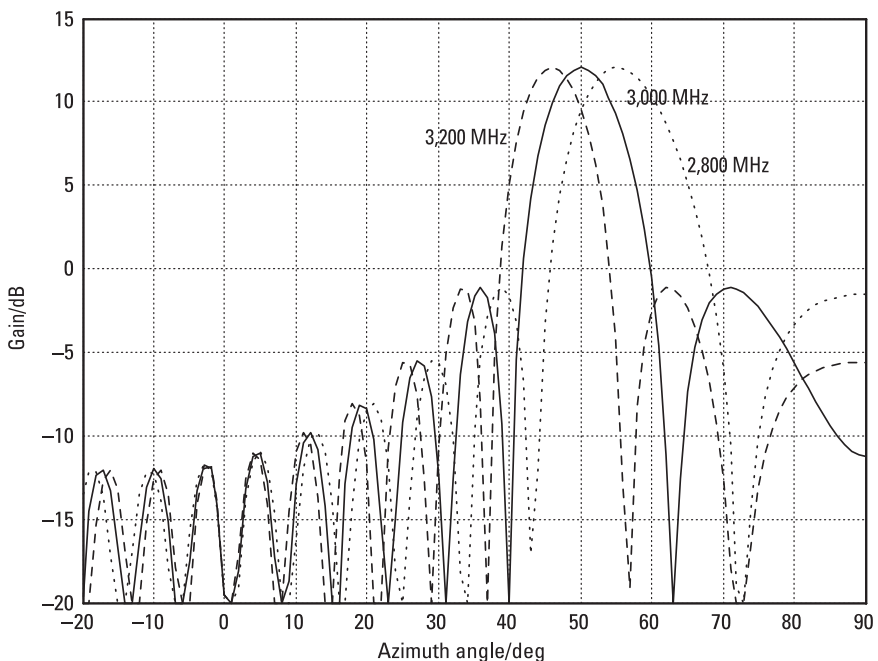
Figure 7.6 Array response with narrowband weights.

difference beam, which is more complex and uses the results of Sections 7.2 and 7.3. We illustrate this using the same array and signal spectrum.

The system we model is a 16-element linear array of omnidirectional elements at half-wavelength spacing operating at 3000 MHz. (More generally, the elements need not be omnidirectional, but should be similar, should be orientated in parallel, and are taken to be frequency independent.) The actual frequency is not particularly significant; what is more important are the relative frequencies. To illustrate the problem, Figure 7.6 shows the gain (more precisely the array factor) at three frequencies, for the array when steered at 50° from broadside. The steering weights are the correct phases at the center frequency, and this beam has its peak at the correct position. With the same weights, the beams at the frequencies 200 MHz above and 200 MHz below (at about ±6.7 percent offset) are displaced in position. (This effect is known as *squint*.) Thus for a broadband signal arriving from 50° and with the array steered in this direction, there will be a variation in gain, with a fall of about 2½ dB at ±200 MHz from the center frequency in this case and hence a distortion of the received signal.

Using the equalization method described in Section 7.2, we use (7.9) for the weights on the FIR filter taps, where the components of **a** and **B** are given in general form in (7.6) and (7.7). For this example, we take a symmetric trapezoidal shape for the spectral power density, U, with a flat top 80 percent of the full width of 500 MHz. The channel response requiring compensation, or equalization (G in Section 7.2) is just that due to a simple delay, different in each element channel, in general. For this delay equalization case, the problem is the same as that considered in Section 6.3, and the components of **a** and **B** are given more specifically by (6.47a) and (6.47b). The result of implementing this delay equalization is shown in Figure 7.7. Responses for the same set of frequencies as in Figure 7.6 are shown, with those at ±200 MHz being toward the edges of the 500-MHz band (at the corners of the trapezoidal spectrum, in fact). We see that the squint has been removed effectively, with the main lobes of the responses at the three frequencies virtually coincident, though the sidelobes have risen slightly in Figure 7.7(b).

Two processing alternatives are shown; in Figure 7.7(a) only five taps are used for each delay, with an oversampling rate of 1.2, or 20 percent above the minimum rate, and in Figure 7.7(b) only three taps are used, but the sampling rate increase has been raised to 50 percent. The difference is small, with the three-tap responses slightly poorer, but on raising the oversampling factor to 2, the performance with three taps is much the same as with five at 1.2.

In fact, if we reduce the taps to two we still get good equalization with q raised to 5. Taking this further, if we take $m = 1$ (i.e., with no FIR filters), we
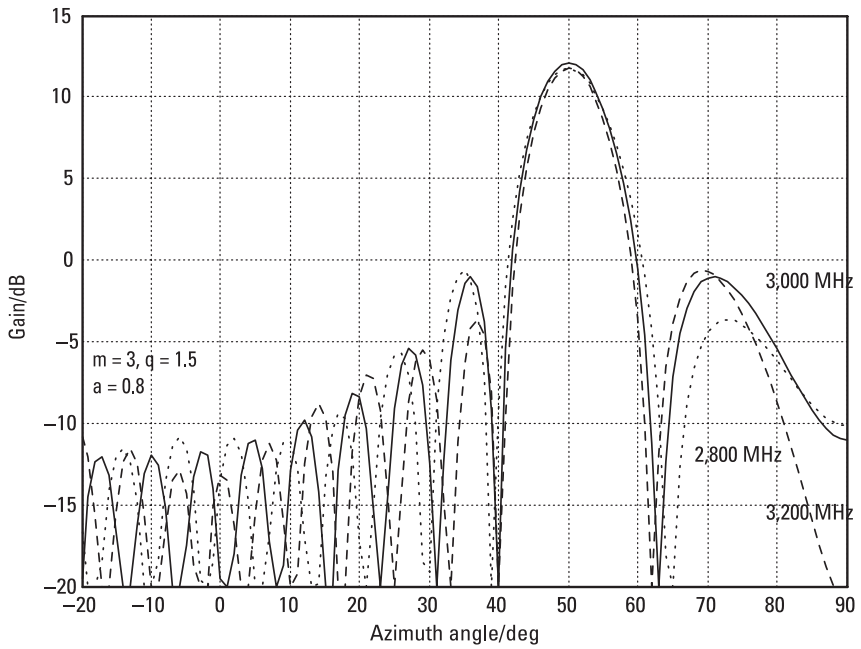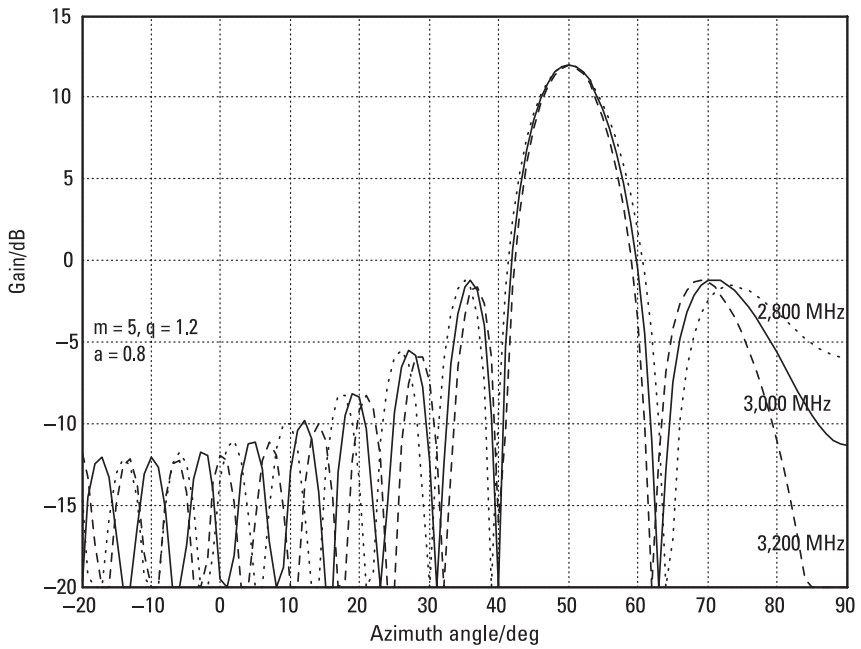
Figure 7.7 Array response with equalization. (a) Five taps, 20% oversampling, and (b) three taps, 50% oversampling.
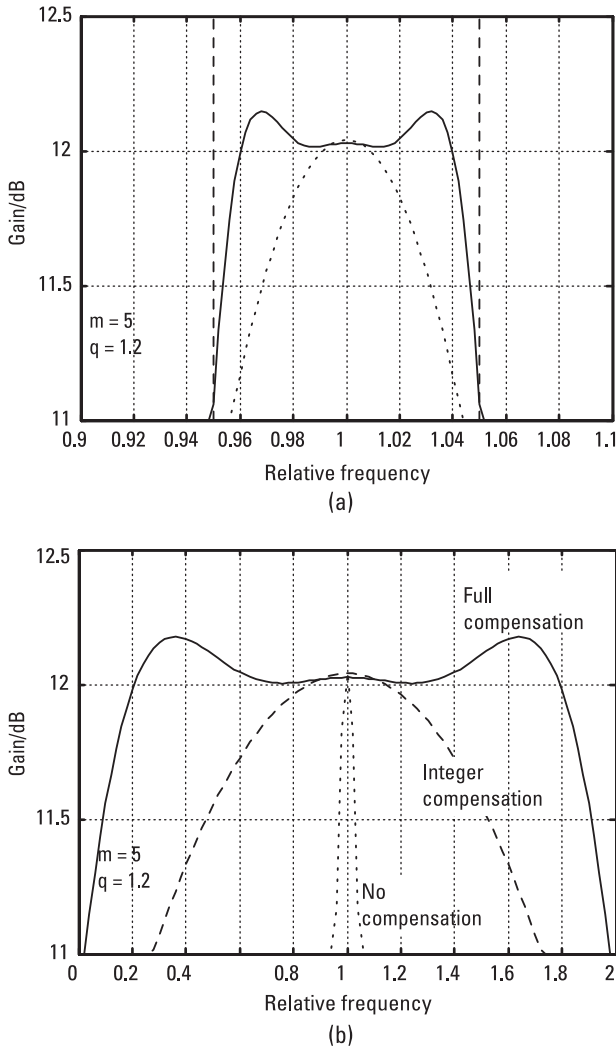
Figure 7.8   Sum beam frequency response; effect of bandwidth. (a) 10% bandwidth, and (b) 200% bandwidth.

get a useful degree of compensation by oversampling (with the least squares processing)—with $q = 2$ the main lobes are close, but the sidelobe patterns are considerably degraded and the gain is reduced by about ½ dB for the upper and lower frequencies.

To study the response at the peak of the beam more closely, the gain in the steered direction has been plotted in Figure 7.8 as a function of frequency

normalized to the center frequency. The plots are for the case of five taps and a 20 percent oversampling rate, as in Figure 7.7(a), and it can be seen that there is only a slight variation with frequency—a rise of less than 0.2 dB and a fall in gain at the very edges of the trapezoidal band taken, where the signal power density is falling and the matching is not required to be so good. In Figure 7.8(a), the vertical lines mark the edge of the 10 percent band over which equalization is required, and the dotted curve shows the response in the absence of equalization. In Figure 7.8(b) the parameters of the equalization filters are the same, but the receiver bandwidth is now 200 percent, extending from zero to twice the center frequency. Again the dotted line shows the frequency response without any equalization, and the dashed response is that for the case of only integer delay compensation (in units of the sampling interval). (In Figure 7.8(a) there is no dashed curve, as all the delays are within ±0.5 sampling intervals, so no integer compensation is feasible.) We note that, with the same set of parameters, the response is essentially independent of the fractional bandwidth—the shapes of the responses are virtually identical. In the second case, the sampling rate is much higher, of course; in this case, as the bandwidth is $2f_0$, where f_0 is the center frequency, the sampling rate is $2.4f_0$. To sample at this rate may be impracticable at radar frequencies but may well be feasible for sonar, where broadband (or even wideband) operation is much more commonly required and the actual signal frequencies are much lower. We also note that the response with integer delay compensation in the wideband case is the same, in proportion to the bandwidth, as the uncompensated curve in the narrower band case. This is because, in the latter case, as all the matching delays required are less than one sampling interval, the integer compensated case is the same as the uncompensated case.

The fact that these responses are very similar is not a coincidence, but illustrates that the response is essentially independent of the fractional bandwidth and depends only on how well the delays are matched. This depends, for a given set of equalization filter parameters (m and q) on how close the required delays are to integer multiples of the sampling period. This will vary, in general, from one element to another and will depend on the beam steered direction and the element separation. In particular cases, the delays required may all be integral, in sampling periods, in which case the matching will be exact, in principle, and the response will be completely flat. At the other extreme, the delays required may all be half-integral, which is the worst case for matching. In general, however, there will be spread of delays, and the performance will be intermediate. This is illustrated in Figure 7.9, which shows the gain in the look direction as a function of frequency. Here, the frequency axis is the frequency offset from the center, normalized to the
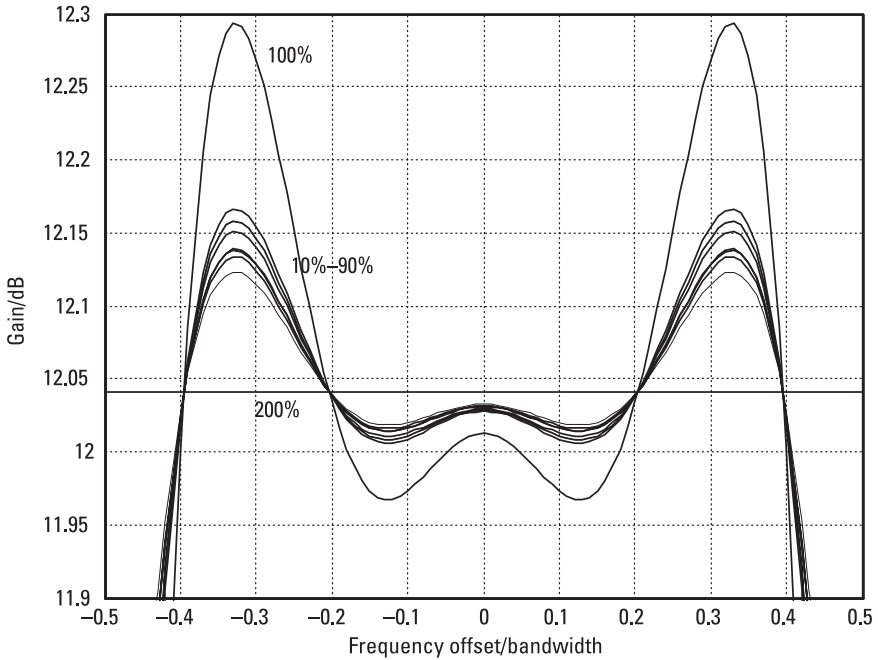
Figure 7.9   Sum beam response with frequency offset, for various bandwidths.

bandwidth, so the range shown is just the band over which equalization is required. For this figure, the parameters were chosen in order to include the two extreme cases described earlier. The delay required for an element at distance d from the array center is given in (7.28), and putting $c = f_0\lambda_0$, and dividing by the sampling period $1/qF$, the required delay in units of sampling periods is given by

$$\beta = (d/\lambda_0)q\sin\theta(F/f_0) \qquad (7.30)$$

The element separation was increased to one wavelength, so that the element positions are given as $(2n + 1)/2$ wavelengths (n an integer from -8 to $+7$ for the 16 element array). The steer direction remained at 50°, but q was increased to 1.3054 so that $q\sin50° = 1$. The delay required (in sampling intervals) for element n is then given, from (7.30), by $(2n + 1)(F/2f_0)$. If we choose $F = f_0$, the 100 percent bandwidth case, we see that all the delays are half integral (the worst case), while if $F = 2f_0$, the 200 percent case, the delays are integral and we have the flat response shown. The other curves are for the cases of 10 percent, 20 percent . . . 90 percent bandwidths (*not* giving a
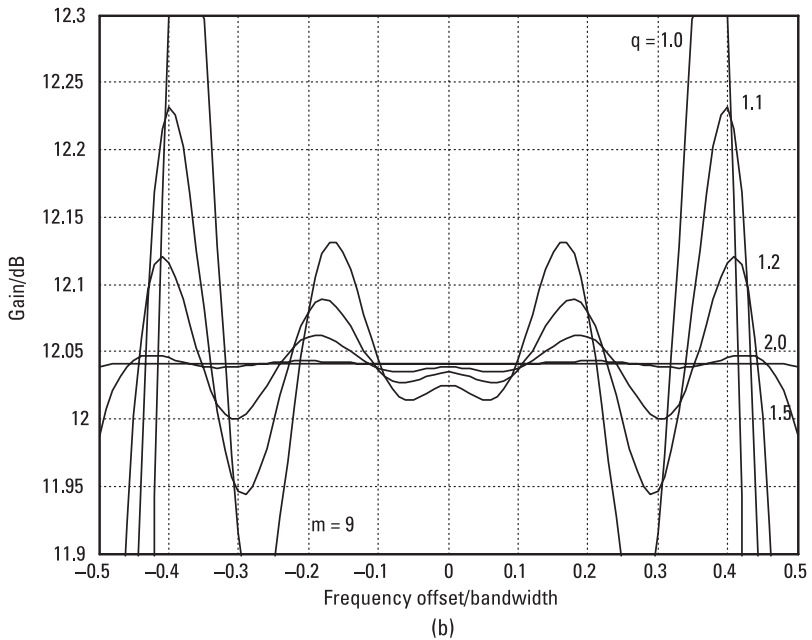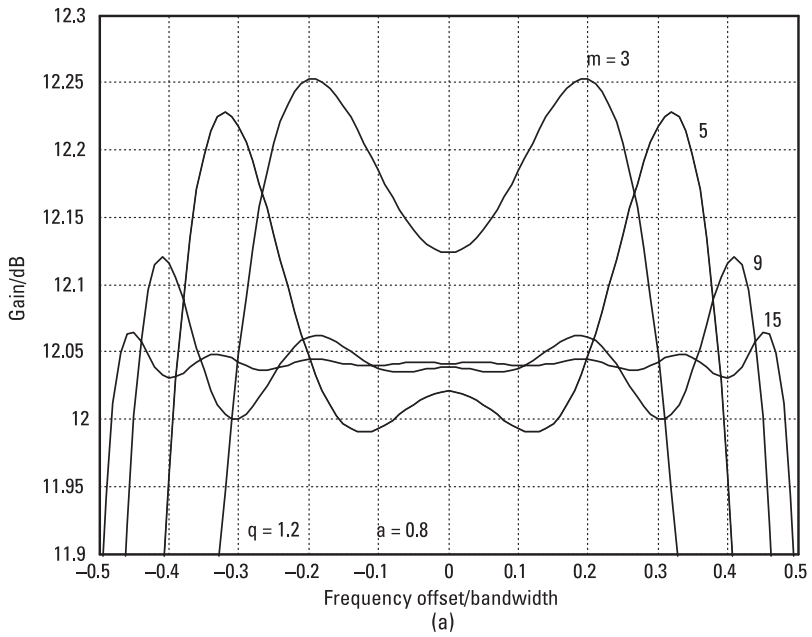
Figure 7.10 Sum beam frequency response; variation with equalization parameters. (a) Variation with *m*, and (b) variation with *q*.

monotonic sequence of peak ripple levels, with some curves overlying others), and because the fractional delays are distributed over the full range the results for these cases are much the same and intermediate between the extreme cases. These are also the same results as for bandwidths of 110 percent to 190 percent because it can be seen that for this case (where $q\sin\theta = 1$) the results for a fractional bandwidth F/f_0 of r and $2 - r$ will give the same result.

The effect of varying the equalization parameters is shown in Figure 7.10, for the 50 percent bandwidth case, and for the array separation of 0.5 wavelengths. In Figure 7.10(a), we fix the sampling rate at 1.2 or 20 percent above the minimum and vary the number of taps m in the equalizing filters. We note that even with three tap filters, the ripple in the center of the band is quite small (less than 0.25 dB above the fully equalized level), but there is a rather rapid fall in gain at the edges of the trapezoidal band, starting well within the flat top region (from –0.4 to +0.4 bandwidths offset). As m increases the response improves, and at $m = 9$ the gain falls off rather sharply only outside the flat top of the signal spectrum. With $m = 15$ the equalization
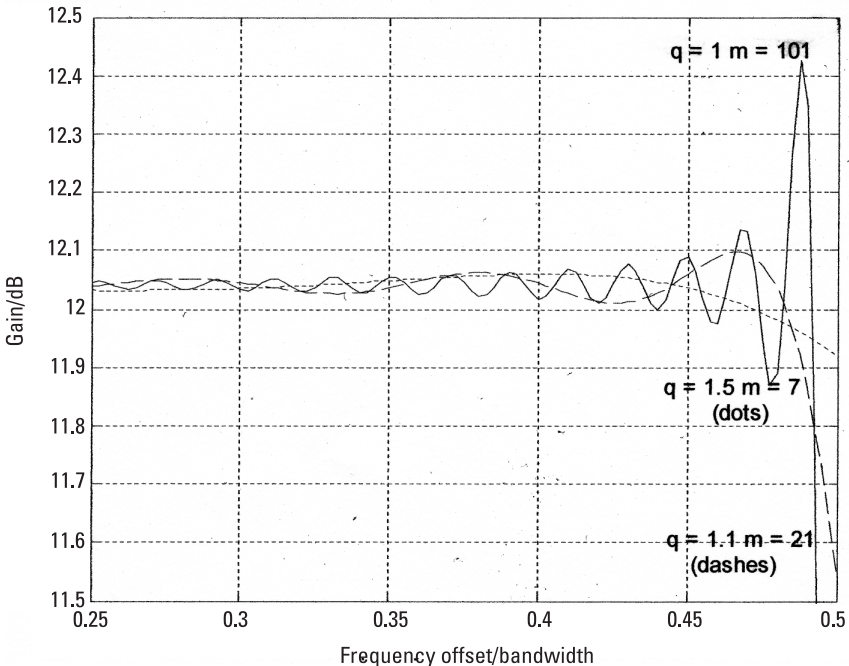
Figure 7.11   Effect of increasing oversampling rate.

is excellent, with a gain ripple of only a few hundredths of a decibel. The filter length has been kept at nine in Figure 7.10(b) and the relative sampling rate q varied. With no oversampling ($q = 1$), the nine tap filters do achieve a considerable degree of equalization, but there is a large ripple near the edges of the band. This is rapidly reduced with oversampling, and at $q = 2$ the response is almost perfect. (It should be remarked that these are nominal gain plots and give an ideal figure of 12.04 dB for an array of 16 elements. They should be corrected slightly if directivity is required, but any correction will generally be small, particularly for larger arrays not steered too close to a grating lobe condition.)

Finally Figure 7.11 shows clearly the benefit of oversampling. At the minimum sampling rate, a very long filter is needed for effective equalization—in this example, 101 elements are required (continuous curve) to give low ripples in the response. If the sampling rate is increased to just 1.1, comparable ripples result at a filter length of only 21 (dashed curve), a reduction of nearly five times in the computation required. Oversampling at 50 percent (dotted curve) allows an improvement by a further factor of three to only seven elements. For planar arrays with a large number of elements, typically required for many radars, it could be important and valuable to keep the complexity of equalization down to a modest level in each channel; in some applications, with a moderate degree of oversampling, filters of length as low as three or four may be adequate.

7.7   Difference Beam Equalization

We take the difference beam pattern to be given essentially by the derivative with respect to angle of the sum beam pattern. We will use the "sine-angle" coordinate u, where $u = \sin\theta$, as this simplifies the following expressions, particularly for the difference beam slope, but otherwise does not affect the principles being illustrated. (In this form, the beam shape, plotted against u, remains unchanged in shape as the beam is scanned.) Thus, in this section we replace $\sin\theta$ with u, where θ is the look direction measured from broadside, in particular in equations that use (7.28). If $w_k(u_0)$ is the weight applied to the output of element k to steer in direction θ_0, where $u_0 = \sin\theta_0$, then the sum beam gain (array factor) is given, as a function of frequency and angle, by

$$g(u, f; u_0) = \sum_k w_k(u_0) \exp 2\pi i f \tau_k(u) \tag{7.31}$$

For narrowband steering, we take $w_k(u_0) = \exp(-2\pi i d_k f_0 u_0/c)$ so that the signals add in phase in the look direction θ_0 at the center frequency, f_0. The sum is over all elements and the signal delay τ_k relative to the center of the array is given by $d_k u/c$ (from (7.28)), where the element is at distance d_k from the array centroid, the mean element position, such that the sum of the element positions measured from this point is zero.

We now want to define a difference beam pattern whose response in angle is a derivative of the sum beam. The differential of this beam with respect to u, is given, from (7.31), by

$$g'(u, f; u_0) = \sum_k w_k(u_0)(2\pi i f d_k/c) \exp(2\pi i f d_k \, u/c) \tag{7.32}$$

In fact to define a difference beam, we do not need the factor f; we require only the frequency-sensitive element delay compensation factors $w_k(u_0) = \exp(-2\pi i f d_k u_0/c)$, which allow the signals to sum in phase across the frequency band. The element distances d_k, are weighting factors that result in zero gain in the look direction with these weights applied. This set of weights $\{w_k\}$ is the same as those required for the sum beam, so the same frequency compensation is required on each element. Thus, excluding the factor f in (7.32) and other factors independent of frequency, we *define* the required difference beam response, within a scaling factor, by

$$h(u, f; u_0) = \sum_k w_k(u_0) i d_k \exp 2\pi i f d_k \, u/c. \tag{7.33}$$

However, for an ideal difference beam, we require its *slope*, with respect to angle, at the beam pointing position θ_0 to be constant across the band, and this is the derivative of h with respect to angle:

$$h(u, f; u_0)' = -\sum_k w_k(u_0) d_k 2\pi f (d_k/c) \exp 2\pi i f d_k u/c$$

In this case we cannot remove the variable f from the expression because this is not a *definition* of the slope but is a derivation from the pattern as defined

in (7.33). Omitting the constant $2\pi/c$ we have for the difference beam slope, within a scaling factor,

$$s(u, f; u_0) = -\sum_k w_k(u_0) d_k^2 f \exp 2\pi i f d_k u/c \qquad (7.34)$$

In (7.34) f is a frequency within the RF band (i.e., $f_0 - F/2 < f < f_0 + F/2$), but if we now want to represent the gain pattern in terms of the baseband frequency, we replace f with $f_0 + f$, where now we have $-F/2 < f < F/2$. With this change, the response at baseband frequency f, after down-conversion (which removes f_0 from the exponential factor), is given by

$$s(f, u; f_0, u_0) = -\sum_k w_k(u_0)(f_0 + f) d_k^2 \exp 2\pi i f d_k \, u/c$$

Rescaling by f_0, we redefine s as

$$s(f, u; f_0, u_0) = -\sum_k w_k(u_0)(1 + f/f_0) d_k^2 \exp 2\pi i f d_k \, u/c \qquad (7.35)$$

This response varies with angle and frequency, but we require it to be independent of frequency at the direction of interest, θ_0. Thus, excluding constants with respect to frequency, we see that the frequency variation to be compensated is now of the form

$$S(f) = (1 + \phi f/F) \exp 2\pi i f \, \tau_k(u_0) \qquad (7.36)$$

where the delay τ_k varies with the element position, and we have expressed the function S in terms of ϕ, the fractional bandwidth, F/f_0.

Before putting this expression for S into (7.6) and (7.7) we note, as before, that for the band-limited signal we effectively have a factor $\mathrm{rect}(f/F)$ in $|U(f)|^2$, so multiplying $S(f)$ by this rect function will make no difference to the integrals in (7.6) and (7.7). Thus, we can replace S with

$$S(f) \mathrm{rect}\left(\frac{f}{F}\right) = \left(\mathrm{rect}\left(\frac{f}{F}\right) + \frac{\phi}{2} \mathrm{ramp}\left(\frac{f}{F}\right)\right) \exp(2\pi i f \, \tau) \qquad (7.37)$$

Putting this into (7.6) and (7.7) in place of G gives

$$a_r = \int_{-\infty}^{\infty} \left(1 + \frac{\phi}{2} \operatorname{ramp}\left(\frac{f}{F}\right)\right) |U(f)|^2 \exp 2\pi i f (rT - \tau) df \qquad (7.38)$$

and

$$b_{rs} = \int_{-\infty}^{\infty} \left(1 + \phi \operatorname{ramp}\left(\frac{f}{F}\right) + \frac{\phi^2}{4} \operatorname{ramp}^2\left(\frac{f}{F}\right)\right) |U(f)|^2 \exp \left(2\pi i f (r - s)T\right) df$$

$$(7.39)$$

Now let ρ_a, ρ_b, and ρ_c be the inverse Fourier transforms of $|U(f)|^2$, $\operatorname{ramp}(f/F)|U(f)|^2$ and $\operatorname{ramp}^2(f/F)|U(f)|^2$, respectively, and also let us put $\tau = (k + \beta)T$, where $-0.5 < \beta \le 0.5$ and k is integral. As before, we assume that the delays are compensated to the nearest integer multiple k of the sampling period by taking the appropriate sampled pulse train (e.g., from a shift register) and that we only have to equalize the fractional parts using the filter. Introducing these, with βT for τ, we see that (7.38) and (7.39) can be written

$$a_r = \rho_a \left((r - \beta)T\right) + (\phi/2)\rho_b \left((r - \beta)T\right) \qquad (7.40)$$

and

$$b_{rs} = \rho_a \left((r - s)T\right) + \phi \rho_b \left((r - s)T\right) + (\phi^2/4)\rho_c \left((r - s)T\right) \qquad (7.41)$$

Now, for the trapezoidal spectrum we have (as in Section 6.3.2, equation (6.45))

$$|U(f)|^2 = \frac{4}{(1 + a)(1 - a)F^2} \operatorname{rect}\left(\frac{2f}{(1 - a)F}\right) \otimes \operatorname{rect}\left(\frac{2f}{(1 + a)F}\right) \qquad (7.42)$$

Although the function $\operatorname{rect}(f/F)$ does not appear in this expression, the spectral function would be unchanged on multiplying by this rect function, as the convolution of the rect functions in (7.42) has a base width of $(1 - a)F/2 + (1 + a)F/2 = F$, the same as $\operatorname{rect}(f/F)$. The rect function is unity within the region where the trapezoidal function is nonzero and zero where the trapezoidal function is zero. This justifies the statement (7.37) that this rect function can be included in the integral and hence also with S.

The Fourier transform of the power spectrum in (7.42) is (as in (6.45)):

$$\rho_a(t) = \operatorname{sinc}\big((1-a)Ft/2\big)\operatorname{sinc}\big((1+a)Ft/2\big) \tag{7.43}$$

To find ρ_b, the transform of $\operatorname{ramp}(f/F)|U(f)|^2$, we see from (7.42) that we require the product of the ramp function with a convolution of two rect functions. Now, in general it is not the case that $u(v\otimes w) = (uv)\otimes w$, but in the particular case where w is a δ-function at the origin, then, as $\delta(x)\otimes y(x) = y(x)$, this relation is true (i.e., $u(v\otimes\delta) = uv = (uv)\otimes\delta$). In this case, where a is near to unity, the smaller rect function (with the factor $2/(1-a)F$, to make its integral unity) is near to a δ-function, and we will make the small approximation of rearranging the product with the convolution in the form

$$\operatorname{ramp}\left(\frac{f}{F}\right)|U(f)|^2 \approx \frac{4}{(1+a)(1-a)F^2}\operatorname{rect}\left(\frac{2f}{(1-a)F}\right)$$

$$\otimes\operatorname{ramp}\left(\frac{f}{F}\right)\operatorname{rect}\left(\frac{2f}{(1+a)F}\right) \tag{7.44}$$
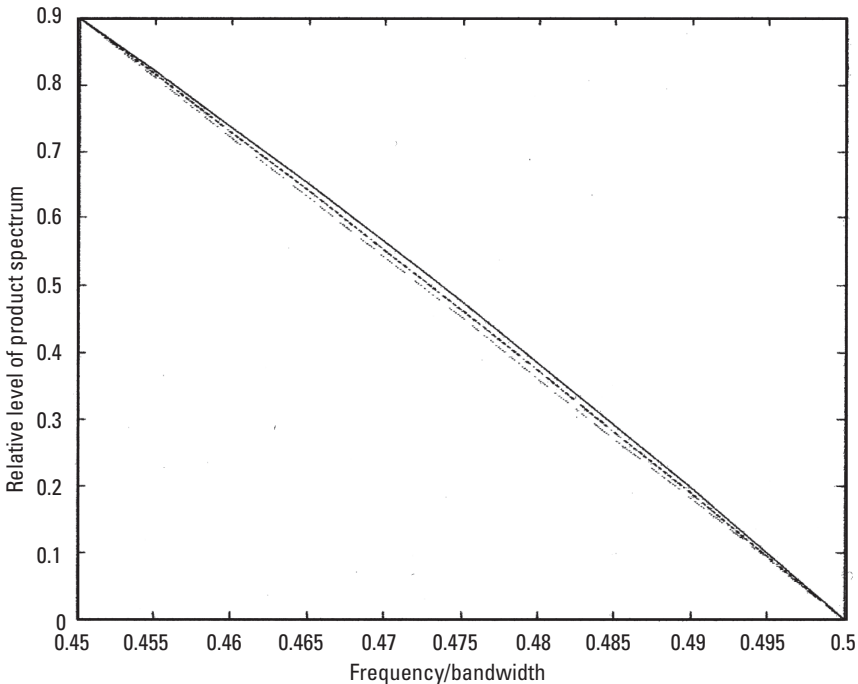
Figure 7.12   Effect of approximation of product spectrum on falling edge of trapezoid.
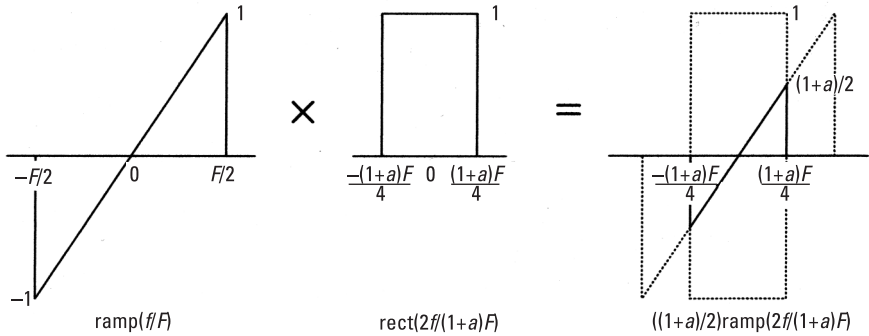
Figure 7.13   Product of ramp and rect functions.

Figure 7.12 shows the scale of the approximation. The lowest trace (dotted) is the straight line of the falling edge of the trapezoid, which results if we take a δ-function instead of the factor $(2/(1-a)F)\,\mathrm{rect}\big(2f/(1-a)F\big)$. The highest trace (continuous) is a shallow quadratic given by the product of the trapezoid edge with the ramp function over this interval and is the correct shape. The middle trace (dashed), an even shallower quadratic, corresponds to (7.44), the result of convolving the narrow rect function with the product of the ramp function with the wider rect function, which is illustrated in Figure 7.13. (It can be shown that the middle trace is in fact halfway between the other two.) The differences are seen to be very small. With different spectral shapes, without convolutions, such as the raised cosine or Gaussian, this problem does not arise.

We now consider just the product of the ramp function with the wider rect function. As the rect function is narrower than the ramp function, the product is smaller than the unit ramp function, which reaches values of +1 and −1 at its edges. The result, as illustrated in Figure 7.13, is a scaled ramp function; the scaling factor is the relative width of the rect function, which is $(1 + a)/2$. The spectrum to be transformed is thus

$$\mathrm{ramp}\!\left(\frac{f}{F}\right)\!\big|U(f)\big|^2 = \frac{4}{(1+a)(1-a)F^2}\,\frac{(1+a)}{2}\,\mathrm{ramp}\!\left(\frac{2f}{(1+a)F}\right) \otimes \mathrm{rect}\!\left(\frac{2f}{(1-a)F}\right)$$

$$(7.45)$$

and its inverse transform is, using P13b (and P3b, R5):

$$\rho_b(t) = -i\left(\frac{1+a}{2}\right)\mathrm{snc}_1\left(\frac{(1+a)Ft}{2}\right)\mathrm{sinc}\left(\frac{(1-a)Ft}{2}\right) \qquad (7.46)$$

Finally, for ρ_c the function to be transformed is $\mathrm{ramp}^2(f/F)|U(f)|^2$, and (again making the small approximation by rearranging the expression) we can see that the product of $\mathrm{ramp}^2(f/F)$ with $\mathrm{rect}(2f/(1+a))$ is $((1+a)/2)^2\mathrm{ramp}^2(2f/(1+a))$, and, again using P13b, the transform is given by

$$\rho_c(t) = -\left(\frac{1+a}{2}\right)^2\mathrm{snc}_2\left(\frac{(1+a)Ft}{2}\right)\mathrm{sinc}\left(\frac{(1-a)Ft}{2}\right) \qquad (7.47)$$

Using (7.43), (7.46), and (7.47) to substitute for ρ_a, ρ_b, and ρ_c in (7.40) and (7.41) and also putting $FT = 1/q$, as the sampling interval is the reciprocal of the (oversampled) sampling rate qF, we obtain

$$a_r = \mathrm{snc}_0(\alpha_1)\left(\mathrm{snc}_0(\alpha_2) - i\frac{(1+a)\phi}{4}\mathrm{snc}_1(\alpha_2)\right) \qquad (7.48)$$

and

$$b_{rs} = \mathrm{snc}_0(\beta_1)\left(\mathrm{snc}_0(\beta_2) - i\frac{(1+a)\phi}{2}\mathrm{snc}_1(\beta_2) - \frac{(1+a)^2\phi^2}{16}\mathrm{snc}_2(\beta_2)\right),$$
$$(7.49)$$

where

$$\alpha_1 = \frac{(1-a)(r-\beta)}{2q}, \quad \alpha_2 = \frac{(1+a)(r-\beta)}{2q}, \quad \beta_1 = \frac{(1-a)(r-s)}{2q}$$

$$\text{and } \beta_2 = \frac{(1+a)(r-s)}{2q}$$

Using these expressions for the components of **a** and **B**, we compute the weights of the equalization filters for each element and then plot the difference beam patterns, in Figure 7.14, corresponding to the sum beam patterns of Figures 7.6 and 7.7(a). In this case, however, we plot the linear response with angle (rather than the logarithmic power response) in order to show the response passing through zero at the required angular position. The parameters for the equalizing processing are the same, using five tap equalizing filters with oversampling
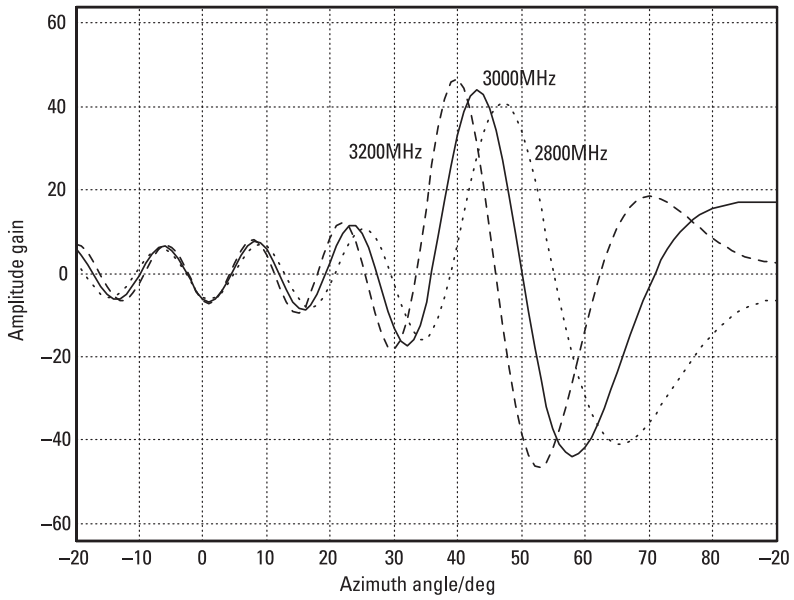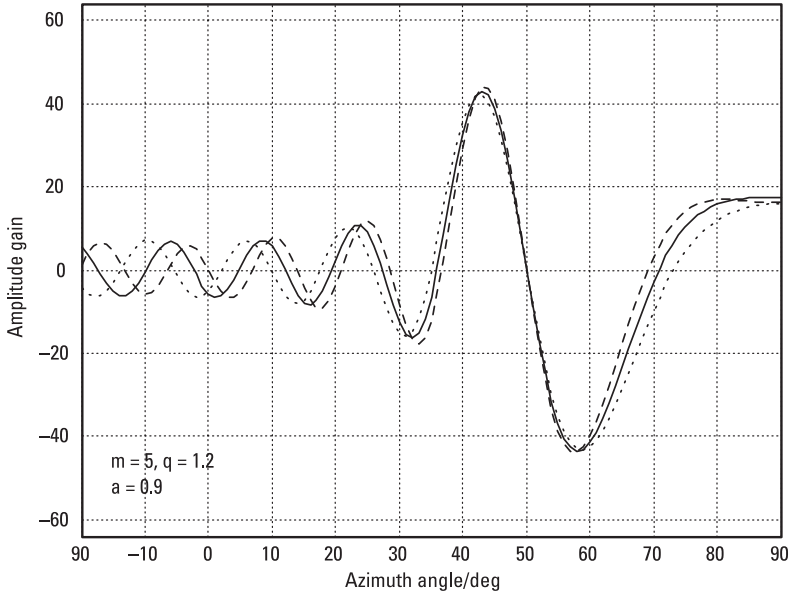
Figure 7.14   Difference beam responses with (a) narrowband weights, (b) equalization, (c) center region of scan (a), and (d) center region of scan (b).

(c)

(d)
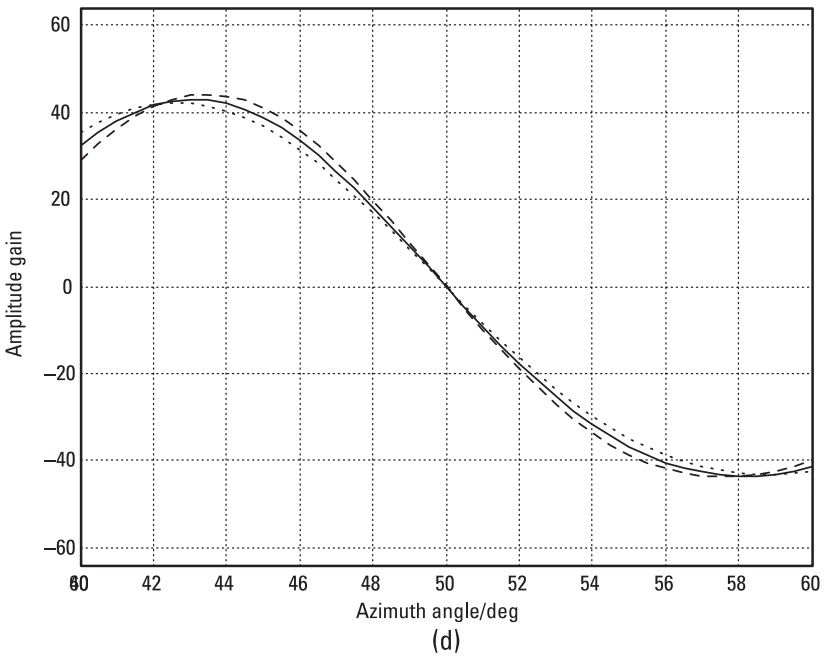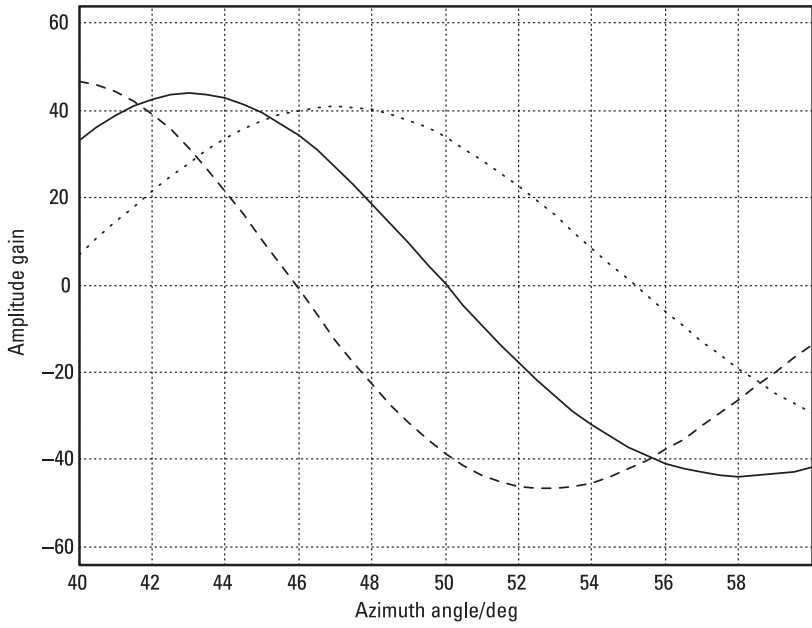
Figure 7.14   (Continued)
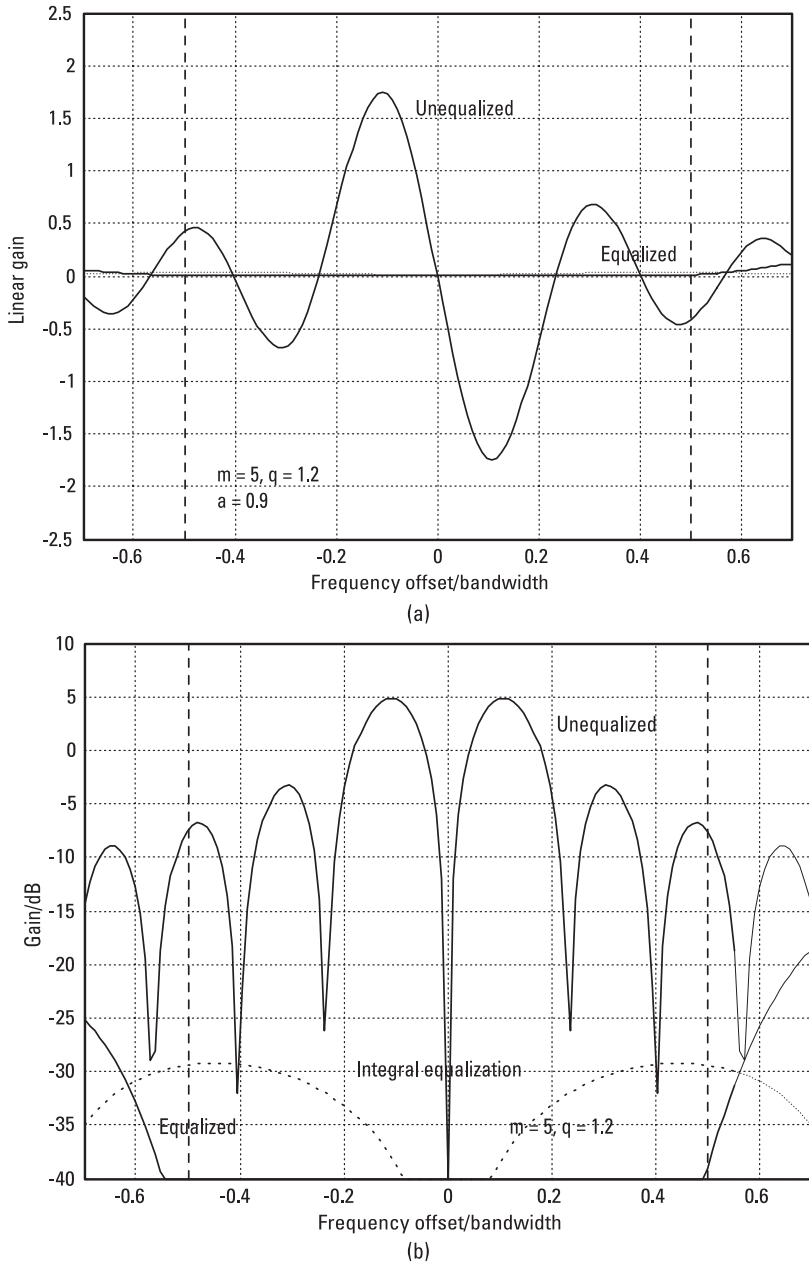
Figure 7.15   Difference beam gain response against frequency offset: (a) linear response, (b) logarithmic response, (c) expanded equalized response, and (d) response with more processing.
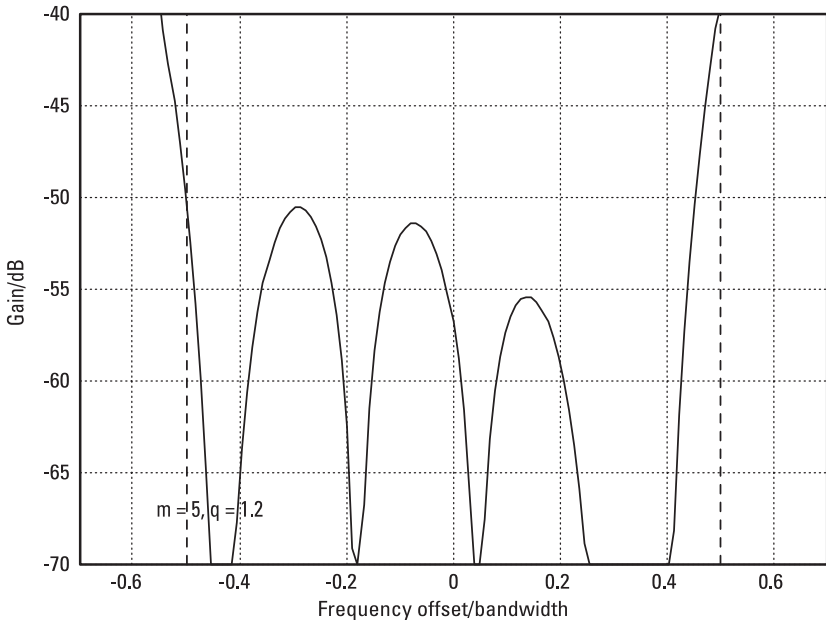
(c)
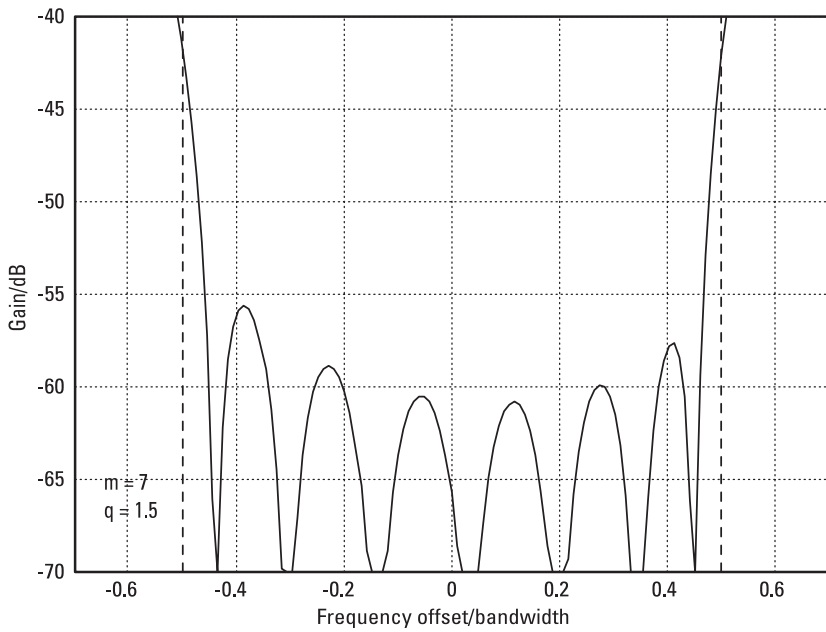
(d)

Figure 7.15 (Continued)
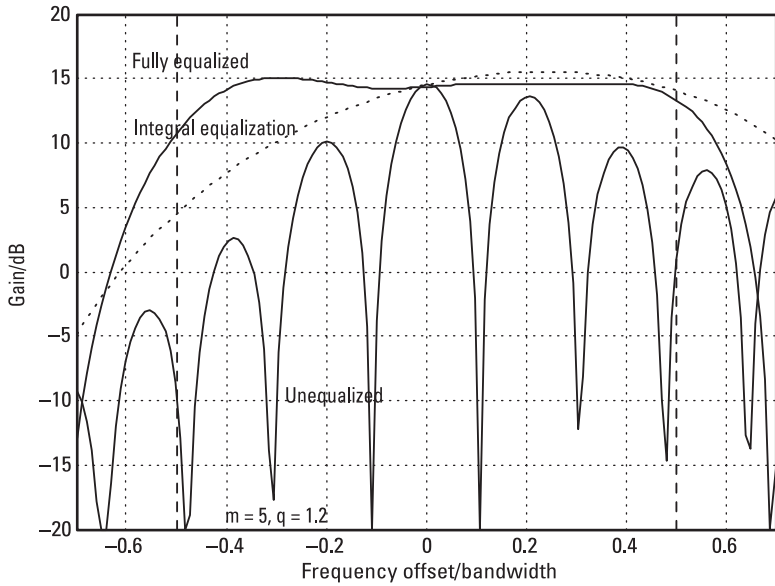
(a)
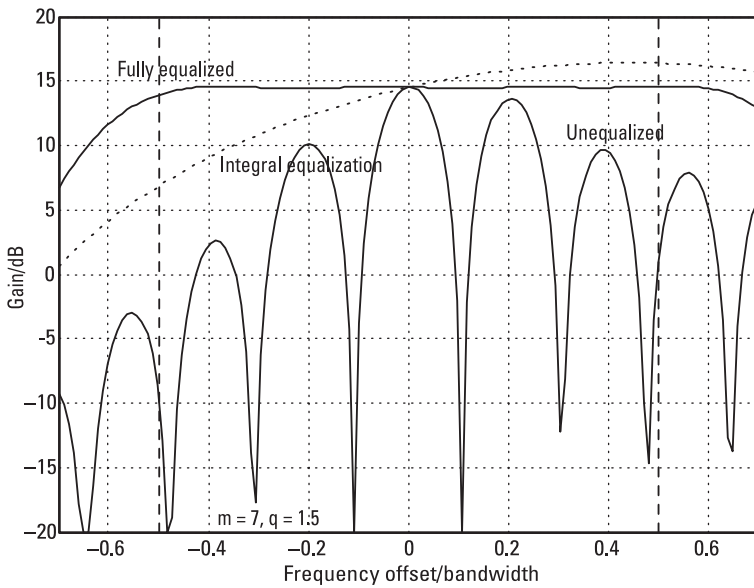
(b)

Figure 7.16   Difference beam slope: (a) small filter response, (b) larger filter response, (c) expanded small filter response, and (d) expanded larger filter response.

m = 5, q = 1.2

(c)

m = 7, q = 1.5

(d)
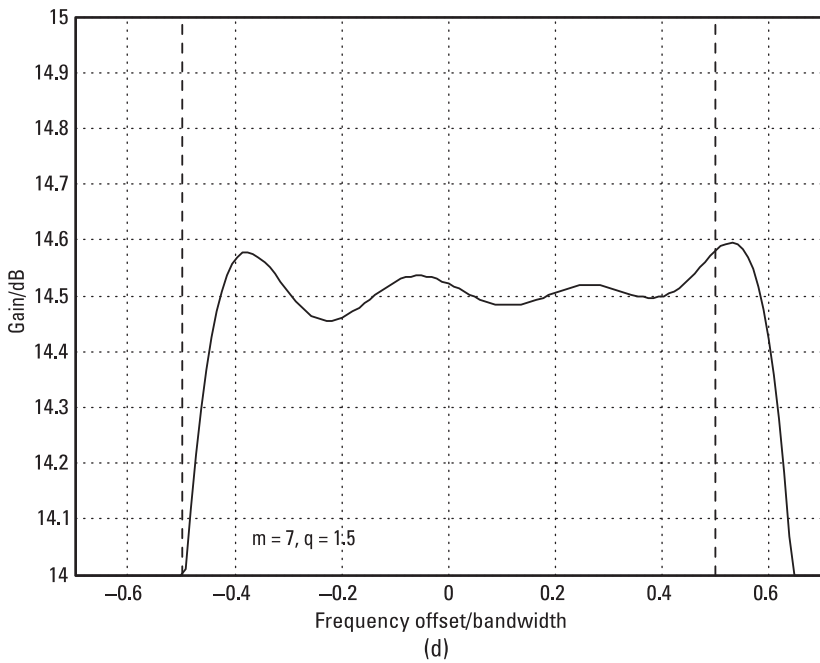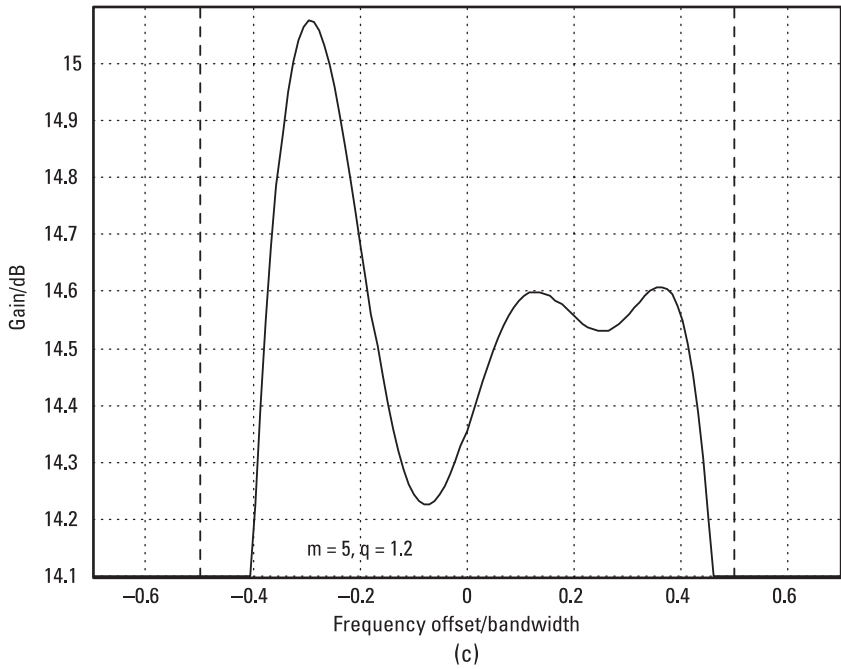
Figure 7.16   (Continued)

by 20 percent, except that the trapezoidal signal spectrum now has a flat top of 90 percent of the bandwidth. (This makes the approximation of the convolving narrow rect function nearer to a δ-function, in fact.) We have also taken a relative bandwidth of 100 percent (i.e., equal to the center frequency), though Figure 7.8 shows that the relative bandwidth has very little effect. Again, we see that equalizing has been highly effective. We note that although **a** and **B**, used in the process (with components given in (7.48) and (7.49)) are complex, the gain is real to a high degree of accuracy; this is because the response to be matched is real. Figures 7.14(a) and (b) are the difference beams equivalent to the sum beams of Figures 7.6 and 7.7(a). Figures 7.14(c) and (d) show the regions round the look direction (50°) in more detail, and we see that the difference beam gains (of zero) and slopes at this point have been matched accurately.

As before, we look at the response in the steered direction as a function of frequency; in this case, we require the gain in this direction to be zero and the slope to be constant. The variation of gain over the normalized bandwidth at baseband is shown in Figure 7.15, for the same parameters as for Figure 7.14. We first show the gain in linear form in Figure 7.15(a). The unequalized response in the look direction, as a function of frequency, is rather similar to the response as a function of direction, at the center frequency, shown in Figure 7.14. The fully equalized response is excellent, rising slightly just at the edges of the band. Integral equalization only (the dotted curve) gives a considerable improvement on the unequalized response but is still much poorer than the fully equalized case. Figure 6.15(b), showing the power response in decibels, also illustrates these points.

Neither Figure 7.15(a) nor (b) shows clearly how well the gain has been kept near to zero in the look direction across the band. Changing the scale, in Figure 7.15(d), shows that the gain ripples are more than 55 dB below the peaks of the difference beam response, and this is with only five tap filters and oversampling at 20 percent. Increasing either of these will reduce the ripple level to lower values, as shown in Figure 7.15(d), where there are seven taps and 50 percent oversampling, giving ripples about 10 dB lower in the band center. We note that the ripple pattern is not symmetrical about the look direction. In fact it would be so if we had performed optimum equalization of the difference beam, which requires only delay compensation, rather than its slope. In this case, we have equalized the pattern slope, which requires compensation for both delay and the amplitude variation with frequency seen in (7.35), and as this amplitude rises with frequency the compensation factor (like K in Figure 7.4) falls, and we see that the ripples on the higher frequency side in Figure 7.15(c) and (d) are indeed smaller than the corresponding ones at lower frequency.
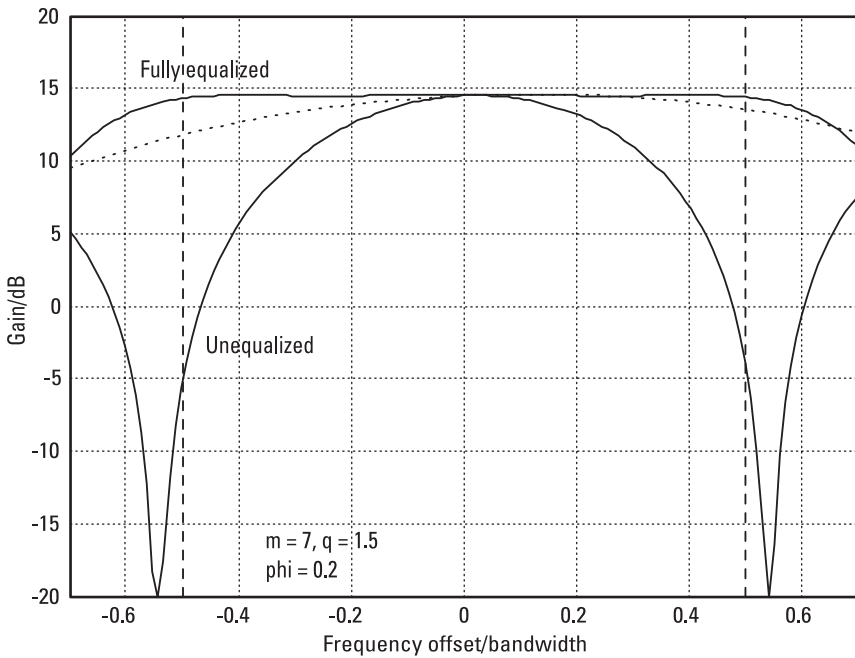
Figure 7.17   Difference beam slope, 20 percent bandwidth.

Finally we show, in Figure 7.16, the equalized slope for the two sets of filter parameters used in Figure 7.15. Figures 7.16(a) and (b) show the difference between the unequalized and equalized responses. We see that the equalization has been remarkably effective. The equalization using only integral delays gives a considerable improvement, but is still far from adequate. It is slightly better with the higher sampling rate used in Figures 7.16(b). The nearly flat equalized responses are shown amplified in Figures 7.16(c) and (d). In the first case, the total variation is just under a decibel, but with the slightly longer filter and greater sampling rate, it is only about 0.15dB (except at the band edges, where the signal power is falling rapidly).

It should be emphasized that Figures 7.15 and 7.16 are for the case of 100 percent bandwidth—the bandwidth is equal to the center frequency (e.g., 100 to 300 MHz). As pointed out following Figure 7.9, the fractional bandwidth is not very significant, except that, of course, as the actual bandwidth increases the sampling rate rises correspondingly, so that while it may be possible to achieve equalization over remarkable fractional bandwidths in principle, in practice there may be difficulty sampling fast enough (and over-

sampling, while highly desirable, will increase this difficulty). If we consider different bandwidths, we see that the initial equalization problem is different. Figure 7.17 shows the difference beam slope in the case of 20 percent bandwidth (e.g., 180 to 220 MHz). We see that there is less sensitivity (fewer lobes) in the unequalized response, but the equalized result is comparable. If the fractional bandwidth is small enough, (e.g., 1 percent) the unequalized response may be flat enough for equalization not to be necessary, of course, and this is when the narrowband solution is adequate.

7.8   Summary

In this chapter, we have looked at equalization of both linear phase variation (due to delay error) and polynomial amplitude error across the band of interest. In the latter case, we saw that the amplitude response requiring equalization could be expressed as a sum of ramp functions. The equalizing weights that minimize the weighted mean square error across the signal band are found as the solution of a matrix equation, the components of which
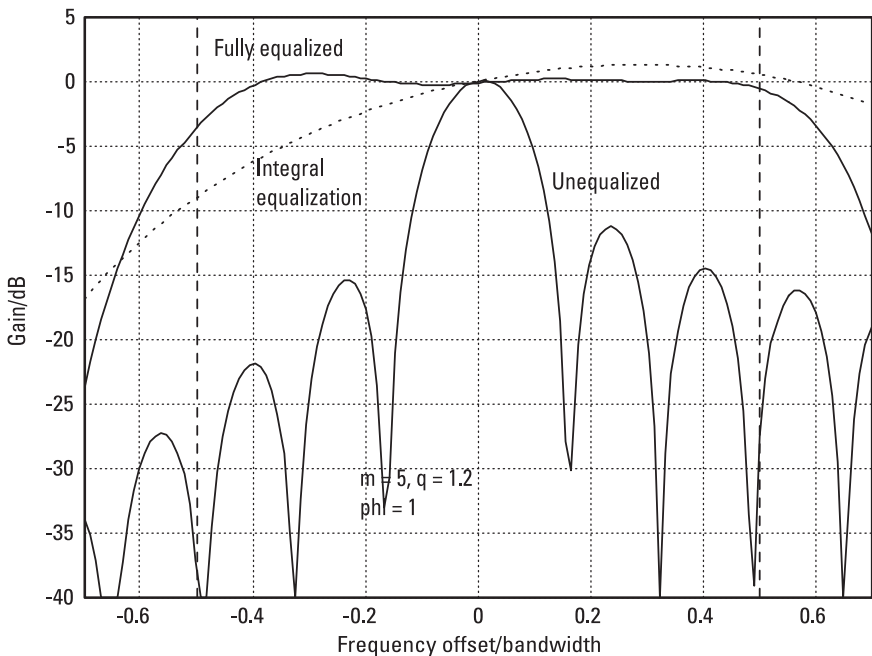
Figure 7.18   Sum beam gain with frequency sensitive elements.

are values of the Fourier transforms of the distorted responses. Thus, for the amplitude distortions, we require the transforms of the ramp functions, and these are found to be derivatives of the sinc function. Including the ramp^r – snc$_r$ pairs in the set of transform pairs we now have the tools for carrying out effective equalization for a range of problems without having to perform explicitly any integration whatever.

After showing that the method is successful in a single channel, including compensating for both amplitude distortion and delay mismatch, the case of forming sum and difference beams using an array was taken. Very effective equalization indeed was found to be possible, and, as shown in the interpolation study of Chapter 5, quite short equalization filters are adequate for high performance, if there is some degree of oversampling. This does not mean sampling at several times the minimum rate but typically at only 20 percent, or 50 percent higher. Only a simple array, of 16 elements in a regular linear configuration, was taken, but the method is general and is also applicable to much larger arrays and arrays of different configurations, such as regular or irregular, planar or volume arrays. Each complex digital channel (whether fed by a single element or a subarray) has a delay and amplitude response that requires equalization, and the process is the same however the elements are distributed.

In the example, the elements were taken to be frequency independent, so the sum beam equalization required only delay compensation. However, for the difference beam slope, it was found that linear amplitude compensation is required as well. If the elements were frequency-sensitive, then the equalization could be made to include this effect as well. We illustrate the case of element amplitude sensitivity (taken to be proportional to frequency at RF) on the sum beam in Figure 7.18. We note higher lobes in the unequalized response at the higher frequencies due to the element responses (and also the similarly asymmetric partially equalized response), but the equalized response is flat to a high degree of accuracy, with only five taps for the delay filters and oversampling at 20 percent.

Finally, we noted that the effectiveness of the equalization is largely independent of actual fractional signal bandwidth (the ratio of the bandwidth to the center frequency), and bandwidths up to 200 percent (from zero to twice the carrier frequency) can be handled, though of course wider signal bandwidths require proportionally higher sampling rates (further raised by oversampling).

8

Array Beamforming

8.1 Introduction

In this chapter, we consider how the rules-and-pairs technique can be applied to relate aperture distributions to antenna beam patterns, particularly for antennas made up of linear arrays of similar elements. Beamforming suggests forming an antenna pattern with a dominant main beam, steered in a direction of interest, and this is indeed an important application. This is achieved by weighting the received (or transmitted) signals so that they sum in phase in the given direction. The weights here are complex phase factors, but amplitude factors can also be used to adjust the pattern, in particular to give low principal sidelobes. The principle of applying complex weights to the array elements can be extended to form other gain patterns, such as a beam covering a wide sector, as shown later. One problem arising with a regular array is that of grating lobes. These (named by close analogy of the antenna array with diffraction gratings) are highly undesirable in several respects. On reception they make the array vulnerable to interference from sources in the lobe direction and cause ambiguity as to the direction of a received signal. On transmission they are a cause of wasted power, reducing the power emitted in the wanted direction and causing interference in other directions.

We start by showing there is a Fourier transform relationship between linear aperture distributions and beam patterns. This relationship holds in general, including for continuous distributions, but we subsequently restrict

our study here to multielement arrays, which are in effect discretely sampled apertures. In the case of uniform, or regular (evenly spaced) linear arrays, the aperture distribution is of the form of a comb function, which has a rep function as its transform. For this kind of array, the rules-and-pairs method works well and is easy to apply to suitable problems. Two sets of examples are given. In one case, a simple beam is required (with further study of variations with low sidelobe patterns), and in the other case a beam covering a sector at a uniform gain level is generated.

   If the array elements are not uniformly distributed, then the convenience of the comb/rep transform is not applicable and a more general least squares error solution is required. As the Fourier transform is a least squares error solution also, this general approach, if applied in the uniform array case, would result in the same solution, if not quite so directly achieved. The general approach still requires Fourier transforms and is presented in Section 8.4. Although we cannot use the Fourier transform of the aperture in the general array case, the transform is still required in determining the components of the matrix and vector used to obtain the weights. The Fourier transform is also useful for general results on the relationship between the weights and the patterns, as shown in Sections 8.2 and 8.3.

   In this chapter we consider only the narrowband case, where the bandwidth is small enough for the effect of delay across the aperture to be adequately approximated as a phase shift at the center frequency of operation. This condition holds for a very wide range of radio and radar problems, but when it does not the equalization methods of Chapter 7 can be applied. We also consider only the case of the linear aperture as, again, this is very widely encountered, and in the form of the uniform linear array (ULA) is particularly suitable for analysis by the rules-and-pairs method. Furthermore, the linear solution is also applicable to regular rectangular *planar* arrays, for which the two-dimensional beam pattern (e.g., in direction cosine coordinates u and v) is simply the product of the two patterns given by the orthogonal linear apertures.

8.2   Basic Principles

Given a linear aperture, the far field signal strength is proportional to the sum across the aperture of the current at each point, which may be weighted by a factor that depends on the position in the aperture and the direction for which the response is to be calculated (Figure 8.1(a)). We consider the signal received in the far field in the direction θ, measured from broadside to the
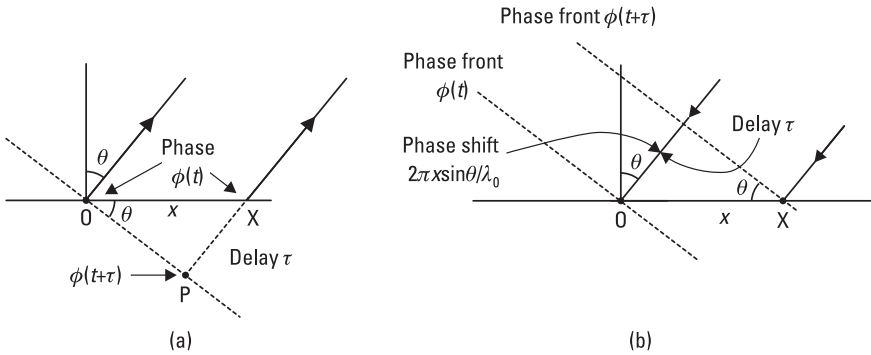
Figure 8.1 Aperture phase shift: (a) on transmission, and (b) on reception.

linear array (initially unweighted). We consider that a signal, phase $\phi(t)$, is applied to the elements of the array, along the line OX. A point in direction θ in the far field sees points on the line OP as equidistant, so in effect the far field response in this direction is given by the sum of signal phases along this line (or any parallel line). The signal at X, with phase $\phi(t)$, is equivalent to a source of phase $\phi(t + \tau)$ at P, as the phase at X is that at P at time τ earlier, where τ is the time taken to travel along PX. We note that $\tau = x\sin\theta/c$, where c is the speed of light and x is the distance of the element X, from the origin. The phase at P for a signal at frequency f_0 is $2\pi f_0(t + \tau) = \phi(t) + 2\pi f_0\tau = \phi(t) + 2\pi x\sin\theta/\lambda_0$, where λ_0 is the wavelength at this frequency (so $f_0\lambda_0 = c$). Thus, the effective contribution from element X differs from that at O by the complex factor $\exp(2\pi ix\sin\theta/\lambda_0)$.

If the signal is weighted across the array by a (complex) amplitude factor $a(x)$, then we see that, summing the contributions along the array, the gain within a scaling factor is

$$g(\theta) = \int_{-\infty}^{\infty} a(x)\exp(2\pi ix\sin\theta/\lambda_0)dx \qquad (8.1)$$

The same considerations apply on reception. In this case, a plane wavefront is received from a distant source, Figure 8.1(b). If the phase at O is $\phi(t)$, the phase of the wavefront at X is given by $\phi(t + \tau)$ as this front reaches O at time τ later. This gives the same phase shift as given earlier, and, with the weighting factor $a(x)$, we have the same expression (8.1) for the gain on reception.

In general a is complex, and in the form of the phase factor $\exp(-2\pi i x \sin\theta/\lambda_0)$ it provides the correct compensation to steer the beam in direction θ (for both transmission and reception). This compensates for the delay at a single frequency. For wideband steering, we need to compensate for the delay, rather than just phase—that is, we need to delay by τ the signal applied at X (or received at X) relative to that at the array origin. In the form of amplitude tapering, with smaller weights toward the edges of the array, it can give lower sidelobes, as shown later in this chapter.

The integral in (8.1) is over the whole domain of x, though with a finite aperture $a(x)$ will be zero outside this finite region. It is convenient to define the array in units of the wavelength of operation, λ_0, so with this convention we replace x/λ_0 with x subsequently in this chapter. If we also define $u = \sin\theta$, as in Section 7.7, then (8.1) becomes (within a scaling factor, which now includes λ_0)

$$g(u) = \int_{-\infty}^{\infty} a(x)\exp(2\pi i x u)dx \qquad (8.2)$$

and we see that g is formally the inverse Fourier transform of the aperture distribution a, and correspondingly the distribution a is the Fourier transform of the pattern g. However, we must treat this with some caution, because, although (8.2) defines values for $g(u)$ when $|u| > 1$, these u values do not correspond to real directions. If we wanted to determine the aperture distribution for a given pattern, and the pattern is defined only for the real angles $-\pi/2 \leq \theta \leq \pi/2$, then we only have the information for the integration over this finite interval for u $(-1 \leq u \leq 1)$. However, if g can be defined as the required function in this range of u, even though the function extends outside this range, then we can integrate over the whole u domain, knowing that the resultant aperture distribution a will give the required pattern over the basic interval. An example is the case of a uniform aperture distribution $a(x) = \text{rect}(x/X)$, where the aperture is given by $-X/2 \leq x \leq X/2$ and the distribution is uniform over this interval. This has the transform $g(u) = X\text{sinc}Xu$, a sinc function response, with first zeros at $\pm 1/X$. This response is curtailed, for the pattern over real angles, at $\pm\pi/2$ radians (i.e., for $u = \pm 1$). However, if we were given that the required pattern over the real angles $(-1 \leq u \leq 1)$ is $\text{sinc}Xu$, by integrating $\text{sinc}Xu$ over the whole range of u $(-\infty < u < \infty)$, we obtain the rect function for the aperture distribution, which gives the wanted pattern in the real angle region.

We should still treat this with caution, however, because we could use the function rect($u/2$)sinc(Xu), which gives the correct response in the real angle region, but transforms to sinc($2x$)⊗rect(x/X), which is not the same weight distribution. Nevertheless, these weights will give the correct pattern in the real angle region.

In the case of an array of identical elements, with their patterns (if not omnidirectional) oriented similarly, we can separate the array response into an array factor, which would be given by using omnidirectional elements, and the element factor, which multiplies the array factor at each angle. The array factor is obtained by summing the contributions from each element with the appropriate phase factor, as in (8.1). For an array of elements, we have a sampled aperture; we can still use the Fourier transform but the aperture distribution is now described by a set of delta-functions. If the array is taken to be a regular linear array, we note that a regular set of delta-functions corresponds to the transform of a periodic function, so we expect the array factor to be periodic in this case. If we do not want the pattern to be periodic in the real angle region, we could make the period such that it has just one cycle in this interval, requiring it to repeat at a period of 2 in u. This will correspond to the element separations being ½ (i.e., half a wavelength), a well-known result for a pattern free from grating lobes, for all steered directions. (It could also have a greater repetition period than 2, but this would require an element separation closer than a half wavelength; however, this is undesirable, increasing mutual coupling and causing driving impedance problems on transmission.) If the main lobe is narrow and is fixed at broadside to the array (at $\theta = 0$), then a repetition period in u of just over 1 could be allowed, corresponding to an element separation of just under one wavelength. (With a period of unity in u, repetitions of the main beam (i.e., grating lobes) will occur at $u = \pm 1$, which lie along the line of the array, and also at higher integral values for u, of course, which are not in real angle space.)

Finally we note that, as $\sin(\pi - \theta) = \sin\theta = u$, if we consider the array factor pattern from $-\pi$ to π radians, or $-180°$ to $+180°$, we see that the pattern from $90°$ to $180°$ is the reflection, about $90°$, of the pattern from $90°$ to $0°$ and similarly on the other side—in other words, the pattern has reflection symmetry about the line of the array. Thus, if a main lobe is produced at angle $\theta_0°$, then there will be an identical lobe at $180°-\theta_0°$ and, in particular, if there is a broadside main beam (at $0°$) there will be a lobe of equal size at $180°$. Later in this chapter, we take the case of reflector-backed elements, which have a $2\sin[(\pi/2)\cos\theta]$ pattern for $-\pi/2 \leq \theta \leq \pi/2$ and a response of zero for $\pi/2 \leq |\theta| \leq \pi$, and this removes the unwanted response in the back direction.

8.3 Uniform Linear Arrays

8.3.1 Directional Beams

Initially we consider a uniform weighting over the aperture of width X. If the element separation is d wavelengths, then the aperture distribution function is given by

$$a(x) = \text{comb}_d\,[\text{rect}(x/X)] \tag{8.3}$$

and the beam pattern is (from P3b, R5, and R8b)

$$g(u) = (X/d)\text{rep}_{1/d}[\text{sinc}(Xu)] \tag{8.4}$$

If we want the beam to be steered in some direction u_1, then we require the pattern shape to be of the form $\text{sinc}(X(u - u_1))$ instead of $\text{sinc}(Xu)$; this will place the peak of the sinc function at u_1 rather than at zero. Transforming back to the aperture domain (using R6a), we see that this requires the distribution to be

$$a(x) = \text{comb}_d[\text{rect}(x/X)\exp(-2\pi i u_1 x)] \tag{8.5}$$

We see we need to put an appropriate phase slope across the aperture to steer the beam (i.e., to offset it in the angle domain). If, on the other hand, we offset the array in the aperture domain, so that the distribution is given by $a(x) = \text{comb}_d(\text{rect}((x - x_1)/X))$, then (by R6b) the pattern is

$$g(u) = (X/d)\text{rep}_{1/d}[\text{sinc}(Xu)\exp(2\pi i u x_1)] \tag{8.6}$$

and there is a phase slope with angle across the pattern. This will have little significance in practice, as there is normally no reason to combine or compare signals received at different points in the far field. This result can be used to help equalize the power levels across the elements of a transmitting array, as outlined at the end of Section 8.3.3.

The distinction between the patterns in the u domain and in the real angle domain is illustrated in Figure 8.2. An array of 16 elements was taken with an element spacing of 2/3 wavelengths, which gives a repetition period for the pattern of 1.5 in u. This is shown (in decibel form) in Figure 8.2(a), and this pattern is described by (8.4), repeating as expected, even though values of u outside the interval $[-1,1]$ do not correspond to real angles. The vertical
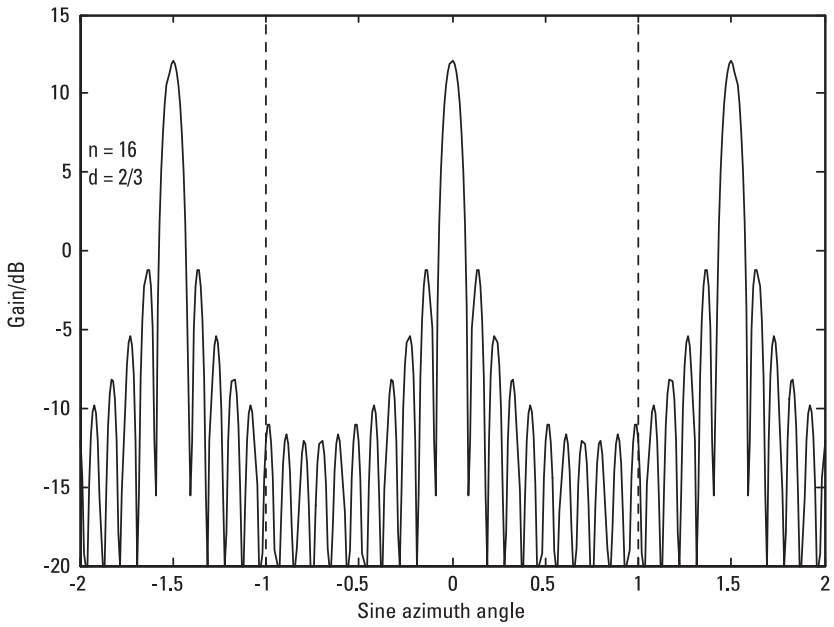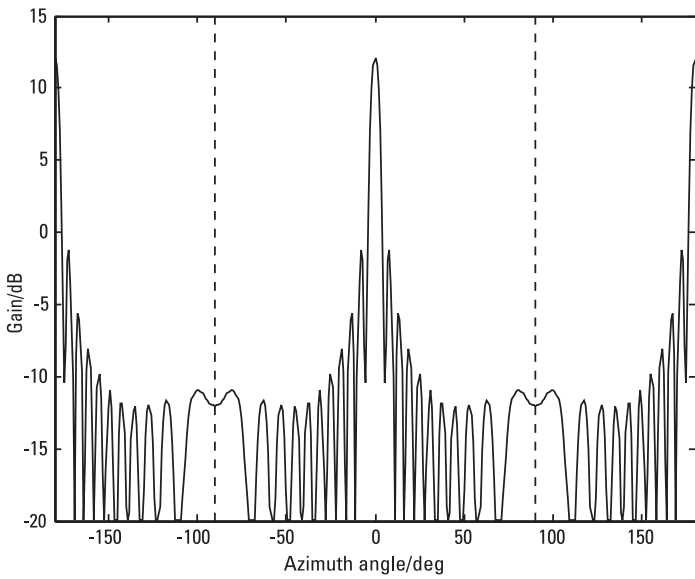
Figure 8.2 Beam patterns for a uniform linear array. (a) Broadside beam, *u*-space,
(b) broadside beam, angle space, (c) beam at 60 degrees, *u*-space, and
(d) beam at 60 degrees, angle space.
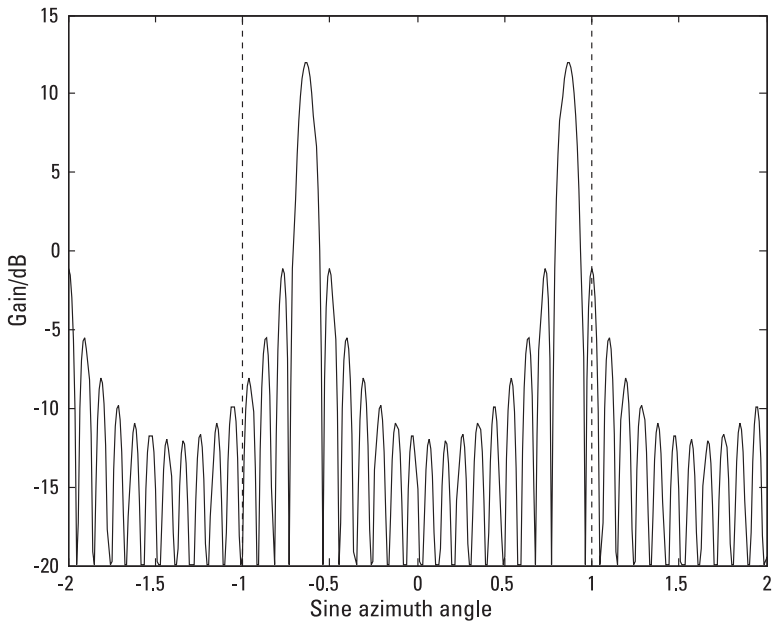
(c)
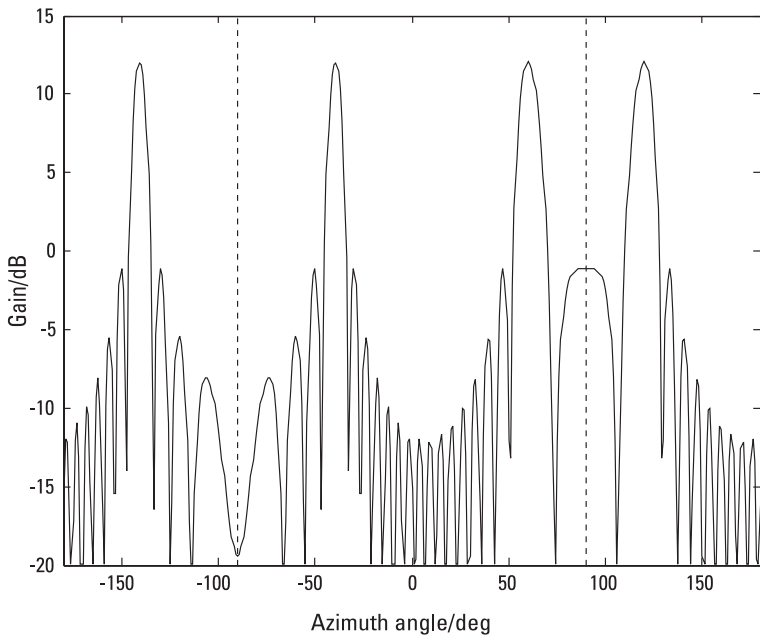
(d)

Figure 8.2   Continued

lines show the segment of the u pattern that corresponds to real angles. In Figure 8.2(c), the beam has been steered to 60° ($u = 0.866$), and we see that the pattern has moved along so that a second beam, a grating lobe, lies within this interval. Figures 8.2(b) and (d) show the corresponding real beams plotted over the full 360° interval. These show two significant differences—the stretching of the pattern toward the ±90° directions with the lobes becoming wider, and the reflection of the pattern about these directions. If the patterns in u-space and angle space are g_u and g_θ, then the gain in direction θ is given by $g_\theta(\theta) = g_u(\sin\theta)$.

In plotting this curve, (8.4) was not used, as that would require summing a large number of sinc functions—in principle, an infinite number. We can describe the aperture distribution given in (8.3) alternatively by

$$a(x) = \sum_{k=-(n-1/2)}^{(n-1)/2} \delta(x - kd) \tag{8.7}$$

where n is the number of elements in the aperture X (and is such that $(n-1)d \leq X < nd$). This has the inverse transform, from P1a and R6b,

$$g(u) = \sum_{k=-(n-1/2)}^{(n-1)/2} \exp(2\pi i k d u) \tag{8.8}$$

and this finite sum is much easier to evaluate. However, the form given in (8.4) is still useful, making much more explicit the periodic form of the pattern in the u domain.

8.3.2 Low Sidelobe Patterns

In Sections 3.2, 3.3, and 3.6, the spectrum of a pulse was shown to improve, in the sense of producing lower sidelobes and concentrating the spectral energy in the main lobe, by reducing the discontinuities (in amplitude and slope) at the edges of the pulse. The same principle is applicable for improving antenna patterns, by shaping (or *weighting*, *tapering*, or *shading*) the aperture distribution in the same way—in fact, if the aperture distributions are given by the pulse shapes of Chapter 3, the beam patterns (in u-space) will be the same as the pulse spectra, as the same Fourier relationship holds. (Strictly speaking, for the pulse spectra the forward Fourier transform is required,
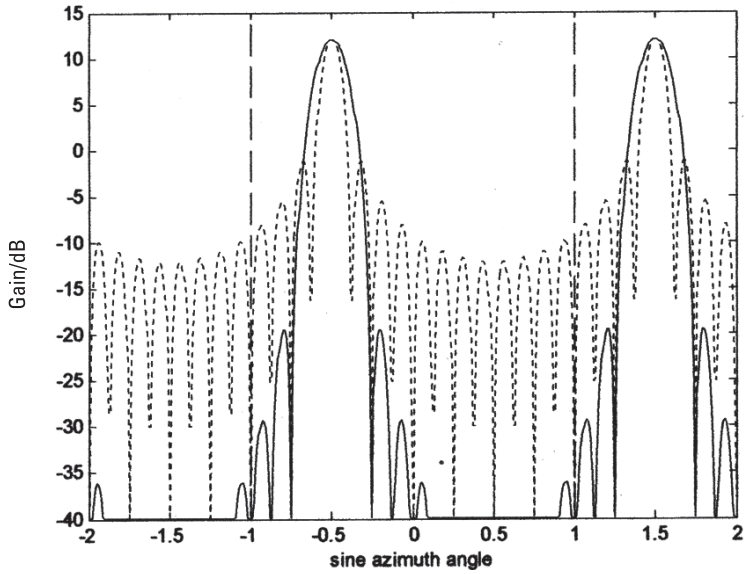
(a)
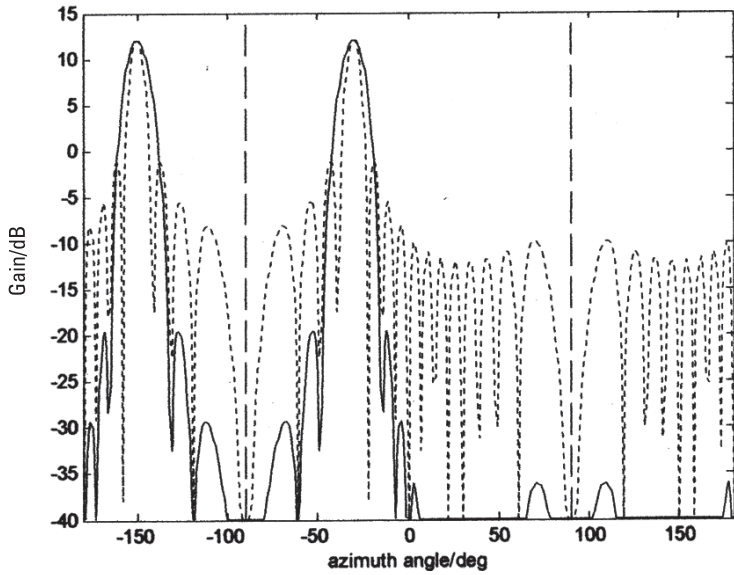
(b)

Figure 8.3   Beam patterns for uniform linear array with raised cosine shading. (a) *u*-space, and (b) angle space.

while for the beam patterns on reception it is the inverse transform. However, for the frequently encountered case of symmetric distribution functions, there is no distinction.) This is actually the case for continuous apertures, but in the case of a regular linear array, corresponding to a sampled aperture, the pattern is repetitive and is given (over the fundamental interval $-1 \le u \le 1$) by the sum of repeated versions of the continuous aperture pattern (as in (8.4) and (8.6), for the rectangular distribution). For a reasonably narrow beam, particularly one with low sidelobes, the effects of the overlaps will be very small, and often negligible. Figure 8.3 shows array patterns for a regular linear array, again of 16 elements, for both the unweighted case (rectangular aperture weighting, dotted line) and with raised cosine weighting (solid line). The effect of overlap of the low sidelobe waveforms is clearly negligible in this case. Thus, in this section, we ignore the repetitive response given by a discrete aperture (an array) and explore the possibilities of obtaining low sidelobe patterns as if from a continuous aperture.

In the raised cosine case, the aperture distribution is given by rect(x/X)(1+cos$2\pi x/X$) with transform (as in Section 3.6, with $X = 1/U$ replacing $2T = 1/f_0$ and omitting the scaling factor) sinc(u/U) + ½sinc [($u–U$)/U] + ½sinc[($u+U$)/U]. The figure shows both the response in u-space and with angle, as in Figure 8.2, but in this case the element spacing is 0.5 wavelengths, so the repetition interval in u is 2, as seen in Figure 8.3(a), and the beam direction is –30°. The weighting has been very effective in reducing the sidelobe levels, though at the cost of broadening the main lobe.

Clearly we could apply different weighting functions, obtaining the corresponding beam patterns, given by their Fourier transforms, but this would be simply going over the ground of Chapter 3, where pulses of various shapes and their spectra were studied. Instead, we look at two other possibilities for improving the pattern, not necessarily for practical application but as illustrations of approaches to problems of this kind that could be of interest. First, we note that the main lobe in Figure 8.3 consists of the sum of the main sinc function with two half amplitude sinc functions, offset on each side by one natural beamwidth (the reciprocal aperture; this is actually the beamwidth at 4 dB below the peak). This suggests continuing to use sinc functions to obtain further improvement. We could reduce the largest sidelobes, near ±2.5 beamwidth intervals by placing sinc functions of opposite sign at these positions. This will have to be done quite accurately because these sidelobes are already at about –31 dB below the peak, or at a relative amplitude of 0.028 so an amplitude error of 1 percent, for example, would not give much improvement. To find the position of these peaks, we can use Newton's method for obtaining the zeros of a function. In this case, the function is the *slope* of the pattern, as we want the position of the peak of a lobe

rather than a null. In this discussion, we neglect the overlapping of the repeated functions on the basis that, for an aperture of moderate size (such as that of this 16-element array, which is effectively eight wavelengths), the effect of overlap is small, especially in the low sidelobe case—in fact, by dropping the rep function we are studying the pattern of the continuous aperture. In addition, we plot the pattern in units of the beamwidth U, as this simply acts as a scaling factor (in u-space).

Differentiating the previous expression for the beam shape $g(u)$ to obtain its slope $g'(u)$ we have

$$g'(u) = (\pi/U)(\text{snc}_1(u/U) + \tfrac{1}{2}\text{snc}_1[(u - U)/U] + \tfrac{1}{2}\text{snc}_1[(u + U)/U]) \quad (8.9)$$

where πsnc_1 is the derivative of the sinc function, as defined in Section 7.3 (see (7.17)). Using Newton's approximation method to find the peak of a lobe (a point of zero slope) we have

$$u_{r+1} = u_r - g'(u_r)/g''(u_r) \quad (8.10)$$

and if we put $v = u/U$, to give the pattern in terms of natural beam widths, then this becomes

$$v_{r+1} = v_r - (1/U)g'(Uv_r)/g''(Uv_r). \quad (8.11)$$

Here u_r and v_r are the approximations after r iterations. Putting in g' from (8.9) and g'' from another differentiation of (8.9), we obtain

$$v_{r+1} = v_r - \frac{2\,\text{snc}_1(v_r) + \text{snc}_1(v_r - 1) + \text{snc}_1(v_r + 1)}{\pi(2\,\text{snc}_2(v_r) + \text{snc}_2(v_r - 1) + \text{snc}_2(v_r + 1))} \quad (8.12)$$

Starting with $v_0 = 2.5$, this converges rapidly (v_4 is equal to v_3 to 4 decimal places) to give a value of -0.0267 at $v = 2.3619$. Adding sinc functions to cancel the lobes near ± 2.5 the pattern in v is now

$$g(v) = \text{sinc}(v) + \tfrac{1}{2}[\text{sinc}(v - 1) + \text{sinc}(v + 1)] + 0.0267[\text{sinc}(v - 2.362) + \text{sinc}(v + 2.362)] \quad (8.13)$$

This pattern is shown in Figure 8.4, with the raised cosine shaded pattern for comparison (dotted curve). We see that the original first sidelobes have been removed and the new largest sidelobes are at almost -40 dB, an improvement of nearly 10 dB. To find the weighting function that gives this
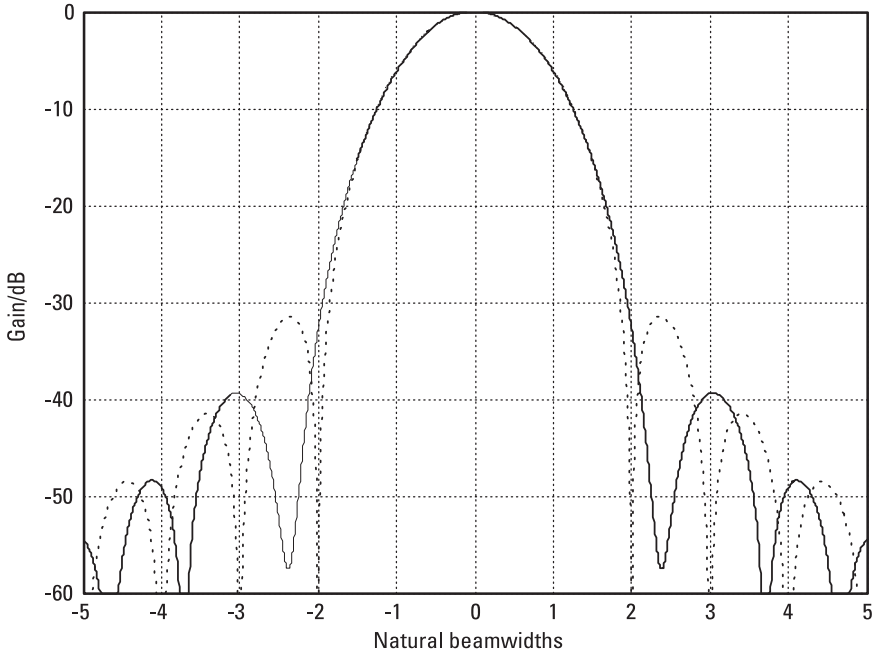
Figure 8.4 Beam pattern for ULA with additional shading.

pattern, we require the Fourier transform of (8.13). This can be seen almost by inspection, following, in reverse direction, the route that gave the raised cosine transform. More formally, we have

$$g(v) = \text{sinc}(v) \otimes \{\delta(v) + \tfrac{1}{2}[\delta(v-1) + \delta(v+1)] + 0.0267[\delta(v-2.362) + \delta(v+2.362)]\}, \tag{8.14}$$

giving, on Fourier transforming,

$$a(y) = \text{rect}(y)\{1 + \tfrac{1}{2}[\exp(2\pi iy) + \exp(-2\pi iy)] + 0.0267[\exp(2\pi i2.362y) + \exp(-2\pi i2.362y)] = \text{rect}(y)\{1 + \cos(2\pi y) + 0.0534\cos(4.724\pi y)\} \tag{8.15}$$

As we started with the normalized variable $v = u/U$, this distribution is in terms of the normalized aperture $y = x/X$.

Clearly this could be generalized, so that if we put for the pattern

$$g(v) = \text{sinc}\, v \otimes \left\{ \delta(v) + \sum_k \alpha_k (\delta(v - \beta_k) + \delta(v + \beta_k)) \right\}$$

then the weights are given by

$$a(y) = \text{rect } y \left(1 + 2\sum_k \alpha_k \cos(2\pi\beta_k y) \right)$$

For the second example, we produce a pattern with the closest sidelobes to the main beam (and the largest) all at almost the same level, similar to the pattern given by Taylor weighting. In this case we take the pattern to be given by a sum of sinc functions at 0, ±1, ±2, . . . ±m natural beamwidths (reciprocal aperture units) from the center. In this case, we do not take the amplitudes of the sinc functions at ±1 to be 0.5. Thus, we have, again using a normalized u-space variable,

$$g(v) = \text{sinc}(v) + a_1[\text{sinc}(v-1) + \text{sinc}(v+1)]$$
$$+ a_2[\text{sinc}(v-2) + \text{sinc}(v+2)] + \dots$$
$$+ a_m[\text{sinc}(v-m) + \text{sinc}(v+m)] \qquad (8.16)$$

The m coefficients are determined by setting the gain to particular values at m points, in the form $g(v_r) = g_r$. The values we choose are the constant level A, or $-A$, at the sidelobe peaks, where $20\log_{10}(A)$ is the required peak level in decibels. We do not know exactly where these peaks are, but we should be near the peak positions if we choose the points to be midway between the nulls in the sinc patterns; thus, we have

$$g(r + 1.5) = (-1)^{r+1}A. \qquad (r = 1 \text{ to } m) \qquad (8.17)$$

(The factor $(-1)^{r+1}$ is required as the amplitudes of the sidelobe peak magnitudes alternate in sign.) The set of m equations given by putting the conditions of (8.17) into (8.16) leads to the vector equation $\mathbf{Ba} = \mathbf{b}$, with solution

$$\mathbf{a} = \mathbf{B}^{-1}\mathbf{b} \qquad (8.18)$$

where $\mathbf{a}$ contains the required coefficients, the components of $\mathbf{b}$ are given by

$$b_j = (-1)^{j+1}A - \text{sinc}(j + 1.5) \qquad (8.19)$$

and the components of $\mathbf{B}$ by

$$B_{jk} = \text{sinc}(j - k + 1.5) + \text{sinc}(j + k + 1.5) \qquad (8.20)$$
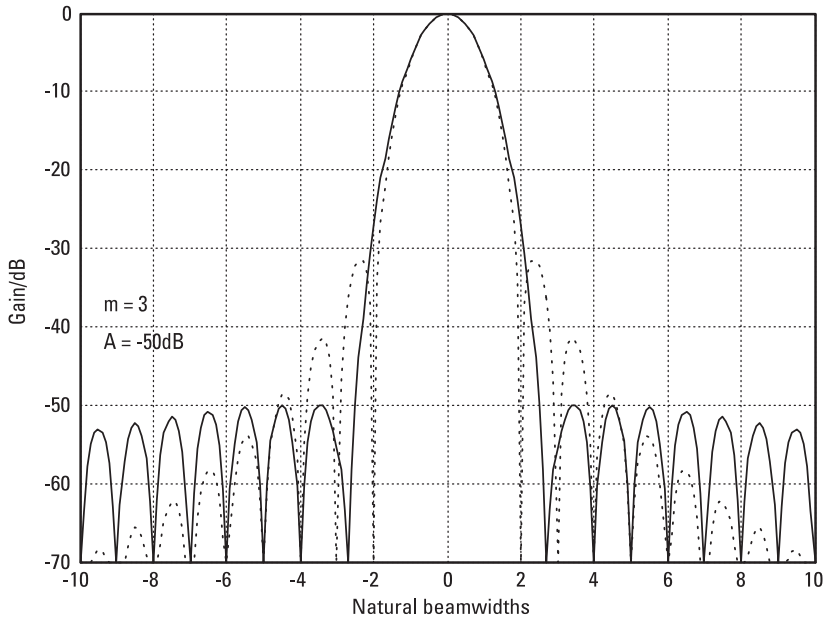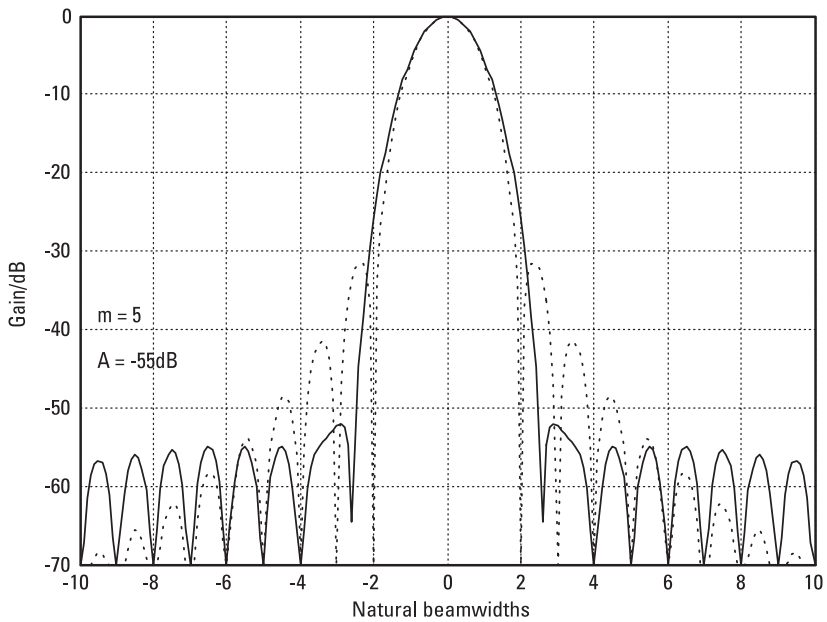
Figure 8.5 Constant level sidelobe patterns. (a) *m* = 3, levels-50 db, and (b) *m* = 5, levels –55 db.

We note that the first points, at ±2.5, are on the edge of the main lobe, rather than the peak of a separate sidelobe, and the value is positive, with subsequent points on (or near) sidelobe peaks and alternating in sign. Two patterns given by (8.16), with coefficients from (8.18), are shown in Figure 8.5, again with the raised cosine pattern for comparison. In Figure 8.5(a) we took $m = 3$ and the required level to be –50 dB. The two nearest-in lobes on each side are seen to be very close to this level—the pattern levels at ±2.5, ±3.5, and ±4.5 are precisely –50 dB, by construction, but the peaks of the lobes will not be at exactly these points, so the actual peaks will rise slightly above the required value. (In fact the third lobe is also very close to the set level, although not included in the constraint.) However, the range of levels for which this works well is limited, and Figure 8.5(b) shows it starting to fail. In this case, $m = 5$ and the nominal level is –55 dB. This is seen to be attained very closely for the lobes at ±4.5, ±5.5, and ±6.5, but the pattern has bulged between ±2.5 and ±3.5, giving a lobe appreciably above the specified level. Nevertheless these are good sidelobe levels and have been obtained quite easily. The pattern is well-behaved when designed for –50-dB sidelobes, but the first sidelobe, near ±2.5, starts to rise when the specified level is about −48 dB or higher. In general, for these patterns the coefficient a_1 is near 0.5, and the other coefficients fall rapidly in magnitude. To find the corresponding weighting function we transform the pattern to obtain

$$a(y) = \text{rect}(y)\{1 + 2a_1\cos(2\pi y) + 2a_2\cos(4\pi y) + \ldots + 2a_m\cos(2m\pi y)\}$$

(8.21)

This is evaluated at the normalized points $y = x/X$, where $x = kd$ and $X = nd$, so $y = k/n$, $k = -(n-1)/2$ to $(n-1)/2$ for the array of n elements.

8.3.3   Sector Beams

We now consider a quite different problem—that of providing a flat, or constant gain, beam for reception or transmission over a sector, generally wide compared with the natural beamwidth. In this case, as we want the sector gain to be constant over an interval (for simplicity we take the amplitude to be unity), it will be of the form $\text{rect}(u/u_0)$, where the width of the sector is u_0 centered on broadside initially. For a uniform linear array, we want a regularly sampled aperture distribution, rather than a continuous one, so we take the required pattern to be repetitive in the u domain and to be given by

$$g(u) = \text{rep}_U(\text{rect}(u/u_0))$$

(8.22)

so the element weights across the aperture are given by

$$a(x) = (u_0/U)\text{comb}_{1/U}\text{sinc}(u_0 x) \tag{8.23}$$

This is a sinc function envelope, with width proportional to $1/u_0$ and sampled at intervals $1/U$ wavelengths, where U is the repetition interval in the u domain. If we take the beam to have an angular width θ_0, then the edges of the beam are at $\pm\theta_0/2$, and the corresponding u_0 value is given by

$$u_0 = 2\sin(\theta_0/2) \tag{8.24}$$

(It is important not to put $u_0 = \sin(\theta_0)$, because of the nonlinear relationship between these variables. For example, if we chose $\theta_0 = 90°$ then the first, correct, expression makes $u_0 = \sqrt{2}$, while the second makes $u_0 = 1$; this would actually give a 60° beam, rather than 90°.)

Figure 8.6(a) shows an example of a sector beam generated this way, with the weights applied to the elements shown in Figure 8.6(b). The aperture distribution is a sampled sinc function and, for perfect patterns, extends in principle over the whole x-axis. In practice it is limited to n elements so is effectively gated by a rect function, $\text{rect}(x/nd)$, where $d = 1/U$ is the separation between elements and nd is the effective aperture. In this case $U = 2$ and d is a half wavelength. The transform of this rect function is a relatively narrow sinc function; this is convolved with the ideal rectangular pattern given by an infinite array to produce the ripple seen in the figures. The figure is for a nominal 50° sector beam (from –25° to 25°) given by an array of 21 elements.

The sidelobe ripples indicate the width of the natural beam from this aperture—the main lobe width, between the first zeros, would be the width of two of these sidelobes. With an even number of elements, the distribution is rather different in appearance, with two equal values in the center but a very similar beam pattern. There is no simple relation between the sidelobe levels and the number of elements (or whether this number is odd or even)—the levels vary with both the number of elements and the beamwidth. Because of the repetitive form of the response in the u domain, these lobes are the result of summing the convolution ripples of mainly two basic patterns, as given by the continuous aperture, at a separation of $U = 1/d$, and these may sometimes reinforce and sometimes tend to cancel (e.g., the lobe at 90° is essentially the sum of contributions from the pattern in u-space centered at 0 and the next repetition of the pattern at 2). The fluctuations with parameter variation of these lobes will tend to be greater as the sector width increases and the edges of the beam and its repetition become closer.
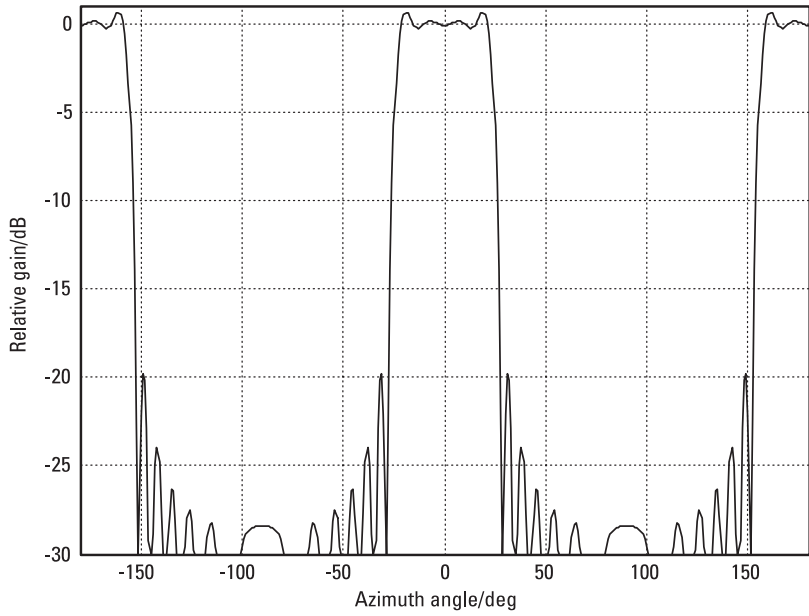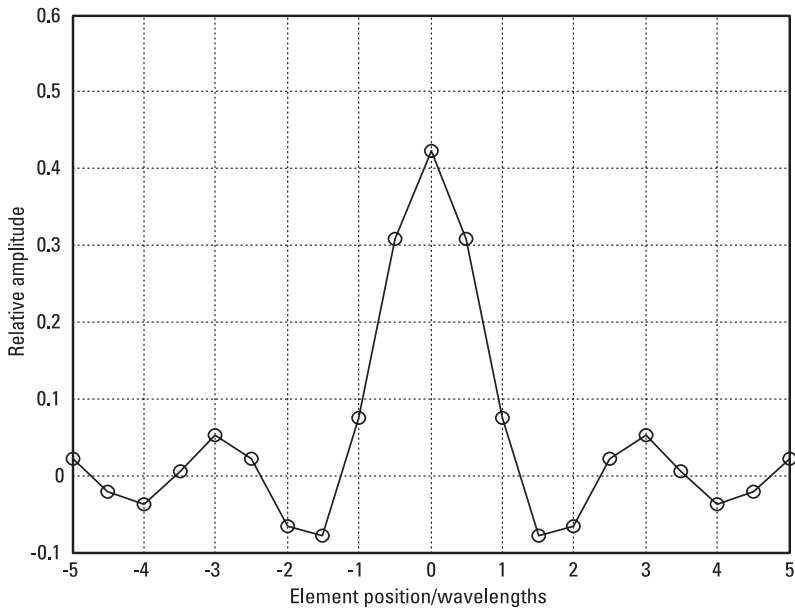
Figure 8.6   Fifty degree sector beam from an array of 12 elements. (a) $m = 3$, levels-50 db, and (b) $m = 5$, levels –55 db.

We also note the appearance of the back lobe in Figure 8.6(a). In many applications, this is undesirable, whether on transmission, when only half the power goes into the forward lobe, or on reception, when interference or external field noise will enter through this lobe. This lobe can be removed by mounting a reflecting plane at a quarter wavelength behind the element (Figure 8.7). Combining the direct signal with the reflected one, effectively arriving at a point a quarter wavelength behind the reflecting plane, and including the phase change of π on reflection at a denser medium, the element response becomes $2\sin((\pi/2)\cos\theta)$ for a signal at angle θ to broadside. That is, $\exp(i(\pi/2)\cos\theta) - \exp(-i(\pi/2)\cos\theta) = 2i\sin((\pi/2)\cos\theta)$; i gives an overall phase shift, not affecting the amplitude response. We have used the fact that a signal path of a quarter wavelength leads to a phase shift of $\pi/2$ radians. This is in the forward half azimuth plane, with no response in the back half plane (for an infinite reflecting plane). This is a pattern with a single broad lobe (Figure 8.7), falling to 3 dB below the peak at $\pm60°$, and increases the directivity of the elements by 6 dB; part of this gain (3 dB) is due to limiting the power to one side of the array and part due to reducing the beam from a 180° semicircle to this 120° lobe. Because this response is so flat, it will make very little difference to the shape of sector beams centered at, or near, broadside, though it will more noticeably distort beams steered toward the edges of the forward sector.

If we want to steer the beam so that its center is at θ_1 and its width is still θ_0, then its edges are at $\theta_a = \theta_1 - \theta_0/2$ and $\theta_b = \theta_1 + \theta_0/2$, and the corresponding u values are $u_a = \sin\theta_a$ and $u_b = \sin\theta_b$. In this case, the center of the beam in u space is at $u_1 = (u_b + u_a)/2$ and its width is $u_0 = u_b - u_a$. With these definitions of u_0 and u_1, the required sector beam pattern is, from (8.22),

$$g(u) = \text{rep}_U[\text{rect}((u - u_1)/u_0] \tag{8.25}$$
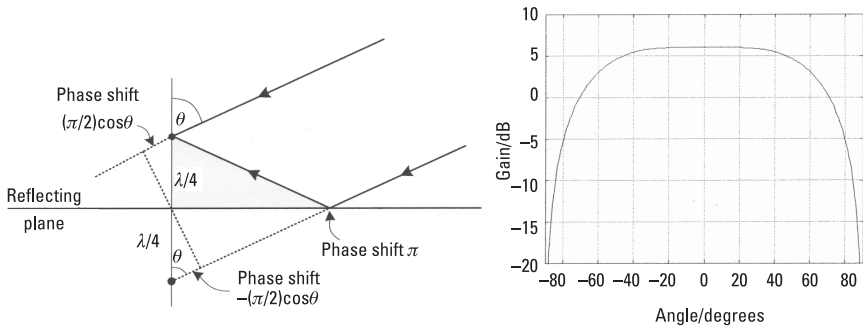
Figure 8.7   Element response with reflector.

This has the (forward) transform (using R6a)

$$a(x) = (u_0/U)\text{comb}_{1/U}[\text{sinc}(u_0 x)\exp(-2\pi i x u_1)] \qquad (8.26)$$

and we see that this requires putting a linear phase slope across the array elements; this corresponds to the effect of the delay across the aperture for a waveform received from (or transmitted to) this direction, causing a phase shift at the carrier frequency, f_0. This requires an infinite aperture (to give a perfectly rectangular pattern); with a finite aperture, of width between nd and $(n + 1)d$, we include a rect function within the comb argument in (8.26). Putting (8.26) in the alternative form of a sum of δ-functions, as in (8.7) (but weighted by $(u_0/U)\text{sinc}(u_0 kd)\exp(-2\pi ikdu_1)$ in this case, with $d = 1/U$), and carrying out the inverse transform gives

$$g(u) = \frac{u_0}{U} \sum_{k=-(n-1)/2}^{(n-1)/2} \text{sinc}(u_0 kd)\exp\big(2\pi i(u - u_1)kd\big) \qquad (8.27)$$

as the alternative to (8.25) for practical evaluation.

Figure 8.8 illustrates a steered sector beam, with a reflector-backed array. In this case the beam is formed from a uniform linear array of 12 elements, at half-wavelength spacing, and is 90° wide, centered at 20°. The response with omnidirectional elements is shown (dotted line) for comparison (except that it would be 6 dB lower, not having the gain of the reflector elements). The reflector removes the back lobe and also distorts the sector beam slightly. The weights are complex, as indicated in (8.26), and, as the pattern is specified to be real, the weight distribution, as the transform of the pattern, has conjugate symmetry, with the real part symmetric and the imaginary part antisymmetric (see Section 2.3).

The sector beams defined so far have the same phase across the sector, so that, when used for transmission, the signal received in the far field will have the same phase at points in all directions at the same distance from the center of the array. If we put a phase slope across the pattern, this will not change the power transmitted in a given direction but will change the weights required. In this case, let the slope be such as to produce a phase difference of r cycles across a unit range of u, where the phase variation is linear in u space. The required pattern, from (8.25), is now

$$g(u) = \text{rep}_U[\text{rect}((u - u_1)/u_0)\exp(2\pi iru)] \qquad (8.28)$$
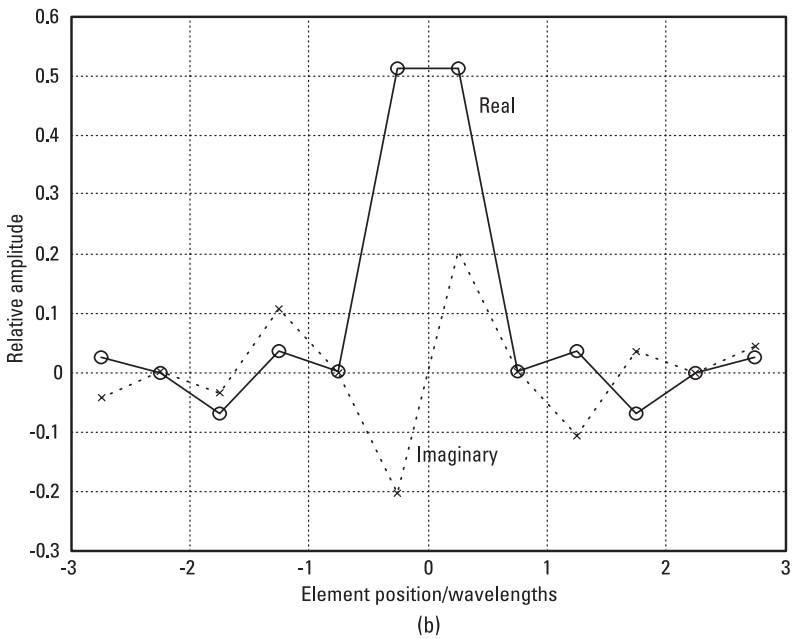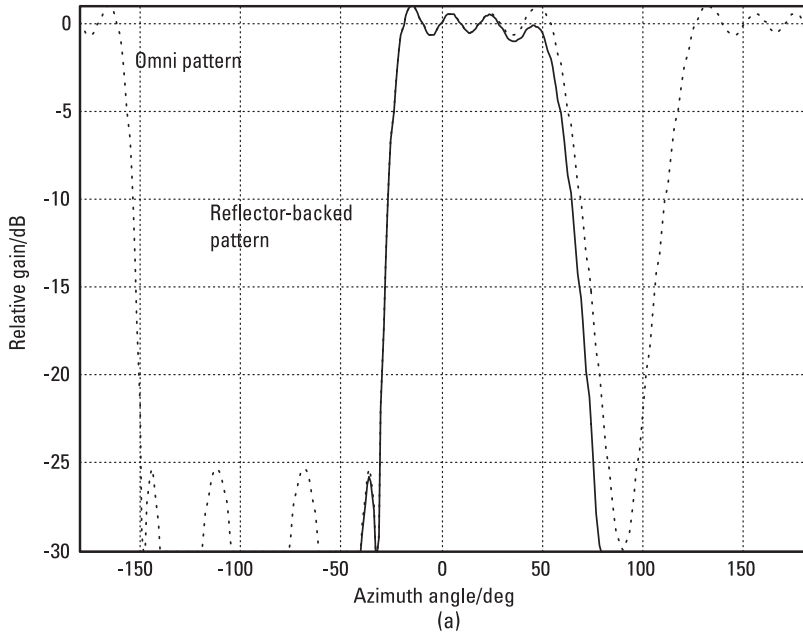
Figure 8.8 Steered sector beam with 12 reflector-backed elements. (a) Beam patterns, and (b) element weights.

and the weight function, given by the Fourier transform of (8.28), is

$$a(x) = (u_0/U)\mathrm{comb}_{1/U}[\mathrm{sinc}(u_0 x)\exp(-2\pi i x u_1)\otimes\delta(x-r)]$$

$$= (u_0/U)\mathrm{comb}_{1/U}[\mathrm{sinc}(u_0(x-r))\exp(-2\pi i(x-r)u_1)] \qquad (8.29)$$

We see that the envelope of the set of δ-functions from the comb function, which defines the weights on the elements, is shifted by r wavelengths with this linear phase slope.

Figure 8.9(a) shows the array factor for a 60° sector beam from an array of 20 elements at half-wavelength spacing, steered to broadside. The beam also has a phase slope of one cycle per unit of u (i.e., $r = 1$), and this requires the sampled sinc function distribution for the weights to be displaced one wavelength from the center of the array, as seen in Figure 8.9(b). As $u = \pm\frac{1}{2}$ at $\pm30°$, the phase variation should be 360° across this interval, and this is seen in Figure 8.9(c), which shows the phase relative to that at the center of the beam. The slope varies
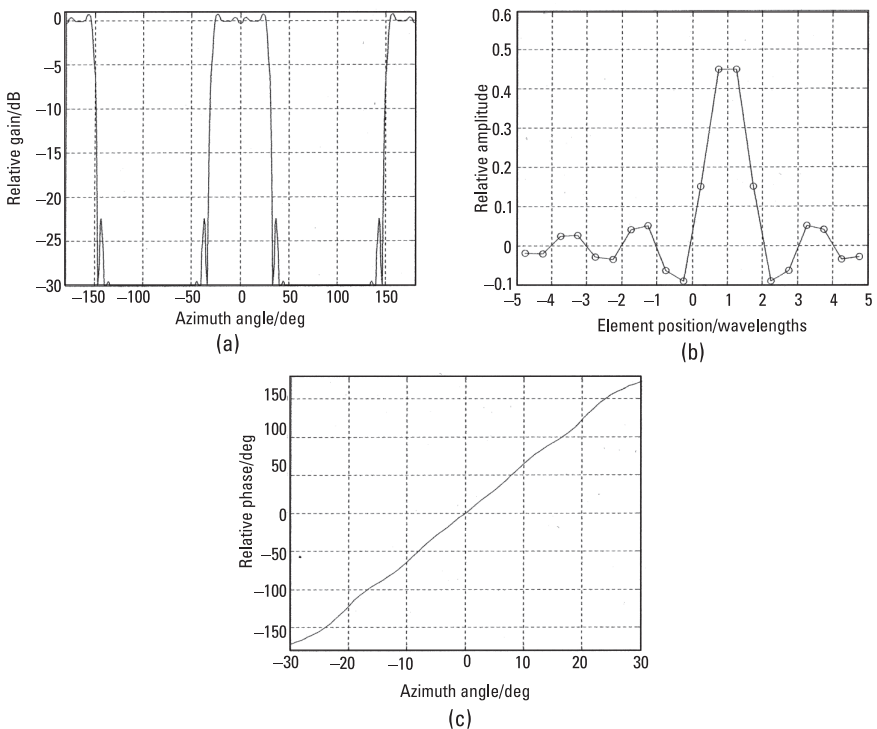
Figure 8.9   Sector beam with phase variation across beam. (a) Beam pattern, (b) element weights, and (c) relative phase.

slightly (because of the finite aperture effect, which causes the amplitude ripples, and the stretching of the pattern in angle space, at higher angle values, compared with u space), but is close to the set value.

By splitting the sector into two or more subsectors with linear phase slopes, and so with offset peak amplitude values, as in Figure 8.9(b), it is possible to generate beams with more uniform weight magnitudes, which is desirable for transmitting arrays, with similar power amplifiers on each element. The subsectors are given different phase slopes so that the peak weights for these sectors are at different points on the array. Even for a beam centered at broadside (normally with real weights), there will be phase variation between elements, as the centers of the sectors will be steered off broadside in general, requiring phase shifts. However, there may be some beam shape degradation and difficulty in balancing flatness of the weight magnitudes and the quality of the sector beam.

8.4 Nonuniform Linear Arrays

8.4.1 Prescribed Patterns from Nonuniform Linear Arrays

We have seen in (8.2) that the beam pattern, in u space, is the inverse Fourier transform of the aperture distribution, and we can use the rules-and-pairs technique for a useful range of distributions for continuous apertures and, as demonstrated in Section 8.3, for regularly sampled apertures corresponding to uniform linear arrays. In this case, the regularly sampled aperture is represented as a comb function, for which the transform is known (Rule 8b). However for nonuniform sampling, no general rule is available and a different approach is required. In this case, given a desired beam shape and a set of element positions, the problem tackled is to find the weights to be applied to each element to match the desired pattern in a least squared error sense. This problem is very similar to those of Sections 6.3 and 7.2. By pattern, we mean here the array factor, taking the case of similar gain elements, oriented in parallel, so the actual array pattern is the product in each direction of the array factor and the element response. For omnidirectional elements, of course, the array factor gives the overall pattern (within a scaling factor).

For a linear array, the aperture distribution is of the form

$$a(x) = \sum_{r=1}^{n} a_r \delta(x - x_r)$$

where the n elements are at positions x_r, with weights a_r. The gain pattern (in u space) is given by the transform of this:

$$g(u) = \sum_{r=1}^{n} a_r \exp(2\pi i x_r u) \qquad (8.30)$$

Now let $g(u)$ be a desired beam pattern, not necessarily exactly realizable by any linear combination of the n complex exponentials in (8.30). We now want to find the set of n coefficients a_r, which gives a least squared error fit to $g(u)$. Let the error at point u be $e(u)$, and defining $f_r(u) = \exp(-2\pi i x_r u)$, we have

$$e(u) = g(u) - \sum_{r=1}^{n} a_r \exp(2\pi i x_r u) = g(u) - \sum_{r=1}^{n} a_r f_r{}^*(u) = g(u) - \mathbf{f}(u)^H \mathbf{a}$$

$$(8.31)$$

where $\mathbf{a}$ and $\mathbf{f}$ are n-vectors with components a_r and f_r (and the suffix H indicates complex conjugate transpose). The square modulus of e is

$$|e(u)|^2 = |g(u)|^2 - \mathbf{f}(u)^H \mathbf{a} g(u)* - g(u)\mathbf{a}^H\mathbf{f}(u) + \mathbf{a}^H\mathbf{f}(u)\mathbf{f}(u)^H\mathbf{a} \quad (8.32)$$

We have used $(\mathbf{f}^H\mathbf{a})^* = \sum_k f_k a_k{}^* = \mathbf{a}^H\mathbf{f}$. The total squared error as a function of the weights $\varepsilon(\mathbf{a})$ is given by the integral of $|e(u)|^2$ over the interval I in u over which we want the specified response. In some cases, this will be the whole real angle region, from $u = -1$ to $u = +1$, but this need not necessarily be the case. The integrated error, as a function of the vector $\mathbf{a}$ is thus $\varepsilon(\mathbf{a})$, given by

$$\varepsilon(\mathbf{a}) = \int_I |e(u)|^2 \, du = p - \mathbf{b}^H\mathbf{a} - \mathbf{a}^H\mathbf{b} + \mathbf{a}^H\mathbf{B}\mathbf{a} \qquad (8.33)$$

where $p = \int_I |g(u)|^2 \, du$, and the components of $\mathbf{b}$ and $\mathbf{B}$ are given by

$$b_r = \int_I f_r(u)g(u)du = \int_I \exp(-2\pi i x_r u)g(u)du$$

$$B_{rs} = \int_I f_r(u)f_s(u)^* \, du = \int_I \exp(-2\pi i(x_r - x_s)u)du. \qquad (8.34)$$

The value of **a** that minimizes ε (or more generally gives a stationary point of ε) $\mathbf{a}_0$ is given by $\partial\varepsilon/\partial\mathbf{a}^* = \mathbf{0}$ or, from (8.33), $-\mathbf{b} + \mathbf{B}\mathbf{a}_0 = \mathbf{0}$, so that

$$\mathbf{a}_0 = \mathbf{B}^{-1}\mathbf{b} \qquad (8.35)$$

This gives the set of weights for the functions $\{f_r\}$, which gives the best fit in a least squares sense to the required pattern function g, over the interval I, where the components of **b** and **B** are given in (8.34). We see that these components are of the form of (forward) Fourier transforms: if g is within the interval I then the components of **b** are given by the Fourier transform of g, evaluated at x_r. If I is put in the form of a rect function, then the components of **B** are given by the corresponding sinc function, evaluated at $(x_r - x_s)$.

8.4.2 Sector Beams from a Nonuniform Linear Array

Taking first the case of forming a sector beam from a regular array, let the element separation be d and so $1/d$ is the pattern repetition interval, U, in the u domain. Then it seems a natural choice of I to take the interval $[-U/2, U/2]$ (i.e., one repetition period), centered at $u = 0$ (broadside), which is equivalent to including the factor rect(u/U) in the integrands in (8.34). In this case B_{rs} is the Fourier transform of rect(u/U) evaluated at $(x_r - x_s)$ (i.e., Usinc$((x_r - x_s)U)$). However, as $x_r - x_s$ is an integer times d and $dU = 1$, then the sinc factor is zero except when $x_r = x_s$ so that $B_{rs} = U\delta_{rs}$ and $\mathbf{B} = U\mathbf{I}$. For the sector beam, width u_0, centered at u_1, $g(u) = $ rect$((u - u_1)/u_0)$, and as this is taken to be within rect(u/U), the product is still $g(u)$. Then b_r is the Fourier transform of $g(u)$ evaluated at x_r, and we find that the weights a_r given by (8.34) and (8.35) in this case are exactly the same as given by (8.26), rather more directly, confirming the point that the Fourier transform solution is also the least squared error solution.

The solution given by (8.34) and (8.35) is more general than that of (8.23), which is for the regular array, so that a solution can be found for the weights of an irregular linear array giving a close approximation to a given required pattern. Figure 8.10 shows a sector pattern obtained from an irregular array. For this plot, the array elements were displaced from their regular positions, with separation d wavelengths, by a pseudo-random step chosen within an interval of width $d - 0.5$, which ensures that the elements are at least half a wavelength apart. Figure 8.10(a) shows the response in u space for an array of 21 elements at an average spacing d of 2/3. A sector beam of width 40° centered at broadside was specified. A regular array would have a pattern
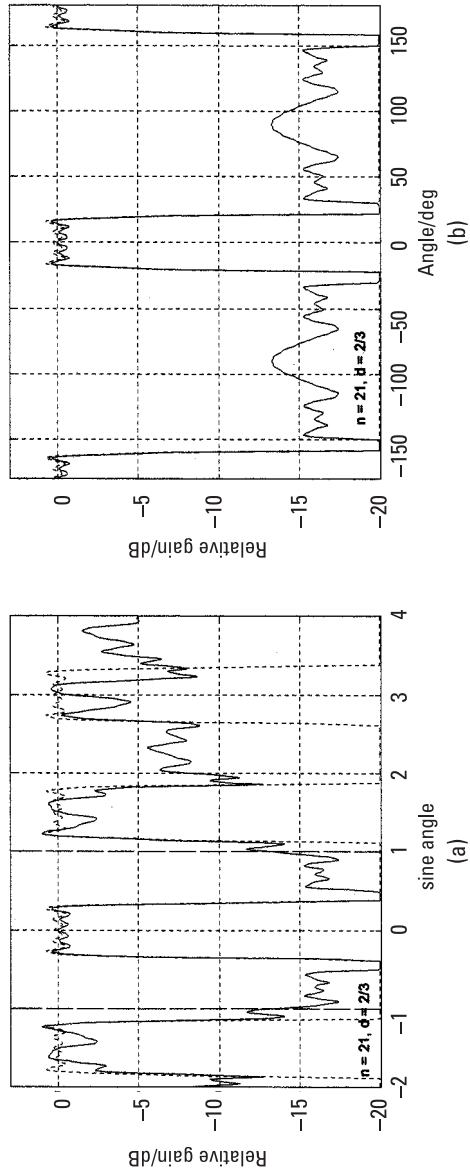
Figure 8.10   Sector pattern from an irregular linear array. (a) Response in u-space, a nd (b) beam pattern.

strictly repetitive at an interval of 1.5 in u (equal to $1/d$), and this is shown by the dotted response. The irregular array "repetitions" are seen to degrade rapidly, but the pattern that matters is that lying in the interval $[-1,1]$ in u. This part of the response leads to the actual pattern in real space, shown in Figure 8.10(b). We note that the sidelobes are up to about -13 dB, much poorer than for the patterns from regular arrays shown in Figures 8.6, 8.8, and 8.9, though this level varies considerably with the actual set of element positions chosen. The integration interval I was chosen to be $[-1,1]$, to give the least squared error solution over the full angle range (from $-90°$ to $+90°$ and its reflection about the line of the array). This is equivalent to including $\text{rect}(u/2)$ in the integrands in (8.34). This, again, makes no difference to the components of **b** (as $g(u)$ is within this rect function), but for the components of **B** it gives values $B_{rs} = 2\text{sinc}2(x_r - x_s))$. This compares with the case of taking one period of u, where the rect function is of width U so we include $\text{rect}(u/U)$ and obtain $B_{rs} = U\text{sinc}U(x_r - x_s)$.

A second example is given in Figure 8.11 for an array of 51 elements but illustrating the effect of steering. In this figure, the 40° sector beam is steered to 10°, and again we see the rapid deterioration of the approximate repetitions in u space of the beam and a nonsymmetric sidelobe pattern, though the levels are roughly comparable with those of the first array. The average separation is 0.625 wavelengths, giving a repetition interval of 1.6 in u. If we steer the beam to 30° (Figure 8.12, using the same array), there is a marked deterioration in the beam quality. This is because part of one of the repetitions falls within the interval I over which the pattern error is minimized, so the part of this beam (centered near $u = -1$) that should be zero in the required pattern is reduced. At the same time, the corresponding part of the wanted beam (centered at $u = \frac{1}{2}$, for the steering direction of 30°) should be unity, so the solution tries to hold this level up. We note that the levels end up close to -6 dB, which corresponds to an amplitude of 0.5, showing that the error has been equalized between these two requirements. We note, from the dotted responses, that the result would be much the same using a regular array (where the repetitions are identical).

In fact this problem would be avoided by choosing I to be of width 1.6 (the repetition interval) instead of 2, preserving the quality of the sector beam. Also, if we center I at u_1, the center of the sector, then we ensure that the full sector is within the interval I. Thus, we include a factor $\text{rect}((u - u_1)/U)$ in the integrals, with $U = 1/d = 1.6$ in this case. Again the integral for the components b_r is unaffected, but the components B_{rs} will now be given by the transform of this rect function, $U\text{sinc}(x/U)\exp(-2\pi i u_1 x)$ evaluated at $(x_r - x_s)$. The result is shown in Figure 8.13 (for the same array), showing that the
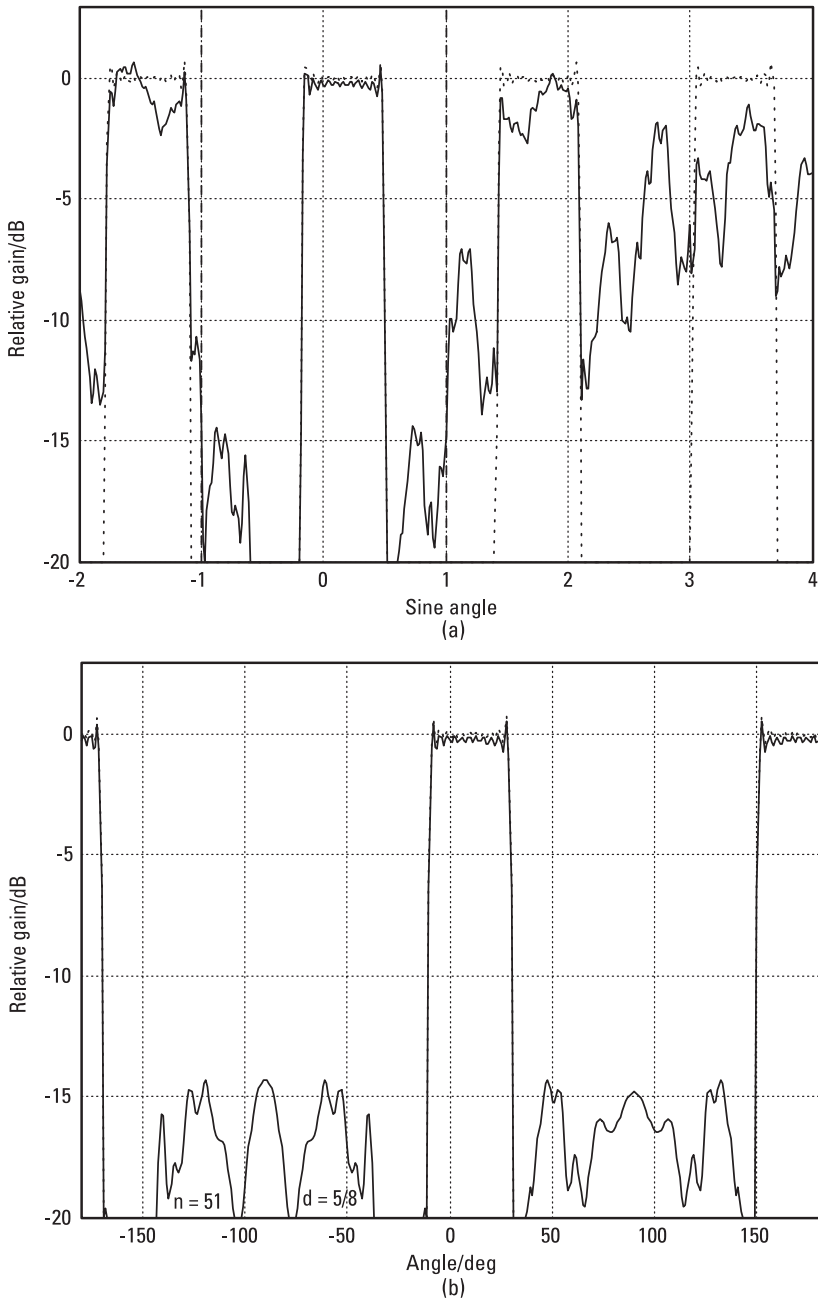
Figure 8.11   Sector pattern from an irregular linear array, beam at 10°. (a) Response in
u-space, and (b) beam pattern.
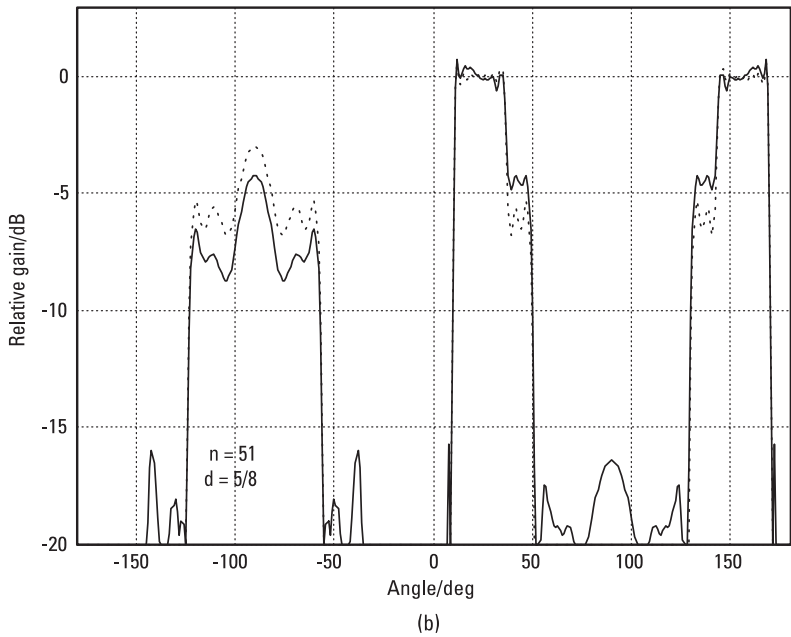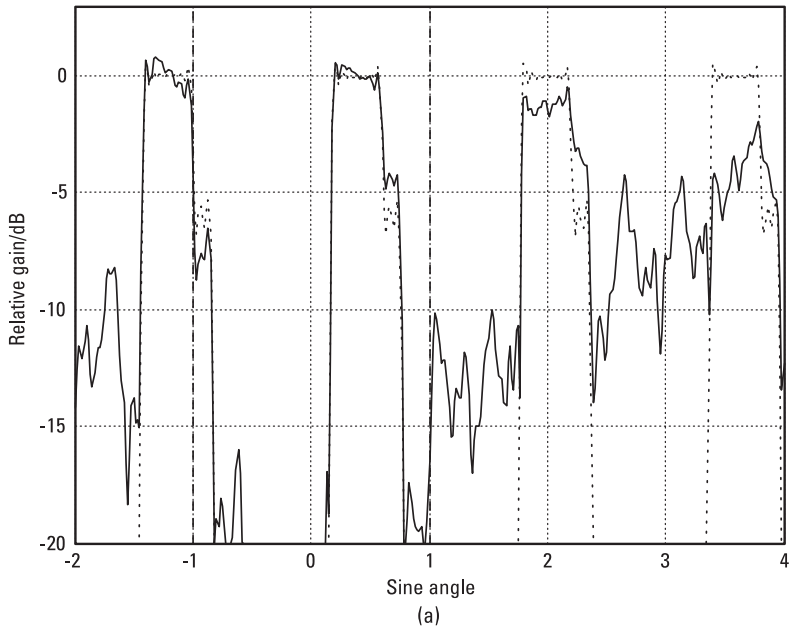
Figure 8.12   Sector pattern from a steered irregular linear array, beam at 30°. (a) Response in *u*-space, and (b) beam pattern.
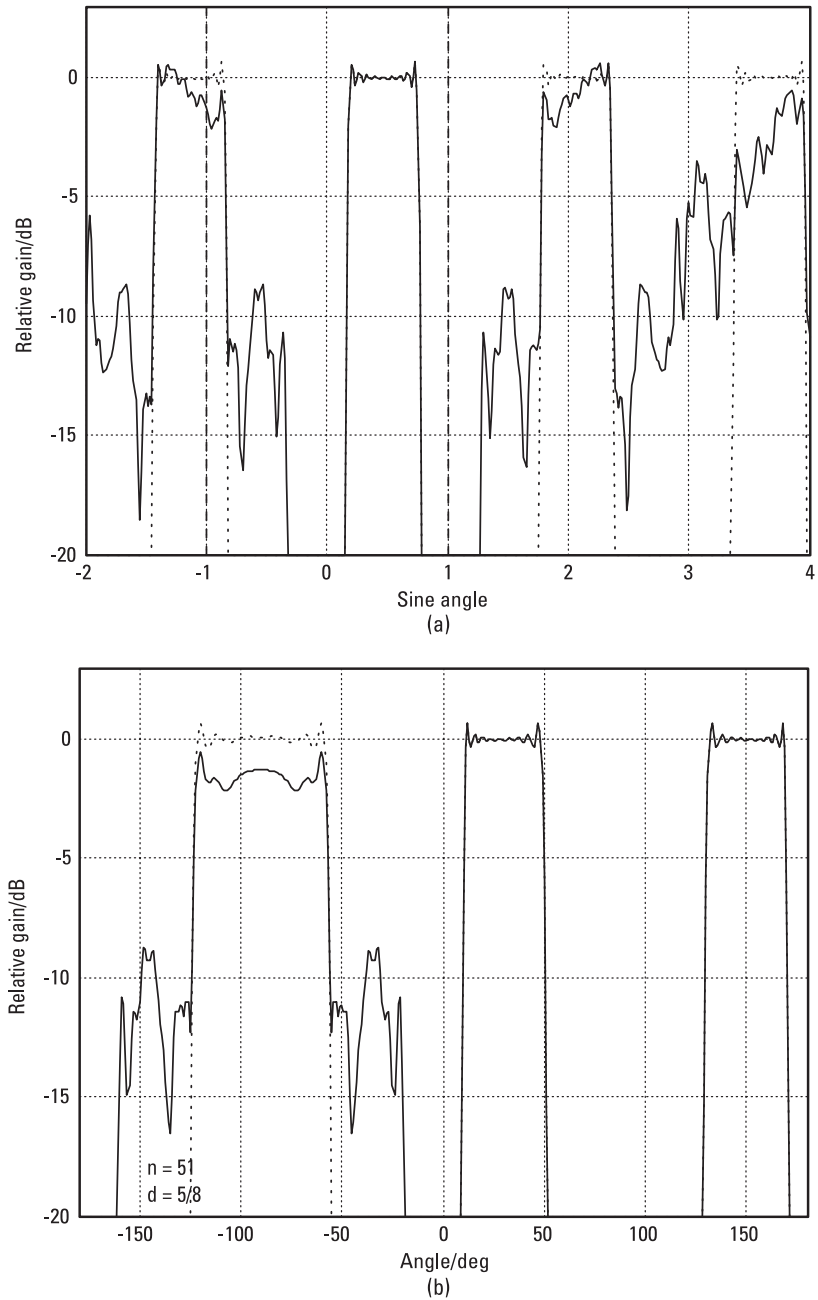
Figure 8.13   Sector pattern from an irregular linear array, beam at 30°, optimization over one period in *u*. (a) Response in *u*-space, and (b) beam pattern.
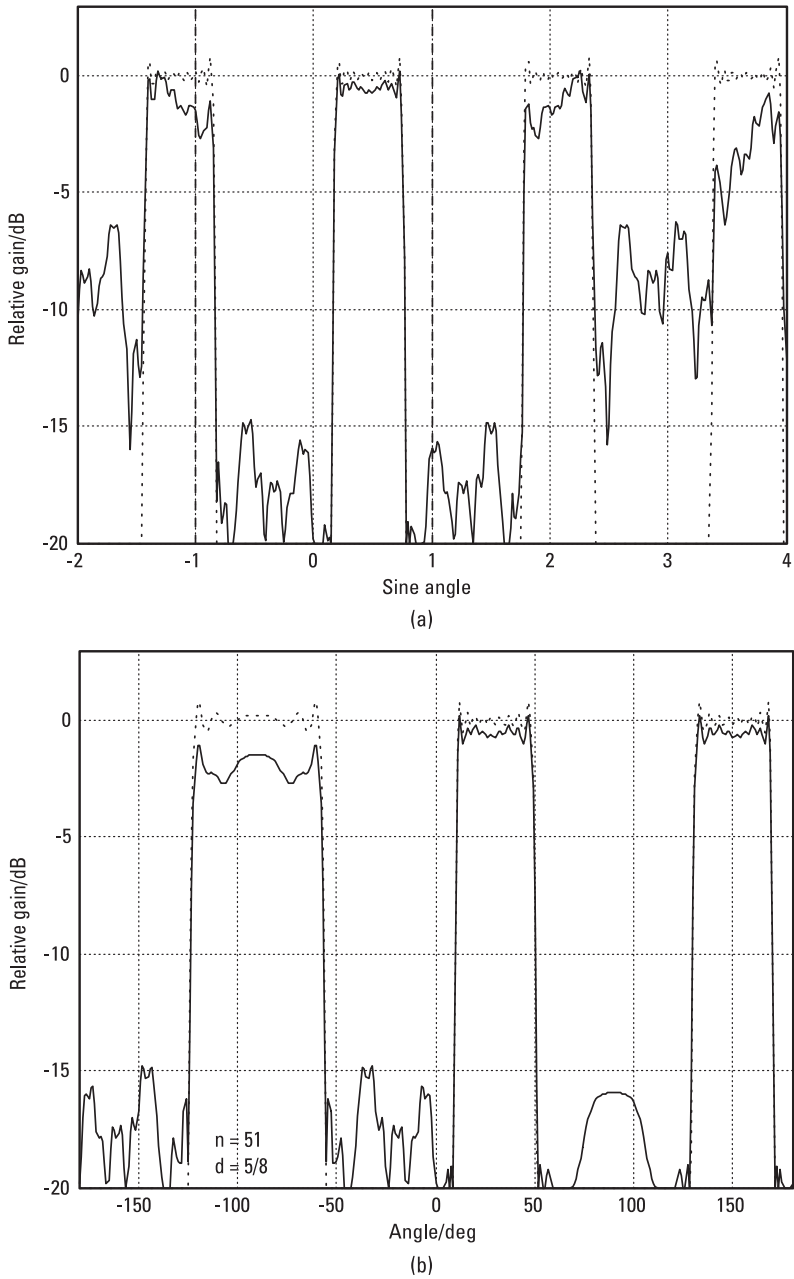
Figure 8.14 Sector pattern from an irregular linear array, beam at 30°, optimization over two periods less the sector width. (a) Response in *u*-space, beam at 30°, and (b) beam pattern, beam at 30°.

required sector beam is now preserved, but in this case there is a large lobe around −90°, nearly the full height of 0 dB. This is derived from the edge of the approximate grating lobe near $u = -1$, within the real angle region ($-1 \leq u \leq 1$). The large lobe at 150° is the reflection about 90° of the wanted lobe, at 30°. This lobe could be removed by using reflector-backed elements, as discussed earlier, but some of the large lobe (in the region −50° to −90°) will not be removed. Furthermore, there are quite high sidelobes in the region −20° to −50°, which are derived from parts of the u response that were not within the pattern optimizing region chosen for I.

    We see from the discussion of Figures 8.11 through 8.13 how the choice of I affects the pattern. Finally, we choose I to be the whole region between the first two approximate grating lobes, so it is of width $2U - u_0$, where u_0 is the width of the required sector, and we center I at the sector center, u_1, as before. Thus, using rect($(u - u_1)/(2U - u_0)$) in (8.34), so that

$$B_{rs} = (2U - u_0)\operatorname{sinc}((2U - u_0)(x_r - x_s))\exp(-2\pi i(x_r - x_s)u_1)$$

we obtain Figure 8.14 (for the same array as in Figures 8.11 through 8.13). We still have the large lobe around −90°, caused by the approximate grating lobe near $u = -1$, but the sidelobes between the main lobes are now rather smaller, as the regions of the u response that they originate from are now included in the least squared error solution.

    Thus, although a solution can be found for the irregular array, its usefulness is limited for two reasons; the set of nonorthogonal exponential functions (from the irregular array positions) used to form the required pattern is not as good as the set used in the regular case, and, if the element separation is to be 0.5 wavelengths as a minimum, an irregular array must have a mean separation of more than 0.5 wavelengths, leading to grating (or approximate grating) effects.

8.5 Summary

As there is a Fourier transform relationship between the current excitation across a linear aperture and the resultant beam pattern (in terms of u, a direction cosine coordinate), there is the opportunity to apply the rules-and-pairs method for suitable problems in beam-pattern design. This has the now-familiar advantage of providing clarity in the relationship between aperture distribution and beam patterns, where both are expressed in terms of combinations of relatively simple functions.

However, there is the complication to be taken into account that the "angle" coordinate in this case is not the physical angle but the direction cosine, along the line of the aperture. In the text, we have taken the angle θ to be measured from broadside to the aperture and defined the corresponding Fourier transform variable u as $\sin\theta$, so that $u = \cos(\pi/2 - \theta)$, the cosine of the angle measured from the line along the aperture. In this u domain beam shapes remain constant as beams are steered, while in real (or angle) space they become stretched out when steered toward the axis of the aperture. Furthermore, the transform of the aperture distribution produces a function that can be evaluated for all real values of u, but only the values of u lying in the range -1 to 1 correspond to real directions.

Both continuous apertures and discrete apertures can be analyzed, the latter corresponding to ideal antenna arrays with point, omnidirectional elements. In this chapter, we have concentrated on the discrete, or array, case. The regular linear array, which is very commonly encountered, is particularly amenable to the rules-and-pairs form of analysis. In this case, the regular distribution (a comb function) produces a periodic pattern in u space (a rep function). In the case of a directional beam, the repetitions of this beam are potential grating lobes, which are generally undesirable, but if the repetition interval is adequate (large enough), there will be no repetitions within the basic interval in u corresponding to real space and hence no grating lobes. The condition for this (that the elements be no more than half a wavelength apart) is very easily found by this approach. Two variations on the directional beam for producing different low sidelobe patterns were studied in Section 8.3.2. These exercises, whether or not leading to useful solutions for practical application, are intended to illustrate how the rules-and-pairs method can be applied to achieve solutions to relatively challenging problems with quite modest effort. It was seen in Section 8.3.3 that very good beams covering a sector at constant gain can be produced, again very easily using the rules-and-pairs method.

The case of irregular linear arrays can also be tackled by these methods. However, the rules-and-pairs technique is not appropriate for directly finding the discrete aperture distribution that will give a specified pattern when the elements are irregularly placed. Instead, the problem is formulated as a least squared error match between the pattern generated by the array and the required one. In this case, the discrete aperture distribution is found to be the solution of a set of linear equations, conveniently expressed in vector-matrix form. The elements of both the vector and the matrix are obtained as Fourier transform functions evaluated at points defined by the array element positions. Again, the sector pattern problem was taken, and it was shown that

this approach gives the same solution as that given directly by the Fourier transform in the case of the regular array, confirming that the direct Fourier transform solution is indeed the least squared error solution. For the irregular array, we obtain sector patterns as required, though with perhaps higher sidelobe levels and with some limitations on the array (which should not be too irregular or have too wide an aperture for the number of elements) and on the angle to which the beam can be steered away from broadside. These limitations are not weaknesses of the method but a consequence of the irregular array structure, which makes achieving a given result more difficult. If the array elements are not to be too close (so are preferably at least a half wavelength apart), the elements of the irregular array will have a mean separation of over a half wavelength, leading to some grating effects, which seem to be unavoidable (even if directional elements are used to remove the back half of the pattern) except by keeping the average element separation down and not steering too far from broadside.

Final Remarks

The illustrations of the use of the rules-and-pairs technique in Chapters 3 through 8 show a wide range of application and how some quite complex problems can be tackled, using a surprisingly small set of Fourier transform pairs. The method seems to be very successful, but on closer inspection we note that the functions handled are primarily amplitude functions—the only phase function is the linear phase function due to delay. Topics such as the spectra of chirp (linear frequency modulated) pulses or nonlinear phase equalization have not been treated, as the method, at least as formulated at present, does not handle these. There may be an opportunity here to develop a similar calculus for these cases.

A considerable amount of work, in Chapters 6 and 7, is directed at showing the benefits of oversampling (by only a relatively small factor, in some cases) in reducing the amount of computation needed in the signal processing under consideration. As computing speed is increasing all the time, it is sometimes felt that little effort should go into reducing computational requirements. However, apart from the satisfaction of achieving a more elegant solution to a problem, there may be good practical reasons. Rather analogously to C. Northcote Parkinson's law, "Work expands to fill the time available for its completion," there seems to be a technological equivalent: "User demands rise to meet (or exceed) the capabilities of equipment." While at any time an advance in speed of computation may enable current problems to be handled comfortably, allowing the use of inefficient implementations, requirements will soon rise to take advantage of the increased performance—higher bandwidth systems, more real-time processing, more comprehensive simulations, and so on. Cost could also be a significant factor, particular for real-time signal processing—it may well be much more economical to put some

theoretical effort into finding an efficient implementation on lower performance equipment than require expensive equipment for a more direct solution, or alternatively to enable the processing to be carried out with less hardware.

Finally, while it is tempting to use simulations to investigate the performance of systems, there will always be a need for theoretical analysis to give a sound basis to the procedures used and to clarify the dependence of the system performance on various parameters. In particular, analysis will define the limits of performance and, if practical equipment is achieving results close to the limit, it is clear that little improvement is possible and need not be sought; on the other hand, if the results are well short of the limit, then it is clear that substantial improvements may be possible. The Fourier transform (now incorporating Fourier series) is a valuable tool for such analysis, and as far as Woodward's rules-and-pairs method makes this operation easier and its results more transparent, it is a welcome form of this tool.

About the Author

After graduating in physics at Oxford University (where, coincidentally, he was a member of the same college as P. M. Woodward, whose work is the starting point for this book), the author joined, in 1959, the Plessey Company's electronics research establishment at Roke Manor—now Roke Manor Research. Apart from one short break, he remained there until retiring in 2002, studying a variety of electronic systems and taking a degree in mathematics at the Open University to assist this work. His principal fields of interest have been adaptive interference cancellation, particularly for radar, adaptive arrays, superresolution parameter estimation, blind signal separation, and multilateration. His thesis, for a Ph.D. from University College London, was on the theoretical performance of superresolution systems.

Index